CRANFIELD UNIVERSITY

ARUBI ISAAC MARCUS TESI

MULTIPHASE FLOW MEASUREMENT USING GAMMA-BASED TECHNIQUES

SCHOOL OF ENGINEERING

PHD THESIS
Academic Year: 2010 - 2011

Supervisor: PROFESSOR HOI YEUNG
MARCH 2011

CRANFIELD UNIVERSITY

SCHOOL OF ENGINEERING

DEPARTMENT OF OFFSHORE, PROCESS AND ENERGY ENGINEERING

PHD THESIS

Academic Year 2010 - 2011

ARUBI ISAAC MARCUS TESI

MULTIPHASE FLOW MEASUREMENT USING GAMMA-BASED TECHNIQUES

Supervisor: PROFESSOR HOI YEUNG

March 2011

This thesis is submitted in partial fulfilment of the requirements for the degree of Doctor of Philosophy

© Cranfield University 2011. All rights reserved. No part of this publication may be reproduced without the written permission of the copyright owner.

Every investigation whose complete success is now acknowledged was subject to numerous failures during the previous period of research…..

ABD-DRU-SHIN

ABSTRACT

The oil and gas industry need for high performing and low cost multiphase meters is ever more justified given the rapid depletion of conventional oil reserves. This has led oil companies to develop smaller/marginal fields and reservoirs in remote locations and deep offshore, thereby placing great demands for compact and more cost effective solutions of on-line continuous multiphase flow measurement. The pattern recognition approach for clamp-on multiphase measurement employed in this research study provides one means for meeting this need.

High-speed gamma densitometers and Coriolis meters were installed vertically at the top of a 50.8mm and 101.6m riser as well as horizontally close to the riser base in the Cranfield University multiphase flow test facility. A comprehensive experimental data collection of the densitometer and the Coriolis meter response to a variety of multiphase flow conditions typical of operating conditions found in the petroleum industry was undertaken.

Signal analysis of the densitometer data in the time and frequency domain gave a good indication of the gas and liquid phase distribution in the flow and discriminatory correlations between statistical features of the gamma count data and key multiphase flow parameters were revealed.

The flow pattern prevalent in the 50.8mm and 101.6mm pipe sizes in the horizontal as well as vertical orientation were identified from statistical parameters. Based on the results, the experimental flow regime maps were developed and compared with the existing regime maps and good agreement was found.

The effect of upstream conditions on the 50.8mm vertical riser flow behaviour was also investigated via two different air inlet configurations (i) upstream flowline mixing and (ii) riser base injection. No significant difference exist in flow behaviour at low superficial air-liquid velocities for both configurations, but at higher superficial air-liquid velocities, the intermittent flow behaviour due to

hydrodynamic slugging in flowline influences the riser flow pattern characteristics, thus controlling the riser dynamics.

The drift flux modeling approach was employed in predicting void fraction. It was found that with increase in superficial gas velocity and enlargement of bubble sizes, the drift velocity also increases in vertically upward flows. Furthermore it was shown that the drift velocity in horizontal flows is not normally zero.

Large phase fraction measurement uncertainties, using Monte Carlo simulation methods were found from the densitometer data.

The use of pattern recognition techniques to correlate the gamma densitometer data with the individual phase superficial velocities and the water cut was investigated. A feedforward multi-layer perceptron network model was developed and trained to map the temporal fluctuations in the multiphase mixture density with the individual phase flow rates using statistical features extracted from the gamma count signals as their inputs. Individual phase flow rate predictions to within ±5% relative error for the two phase air-water flows and ±10% for three phase air-oil-water flows were achieved.

Keywords: *gamma densitometry, multiphase flow, multiphase measurement, measurement uncertainty, pattern recognition, flow regime, signal analysis, drift flux, phase inversion.*

ACKNOWLEDGEMENTS

This thesis would not have been possible without the valuable contributions of a number of people over the past three years. Therefore it is an honour for me to acknowledge the support of the following people.

I would like to show my gratitude to my supervisor Professor Hoi Yeung who has been a constant source of guidance, support and ideas throughout the duration of this work.

I am indebted to Mr David Whittingham, Mr Andrew Jamieson, Dr. Vladimir Kratirov (deceased), Mr Ivan Endovitsky, Dr. Dmitry Gazin and the entire staff and associates of the Neftemer family who have offered a considerable amount of assistance and encouragement.

I wish to express my sincere thanks to the entire staff and student of the Process Systems Engineering Group with special mention of Professor Mike Sanderson, Dr. Yi Cao, Dr. Meihong Wang, Dr. Liyun Lao, Mr. Clive Wood, Mr. Derek Brown, Mr. David Whittington and Mrs Samantha Skears for their input in various capacities.

This work was undertaken with the financial assistance of EPSRC and De Flow Ltd and I am eternally grateful for their support.

Lastly, my deepest gratitude to my wife Adaze for her love and support and blessings to my son Aninoritse and daughter Oritsemisan.

TABLE OF CONTENTS

LIST OF FIGURES

LIST OF TABLES

NOMENCLATURE

A. Symbols

Symbol	*Units*	*Description*
A	[m^2]	Area
A_g	[m^2]	Cross-sectional area occupied by gas
A_l	[m^2]	Cross-sectional area occupied by liquid
a_k,	[-]	Linear predictor filter output coefficient
A_o	[m^2]	Cross-sectional area occupied by oil
A_p	[m^2]	Pipe cross-sectional area
A_w	[m^2]	Cross-sectional area occupied by water
b	[-]	Neuron bias
b_l	[-]	Linear predictor filter input coefficient
b_0	[-]	Initial term of linear predictor transfer function
B	[-]	Build up factor
B_s	[m]	Bandwidth
c	[ms^{-1}]	Speed of light in a vacuum or intercept
C_e	[farad]	Measured capacitance
C_m	[farad]	Multiphase fluid mixture capacitance
C_o	[-]	Distribution/concentration parameter
C_p	[farad]	Electrode-pipe wall capacitance
d	[m]	Euclidean distance or bubble diameter
D	[m]	Diameter
Dp	[bar]	Differential pressure
E	[eV]	Photon energy
e	[volts]	Final voltage being measured by the sensing device.

E_b	[eV]	Electron binding energy
E_d	[-]	Objective function for neural network error minimisation
E_e	[eV]	Electron energy
e_n	[-]	Residual error of linear prediction
E_o	[eV]	Original photon energy
e_o	[volts]	Voltage measured at zero value of physical variable.
E_{pe}	[eV]	Photoelectric energy
E_q	[-]	Average quantisation error
E_r	[-]	Neural network output associated relative error
E_R	[-]	Residual error of linear prediction coefficients
E_t	[-]	Topographic error
E_T	[j]	Total signal energy
E_W	[-]	Sum of squares of network weights
f	[-]	Neural network activation function, Friction factor
F	[-]	Modified objective function or input vector scale factor
F_c	[Hz, N]	Signal psuedo-frequency or Coriolis force
f_s	[Hz]	Sampling frequency
G	[S,kg·m^{-2}·s^{-1}]	Conductivity or mass flux
G_t	[Kgs^{-1}]	Total mass flow rate
g	[m/s^2]	Acceleration due to gravity
h	[-,m,-]	Planck constant, thickness of absorber, or number of hidden nodes
h_a	[m]	Gamma beam path length through air
h_l	[m]	Gamma beam path length through liquid
h_o	[m]	Gamma beam path length through oil

h_w	[m]	Gamma beam path length through water
H_L	[-]	Holdup
I	[-]	Current or measured gamma radiation intensity
I_0	[-]	Initial gamma radiation intensity
I_a	[-]	Gamma radiation intensity of air filled conduit
I_g	[-]	Gamma radiation intensity of gas filled conduit
I_l	[-]	Gamma radiation intensity of liquid filled conduit
I_o	[-]	Gamma radiation intensity of oil filled conduit
I_w	[-]	Gamma radiation intensity of water filled conduit
k	[-]	Gain
K	[-]	Slip constant
L	[m]	Length
m	[kg/s,-, kg]	Mass flow rate, gradient, mass
m_c	[-]	Best matching unit vector
m_o	[kg]	Rest mass of an object
n	[-]	Number of layers in neural network
N	[-]	Total number of points in a sampled record or number of radioactive nuclei
N_{Re}	[-]	Reynolds's number
P	[bar, - , -]	Pressure, linear predictor filter order, neural network input
P_{base}	[bar]	Riser base pressure
P_{top}	[bar]	Riser top pressure
$P(x)$	[-]	Probability density function
$P(z)$	[-]	Symmetric polynomial
ΔP	[bar]	Differential Pressure
Q	[-]	Physical variable (e.g. pressure)

Q_g	[m^3/s]	Volumetric gas flow rate
Q_l	[m^3/s]	Volumetric liquid flow rate
Q_{MA}	[S m^3/hr]	Air flowrate
Q_{MO}	[kg/s]	Oil flowrate
Q_{MW}	[kg/s]	Water flowrate
Q_{total}	[kg/s]	Total flowrate
Q_o	[m^3/s]	Volumetric oil flow rate
Q_t	[m^3/s]	Total volumetric flow rate
Q_w	[m^3/s]	Volumetric water flow rate
$Q(z)$	[-]	Anti-symmetrical polynomial
R	[m,-]	Radius, Covariance coefficient, Input vector range
r_o	[m]	Classical electron radius
R_e	[Ω]	Effective resistance
R_m	[Ω]	Multiphase fluid mixture resistance
R_{xx}	[-]	Autocorrelation function
R_{xy}, R_{y0y1}	[-]	Cross-correlation function
s	[-]	Slip
T	[ºC]	Temperature
t	[s,-]	Time, Neural network target output
T_{base}	[ºC]	Riser base temperature
U_g	[m/s]	Drift flux velocity
u_g	[m/s]	Mean gas velocity
u_l	[m/s]	Mean liquid velocity
$u(y)$	[-]	Standard uncertainty associated with y
v	[V, m/s]	Voltage, velocity
V	[m/s]	Velocity

V'	[m^3]	Volume
V_a	[m/s]	Air phase velocity
V_{drift}	[m/s]	Drift velocity
v_f	[V]	Final voltage
V_g	[m/s]	Gas phase velocity
V'_g	[m^3]	gas volume
V_l	[m/s]	Liquid phase velocity
V'_l	[m^3]	Liquid volume
V_m, V_{mix}	[m/s]	Mixture velocity
V_o	[m/s]	Oil phase velocity
V_{sg}	[m/s]	Gas superficial velocity
V_{sl}	[m/s]	Liquid superficial velocity
V_{slip}	[m/s]	Slip velocity
V'_t	[m^3]	Total Volume
V_w	[m/s]	Water phase velocity
W	[-]	Neural network weight
x	[-]	Data set
$\overline{x}$	[-]	Mean
$x(t)$	[s]	Sampled time history
X	[-]	Lockhart and Martinelli number, Input Quantity
Y	[-]	Neural network output, output quantity
z	[m]	Height
Z	[-]	Atomic number
Z_e	[Ω]	Electrical impedance

B. Greek Symbols

Symbol	*Units*	*Description*
α	[-]	Void fraction, control parameter in Bayesian regularisation
α_g	[-]	Gas volume fraction
α_l	[-]	Liquid volume fraction
β	[-]	Water volume Fraction, control parameter in Bayesian regularisation
γ	[-]	Oil volume fraction; linear attenuation coefficient; or number of effective parameters
γ_a	[-]	Air linear attenuation coefficient
γ_l	[-]	Liquid linear attenuation coefficient
γ_o	[-]	Oil linear attenuation coefficient
γ_w	[-]	Water linear attenuation coefficient
δ	[m]	Outer layer error
Δ	[-]	Sampling period
ε_a	[-]	Air chordal hold-up
ε_o	[-]	Oil chordal hold-up
ε_w	[-]	Water chordal hold-up
ε	[-]	Pipe roughness
η	[-]	Step size
θ	[-]	Photon deflection angle
λ	[-]	Mean free path or radioactive decay constant
λ_g	[-]	Gas hold-up
λ_l	[-]	Liquid hold-up
μ_l	[-]	Mean
μ_g	[Pa-s]	Dynamic Gas viscosity

μ_l	[Pa-s]	Dynamic Liquid viscosity
ν_l	[m^2s^{-1}]	Kinematic Liquid viscosity
ρ_g	[kgm^{-3}]	Gas density
ρ_l	[kgm^{-3}]	Liquid density
ρ_m	[kgm^{-3}]	Mixture density
ρ_o	[kgm^{-3}]	Oil density
ρ_w	[kgm^{-3}]	Water density
ρ_{TP}	[kgm^{-3}]	Two phase density
$\Delta\rho$	[kgm^{-3}]	Density difference between the two phases
σ	[Nm^{-1},-,-]	Surface tension, standard deviation or photon interaction probability
Y	[Hz]	Frequency of electromagnetic radiation
ϕ_l	[-]	Liquid Friction multiplier
ψ_g	[-]	Mass transfer rate between phases
ψ_e	[-]	Entrainment rate
υ	[-]	Excitation frequency of electronic circuitry
ω	[m/s, Hz]	Angular velocity or frequency

C. Subscripts

a	Air
b	Bubble
g	Gas
i	Interface, initial
l	Liquid
m	Mixture
o	oil

w	Water

D. Acronyms

Acronym	*meaning*
ACF	Auto Correlation Function
BMU	Best Matching Unit
CAPEX	Capital Expenditure
CK	Coefficient of Kurtosis
CS	Coefficient of Skewness
FFT	Fast Fourier Transform
FMLP	Feedforward Multi-layer Perceptron
Fr	Froude number
FT	Air flow meters of three phase facility
GOR	Gas/Oil ratio
GVF	Gas Volume Fraction
LM	Levenberg-Marquardt
LPC	Linear Prediction Coefficient
LSF	Line Spectral Frequency
MCS	Monte Carlo Simulation
MLP	Multi-Layer Perceptron
MPFM	Multiphase Flow Meter
OPEX	Operating Expenditure
PCA	Principal Component Analysis
PDF	Probability Density Function
PLC	Programmable Logic Controller
PMF	Probability Mass Function

PR	Pattern Recognition
PSD	Power Spectral Density
PVC	Polyvinyl chloride
PVT	Pressure-Volume Temperature
RMS	Root Mean Square
RSS	Root Sum Square
SCG	Scaled Conjugate Gradient
SD	Standard Deviation
SG	Specific Gravity
SSE	Sum of Square Error
TLD	Thermoluminescent Dosimeters
WC	Water Cut
ZMUV	Zero-Mean and Unit Variance

CHAPTER ONE

1. INTRODUCTION

1.1 Background

This research study focuses on the measurement of multiphase flows of gas, oil, and water in flowlines found in oil and gas production operations. In this context, multiphase flow is a flow in which the phases are not chemically related or where more than two phases are present in a conduit.

Multiphase metering is an exciting solution to the growing production measurement issues in the petroleum industry. Oil and gas production operations is occurring in more remote locations and deeper water depths (e.g. BP's PSVM Block-31, offshore Angola is located in water depth of 2000m; also the Great White, Silvertip and Tobago developments in the Gulf of Mexico are in water depths ranging from 2360 to 2940m, (Letton *et al*, 2010)), and with increasing tieback distances, calling traditional measurement employing three phase separator well testing into question. Moreover, new oil and gas developments commingled with existing infrastructures leads to various royalty payment requirements and further complicate the allocation process. These issues, coupled with widening operating envelope and improve measurement quality, is driving the development of multiphase meters to realize their full potential for reservoir monitoring, flow assurance calculations, production optimization, and reservoir engineering analysis (Kelner, 2009).

The need for multiphase flow metering arises when it is desirable or necessary to meter the well streams before they are conditioned (Dykesteen *et al*, 2005). This is done to facilitate reservoir management, field development, operational control, flow assurance, and production allocation (DTI, 2003). Thus the main areas of application for multiphase flow metering are well surveillance or monitoring, well testing, production allocation metering and fiscal or custody transfer measurements.

Multiphase meters today are vital to oil companies' field development and production plans. This is because over the past decade multiphase measurement technology has undergone a significant transformation such that the number of multiphase flow

meters (MPFMs) installed globally has been on the increase (Joshi and Joshi, 2007). Industry analysts predict that there will be 1,000 additional subsea multiphase meters deployed by 2015 (Ruden, 2010). A number of factors are responsible for this rapid uptake of multiphase measurement technology. These are improved meter performances, decreases in meter costs, more compact meters enabling deployment of mobile systems, increases in oil prices, a wider assortment of operators (Blaney, 2008) and the development of compact subsea MPFMs.

The *2010 BP Statistical Review of World Energy* shows that oil prices has been on an upward path for the past decade albeit the decline in 2009, Figure 1-1 (BP, 2010). Given this trend, and with the current economic climate, the initial capital cost as well as the operational/maintenance cost of the multiphase meter will easily be recovered. In another light, this increasing crude oil prices, coupled with the reduced hardware and installation costs associated with deploying MPFMs, would facilitate economic justification of a per well installation basis (Jamieson, 1998).

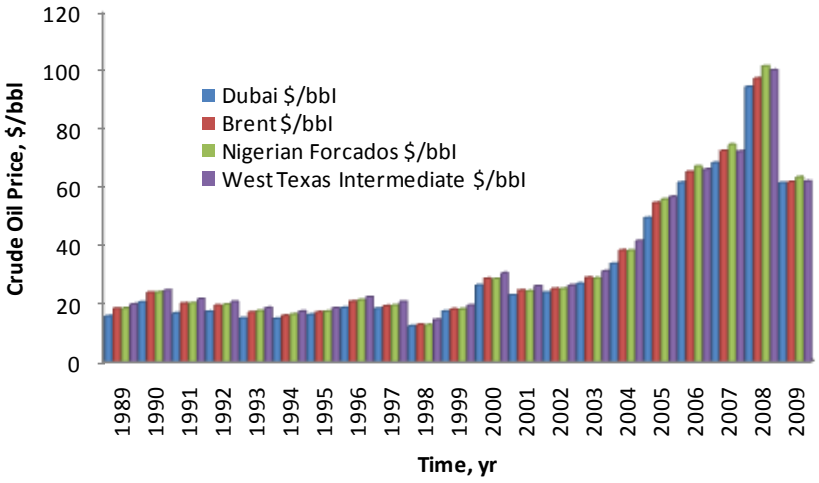

Figure 1-1 World Crude Oil Prices 1989-2009 (BP, 2010)

However with the increased market penetration of multiphase meters come challenges: particularly in environments such as deepwater operations where scaling, meter fouling and high temperature-high pressure (HTHP) conditions are prevalent, sour gas fields with fluctuating H_2S concentration and heavy oil fields with high viscosity and low flow rates. Aligned to these market drivers is the increased pressure on operators to manage costs, increase efficiency, guarantee flow assurance and enhance production. This means MPFMs:

- Must have a measurement principle that can handle and accurately describe complex flow regimes so that appropriate multiphase flow models can be applied.

- Must be able to detect the timing of well flow changes and such factors like slug pattern, emulsions and paraffin deposition which can affect the flow stream.

- Must be operational and effective at lower costs in previously inaccessible locations, and have the necessary flexibility to react to changing production conditions during the field's lifecycle (Ruden, 2010).

To date no single commercial multiphase meter is able to meet all the above requirements and in spite of the advances in multiphase metering technology, industrial utilisation of this technology remains relatively expensive for meters that offer an acceptable level of performance. This justifies the need for further development of MPFMs.

Clamp-on gamma-densitometry is a suitable technique to facilitate non-intrusive multiphase flow metering as it does not require breaking into the pipeline for installation, thus eliminating the cost of production deferment; the unit is simply clamped onto the pipe's exterior surface (Kratirov *et al*, 2006). Consequently, it is suitable for different line sizes, and can be retrofitted on land and offshore wells without breaking into flow lines. Many commercially available multiphase meters uses gamma-densitometry techniques as part of their measurement systems (Thorn *et al*, 1997) because low intensity gamma radiation sources does not present significant technical problems during installation or use in onshore environments. Although restrictive logistics and administrative barrier hinders the deployment of nucleonic instrumentation in certain countries, nevertheless there remain growing markets in countries where radiation-based MPFMs can be installed.

1.2 Objective

This research study is a follow up on and an extension to a previous work on the application of a single gamma-densitometer unit to determine both phase volume fraction and velocities to yield oil, water and gas flow rates as part of a research and

development programme for a commercial clamp-on multiphase meter. The objectives of this research study are:

- Carry out a literature review on multiphase flow, multiphase flow measurement, gamma radiation and pattern recognition techniques in multiphase metering, and measurement uncertainty estimation.
- Undertake experimental data collection of a gamma-densitometer and Coriolis mass flow meter response to a comprehensive multiphase flow conditions typical of operating conditions found in the oil and gas industry.
- Undertake sensors' signal analysis in relation to key multiphase flow parameters and evaluate three phase flows characteristics in horizontal as well as vertical upward flows.
- Apply pattern recognition modelling to predict individual phase flow rates and the liquid phase water cut and validate the claim that gamma densitometer, when mounted horizontally, produces better prediction results in a pattern recognition based multiphase flow measurement system.
- Investigate the effects of upstream conditions on the flow behaviour in the 50.8mm diameter vertical riser.
- Investigate the suitability of predicting the point of phase inversion in the 50.8mm diameter vertical riser using pressure gradient analysis.
- Perform uncertainty evaluation of the gamma densitometer measurement using Monte Carlo Simulation (MCS) methods.

1.3 Thesis Structure

Chapter 1: Introduction

This chapter gives a brief discussion of the background for this dissertation, the objectives and scope of the thesis.

Chapter 2: Literature Review

This chapter provides an extensive review of literature relevant to the subject matter. It comprises the following sections: fundamentals of multiphase flow, multiphase flow measurement, gamma radiation methods, pattern recognition techniques and measurement uncertainty.

Chapter 3: Experimental Setup and Data Acquisition

This chapter presents the experimental facility and outlines the instrumentation used, data acquisition and processing and sensor calibration. Details of the experimental campaign are also presented here.

Chapter 4: Experimental Results

In this chapter, flow pattern characterization, flow regime maps and the effects of inlets conditions on three phase flows in the vertical riser are presented. Also included in this chapter are the evaluation of void fraction correlations (drift-flux model) against the experimental data, uncertainty estimation in phase fraction measurement and the performance assessment of Coriolis and Gamma density measurements.

Chapter 5: Signal Analysis

This chapter presents details of the sensors response to different multiphase flow conditions, signal analysis in the time and frequency domain and orientation effects on sensor response.

Chapter 6: Pattern Recognition Techniques

This chapter details the application of pattern recognition techniques to predict individual phase flow rates for both horizontal and vertically upwards multiphase flows. Results of the single multilayer perceptron model and how sensors orientation affects the model predictions is also part of this chapter.

Chapter 7: Conclusions and Future Work

This final chapter presents a summary of the main conclusions drawn from the research and recommendations for future work.

CHAPTER TWO

2. LITERATURE REVIEW

This chapter outlines the fundamentals of multiphase flow. It provides an up to date review of literature relevant to the subject matter and comprises of the following sections: fundamentals of multiphase flow, multiphase flow measurement, gamma radiation methods, pattern recognition techniques, and measurement uncertainty.

2.1 Fundamentals of Multiphase Flow

2.1.1 Multiphase Flow

The subject of multiphase flows encompasses a vast field, a host of different technological contexts, a wide spectrum of different scales, a broad range of engineering disciplines and a multitude of different analytical approaches. Multiphase flow is the term used to describe the simultaneous passage through a system of a stream composed of two or more phases (components). The flow of blood in our body, the rising gas bubbles in a glass of beer and steam condensation on windows are all common examples of naturally occurring multiphase flows. Industrially, multiphase flow systems abounds: heat transfer process equipment (such as heat exchangers), oil and gas production and transportation, condensing systems, geothermal operations, evaporation or refrigeration plants, pneumatic transportation of solids, etc.

In the context of this research study, multiphase flow refers to the flow of oil, gas, and water in onshore/offshore oil and gas production operations. During the past twenty years multiphase flow technology has become increasingly important for the economic transportation of well streams from reservoir to process particularly for offshore production, where the trend is to develop numerous small fields by transporting untreated well fluids via existing infrastructures (Oliemans, 1994).

Multiphase flow systems can be very complex, difficult to understand, predict and model due to the simultaneous presence of different phases and, usually of different compounds in the same stream. Single-phase characteristics including velocity

profile, turbulence, and boundary layer are inappropriate for describing the nature of such flows (Dykesteen *et al*, 2005). Thus, the development of adequate models presents a formidable challenge. However, the combination of empirical observations and numerical modelling has aided the understanding of multiphase flows.

Figure 2-1 illustrates an approximate model of multiphase flow in a pipe (Mehdizadeh and Williamson, 2004). As can be seen, each phase occupies a fraction of the total cross sectional area of the pipe.

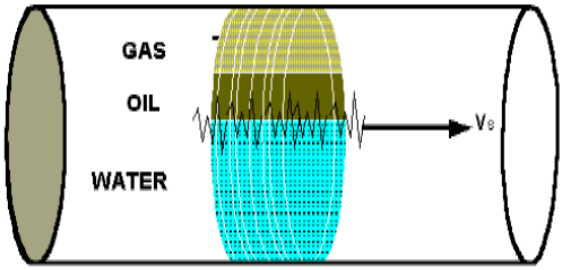

Figure 2-1 Multiphase Flow in a Pipe

The total (mixture) volumetric flow rate through the pipe (Q_t) is the sum of the flow rates of each phase, i.e., gas, water and oil (Q_g, Q_w, and Q_o respectively):

Eqn. 2.1

The total mass flow rate is calculated by multiplying each phase volumetric flow rate by their respective density. The densities of gas, water, and oil are calculated by means of pressure, volume, and temperature (PVT) data.

Eqn. 2.2

Taking a cross-sectional schematic of the multiphase flow in the pipe, Figure 2-2, the volumetric fraction can be expressed in terms of the individual phase velocity Thus. volume fraction, α, is fractional volume flow rate of particular phase. In terms of superficial velocity, the volume fraction of gas is given by:

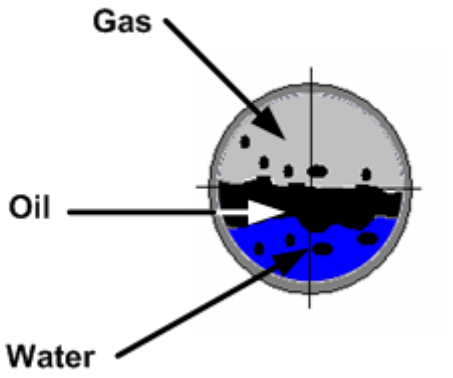

Figure 2-2 Cross-Sectional View of Multiphase Flow

— Eqn. 2.3

where V_g, V_l, and V_m are the gas, liquid and mixture velocity, while *s* denotes superficial. But

Eqn. 2.4

Hence, total mass flow rate can be expressed as shown below where is the liquid density

– Eqn. 2.5

The water fraction or water cut (*WC*) is defined as the ratio of the water mass flow to the total liquid mass flow, expressed in percentage as shown below.

——— Eqn. 2.6

2.1.2 Pressure Gradient

The change in pressure measured across a given distance is called a "pressure gradient". Assuming one-dimensional flow and a constant pressure gradient, the pressure drop in a pipe can be expressed by the equation (Keska and Wang, 2006):

— Eqn. 2.7

where ΔP is the pressure difference between two measurement points in the pipe, ΔL is the distance between these points and dP/dL is the pressure gradient in the pipe. The total pressure gradient can be seen as a superposition of three components due to the mixture acceleration (*a*), friction (*f*) and gravity (*g*). Represented mathematically as:

— — — — Eqn. 2.8

For the steady-state flow conditions in horizontal and vertical pipes and for small and moderate pressure differences between the input and output, it is assumed that the averaged pressure gradient contribution due to acceleration is insignificant. Thus the dP/dL_a, is neglected leaving only the frictional and gravitational to be considered. The frictional pressure is given by:

— ——— Eqn. 2.9

and the gravitational pressure gradient by:

— Eqn. 2.10

where ρ_m is the mixture density, g the acceleration due to gravity, f_m the friction factor, V_m the mixture velocity and D the pipe diameter. If the liquid mixture is considered as a homogeneous dispersion with an effective viscosity μ_m, f_m can be expressed as a function of the mixture Reynolds number $N_{Re} = q_m V_m D/\mu_m$ using existing empirical correlation for a single-phase fluid (Descamps *et al*, 2006). It should be note that Equation 2.9 is applicable for low flows conditions and Equation 2.10 is applicable to vertical flows only.

2.1.3 Drift and Slip-The Definition

When gas and liquid flow in a pipe, the cross sectional area covered by liquid is greater than under static conditions, this is due to the effect of slip between liquid and gas. The lighter gas phase will normally move much faster than the liquid phase while the liquid phase has the tendency to accumulate in horizontal and inclined pipe segments. This difference in the gas - liquid phase velocities is called the slip, while

the deviation of the gas velocity from a homogenised flow velocity is termed the drift, given by Equations 2.11 and 2.12 respectively. The slip ratio, *S*, is equal to unity when the gas and liquid velocities have equal magnitude.

Eqn. 2.11

Eqn. 2.12

— Eqn. 2.13

The liquid or gas fraction of the pipe cross sectional area (*A*) as measured under two-phase flow conditions is known as liquid hold-up (λ_l) and gas void fraction (λ_g). Due to slip effects, the liquid hold-up will be larger than the liquid volume fraction. Liquid hold-up is equal to the liquid volume fraction only under conditions of no-slip, when the flow is homogeneous and the two phases travel at equal velocities as shown in Figure 2-3.

— — Eqn. 2.14

Eqn. 2.15

For most of the of flow patterns, the liquid hold-up will be larger than the liquid volume fraction and the gas void fraction will be smaller than the gas volume fraction. Because of phase slip, and .

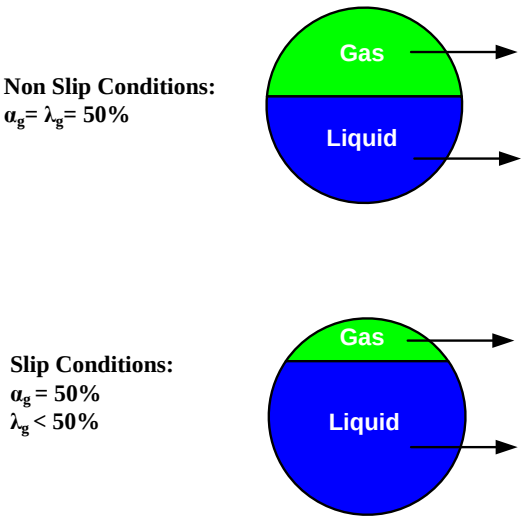

Figure 2-3 Difference between Gas Void Fraction and Gas Volume Fraction

2.1.4 Gas-Liquid Flow Patterns

When gas and liquid flow co-currently in a pipe the phases will distribute themselves in a variety of combinations called flow regimes or flow patterns. This distribution of the fluid phases in space and time differs for the various flow regimes. The configuration of the flow regime is determined by the operating conditions, fluid properties, flow rates, pipe geometry and pipe orientation through which the fluids are flowing. The main mechanisms involved in forming the different flow regimes are transient effects, geometry/terrain effects, hydrodynamic effects and combinations of these effects.

Both vertical and horizontal flow patterns can be grouped into three, namely: dispersed flow, separated flow, intermittent flow or a combination of these. Figure 2-4 and Figure 2-5 illustrate several examples of the flow patterns within each of these groups based on hydrodynamic two-phase gas-liquid system.

- Dispersed flow is characterized by a uniform phase distribution in both the radial and axial directions. Examples of such flows are bubble flow and mist flow.

- Separated flow is characterized by a non-continuous phase distribution in the radial direction and a continuous phase distribution in the axial direction. Examples of such flows are stratified and annular.

- Intermittent flow is characterized by being non-continuous in the axial direction, and therefore exhibits locally unsteady behavior. Examples of such flows are elongated bubble, churn and slug flow.

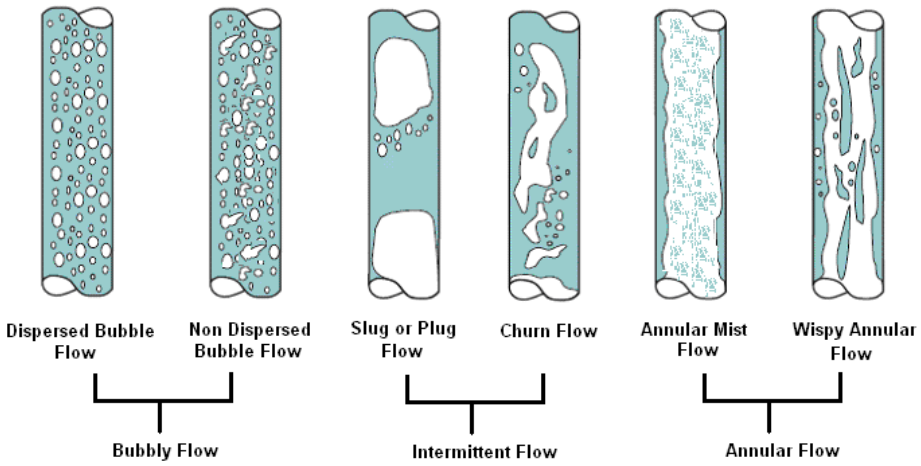

Figure 2-4 Flow Patterns in Vertical Gas-Liquid Flow (Ali, 2009)

Determination of flow patterns is a central problem in multiphase flow analysis. A comprehensive review of flow patterns was carried out by Valle (1998). Since the 1990s, with advance instruments and techniques, different flow pattern parameters have been measured more accurately, and flow patterns of oil-water flow have been analyzed objectively (Xu, 2007).

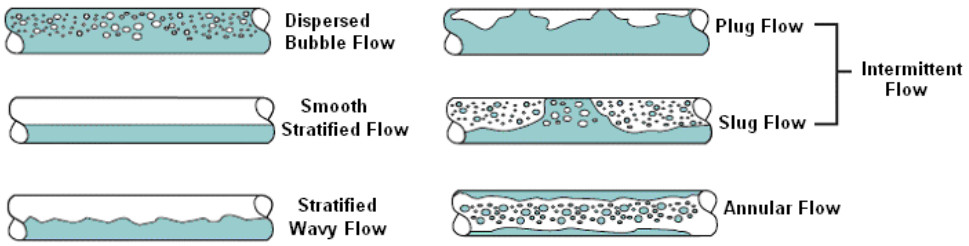

Figure 2-5 Flow Patterns in Horizontal Gas-Liquid Flow (Ali, 2009)

Flow patterns are identified by various methods that can be grouped into two main classes which are visual observation or photography in transparent pipe section, (Griffith and Wallis, 1961; Taitel *et al*, 1980; Fernandes *et al*, 1983 and Hassan and Kabir, 1992) and objective indicator methods (Jones and Zuber, 1975; Vince and Lahey, 1982; Darwich, *et al*, 1989; Stapelberg and Nguyen, 1990; Franca *et al*, 1991; Mi *et al*, 1998; Mi *et al*, 2001; Wu *et al*, 2001; Tjugum *et al*, 2002; Lee *et al*, 2008).

The term superficial velocity is often used when describing multiphase flow regimes. The superficial gas velocity is the velocity of the gas assuming the gas is occupying the whole cross-section of the pipe. It is expressed as the total gas flow rate divided by the total cross-sectional area of the pipe as illustrated below.

— Eqn. 2.16

The superficial liquid velocity is expressed in a similar manner:

— Eqn. 2.17

The multiphase mixture velocity is the sum of the liquid and gas superficial velocities.

Eqn. 2.18

where V_{sg}, V_{sl} and V_m are the superficial gas, liquid and mixture velocities.

2.1.5 Flow Regime Maps

Flow regime maps are graphical representations used to predict the different type of flow patterns that will be encountered in a particular pipe system. Many different types of flow regime maps have been developed for the prediction of flow patterns under various conditions of flow. According to Spedding and Spence (1993), Kosterin (1949) was probably the first to suggest the use of regime maps; thereafter numerous researchers have published flow regime maps employing a variety of parameters as mapping functions. The most widely accepted regime map is that published by Mandhane *et al.* (1974) which use the superficial phase velocities as mapping parameters, Figure 2-6. Another well known flow regime map is the modified flow map of Taitel and Dukler by Taitel *et al* (1980), Figure 2-7.

In the literature, little work on gas-oil-water three phase flows has been published. These have reported the existence of similar flow regimes as those witnessed in standard two-phase flow systems but a particular emphasis is placed on identification of the dispersed and continuous components in the liquid phase (Açikgöz *et al*, 1992; Oddie *et al*, 2003; Spedding *et al* 2005; Wegmann *et al,* 2007). However, some differences have been reported between two and three phase flow

patterns. According to Brill and Arirachakan (1992), at low flow velocities, the liquid density difference may be sufficient to induce separation of the oil and water phases which can result in the production of alternating oil and water slugs and cause substantial slip between the liquid phases in vertical flows. Also Spedding *et al*, (2000) reported that at low gas flow rates, near vertical multiphase flows have been shown to have significant differences when compared to flows contained in a purely vertical pipe.

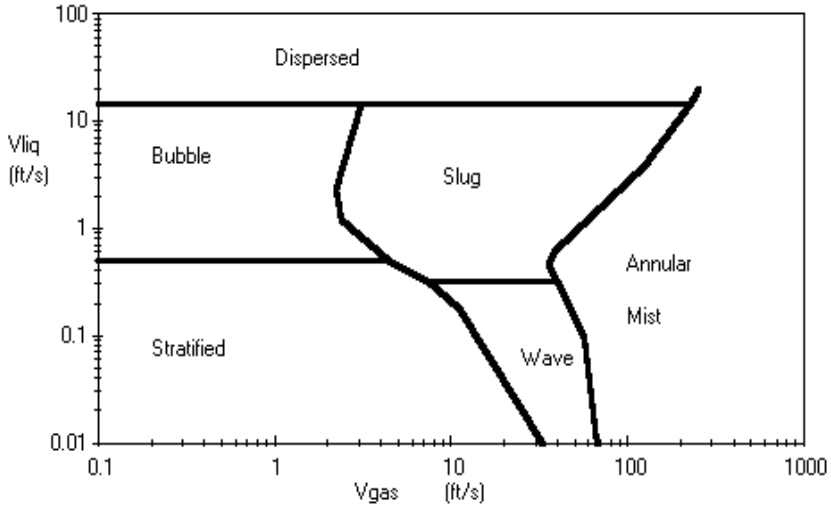

Figure 2-6 Mandhane et al. (1974) Regimes Map for Horizontal Flow

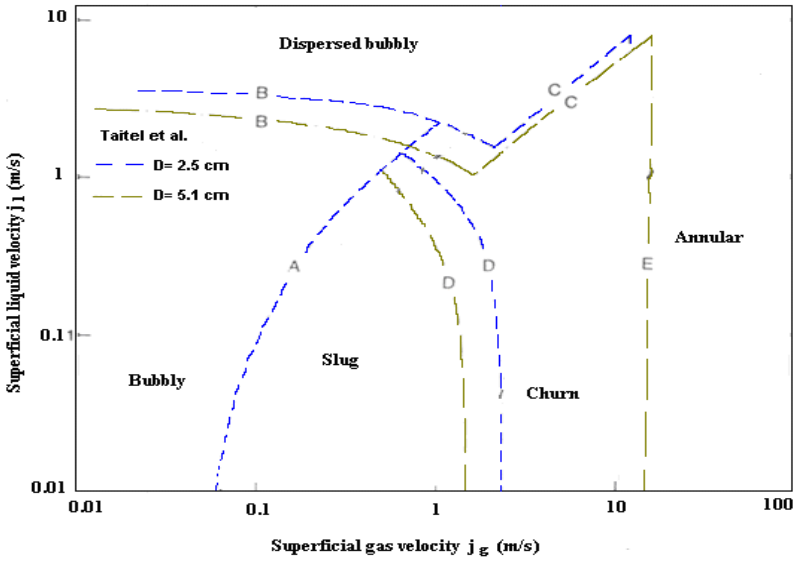

Figure 2-7 Taitel et al. (1980) Regimes Map for Vertical Flow

2.1.5.1 Vertical Flows

Figure 2-8 shows a generic flow regime map based on gas and liquid superficial velocities for co-current multiphase flow in a vertical pipe. As the superficial gas velocity increases the flow will change between all phases in this sequence: bubble - slug - churn and annular. Note that for a particular superficial gas velocity, the multiphase flow is annular for all superficial liquid velocities. The vertical flow regimes are commonly categorised into four main classes:

- **Bubbly Flow:** This type of flow occurs at low gas flow rates wherein the gas is entrained within the continuous liquid phase. The gas bubbles sometimes coalesce to form larger bubbles.

- **Slug Flow:** As the gas superficial velocity is increased, more bubbles will coalesce and form long smooth bubble with the front end shaped like a cap/bullet. This coalescence will continue until the bubble diameter is almost of equivalent cross section as that of the pipe. The resulting flow alternates between high-liquid and high-gas composition.

- **Churn Flow:** This flow is somewhat similar to slug flow, but more disorderedly in nature due to the further increase in gas superficial velocity. The Taylor bubbles have become more distorted to form longer irregular-shaped structures which travel in a churning motion of random oscillatory gas and liquid.

- **Annular Flow:** At very high gas flow rates, the liquid phase exist as film and forced to flow up the pipe wall while the gas flow at the core of the pipe. The gaseous core contains liquid entrainment making the interface between the phases wavy. If this entrained liquid in the gas core becomes significant, the flow is described as annular mist regime.

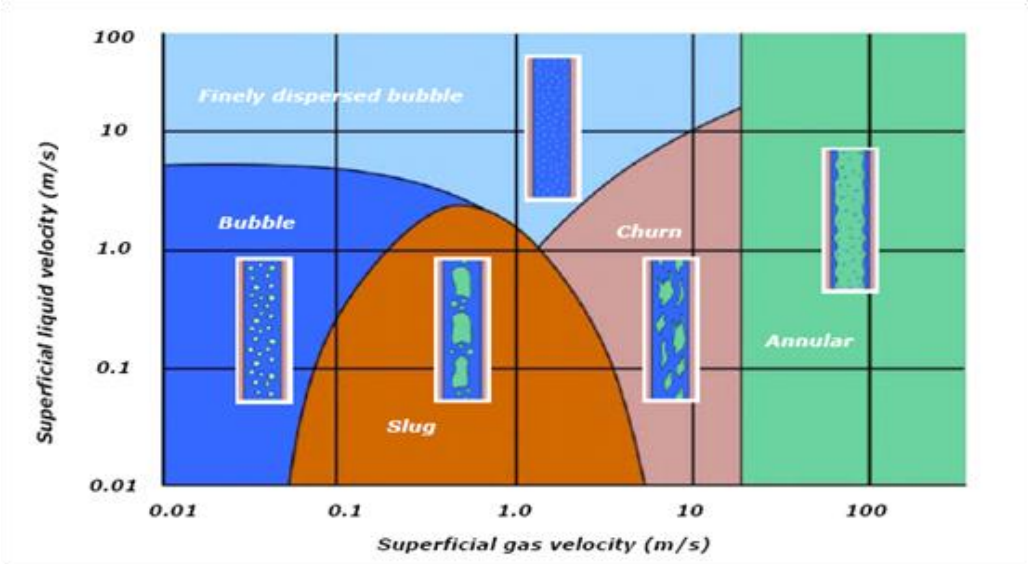

Figure 2-8 Generic Regimes Map for Vertical Flows (Dykesteen et al, 2005)

2.1.5.2 Horizontal Flows

In horizontal flows, the transitions are functions of factors such as pipe diameter, interfacial tension and density of the phases. The flow patterns exhibited in horizontal regimes are not axially-symmetrical and a pipe length equivalent to at least 100 pipe diameters is required for fully developed flow. Figure 2-9 is a qualitative illustration of how flow regime transitions are dependent on superficial gas and liquid velocities in horizontal multiphase flow. A map like this will only be valid for a specific pipe, pressure and a specific multiphase fluid.

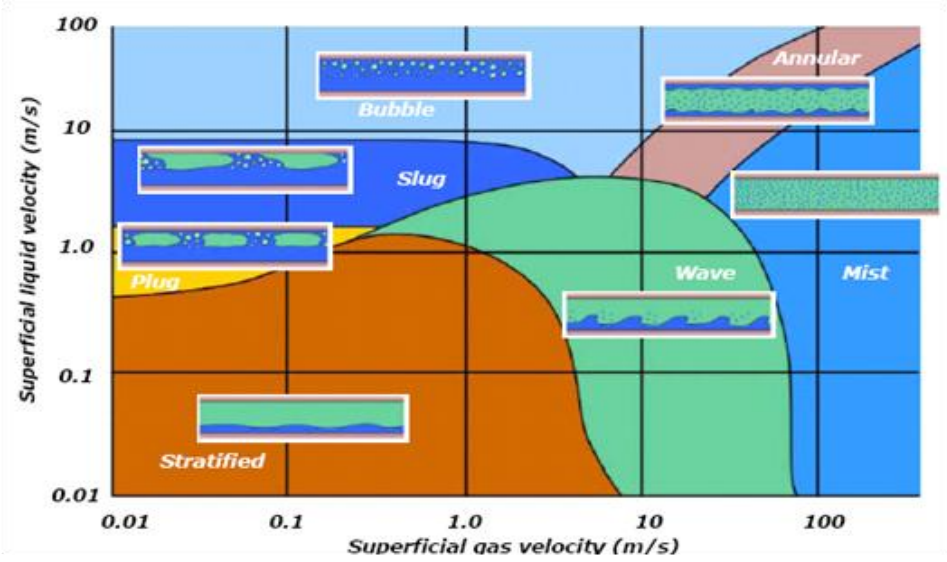

Figure 2-9 Generic Regimes Map for Horizontal Flows (Dykesteen et al, 2005)

- **Bubble Flow**: In horizontal bubbly flow the gas phase exists as discrete bubbles within the liquid and tends to flow at the top of the pipe. At higher liquid and gas velocities the bubbles may become uniformly distributed and appear as froth.

- **Plug Flow**: As the liquid superficial velocity is reduced bubbles become larger and coalesce to form, long bubbles known as plugs, which will occupy the upper section of the pipe.

- **Stratified Flow**: As the gas and liquid superficial velocities are further reduced, the gas phase separates out and flows separately with liquid flowing at the bottom (due to gravity) and gas phase flowing at the upper section of the pipe. There exist two variations of these flows namely; stratified smooth and stratified wavy.

- **Wave Flow**: At higher superficial gas velocity, stratified flow will evolve into wave flow as the increased turbulence will produce a less stable phase interface between the gas and liquid. This interface will be irregular and wavy-like but good separation between phases will still be maintained.

- **Slug Flow**: In this case, higher liquid flow rates produce waves of a much larger magnitude such that the wave touches the top of the conduit and occupies the whole of the pipe cross-section. Thus leading to the propagation of slug down the pipe.

- **Annular/Mist Flow**: At very high gas flow rates, the liquid phase is forced to flow up the pipe wall as a liquid film while the gas flow in the centre. The liquid film will be thicker at the bottom of the pipe owing to gravitational effects.

2.1.6 Phase Inversion Phenomenon

Water-oil dispersions occurring as oil droplets in a water-continuous phase or as water droplets in an oil-continuous phase are frequently encountered in many areas of the process, petroleum and petrochemical industries. In the petroleum industry, oil-water mixtures are transported in wells and flowlines due to formation water break through, particularly at the later years of production. Either water or oil can form the

continuous phase, depending on the operational conditions. A change in condition wherein the continuous phase becomes the dispersed and vice versa is a phenomenon referred to as phase inversion (see Figure 2-10).

The critical volume fraction of the dispersed phase above which this phase becomes the continuous phase is referred to as the inversion point. This transition is usually associated with an abrupt change in the rates of momentum, heat and mass transfer between the continuous and dispersed phases, and between the dispersion and the system solid boundaries, (Wang and Gong, 2009). As such, in designing flowlines, separation facilities and multiphase pumps, phase inversion is a key factor to be considered because of abrupt changes to the rheological properties of the dispersion and the accompanied pressure drop due to high effective viscosity of the mixture (Braumer and Ullman, 2002; Ioannou *et al*, 2004; Gong *et al*, 2006; Piela, *et al*, 2008 and Wang and Gong, 2009).

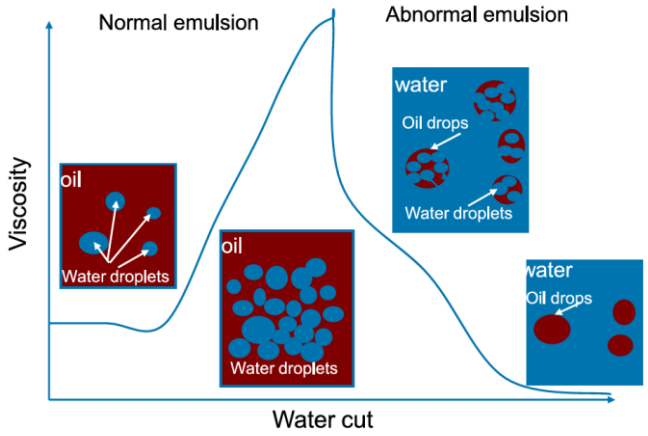

Figure 2-10 Phase Inversion in Crude Oil

Many researchers have investigated phase inversion phenomenon experimentally and computationally, however, work on the influence of gas injection on this phenomenon and the investigations of the pressure gradient characteristics in vertical flows is limited.

Xu *et al* (2010) investigated phase inversion and frictional pressure gradients during simultaneous vertical flow of oil-water two-phase through upward and downward pipes for phase velocities varying from 0 to 1.24 m/s for water and from 0 to 1.87 m/s for oil. They showed that the frictional pressure gradient reaches its lowest value at

the phase inversion point and that this point of inversion occurs at an input oil fraction of 0.8 for upward flow and of 0.75 for downward flow.

Descamps *et al* (2006) carried out experimental study on the influence of gas injection on the phase inversion and the pressure drop increase over the tube during phase inversion of oil-water two phase vertical flows. Their study revealed that gas injection does not significantly change the critical concentration, but the influence on the pressure drop is considerable. They stated that “for mixture velocities larger than 1 m/s, the pressure drop over the tube increases with decreasing bubble size and at inversion can become even larger than the pressure drop during the flow of oil and water without gas injection”.

In another work by Descamps *et al* (2007), experiments on the vertical flow of oil-water-air were performed in order to study the gas-lift technique, with special emphasis on phase inversion for oil-water flows. They also studied the effects of bubble size of the injected air on the efficiency of the gas-lift technique at the point of phase inversion using different types of gas injectors. They found that phase inversion is associated with a sharp increase of the pressure gradient and that with air injection the pressure gradient is always significantly smaller in oil-water-air flow compared with the case of oil-water flow, except at the point of phase inversion where the pressure drop can be even be higher than for oil-water flow. As in their previous work, “it was found that air injection does not significantly change the critical concentration of oil and water where phase inversion occurs”.

In this research, efforts were made to identify the phase inversion point and frictional pressure gradient effects for air-oil-water flow in the 10.5m vertical riser in several different flow patterns. It was found that phase inversion takes place at a water fraction of about 45% and that pressure drop peaked at this point.

2.2 Multiphase Flow Measurement

2.2.1 Principle of Multiphase Flow Measurement

The measurement of flow is one of the most common requirements for processes in industry and research. The measurement and control of fluids into and out of processes are needed to assess the efficiency and/or the quality of the process.

Because flow is so commonly measured, a plethora of flow meters types based on a variety of measurement principles is available (Hardy *et al*, 1999). The MPFM is one of them.

The primary information required from multiphase flow measurement is the mass flow rate of the oil, water and gas components in the flow (Thorn *et al*, 1997). This is done by measuring the mass or volumetric flow rates of the individual components or the individual phase velocities, and the volume fraction of at least two of the flowing phases. The pressure, temperature and vapour-liquid thermodynamic (PVT) equilibrium must be known too. Ideally, the flow meter would make independent direct measurements of each of these quantities. Unfortunately, direct mass flow meters for multiphase flows do not exist yet.

As an alternative to direct mass flow measurement, an inferential method is used. An inferential mass method requires both the instantaneous velocity and cross sectional fraction of each component to be established in order to calculate the individual component mass flow rates and total mixture mass flow rate as illustrated in Figure 2-11.

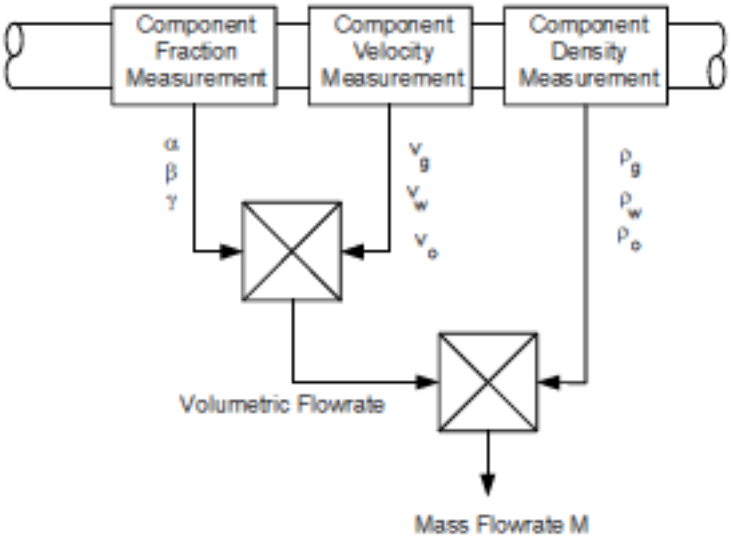

Figure 2-11 Inferential Method of Multiphase Flow Measurement (Thorn et al, 1997)

As the density of oil, water, and gas is readily available from thermodynamic (PVT) data, the problem is therefore reduced to the measurement of the oil, water and gas

phase velocities and two of the three component fractions, usually the gas fraction and the water cut in order to calculate the total mass flow.

Eqn. 2.19

where ρ_g, ρ_w and ρ_o are the densities of the gas, water, and oil fractions. It is assumed that the sum of the component fractions equals unity.

There are currently three main techniques employ in multiphase flow measurement and are categorised as: partial separation of the phases and the measurement of individual phase flow rates using conventional single-phase techniques; flow homogenization and the measurement of composition and velocity averaged over the pipe cross section; and measurement of phase fraction and flow rates in the natural state by non-intrusive methods.

2.2.2 Multiphase Metering Strategies

The following sections discuss the most common techniques that are been applied to measure phase fractions and phase velocities.

2.2.2.1 Phase Fraction Measurements

2.2.2.1.1 Gamma Radiation Attenuation

The measurement of phase fractions in multiphase flows using γ-ray attenuation was first suggested by Abouelwafa and Kendall (1980), and the technique has been used in many current commercial multiphase metering systems (Blaney and Yeung, 2008). Gamma-densitometry exploits the fact that gamma beams are attenuated as they pass through matter owning to interaction of their photons with the matter. The degree of attenuation experienced by the gamma beam is a function of the gamma-beam's energy and the density of the absorbing matter (Blaney and Yeung, 2007). Flow regime dependence and measurement discontinuity over the full component fraction range are the main limitations of gamma ray attenuation methods.

Single Energy Gamma-Ray Attenuation

When a single gamma ray attenuation device is used, the objective is to determine the mixture density which is then used in computing the total multiphase flow rate

(Sanderson, 2008). A collimated gamma ray is directed at the pipe with a sensor placed directly opposite the source on the other side of the pipe, as shown in Figure 2-12. The intensity of the gamma beam decays exponentially as it passes through matter. A gamma ray will be attenuated differently by materials according to their density, a more dense material attenuating the electromagnetic radiation to a greater extent than a less dense material.

The average mixture density is determined by the densitometer and correlated with the densities of the liquid and gas by the following expression:

Eqn. 2.20

where K is gas and liquid velocity ratio.

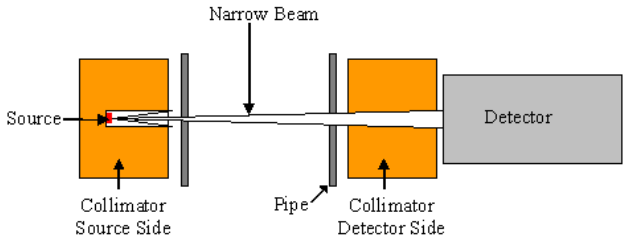

Figure 2-12 Gamma Radiation Method for Component Fraction Measurement

Dual Energy Gamma Ray Attenuation

When two energy levels of the gamma rays are used, the main objective is to determine the volumetric fractions of oil, water and gas. The atomic attenuation coefficients depend not only on the atomic number (hence its density) of a material but also the energy of the gamma beam itself. In a two beam configuration, two equations will be obtained, one for each of the gamma beam energy, giving rise to two of the three equations needed to determine the volumetric phase fractions. The third equation is derived from the fact that the sum of the phase fractions will be equal to unity.

Eqn. 2.21

Eqn.2.22

Where D is the inside diameter of pipe, μ_x is the attenuation coefficient of component x, α_x is the volumetric fraction of component x, I_0 is the intensity of radiation when the pipe is empty pipe, I is the intensity of radiation measured with fluid in pipe and x can be either gas, water or oil.

2.2.2.1.2 Electric Impedance Methods (Capacitance and Conductance)

The basic principle of the electrical impedance methods for component fraction measurements is that the multiphase fluid is characterised as an electrical conductor. Contacting or non-contacting electrodes are used to quantify the electrical impedance across the diameter of the pipe which enables the capacitance or conductance of the fluid mixture to be determined. From the frequency of the input signal one can tell if the measurement is in the impedance or the capacitance mode. If the electrical impedance (Z_e) is measured across two electrodes, the measured resistance (R_e) and capacitance (C_e) can be calculated using these equations:

Eqn.2.23

Eqn.2.24

Where C_p is the capacitance of the electrode-pipe wall, C_m is the capacitance of the multiphase fluid, R_m is the multiphase fluid resistance and ω is the frequency

The resistance and capacitance of the multiphase mixture depends on the conductivity and permittivity of the mixture components, the void fraction, water fraction and flow regime. By installing two electrodes opposite each other on the inner walls within the measurement section, the dielectric constant or permittivity of the mixture can be measured as shown in Figure 2-13. These electrodes will act as a capacitance detector and the resulting capacitance is thus measured. This capacitance will therefore vary when the permittivity changes, i.e. according to the amount of oil, gas, and water in the mixture. Impedance methods are non-intrusive and have almost instantaneous dynamic response.

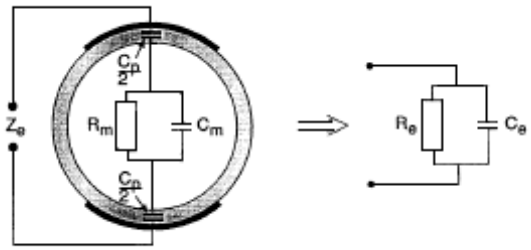

Figure 2-13 Capacitance Method for Component Fraction Measurement

Capacitance measurement technique is suitable for oil continuous systems, i.e. when the water cut is approximately below 60 - 70%. For higher water cuts the flow will normally become water continuous. For these situations the capacitance measurement must be replaced by a conductivity measurement, see Figure 2-14.

The conductivity will typically be measured by injecting a known or controlled electrical current into the flow, and then measure the voltage drop between to electrodes along an insulated section of the pipe. The current can be injected by contact electrodes or in a non-contacting mode by coils (inductive mode). Using the injected current and the measured voltage drop, the resistance (or conductance) is calculated from Ohm's law. The measured resistance can be converted into a conductivity measurement because the distance between the detector electrodes is known.

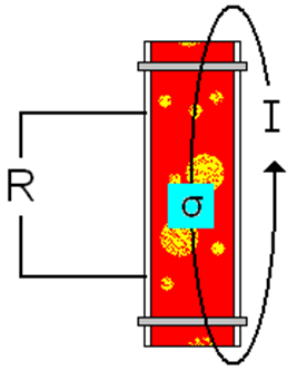

Figure 2-14 Conductance Method for Component Fraction Measurement

Flow regime dependence and measurement discontinuity over the full component fraction range are the main limitations of electrical impedance methods. To

overcome these deficiencies, the flow is homogenised prior to measurement and the electrode designs are modified to reduce bias. Modified electrode designs such as helical (Abouelwafa and Kendal, 1979) and rotating fields (Merilo *et al*, 1977) have been reported in the literature. These sensor designs ameliorate the metering performance within identified flow regimes. Nevertheless, impedance sensors are still not suitable for use in applications where the flow regime is unknown or unstable.

2.2.2.1.3 Microwave Technique

This technology, though similar to capacitance method, is based on measurement of the permittivity of the flowing mixture at microwave frequencies. Water and oil have distinctly different dielectric constants and conductivities and it is this difference that allows a microwave sensor to determine the water content of a water-oil mixture, Table 2-1. The conductivity of the water shown in the table is that of highly purified water measured at 25˚C

Table 2-1 Conductivity and Dielectric Constants of Gas, Oil and Water

Property	Gas	Oil	Water
Dielectric Constant (-)	0	2	75
Conductivity (μScm^{-1})	1	10^{-6}	10

This is done by measuring the amplitude change and phase change of a microwave signal after it has passed through the flow or by using a resonant cavity technique. A resonant cavity comprises a metal structure which confines an electric field, causing it to reflect back and forth within the cavity. By matching one of the dimensions of the cavity to the wavelength of the electromagnetic radiation, a standing wave is produced. When this cavity is filled with a specific fluid, the resonant frequency of the cavity will shift in direct proportion to the permittivity of the fluid present.

According to Nyfors and Vainikainen (1989), the main microwave sensor operation principles are:

I. **Transmission sensor and measurement on a single frequency:** A probe is use to transmit microwave radiation through the multiphase fluid to another receiving probe. Caution must be exercised to prevent reflections in the pipe/sensor and a guided wave sensor may be deployed to prevent against

this. The microwave-receiving sensor may be configured to output the attenuation of or the phase change in the transmitted microwave radiation.

II. **Transmission sensor and measurement on a varying frequency:** Since water continuous liquid phases create high attenuation on high frequency microwaves, it is advantageous to utilize a varying frequency method where the frequency of the transmitted microwave radiation is a function of the dielectric properties of the fluid. This can be implemented by monitoring the change of phase such that the meter can determine the frequency where the phase change is constant.

III. **Resonator sensor:** In this mode of operation, the dielectric properties of the mixture are measured using the resonant cavity method. The resonant cavity is made up of a metal structure which confines an electric field, causing it to reflect back and forth within the cavity. This causes a standing wave to be produced by matching one of the dimensions of the cavity to the wavelength of the electromagnetic radiation. If this cavity is filled with a different fluid, the resonant frequency of the cavity will shift in direct proportion to the dielectric constant of this particular fluid. From measuring the resonant frequency and peak width, the dielectric properties of the fluid can be determined. The system can be calibrated to give the water cut.

A practical microwave MPFM uses the resonator principle for oil-continuous fluids and the varying frequency transmission principle in water-continuous fluids, utilizing the same probes. One of the limitations of this technique is that the water holdup tends to be underestimated as the water cut approaches the phase inversion point, which may be due to the water-oil velocity slippage. Also changing fluids property will affect the accuracy of this technique.

2.2.2.2 Velocity Measurements

2.2.2.2.1 Positive Displacement Flowmeter

A positive displacement (PD) meter is a type of flow meter that requires the fluid being measured to mechanically displace components in the meter in order for any fluid flow to occur. It measures the volumetric flow rate of a liquid or gas by splitting the flow into known-volume collection and counting them over time. Typically, a PD

meter comprise of a number of chambers which are continuously charged and discharged with the fluid. For each ‘cycle’ of fluid charging-discharging, the rotation is transmitted to a mechanical or electrical counter which reads the total volumetric flow (Tuss *et al*, 1996). With appropriate pressure and temperature compensation, the mass flow rate can be accurately determined. The meters come in several forms, including: reciprocating/oscillating piston, oval gear, nutating disk, rotary vane, and diaphragm.

Positive displacement flow meters are very accurate and have high turndown. They can be used in very viscous, dirty and corrosive fluids and essentially require no straight runs of pipe for fluid flow stream conditioning. They are widely used in water metering and in custody transfer of condensates, crude oils and refined petroleum liquids. The performance of positive displacement meters is affected by entrained gas. The mechanical nature of the equipment renders it liable to jamming, leakage, rotor imbalance, and wear. Also, PD meters are relatively expensive and produce high differential pressure.

2.2.2.2.2 Turbine Flowmeter

The turbine flow meter (also known as axial turbine) translates the mechanical action of a turbine rotating in the liquid flow around an axis into a user-readable rate of flow. It consists of a bladed rotor suspended axially in a pipe section in the direction such that the flow through the pipe causes the rotor to rotate. The speed of rotation of the rotor, which is correlated to flow velocity, is measured by means of magnetic pickups, optical fibres or microwave techniques. For a turbine blade with angle (θ) with respect to the pipe axis, the ideal turbine rotational velocity (ω) is related to the flowing velocity (v) and the rotor radius (r) as expressed in Equation 2.25 (Thorn *et al*, 1997).

$$-$$ Eqn. 2.25

Substituting this equation into the relationship between velocity and volumetric flow, the volumetric flow rate q will be:

$$——$$ Eqn. 2.26

where *K*, the *K*-factor, is used to characterised the meter during calibration. Turbine meters are sensitive to swirl, fluid viscosity and other upstream disturbances.

2.2.2.2.3 Differential Pressure Methods (Venturi and Orifice)

In cases of good homogenization of the multiphase flow, single-phase flow meters such as the Venturi meter can be used to determine the velocity of the multiphase flow. In a Venturi meter the differential pressure across the upstream section and the throat section of the device is measured and can be related to the mass flow rate through the Venturi, Figure 2-15. Given the liquid density (ρ_l) and the gas fraction (α), the differential pressure (ΔP) across the Venturi meter can be used to calculate the liquid flow rate (Q_l) from the following expression (Hammer and Nordtvedt, 1991):

Eqn. 2.27

The Venturi meter is much more predictable and repeatable over a wide range of flow conditions. Furthermore, its smooth flow profile minimises frictional abrasion and frictional losses thereby making it more reliable.

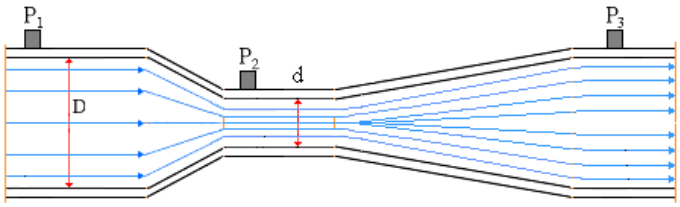

Figure 2-15 Differential Pressure Measurement Systems – Venturi

The orifice plate is the commonest differential pressure flow meter in the industry today. It is typically a flat, metal plate with concentric opening inserted perpendicular to a flow stream as shown in Figure 2-16. Actual flow measurement is achieved by a differential pressure sensor across the orifice. Installing and maintaining it is quite simple and can be interchanged for different flow situations by inserting another plate with different sized opening. However, it causes a complex flow pattern compared with the smooth Venturi flow.

The volumetric flow rate (*Q)* is related to the pressure drop *(ΔP)* across the orifice plate by the following equation derived from the continuity and Bernoulli's equations (Wang, 2008):

Eqn. 2.28

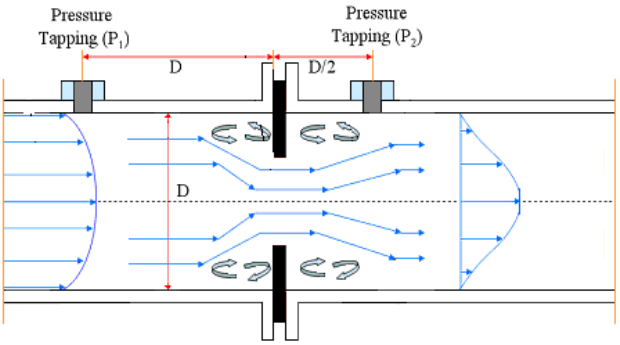

Figure 2-16 Differential Pressure Measurement Systems – Orifice

Eqn. 2.29

where (*C)* is the discharge, (*ε)* is the expansibility factor, and (*β)* is the ratio of the main pipe diameter to the orifice throat diameter.

2.2.2.2.4 Cross Correlation Methods

Determination of phase velocity by cross correlation method is a standard signal processing technique that is frequently used in multiphase flow measurement. Figure 2-17 is an illustration about this technique. Specific properties of the fluid (e.g. density, permittivity or conductivity) are measured by two identical sensors, one located on the downstream of the other separated by a known distance, (*L)*. These sensors will record temporal variations in the measured property and produce output signals (y_0) and (y_1) respectively.

The time delay between these output signals is determined by computing their cross correlation function over a measurement period (*T)*. The cross-correlation function is defined as:

Eqn. 2.30

where $R_{y0y1}(\tau)$ is the value of the cross-correlation function when the upstream output signal (y_1) has been delayed by a time (τ).

The transit time of the flow between the two sensors is found by observing the time lag at which the cross-correlation function is at a maximum (τ_{max}). Thus the velocity (V) of the tracer signal can be found from:

—— Eqn. 2.31

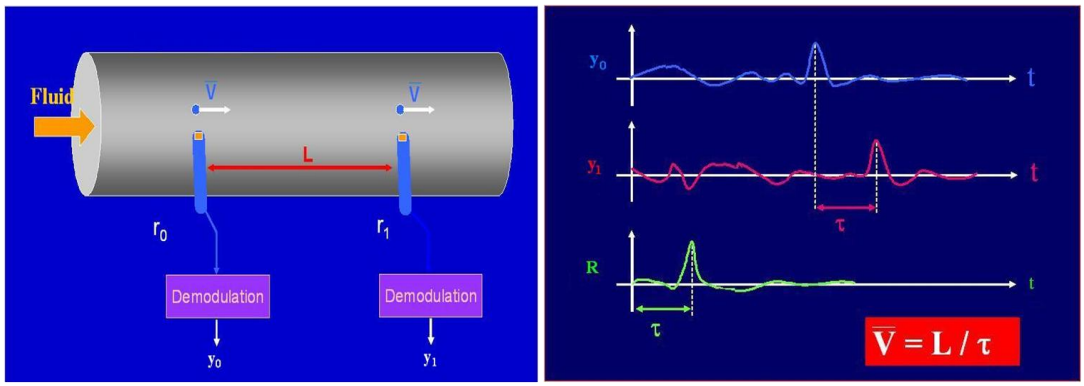

Figure 2-17 Cross Correlation Technique (Shenitech, 2011)

Cross-correlation technique has been successfully implemented utilising a variety of sensors, such as microwave and capacitance. However due to slip effects the velocity measurement could have significant errors. One way of overcoming this error is to homogenise the flow upstream of the sensor by employing in-line mixers (Hewitt *et al*, 1995). Also if transit time of the flow between the two sensors is longer, it will lead to poorer correlation. Furthermore, as the correlation is essentially the square of the signal, so within any volume the largest signal changes, and hence the largest flow structures, dominate the result. Sensors which average across the entire flow cross section give results which are entirely dependent on the flow structure and cannot be reliably interpreted without knowledge of that structure. Thus limiting the range of conditions where this technique can be applied.

2.2.2.3 Electrical Process Tomography

Electrical tomography is a measurement technique for obtaining information about the contents of process vessels and pipelines. Multiple electrodes are arranged

around the boundary of the vessel at fixed locations in such a way that they do not affect the flow or movement of materials. Tomographic measurement techniques differ from point measurement techniques, because they sample a substantial proportion of the process volume rather than at a single point. Circular pipeline-based sensors measure an entire cross-sectional volume (Dyakowski, 1996). The technology can be used for liquid/liquid, solid/ liquid, gas/liquid, and gas/solid/liquid systems. The spatial resolution of the imaging method and the sensitivity of the method depend specifically on the electrical properties of the system being measured and upon the dimensions of the process. Electrical tomography techniques provide the capability for flow visualisation, regardless of material opacity, to enhance the understanding of such complex flow processes.

Many different imaging methods are used in process tomography; however the common ones are Ultrasonic Imaging (UI), Positron Emission Tomography (PET), Electrical Resistance Tomography (ERT), Electrical Impedance Tomography (EIT), Electrical Capacitance Tomography (ECT), and Magnetic Induction Tomography (MIT). In all cases external sensors are used to detect signals from boundary of the object, and the three dimensional material distribution or the velocity field is computed using the measured data. The choice of the process tomographic technique for a given measurement task depends on the physical properties of the fluid to be measured as well as the required time and spatial resolution (Reinecke *et al*, 1998).

Electrical Capacitance Tomography (ECT) is a non-invasive method used to obtain the spatial permittivity distribution within the interior of closed pipes. The principle is based on the measurement of the capacitances between electrodes located on the exterior of the pipe as depicted schematically in Figure 2-18, showing two capacitances (*C*12, 15 and *C*1, 4) as examples (EMT, 2011).

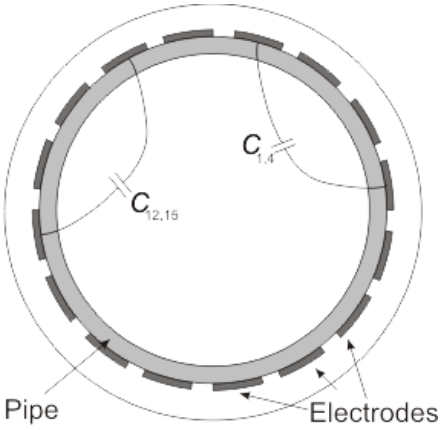

Figure 2-18 Principle of the ECT Measurement System (EMT, 2011)

Since the capacitance depends on the permittivity value of the material located between the electrodes, substances of differing dielectric properties can be distinguished by means of this method (Ismail *et al*, 2005). To obtain a spatially resolved image of the permittivity distribution inside the pipe, multiple electrodes are arranged on the tube and all inter-electrode capacitances are measured. With the application of suitable algorithms the permittivity distribution inside the pipe is determine. This data can then be used to build an image of the pipe contents enclosed by the sensors, based on variations in the permittivity of the material inside the measurement area.

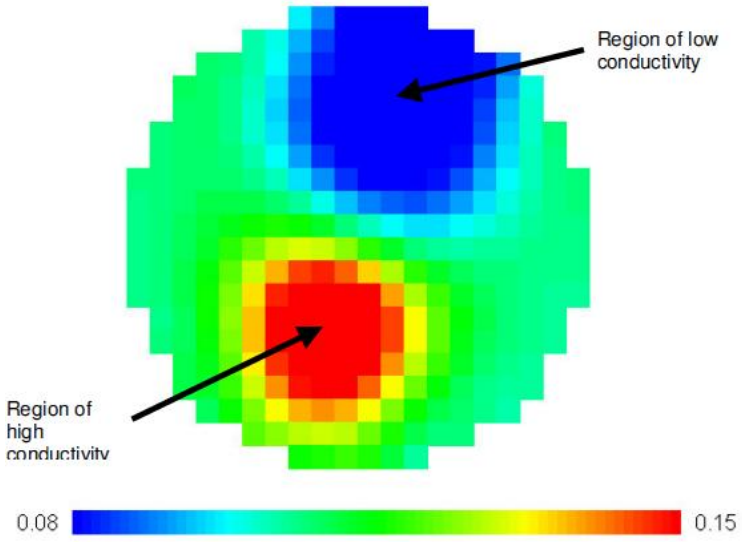

Figure 2-19 Conductivity Tomogram of Oil and Water Mixture showing Regions of High and low Conductivity (ITS, 2000)

Electrical Resistance Tomography, ERT is also a non-intrusive measurement system used for characterization, visualization and control of multiphase fluid flows in conduits. It is similar to ECT, however, it based on measuring the voltage differences between a pair of electrodes when a small amount of current is injected or passed through them. These electrodes make electrical contact with the fluids (electrolytes) contained in the conduits but the contact does not affect fluids flow. Hence, a cross-sectional image of the electrical conductivity distribution of the fluid flow in the conduit is produced and displayed as shown in Figure 2-19. ERT can only be applied to systems where the main continuous phase is at least slightly conductive with other phases with different conductivity values (Dickin and Wang, 1996).

2.2.2.4 Artificial Neural Networks

Application of artificial neural networks (ANNs) to multiphase flow measurement is a recent development in the field. A neural network comprises a large number of simple interconnected processing elements (neurons) operating in parallel and developing their own solutions through exposure to many examples of the correct solution. Training algorithms are used to alter the response of the network so that the output either matches the required pattern (supervised learning) or identifies input pattern clusters (unsupervised learning). The main characteristics of neural networks of particular relevance to the multiphase flow metering problem lies in their ability to represent both linear and non-linear relationships and their capability to learn these relationships directly from the data being modelled (Brown, 2002; and Sheppard and Russell, 1993). Section 2.4 gives a more detailed explanation of neural network and other pattern recognition techniques used in multiphase metering.

2.2.3 A Review of Commercial Multiphase and Water Cut Meters

A review of multiphase and watercut meters that are currently available in the market was undertaken as part of this research work and detailed in **Appendix A** and **Appendix B** respectively. This review consists of information compiled from published papers, sales documentation and vendor's websites, third-party test reports, and personal correspondences with the vendors. Access to details of the research and development undertaken on these measurement technologies was severely limited owing to the reluctance on the part of the manufacturers to divulge

information due to their commercially sensitive nature and trade secrets issues. There are a number of commercially available multiphase flow and water cut meters that are been used in oil and gas operations. These meters employ a diverse range of measurement principles and solutions. Certain types of meters perform better in certain applications than others. Thus, a detailed comparison and selection process is needed to determine the MPFM and watercut meters best suited to a particular application.

2.2.3.1 Commercial MPFMs Metering Systems

As yet there is currently no accepted way of categorising multiphase flow meters in the industry; however they can be grouped in terms of the methods by which the gas and liquid components are handled. The following subsections describe the main categories.

2.2.3.1.1 In-Line Meters

This category of multiphase flow meters is characterised by the fact that they do not involve any separation of the multiphase flow as illustrated in Figure 2-20. Instead, measurement of the phase fractions and phase flow rates are executed directly in the pipeline on the total flow.

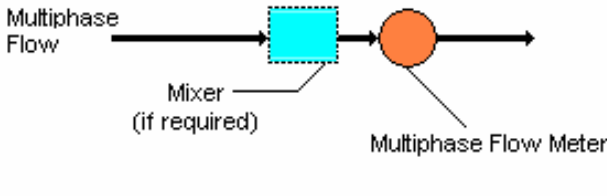

Figure 2-20 Schematic Representation of In-Line MPFM (with/without mixer)

The volume flow rate of each phase of the total flow is determined by calculating the volume fraction of each phase and multiplying these values by the phase velocities. A number of these meters utilise either a mixing operation upstream of the flow meter to homogenise the flow. In-line multiphase flow meters normally apply a combination of two or more of the measuring technologies discussed in previous sections. Examples include Abbon FM, Schlumberger Framo, CCM Meter, ESMER, FlowSys, etc (See Appendix A).

2.2.3.1.2 Complete Separation Meters

These meters are characterised by their separation of the total multiphase flow as schematically depicted in Figure 2-21. This normally entails separating the multiphase stream into gas and liquid streams and then measuring the gas flow rate using a single-phase gas flow meter, corrected to compensate for a tolerated liquid carry-over. The liquid flow rate is then determined using a standard liquid flow rate meter, while the water-cut of the liquid stream is measured using an on-line water fraction meter. Conventional test separators are basically a complete separation MPFM.

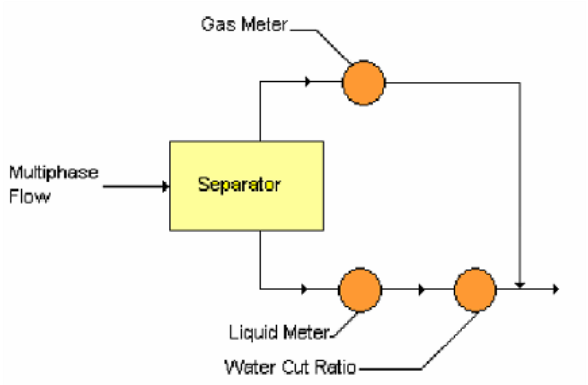

Figure 2-21 Schematic Representation of Complete Separation Meter

2.2.3.1.3 Partial Separation Meters

These meters entail separation of the multiphase flow normally into gas and liquid streams. Essentially the measurements are simplified from one stream of three components to two streams of two components (i.e. a gas stream with small quantity of liquid and a liquid/liquid stream), Figure 2-22. This enables the application of conventional single-phase measurement techniques, with corrections, on the segregated flows. Examples are Agar, Accuflow, REMMS, etc (See Appendix A).

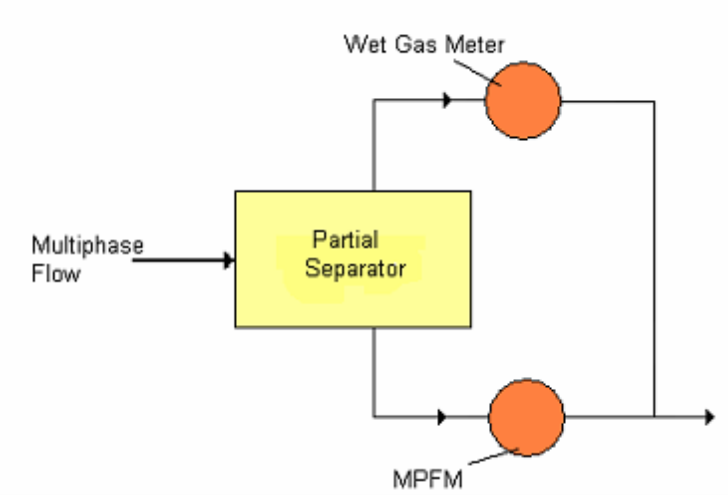

Figure 2-22 Schematic Representation of Partial Separation Meter

2.2.3.1.4 Sample Separation Meters

Though this group of meters carries out separation operation on the multiphase flow, they are characterised by the fact that this separation is not performed on the total multiphase flow as shown in Figure 2-23. Typically, a phase separation is performed on a sample line from the total flow. However, the total flow rate and the gas-liquid ratio must be determined from the total multiphase flow line.

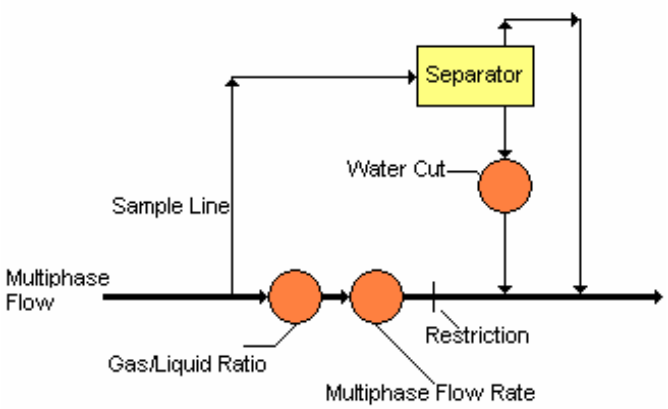

Figure 2-23 Schematic Representation of Sample Separation Meter

2.2.3.1.5 Wet Gas Meters

Wet gas metering encompasses a wide range of measurements due to the specific applications and definition of wet gas. From the perspectives of reservoir engineering, measurement systems, or commercial sales; the definition of wet gas varies depending on which of these areas one is looking at fluids from (Mehdizadeh

et al, 2002). Accordingly, wet gas can be simply defined as gas which contains some liquid. The amount of liquid in a wet gas can vary considerably. Also the quantity and nature of the liquid as well as the flow rate, temperature, and pressure of the stream would have an impact on the selection and accuracy of the measurement system. Below is a system of classification for different wet gas according to Mehdizadeh and Williamson (2004).

The most popular classification of wet gases is that based on the superficial gas and liquid and the Lockhart-Martinelli parameter *(X),* defined as (Mehdizadeh *et al*, 2003):

Eqn. 2.32

The GVF and the liquid to gas ratio (*LGR*) of the multiphase flow stream can be calculated using the following equations:

Eqn. 2.33

Eqn. 2.34

Equations 2.32 – 2.34 are then used to categorize three different regions of wet gas and to calculate the accompanying GVF and LGR in each of these regions. The different classifications of wet gas and their typical areas of application are enumerated in Table 2-2 below. The boundary of these three types of wet gas conditions is dependent on the composition of the liquid fraction, pressure and temperature of the stream, which affects the density of the gas and liquid.

Table 2-2 Wet Gas Types and Typical Areas of Application (Mehdizadeh and Williamson, 2004)

Wet Gas Type	Lockhart-Martinelli Number	Typical Applications
Type 1	≤ 0.025	Typical areas of applications include: production wellheads, unprocessed gas pipelines, allocation points of transfer, separators, and well test facilities.
Type 2	0.025 – 0.03	Typically applied to higher liquid flow ranges at production well head, commingled flow line, or well test application. Users may require increased accuracy in gas and liquid flow rates.
Type 3	≥ 0.03	Commonly applied to gas condensate wells and gas lift wells measurement, these meters must undertake oil, gas and water rate determination at a relatively high GVF (>80%).

Type 1 Wet Gas Meters

Type 1 wet gas meters comprise of single-phase commercial meters that require liquid flow rate so as to compute the gas flow rate. These measurement systems are primarily used for fiscal metering. In these calculations the liquid rate is assumed to be constant over a time period or until new liquid flow rate data updated. The liquid flow rate is determined by such common methods as periodical well tests, tracer injection, pressure-volume-temperature (PVT) predictions, and allocation procedures. For Type 1 wet gas meters, the liquid content of the stream must be corrected for in the gas flow equation so as to avoid any systematic bias error in the gas flow rate. When deploying these measurement systems, due consideration must be given to the selection of flow-metering devices for liquid measurement and their corresponding uncertainty. Table 2-3 lists technologies commonly used in type 1 metering and their corresponding over-reading ranges.

Table 2-3 Type 1 Wet Gas Meters and Gas Rate Over-Reading Data (Mehdizadeh and Williamson, 2004)

Metering Device	Volumetric Over-Reading Range(%) for Lockhart-Martinelli Number ≤ 0.02
Coriolis	0 – 6
Inverted Venturi (V-Cone)	0 – 1.5
Orifice	-1.7 – 2
Turbine	0 – 0.75
Ultrasonic	0 – 10
Venturi	0 – 5
Vortex	0 – 6

Type 2 Wet Gas Meters

These metering systems typically measure the flow stream at the production wellhead, commingled flow line, or during well testing. In some applications direct measurement of produced water in the gas stream can improve process control and reservoir management (Haddelland et al, 2003). Most Type 2 wet gas meters utilize a differential pressure device plus another technique to measure the gas and liquid flow rates. Some systems employ sampling and tracer techniques to determine the liquid flow rate periodically when liquid flow rate remains constant between sampling intervals. These types of wet gas meters are applicable for higher liquid flow ranges where the commercial value of the liquid may be significant.

Type 3 Wet Gas Meters

Metering systems used for Type 3 wet gas are basically multiphase metering systems.

2.2.3.1.6 Other Multiphase Flow Meters

Advanced signal processing systems can estimate the phase fractions and flow rates through analysis of time-varying signals from sensors outputs in multiphase flows. Such sensors are normally acoustic, density fluctuation or pressure monitoring units, although others do exist. The data output from the sensors can then be processed through pattern recognition or statistical signal-processing system. In other cases, process simulation programs combined with techniques for parameter estimation have been developed for the purpose of determining multiphase flow rates. In such systems the temperature and pressure of the flow are measured at the point of

arrival and these are entered into a process simulation software package. Either an upstream or downstream measurement of the temperature and pressure of the flow have to be taken too. Thus, knowing the configuration of the pipe line and the fluid properties, it is possible to develop reasonably accurate estimations of the fluid phase fractions and flow rates.

2.2.4 Multiphase Meters Performance

The performance of MPFMs is a key element in the assessment of whether multiphase flow measurement technologies can be applied to a specific application, and it is also a basis for selecting the most suitable technology. Over the years, the technological evolution has been showing a clear advance in the performance of multiphase flow meters. Such progress was achieved basically due to the Joint Industrial Projects (JIP) strategies, which allowed several technologies to be tested under different conditions over the last decade (Da Costa E Silva *et al,* 2003).

A multiphase metering forum comprising of some major oil companies have reviewed their multiphase metering needs and identified common range and accuracy requirements. The review clearly showed that there is a widespread need for systems that provide adequate oil, water and gas measurements at gas volume fractions (GVF) between 50% and 99% and at the same time handling high volumetric throughputs (exceeding 60,000 m^3/day in some cases). The determination of water cut in a range from zero to above 90% is also needed in many applications (Slijkerman *et al*, 1995). It was also suggested that for petroleum and reservoir engineering needs, meter's accuracy of 5% to 10% error (relative to the individual phases) for both the total liquid flow rate and gas flow rate, and no more than 2% absolute error in water cut is appropriate. Performance specification is not limited to measuring ranges and measurement uncertainties, but also includes other equally important features/properties namely; rated operating conditions, limiting conditions, component performances (performance of primary measurement devices like pressure and temperature transmitters, etc), sensitivities, influence factors, stability and repeatability. Mechanically, MPFMs should ideally be non-intrusive in order to avoid sensor erosion and pressure drop.

2.3 Application of Gamma Radiation to Multiphase Metering

In this context, radiation is defined as the transport of energy emitted from the nucleus or the electron shell of an atom by electromagnetic waves or atomic particles. There are two types of radiation, ionizing and non-ionizing. Ionizing radiation is radiation that has sufficient energy to remove orbital electrons from atoms, leading to the formation of ions. Radioactive decay or disintegration is a spontaneous change within the nucleus of an atom that results in the emission of particles and electromagnetic radiation. It is a process in which unstable atoms stabilises by emitting radiation. There are a number of ways by which a radioactive atom can decay. These are by the emission of Alpha particles *(α)*, Beta particles *(β)* and Gamma rays *(γ)*.

A gamma ray is a packet (or photon) of electromagnetic radiation emitted from the nucleus during radioactive decay and occasionally accompanying the emission of an alpha or beta particle. Gamma rays are identical in nature to other electromagnetic radiations such as light or microwaves but are of much higher energy and have no mass or charge as illustrated in Figure 2-24. Examples of gamma emitters are cobalt-60, zinc-65, cesium-137, and radium-226.

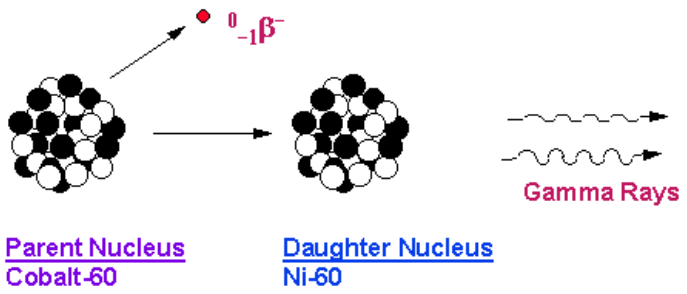

Figure 2-24 Schematic Representation of Gamma Ray Radiation

2.3.1 Interaction Processes

The interaction of ionising radiation with matter is the foundation of every nuclear measurement principle. An energetic photon may travel a long distance in a material without being affected at all, but its history is terminated once it interacts. Gamma photons interact catastrophically with matter by a number of competing mechanisms.

This interaction can be with the entire atom, or with an electron or with the atomic nucleus.

The probability for each of these competing independent processes can be expressed as a collision cross section per atom, per electron, or per nucleus in the absorber. The sum of these collision cross sections, normalized to a per atom basis, is then the probability that the incident photon will have an interaction of some kind while passing through a very thin absorber which contains one atom per cm^2 of area normal to the path of the incident photon (Prepost, 2001). Figure 2-25 shows the linear attenuation of solid sodium iodide (NaI), a common material used in gamma-ray detectors. It demonstrates the different interaction probabilities in relation to radiation energy. From the plot, it is evident that the photoelectric effect dominates at low energies and high atomic numbers; Compton scattering dominates at intermediate energies and low atomic numbers whereas pair production is dominant at high radiation energies and high atomic numbers.

2.3.1.1 Photoelectric Effect

A gamma ray may interact with a bound atomic electron in such a way that it loses all of its energy and ceases to exist as a gamma ray as illustrated in Figure 2-26. Some of the gamma-ray energy is used to overcome the electron binding energy, and most of the remainder is transferred to the freed electron as kinetic energy. A very small amount of recoil energy remains with the atom to conserve momentum. This is called photoelectric absorption because it is the gamma-ray analog of the process discovered by Hertz in 1887 whereby photons of visible light liberate electrons from a metal surface (Knoll, 1979). Photoelectric absorption is important for gamma-ray detection because the gamma ray gives up all its energy, and the resulting pulse falls in the full-energy peak.

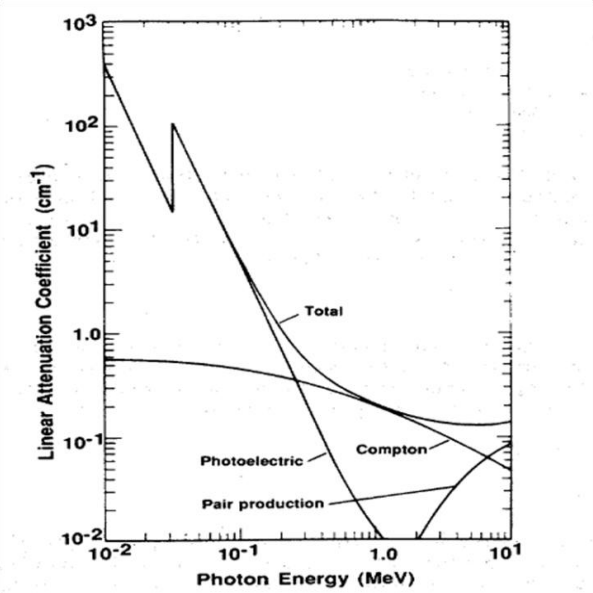

Figure 2-25 Linear Attenuation Coefficient of NaI showing Contributions from Photoelectric Absorption, Compton Scattering, and Pair Production

The probability of photoelectric absorption depends on the gamma-ray energy, the electron binding energy, and the atomic number of the atom. The probability is greater the more tightly bound the electron; therefore, K electrons are most affected (over 80% of the interactions involve K electrons), provided the gamma-ray energy exceeds the K-electron binding energy.

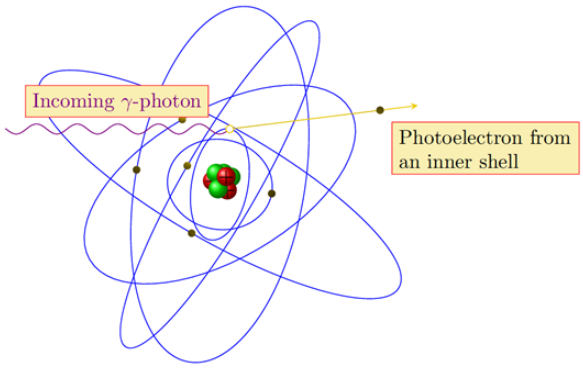

Figure 2-26 Photoelectric Effect

The photoelectric interaction probability cross-section is a function of the absorbing material's atomic number *(Z)* and the incident photon's energy *(E):*

— Eqn. 2.35

where x and y are slowly varying functions of Z and E respectively. This proportionality is only approximate because the exponent of Z varies in the range 4.0 to 4.8. As the gamma-ray energy decreases, the probability of photoelectric absorption increases rapidly (see Figure 2-25). Photoelectric absorption is the predominant interaction for low-energy gamma rays.

The energy of the photoelectron (E_{kin}) released by the interaction is the difference between the gamma-ray energy (E_γ) and the electron binding energy (E_b):

Eqn. 2.36

In most detectors, the photoelectron is stopped quickly in the active volume of the detector, which emits a small output pulse whose amplitude is proportional to the energy deposited by the photoelectron. The electron binding energy is not lost but appears as characteristic x-rays emitted in coincidence with the photoelectron. In most cases, these x-rays are absorbed in the detector in coincidence with the photoelectron and the resulting output pulse is proportional to the total energy of the incident gamma ray.

2.3.1.2 Compton Scattering

Compton scattering is the process whereby a gamma ray interacts with a free or weakly bound electron and transfers part of its energy to the electron as shown in Figure 2-27. Conservation of energy and momentum allows only a partial energy transfer when the electron is not bound tightly enough for the atom to absorb recoil energy. This interaction involves the outer, least tightly bound electrons in the scattering atom. The electron becomes a free electron with kinetic energy equal to the difference of the energy lost by the gamma ray and the electron binding energy. Because the electron binding energy is very small compared to the gamma-ray energy, the kinetic energy of the electron is very nearly equal to the energy lost by the gamma ray according to the expression below:

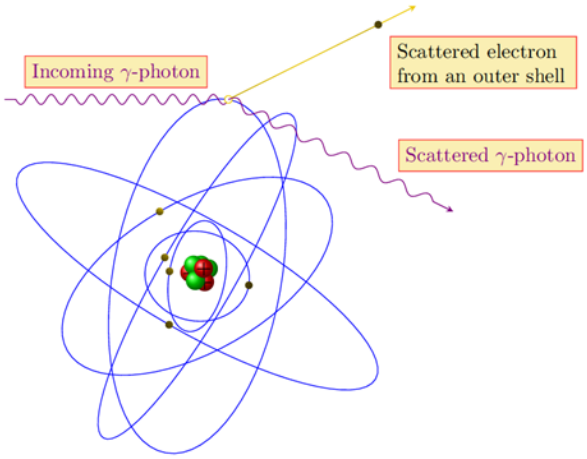

Figure 2-27 Compton Scattering

Eqn. 2.37

where E' = energy of scattered gamma ray. Two particles leave the interaction site, namely, the freed electron and the scattered gamma ray. The directions of the electron and the scattered gamma ray depend on the amount of energy transferred to the electron during the interaction. Equation 2.37 gives the energy of the scattered gamma ray.

Eqn. 2.38

where m_0c^2 is the rest energy of electron, is angle between incident and scattered gamma rays and E_0 is the original photon energy.

When a Compton scattering occurs in a detector, the scattered electron is usually stopped in the detection medium and the detector produces an output pulse that is proportional to the energy lost by the incident gamma ray. Compton scattering in a detector produces a spectrum of output pulses from zero up to the maximum energy. Since Compton scattering involves the least tightly bound electrons, the nucleus has only a minor influence and the probability for interaction is nearly independent of atomic number. The interaction probability depends on the electron density, which is proportional to Z/A and is nearly constant for all materials. The Compton-scattering probability is a slowly varying function of gamma-ray energy (see Figure 2-25). The Compton cross section is a function of the electron density and thus increases linearly with atomic number, Equation 2.39.

Eqn. 2.39

The angular distribution of Compton scattered photons plays an important role in the design of measurement systems. Compton scattering is exploited in some cases for example, in Neftemer multiphase meter, the meter relies on the flowline (which must be metallic) to achieved this interaction process. In other cases it is regarded as an unwanted effect, e.g. in designing shield for high energy gamma rays system.

2.3.1.3 Rayleigh Scattering

Rayleigh scattering is an elastic scattering process between an atomic electron and an incident photon, where the energies of the incident and scattered photons are identical as depicted in Figure 2-28. The photon neither ionises nor excites the atom but interacts coherently with all its atoms. The oscillating transverse electric field of the incident photon induces oscillations at the same frequency in the atomic electrons and the accelerating electric charge emits electromagnetic radiation. This radiation will be of the same frequency and in phase of the original incident photon. Therefore, the electron appears to scatter the incident radiation. The Raleigh scattering cross-section dependence on photon energy and atomic number of the scattering material is defined by the following equation (Blaney, 2008).

—— Eqn. 2.40

Rayleigh scattering is often neglected because its attenuation coefficient is less than those of photoelectric absorption and Compton scattering at low and intermediate energies, respectively.

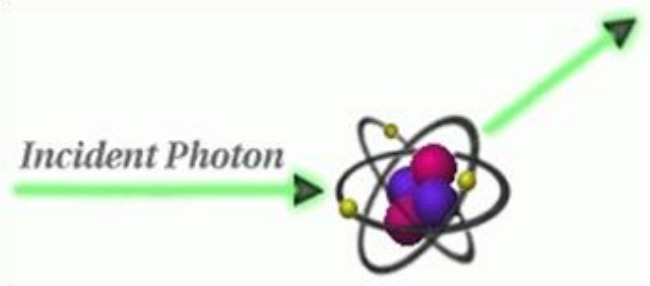

Figure 2-28 Rayleigh Scattering

2.3.1.4 Pair Production

A gamma ray with energy of at least 1.022 MeV can create an electron-positron pair when it is under the influence of the strong electromagnetic field in the vicinity of a nucleus as depicted schematically in Figure 2-29. In this interaction the nucleus receives a very small amount of recoil energy to conserve momentum, but the nucleus is otherwise unchanged and the gamma ray disappears. This interaction has a threshold of 1.022 MeV because that is the minimum energy required to create the electron and positron. If the gamma ray energy exceeds 1.022 MeV, the excess energy is shared between the electron and positron as kinetic energy. Pair production is less important in the context of industrial measurement systems as radiation energy threshold of about 1022 keV is required before it plays any significant role.

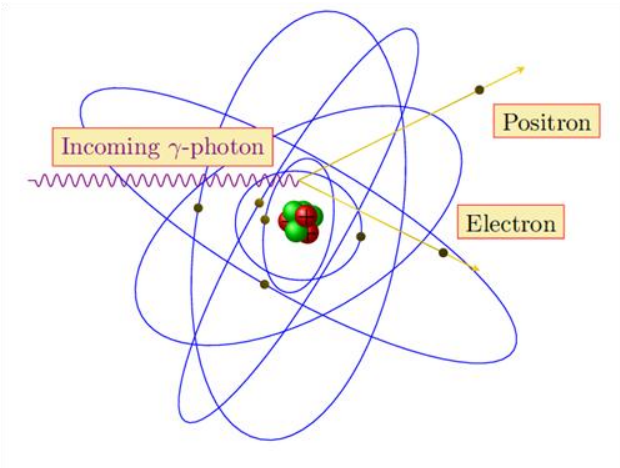

Figure 2-29 Pair Production

The electron and positron from pair production are rapidly slowed down in the absorber. After losing its kinetic energy, the positron combines with an electron in an annihilation process, which releases two gamma rays with energies of 0.511 MeV. These lower energy gamma rays may interact further with the absorbing material or may escape. The kinetic energy of the electron and positron is absorbed in the detector. One or both of the annihilation gamma rays may escape from the detector or they may both be absorbed. The probability of pair production varies approximately as the square of the atomic number Z and and linearly with photon energy (up to 100 MeV).

Eqn. 2.41

2.3.2 Total Mass Attenuation of Gamma

Although attenuation and absorption are used interchangeably for ionising electromagnetic radiation, there is an important difference. Attenuation is removal of photons from the original beam. In other words it expresses the relative number of photons interacting. Absorption, on the other hand, is associated with the energy of the interacting photons.

The four interaction processes described above all contribute to the total mass attenuation coefficient with varying probabilities. The relative importance of these interaction mechanisms depends on the gamma ray energy and the atomic number of the absorber. Thus the total interaction probability is the sum of the individual probability processes:

Eqn. 2.42

To determine the number of photons removed from a beam penetrating an absorber, consider the case of a thin slab of homogeneous material. The attenuation of a narrow and parallel beam of mono-energetic photons penetrating a thin slab of homogeneous material follows the Beer-Lambert's exponential decay law:

Eqn. 2.43

where (I_0) is the incident or initial intensity, (h) is the thickness of the absorber, (I) is the remaining (detected) intensity and (γ) is the linear attenuation coefficient. Figure 2-30 illustrates the exponential attenuation of gamma rays for three different energies levels and shows that the transmission increases with increasing gamma ray energy and decreases with increasing absorber thickness. This attenuation coefficient expresses the photon interaction probability per unit length and it is strongly dependent on radiation energy, density, and atomic number of the absorber.

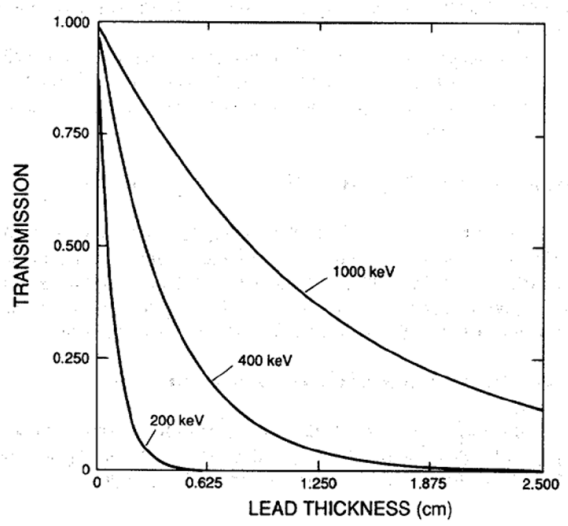

Figure 2-30 Transmission of Gamma Rays through Lead Absorber (Evans, 1955)

Sometimes the attenuation properties of gamma are quoted in terms of mean free path or half-thickness. The mean free path (*λ)* is defined as the average distance a photon travels in an absorber before it undergoes an interaction, Equation 2.44:

– Eqn. 2.44

The half-thickness *(h/2)* is defined as the average thickness in an absorber required to attenuate the beam to half its initial intensity. The mean free path and the half-thickness are given as reciprocals of the linear attenuation coefficient with dimensions in centimetres.

The linear attenuation coefficients of water and kerosene over the same energy range reveals that the differences in the photon absorption may be used to distinguish the two materials (Li *et al*, 2005). Figure 2-31 shows that the photon attenuation in water is greater than that in oil. This is because oxygen has a higher atomic number than carbon, and also because water (ρ=1.00 g/cm^3) has higher density than most mineral oils (typically ρ=0.80~0.90 g/cm^3).

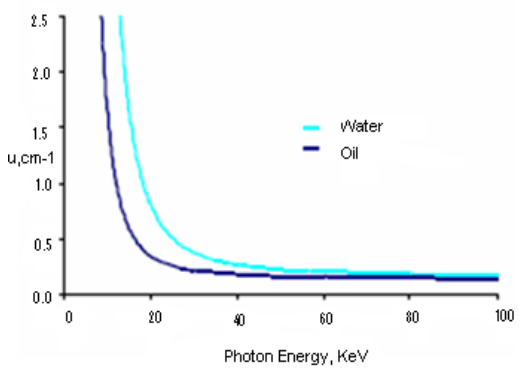

Figure 2-31 Linear Attenuation Coefficients of Oil and Water

2.3.2.1 Two-Phase Systems (Gas-Water)

In two phase multiphase flows, such as oil-water mixtures, in which the components have sufficiently different densities, gamma densitometer can be used to measure the volume fractions of the components. For an empty pipe, the intensity of the transmitted photons at the detector for a given energy level is determined by the following expression:

Eqn. 2.45

where *(I_a)* is the transmitted photons detected, (I_0) is the intensity of transmitted mono-energetic photons reaching the detector assuming the presence of a vacuum within the pipe and (*D*) is the pipe internal diameter. As a result of the relative low density of air, the attenuation experienced by the gamma ray will be low and I_a will be very close to I_0, making the linear attenuation coefficient for air to be very small (nearly zero), regardless of the photon energy. Consequently, the air calibration value (I_a), obtained when the pipe is completely empty, represents the maximum count of transmitted photons reaching the detector for air-water mixtures.

Likewise, when the pipe is full of a liquid, the intensity of the transmitted photons will be:

Eqn. 2.46

where (I_L) is the calibration value when the pipe is full of the liquid. On account of the higher liquid density, and corresponding higher degree of attenuation, I_L will be much smaller than I_a. The attenuation of the photons in the liquid also depends on the

energy of the incident photons, with lower energy photons experiencing a much greater degree of attenuation. The calibration value for a pipe full of water (I_w) represents the minimum count of transmitted photons reaching the detector and is obtained when the is pipe full of water.

With both components present and the measurement section of the pipe is full, then the measured intensity I is given by the following expression:

Eqn. 2.47

where $D = h_a + h_L$. The gas and liquid component fraction is found by measuring the average effective linear attenuation coefficient in the measurement section over the cross-section of the pipe by combining Equations 2.45 - 2.47 to give:

Eqn. 2.48

Therefore the void fraction (α) and the liquid hold-up (ε) are determined by using the detected intensity as given below:

Eqn. 2.49

Equation 2.48 has some deficiencies when applied to describe the correlation between the loss of radiation intensity in a measurement section and its void fraction as it does not take into account the circular geometry of the pipe, the existing flow pattern and phase slip (Åbro and Johansen, 1999).

2.3.2.2 Three-Phase Systems (Gas-Oil-Water)

For three phase flow systems as illustrated in Figure 2-32, the component fraction measurement can be resolved by a second gamma ray source or a source with two different energies (Abouelwafa and Kendall, 1980; Bishop and James, 1993; and Frøystein *et al*, 2005). The intensity of the beam after passing through the measurement section containing gas, oil and water mixtures will be given by:

Eqn. 2.50

For a homogeneous mixture, or a densitometry with narrow beam measurement geometry, the sum of the path length of the gamma ray in gas, oil, and water is equal to the path length within the measurement volume, that is:

Eqn. 2.51

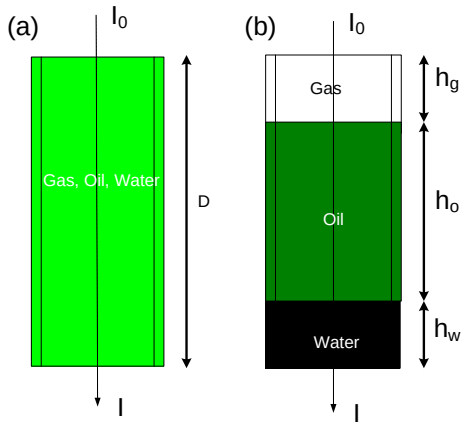

Figure 2-32 Principle of Phase Fraction Measurement: (a) Multiphase – Gas-Oil-Water Mixture; (b) Equivalent Case – Separated Components

For a gamma source with two energy levels, let the detected photon of the low energy be represented by (I_{0L}) and by (I_{0H}) for the high energy. Then the intensity of the beam for the low energy level after passing the three phase system will be:

Eqn. 2.52

Similarly, for the higher energy level the transmitted photon intensity is given by:

Eqn. 2.53

where $\gamma_{gL,}$ $\gamma_{gH,}$ $\gamma_{oL,}$ $\gamma_{oH,}$ γ_{wL}, and γ_{wH} are the linear attenuation coefficients at low energy and high energy levels for gas, water and oil, respectively. The attenuation coefficients may also be express as:

Eqn. 2.54

The linear attenuation coefficients of the components are derived from the calibration measurements of the following intensities:

- I_{gL} for low energy and I_{gH} for high energy level with gas-filled pipe.
- I_{oL} for low energy and I_{oH} for high energy level with oil-filled pipe.
- I_{wL} for low energy and I_{wH} for high energy level with water-filled pipe.

Mathematically,

– — Eqn. 2.55

– — Eqn. 2.56

– — Eqn. 2.57

– — Eqn. 2.58

– — Eqn. 2.59

– — Eqn. 2.60

where where γ_{gL}, γ_{gH}, γ_{oL}, γ_{oH}, γ_{wL}, and γ_{wH} are the attenuation coefficients at the lower energy level and high energy level when the pipe is filled with gas, oil, and water, respectively. From Figure 2-32, it can be deduced that:

— — — Eqn. 2.61

Eqn. 2.62

if it is assumed that the build-up factor in all cases are approximately equal so that the effects of scattered radiation are cancelled out by calibration and α_g, α_o, and α_w are the respective gas, oil and water volume fractions.

The volume fractions of the components can then be expressed as shown below by combining Equations 2.54 - 2.60 and 2.62 and solving for α_g, α_o, and α_w:

Eqn. 2.63

Eqn. 2.64

Eqn. 2.65

The measurement uncertainty in these component fractions due to the statistical errors in the measurement is given as (Rebgetz et al, 1991):

Eqn. 2.66

expressed for one standard deviation for the oil volume fraction. Similarly gas and water fraction uncertainties can be determined.

2.3.3 Gamma Radiation Detection

In nuclear measurement systems, the sensing element is commonly referred to as the radiation detector. In its simplest form, a radiation detector is a device that converts radiation energy into an electronic signal. A variety of methods are available to detect gamma rays, including gas-filled counters, solid-state detectors and

scintillation detectors. However, most commercial multiphase flow meters that employs nucleonic source as part of their measurement system utilizes scintillation detectors made of, for example, inorganic scintillation materials such as crystals of NaI, ZnS, CsI or BaF.

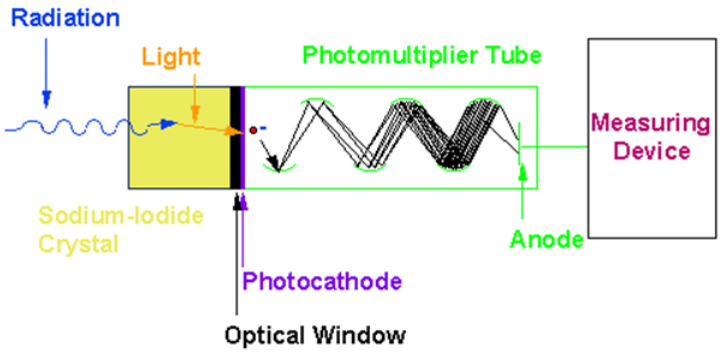

Figure 2-33 Radiation Detection – Scintillation Sensing

Scintillation sensing detectors generates rapid flashes of light when ionised and exited absorber atoms returns to ground state (i.e. de-excite). This scintillation light is in turn directed towards a photodetector where it is detected and converted into an electric charge signal as illustrated in Figure 2-33. The amplitude of this output signal is proportional to the energy deposited in the detector for most detector systems.

The densitometer employed in this research study uses Caesium-137 (, Cs-137), a radioactive isotope of caesium as its gamma source. The Cs^{137} emits an electron *(β)* and a neutrino thus increasing the nuclear charge from 55 to 56 by changing a neutron to a proton:

$$Cs^{137} \rightarrow Ba^{137} + e^{-} + v_e$$

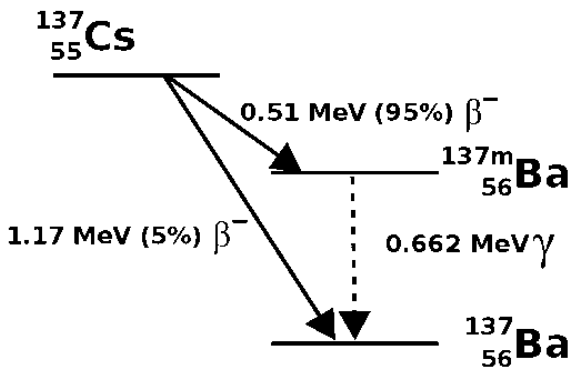

Figure 2-34 Caesium-137 Decay

As shown in Figure 2-34, 95% of the decays result in only 0.51MeV being transferred to the electron and neutrino, leaving the Barium-137 in a metastable, excited state. This will further decay by either emitting a 662 keV gamma (95%) or by 'internally converting' the gamma before it leaves the Barium atom and ejecting a K-shell electron instead. A typical spectrum acquired with a NaI scintillator detector exposed to 662 keV gamma rays and 32 keV characteristic X-rays is shown in Figure 2.30.

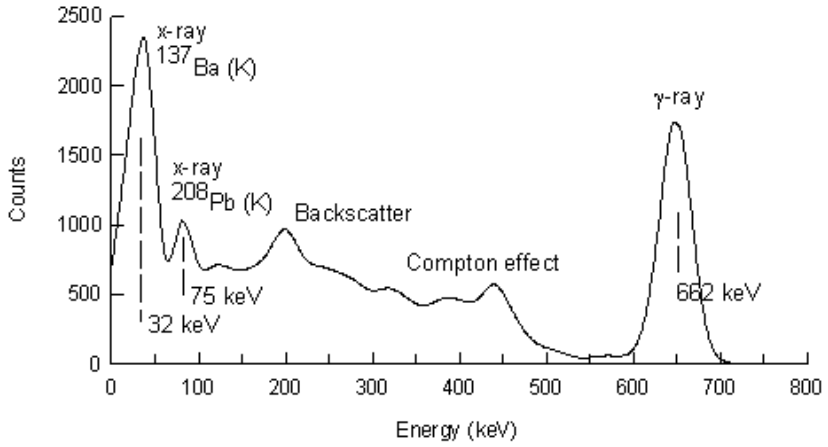

Figure 2.30 Caesium-137 Spectrum

2.3.4 Gamma-Based Techniques in Multiphase Measurement

Employing gamma densitometry for multiphase flow analysis has been documented by a number of researchers (Blaney and Yeung, 2008). Early research works were on component ratio determination in two phase systems and the development of radiation detector units. Mareuge (2000) and Chan and Banarjee (1981) carried out a detail review of gamma attenuation measurement system design and implementation for multiphase flow hold-up measurement.

Jiang and Rezkallah (1993) conducted experiments on void fraction measurements in upward and downward two-phase gas-liquid flow in a vertical tube of 9.525mm (ID) using a single beam gamma densitometer system comprising a caesium-137 (662 keV) source and a sodium iodide (NaI) detector crystal. Measurement error to within ±5% was obtained when compared with reference values from a quick closing valve system. They also found that pipe diameter had no significant influence on the accuracy of the gamma attenuation based void fraction measurement.

Abouelwafa and Kendall (1980) were the first to carry the measurement of component ratios in three phase flow using multi-beam gamma ray attenuation techniques. Using a cobalt-57 (122 keV) and a barium-133 (365 keV) radioisotope with a lithium-drifted germanium based detector, they performed several experiments with static mixtures of oil, water and gas in a 0.1 m diameter pipe section. Gas fraction measurements were detected to within ±1% while oil and water fractions to within ±10%.

In the work of Li *et al* (2005), the concentration of the different components of oil-water-gas multiphase flow was investigated. They used a gamma densitometer system which comprises two radioactive isotopes, amerceium-241 (59.5 keV) and caesium-137 (662 keV); a sodium iodide detector crystal; and a Plexiglas vessel (100mm × 100mm × 600mm). They found that small errors in the intensity measurements may magnify into large errors due to the fact that the linear attenuation coefficients of oil (used for this experiment) and water is too close. To this end, modification algorithm was developed and on application, all phase fraction results have reasonable accuracy maximum error of not more than ±6% of their true values.

Scheers and Slijkerman (1996) reported the results of a multiple energy gamma ray absorption composition measurement system for resolving the oil, water and gas phase fractions and the water salinity. In this study, the gamma measurement system was intrusive with an americium-241 gamma source installed in the centre of 101.8mm pipe with a set of concentric carbon reinforced epoxy cylinders as window material. They reported that measurement uncertainty in phase fractions are in the order of ±2%, when the meter was operated in a standard dual energy mode. With the addition of a third energy level, the calculated phase fractions and water salinity were described as having an ‘acceptable accuracy’ but where not quantified.

Åbro and Johansen (1999) documented the results of a multi-beam low-energy gamma-ray configuration for void fraction measurement. The performance of this multi-beam system was also compared to that of a single-beam. Their setup comprises of an americium-241 (59.5 keV) gamma source, a single CdZnTe semiconductor detector and a pipe of 80mm (ID) and 90mm (OD). Using phantoms of polypropylene, series of static measurement were performed. The detector

responses at several positions around the pipe were obtained for different flow regimes and void fractions. The multi-beam system measurements were within ±10% when measurements of four detector positions around the pipe were combined. They also reported that the system was less sensitive to flow regime than the conventional single beam technique.

The work undertaken by Tjugum *et al* (2002a) is a follow up to that undertaken by Åbro and Johansen. The instrument consists of americium-241 (59.5 keV) source and three detectors, all collimated and embedded in the pipe wall. Two of the detectors measure transmitted radiation across the pipe flow, and the third one measured scattered radiation at a 90° angle. They found that the multi-beam design with three detectors gave more accurate results than the conventional single beam. Also they were able to collect data on the flow regime and salinity as a result of the multi-beam geometry and dual modality of the gamma system.

Tjugum *et al* (2002b) presented a theoretical and experimental work on three phase flow using multi-beam gamma-ray densitometry. They used a fan-collimated americium-241 (59.5 keV) source and a row of nine CdZnTe semiconductor radiation detectors placed on the other side of a 50.8mm pipe. A series of oil, water and gas flow combinations were experimented for three different angles of inclination of the pipe (0°, 45° and 90°). They reported that flow homogeneity increases with increasing inclination and flow rates. Also GVF measurements on non-homogeneous flow were better when compared with those obtained using a conventional single beam configuration, typically to within ±10%. However, there were deviations at high GVF and at separated flows. This deviation was attributed to the effect of slip and backflow.

Stahl and von Rohr (2004) formulated a dimensionless relation that gives the accuracy of void fractions measurements as a function of pipe radius and the attenuation coefficient of the liquid phase. Using a single-beam gamma densitometer which comprises of an iodine-125 (35.5 keV) source and a NaI scintillator detector crystal, they conducted several experiments with air-water flows in a 21mm diameter pipe. They reported that the linear approximation for void fraction calculation is more suitable for flow patterns whose interfaces are mainly oriented parallel to the radiation beam, while profiles with perpendicular interfaces or disperse flow patterns

will yield more accurate results if the logarithmic approximation is used. A maximum accuracy in the void fraction calculation using both approximations was defined as $\Delta\varepsilon \leq 0.21\gamma_L R$ (where γ_L is the liquid attenuation coefficient and R is the pipe internal diameter).

Frøystein *et al* (2005) published results on a dual-gamma tomography system for HTHP multiphase flows. Their setup comprises of a barium-133 (31 keV and 81 keV) source along with a CdZnTe detector and a digital spectrum analyser. Limited static experiments were performed using different fluid configurations. Gamma attenuation for different chordal positions of the pipe cross-section was monitored. The tomography system was able to reconstruct different fluid zones for different flow regimes. Though, for some configurations where different fluid mixtures having similar attenuation coefficient values were located next to each other, the system encountered difficulties in discerning between regions.

Rodriguez and Oliemans (2006) documented the results of oil–water two-phase flow experiments conducted in a 15 m long, 82.8mm diameter, inclinable steel pipe. Steady-state data on flow patterns, two-phase pressure gradient and holdup were obtained over the entire range of flow rates for pipe inclinations of -5°, -2°, -1.5°, 0°, 1°, 2° and 5° with two gamma-ray densitometers (consisting of caesium-137 (662 keV) source and a sodium iodide (NaI) detector crystal) to measure the in-situ volumetric fraction (holdup) of each phase. Their experimental data when compared with results of a flow pattern dependent prediction model, which uses the area-averaged steady-state two-fluid model for stratified flow and the homogeneous model for dispersed flow, reported a maximum accuracy of 10% for low oil/water holdups and 1% for other test points.

More recently, Kumara *et al* (2010) presented the results of a single-beam gamma densitometer to investigate oil-water flow in horizontal and slightly inclined pipes. They performed experiments in a 15m long, 56mm diameter, inclinable stainless steel pipe the (range from 5° upward to 5° downward) using a gamma densitometer with radioactive isotope of Am-241 (59.5 keV) as the source and a NaI(Tl) scintillation detector. They reported that the measured water hold-up and slip ratio profiles are strongly dependent on pipe inclination, i.e., higher water hold-up values are observed in upwardly inclined pipes compared to the horizontal and downwardly

inclined pipes and that there is a marginal difference in frictional pressure drop values for horizontal and downwardly inclined flow.

2.4 Pattern Recognition Techniques in Multiphase Metering

Multiphase flow measurement presents formidable difficulties due to the spatial and temporal inhomogeneities in the flow. Also for transient and intermittent multiphase flows such as slugs, elongated bubble or plug flow, there are added difficulties to the flow measurement. However, responses from instruments do inherently contain all the information they have gathered about the process/plant. In principle, these responses could be used to determine the individual component flow rates if a mapping function relating input to output data is established. Such a metering system can be obtained by the pattern recognition techniques.

“Pattern recognition is the study of how machines can observe the environment, learn to distinguish patterns of interest from their background, and make sound and reasonable decisions about the categories of the patterns” (Jain *et al*, 2000). In terms of Multiphase flow measurement, pattern recognition aims to classify data based on statistical information extracted from the data. The design of a pattern recognition system essentially involves the following four aspects: data acquisition and pre-processing, feature extraction and selection, model determination and model validation. The four best known approaches for pattern recognition are: 1) template matching, 2) statistical classification, 3) syntactic or structural matching, and 4) neural networks. In this study, neural network modelling is employed.

2.4.1 Signal Processing

Signal processing deals with the design, analysis and implementation of systems that extract information of interest from available data. In other words, it is an operation which modifies, analyse or manipulate the information contained in a signal. It is a branch of electrical engineering and applied mathematics that deals with operations on or analysis of signals, in either discrete or continuous time, to perform useful operations on those signals. Signals are analogue or digital electrical representations of time-varying or spatial-varying physical quantities. Advances in digital technology and information theory has stimulated the development of

sophisticated signal processing techniques that are being used in different applications such as speech recognition, audio signal processing, seismic exploration, digital communications, and analysis and control of industrial processes (Jama, 2004).

In signal processing, data is first collected from a sensor. This data is usually in the form of varying voltage waveform (analogue) which is then converted to a digital format with an analogue to digital converter to make it suitable for further mathematical signal processing techniques on a computer system. Sampling is a technique use in digitising analogue signals and it is executed in two stages namely; discretisation and quantisation. In discretisation, the space of a signal is partitioned into a series of equivalent classes then the quantisation process allocates approximated representative signal values to the each of the partitions from a set of finite values.

A fundamental theorem of signal processing states that a signal can only be constructed accurately from a sampled version if it does not contain components, whose frequency is greater than half the frequency at which the sampling takes place (Oppenheim *et al*, 1997). Thus the sampling frequency (f_s) can be expressed as:

Eqn. 2.67

where f_N is the Nyquist frequency defined as the highest frequency below which meaningful information from a set of data can be obtained. Failure to adhere to the condition set out in the above theorem results in the reconstructed waveform effectively contributing only noise. This phenomenon is known as aliasing, as the high frequencies are said to be “under an alias”. A well-known example of this phenomenon is when filming rotating objects such as wheels and aeroplane propellers. The wheel is ‘seen’ to apparently turn at the wrong speed or in the wrong direction. This is because the film samples at a fixed rate, while the wheel can rotate at a range of different speeds.

2.4.2 Components of a Pattern Recognition System

A complete pattern recognition system consists of several components as shown in Figure 2-35. The following sections describe each component in details.

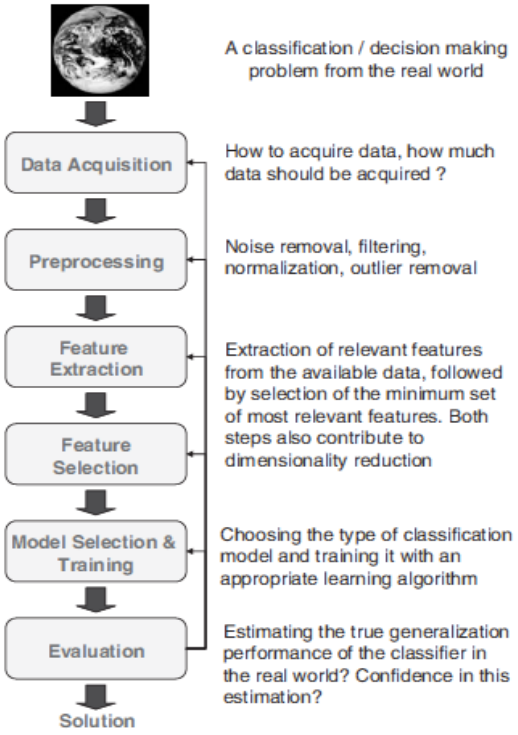

Figure 2-35 Components of a Pattern Recognition System (Polikar, 2006)

2.4.2.1 Data Acquisition

The first step in a pattern recognition system is data gathering via a set of sensors. Adequate and representative training and test data is a key requirement in designing a successful pattern recognition system. There should be adequate amount of data for the model to learn the decision boundary as a functional mapping between the feature vectors and the correct class label. Also the data should contain sufficient level of information concerning the behaviour of the process and that all meaningful variations of this field data that the system is likely to see should be sampled by the training and test data.

2.4.2.2 Preprocessing

Preprocessing involve conditioning the data to remove noises. Different filtering techniques can be employed if the spectrum of the noise is known. Also the data can be normalised with respect to the mean and variance of the features values or with respect to the amplitude of the data. In the former, the data set is normalised such that the normalised data have zero mean and unit variance as expressed below:

Eqn. 2.68

where is the ith feature of the original data set, is its normalised value, is the mean and is the standard deviation of . Whereas in the latter case, the data is simply divided by a constant so that all the features values are within the range of [-1, +1] as shown below:

Eqn. 2.69

where *x* is the feature vector and is its normalised value.

2.4.2.3 Feature Extraction

The performance of the pattern recognition model depends on the interrelationship between input data sizes, number of features, and complexity of the model. Feature extraction is a dimensionality reduction process whereby a small number of features that are particularly distinguishing or informative of the underlying process are mined from the data. The importance of dimensionality reduction in pattern recognition cannot be overstated. A small but informative set of features significantly reduces the complexity of the classification algorithm, the time and memory requirements to run this algorithm, as well as the possibility of overfitting.

Feature extraction is usually obtained from a mathematical transformation (either in a linear or non-linear way) on the data. Some of the most widely used transformations are principal component analysis, factor analysis, and linear discriminant analysis (Jain *et al*, 2000).

2.4.2.4 Feature Selection

Feature selection, which is a special case of feature extraction means the selection of *m* features that provide the most discriminatory information, out of a possible *d* features, where m d. In other words, feature selection entails selecting a subset of features from a set of features that have already been identified by a preceding feature extraction algorithm. Effective feature selection can be difficult as it necessitates the selection of a feature set that will distinguish between different data class volumes and there are an infinite number of features and feature combinations from which to select (Joshi and Joshi, 2007). If too many features are used in the classification, there is a risk that the pattern recognition model gets too complex, and the generalisation capability of the model may then be poor. Therefore it is most useful to reduce the number of original data points to a few sets of features that can represent the system.

According to Polikar (2006) a criterion function is used to assess the discriminatory performance of the features, and a common choice for this function is the performance of a subsequent classifier trained on the given set of features. Generally speaking, only an exhaustive search can guarantee an optimal solution, but this is prohibitively expensive (in terms of computation) even for a relatively small number of features. However search algorithm exists that gives a near optimal solution. They include, branch and bound algorithm, sequential forward and backward selection, sequential forward floating selection, fuzzy set theory and neural networks (Verikas and Bacauskiene, 2002).

2.4.2.5 Model Selection and Training

The classifier is constructed by means of a mathematical model which can be based on one of the following approaches namely; statistical, structural, adaptive, fuzzy, artificial intelligent and neural techniques (Cai, 1995). The classification can be thought of as a function approximation problem, that is, find a function that maps an n-dimensional input to appropriately encoded class information. Once the classification is cast as a function approximation problem, a variety of mathematical tools as enumerated above can be used. Though most common pattern recognition algorithms are categorized as statistical and neural network approaches, there is a

certain amount of overlap between them and it has been shown that they are closely related and with a one-to-one match between certain statistical approaches and their corresponding neural network equivalents established.

2.4.3 Artificial Neural Networks

Artificial Neural Network is an information processing concept that mimics the decision-making ability of the brain. Neural networks can also be viewed as massively parallel computing systems consisting of an extremely large number of simple processors with many interconnections (neurones) working in unison that can be configured for a specific application, such as pattern recognition or data classification, through a learning process.

Unlike conventional computing techniques that use a cognitive approach to problem solving, neural networks do not have to be programmed. Instead, a neural network system will learn to classify inputs through a training process in which the network is presented with a series of inputs and target outputs (Blaney and Yeung, 2007). Based on this training data, the neural network will generate a map between the inputs and outputs. Subsequent input data will then be processed using the relationship derived during the training process to produce corresponding output. Thus one can say that neural networks learn from experience. The main characteristics of neural networks are that they have the ability to learn complex nonlinear input-output relationships, use sequential training procedures, and adapt themselves to the data.

There are many classes and sub-classes of neural networks that are widely used in engineering applications but all of these variations stem from McCulloch and Pitts' original model (McCulloch and Pitts, 1943). The most commonly used family of neural networks for pattern classification tasks are the feed-forward network, the recurrent network, the stochastic network and the modular network.

Numerous neural network models have been developed by researchers worldwide with each model having a different network structure, learning algorithm, performance capability and field of application. In terms of training method, there are three major learning paradigms that can be applied to neural network modelling depending on learning task. These are supervised learning, unsupervised learning

and reinforcement learning. In supervised learning, a set of example inputs and targets are presented to the model and trained to determine a function that describes the relationship between the variables. For unsupervised learning models, the network self-organises data presented to it and detects their emergent collective properties and group them into classes that are self-similar. A detailed description of the different neural network models can be found in (Bishop, 2008). However, the feedforward multi-layer perceptron network implemented in this research study will be examined.

2.4.3.1 Feedforward Multi-layer Perceptron

Multi-layer perceptrons are feed-forward neural networks with one or more layers of neurons between the input and output layers. They have been used as the basis of the majority of practical application of neural networks. As shown in Figure 2-36, the flow of information in the network begins with the input layer, proceeds through the hidden layers and ends at the output layer.

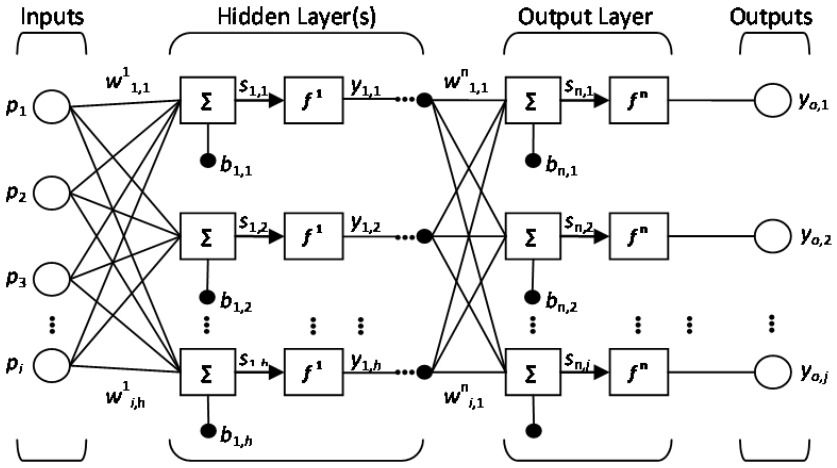

Figure 2-36 The Architecture of a Multi-layer Perceptron (Blaney and Yeung, 2007)

Each input (*p*) is connected to all nodes in the first hidden layer. If there are more than one hidden layers, all outputs from the preceding layer are input to each node in the successive layer. For all nodes, the inputs are first multiplied by their respective weights (*w*), and then summed (*s*) up with subsequent addition of a bias (*b*). The resulting value is used as the input to an activation function (*f*). The first hidden layer

output ($y_{1,h}$) from each processing nodes in the first hidden layer, with *I* inputs parameters, can be expressed by:

Eqn. 2.70

Treating the system as a two-layer system (n=2), the outputs ($y_{o,j}$) can be expressed by:

Eqn. 2.71

Defining the network architecture is a key stage in neural network analysis. For applications where the number of input and output neurons is fixed, the difficulty in defining the network architecture is reduced to the selection of the activation function type(s) and the number of hidden layers and the number of neurons to be employed in the model. There are no rules for the selection of the number of hidden nodes but, generally, the more complex the function one is attempting to model, the greater the number of hidden nodes required. Deciding on the number of hidden nodes is quite tricky because if too many nodes are used the network will memorise the training data thereby displaying poor generalisation, on the other hand, too few hidden nodes will result in a system with insufficient parameters to model the underlying function and severe underfitting will be experienced (Geman *et al*, 1992).

2.4.3.2 Multi-layer Perceptron Training Algorithms

The role of training algorithms is to set the network's weights and thresholds so as to minimize the prediction error made by the network. The network uses historical data gathered to automatically adjust the weights and thresholds in order to minimize this error. This process is equivalent to fitting the model represented by the network to the training data available. All training algorithms use the derivative of the performance function to determine the weight values that will minimise the performance function.

Numerous neural network training algorithms have been published but the best-known ones are the back propagation (with many variations), Levenberg-Marquardt, Quasi-Newton, One-Step Secant, Polak-Ribiere Conjugate Gradient, Fletcher-Powell Conjugate Gradient, Scaled Conjugate Gradient.

2.4.3.2.1 The Backpropagation Algorithm

The backpropagation algorithm is one of the most studied and used algorithms for neural networks learning. The backpropagation algorithm looks for the minimum of the error function in weight space using the method of gradient descent. The combination of weights which minimizes the error function is considered to be a solution of the learning problem. Since this method requires computation of the gradient of the error function at each iteration step, this error function must be a differentiable non-linear function. The error functio to be minimised is the Sum-of-Squared-Error (*SSE*) function:

– Eqn. 2.72

For a specified inputs and outputs, the algorithm starts by calculating the error at the output neurons. This error is the difference between the provided ideal output and the calculated actual output multiplied by the derivative of the activation function on that output point. For the popular sigmoid activation function the derivative is:

Eqn. 2.73

thus;

Eqn. 2.74

Having computed the error for the output layer an error for each neuron in the hidden layers, going backwards, is calculated layer by layer. The error for a neuron in a hidden layer is the sum of the products between the errors of the neurons in the next layer and the weights of the connections to those neurons, multiplied by the derivate of the activation function as expressed below.

Eqn. 2.75

These errors are then used to calculate the variation of the weights as a result of the current input pattern and ideal outputs. The variation (Δ) of a weight is the product of the input neuron output value and the error of the output neuron for that connection.

Eqn. 2.76

This process is repeated for all input patterns and the variations (Δ) are accumulated. At the end of a learning iteration, the actual weights are then changed with the accumulated deltas for all the training patterns multiplied with a learning rate. The MLP neural network weights and biases are then updated accordingly. This process of updating the network weights and biases is repeated iteratively until the sum of squares error function is minimised and this typically involves at least a few hundred iterations in order to learn a set of patterns.

Eqn. 2.77

Eqn. 2.78

2.4.3.3 Preventing Over-fitting

The critical issue in developing a neural network is generalization, that is, how well the network will make predictions for cases that are not in the training data set. Neural networks, like other flexible nonlinear estimation methods such as kernel regression and smoothing splines, can suffer from either underfitting or overfitting. On the one hand, a network that is not sufficiently complex can fail to detect fully the information in a complicated data set, leading to underfitting. On the other hand, a network that is too complex may fit the noise, not just the information, leading to overfitting. Overfitting is especially dangerous because it can easily lead to predictions that are far beyond the range of the training data. It can also produce wild predictions in multilayer perceptrons even with noise-free data.

Given a fixed amount of training data, there are various approaches to avoiding underfitting and overfitting, and hence getting good generalization. These are model selection, jittering, early stopping, weight decay, bayesian learning, and combining networks

2.4.3.3.1 Early Stopping

Early stopping (or cross-validation) is one of the simplest and most widely used means of avoiding overfitting. It involves dividing the data into two sets: a training set and a validation set. During the training process, the training set is used to calculate the network weights and biases and at the same time, the validation set is used to produce a validation error. As the validation data is independent of the training data,

network performance is a good measure of generalization. Also, as long as the network is learning the underlying structure of the data, performance on the validation set will improve with training. Once the network stops learning, performance on the validation set will stop improving, and will typically get worse. Schematic learning curves showing error on the training and validation sets are shown in Figure 2-37. To avoid overfitting, the training is stopped at time *t*, where performance on the validation set is optimal. The weights and biases present at this optimum will be implemented when testing the network. The requirements of independent training, validation and test sets means that early stopping can only be used in a data-rich situation.

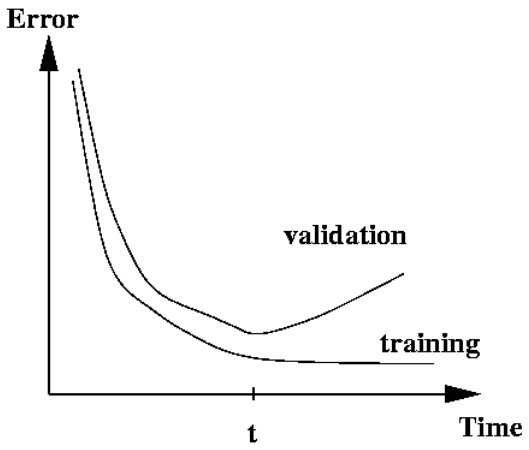

Figure 2-37 A Typical Neural Network Learning Curve

2.4.3.3.2 Bayesian Regularisation

Regularization refers to a set of techniques which help to ensure that the function computed by the network is no more curved than necessary. These approaches offer a tool for control of neural network model complexity as it can be exploited to select the optimal number of neurons in the hidden layer, thus avoiding over-fitting, and offers an alternative approach to error minimisation techniques (Doan and Liong, 2004).

This is achieved by adding a penalty to the error function, giving:

Eqn. 2.79

One possible form of the regularizer comes from the informal observation that an over-fitted mapping with regions of large curvature requires large weights. The large weights are then penalised by choosing:

– Eqn. 2.80

Using this modified error function, the weights are now updated as:

—— —— Eqn. 2.81

where the right hand term causes the weight to decrease as a function of its own size. In the absence of any input, all weights will tend to decrease exponentially, hence this technique is sometimes referred to as "weight decay" (Orr *et al*, 1999).

Bayesian regularisation with the use of Levenberg-Marquardt (LM) algorithm is an alternative approximation technique which is less calculation intensive (Foresee and Hagan, 1997). The LM algorithm is an iterative technique that locates the minimum of a multivariate function that is expressed as the sum of squares of non-linear real-valued functions. It has become a standard technique for non-linear least-squares problems, widely adopted in a broad spectrum of disciplines. LM can be thought of as a combination of steepest descent and the Gauss-Newton method. That is when the current solution is far from the correct one, the algorithm behaves like a steepest descent method: slow, but guaranteed to converge. However when the current solution is close to the correct solution, it becomes a Gauss-Newton method (Lourakis, 2005).

2.4.4 Application of PR Techniques in Multiphase Metering

Pattern recognition techniques are primarily concerned with the description and classification of measurement (data) related to a physical or mental processes. It is one of the techniques employed for multiphase flow measurement and analysis. Pioneering work by Imperial College researchers in developing the ESMER multiphase measurement system is by far the most prominent in this field of study.

Darwich (1989) showed that multiphase flow are reproducible and could be exploited to determine the individual phase flow rates in a air-water two phase flow by the

extraction, classification, and identification of stochastic features from turbulent pressure and void-fraction waveforms. Experiments in a 50.8mm horizontal loop with a spool piece made up of radially mounted pressure transducers and axially mounted capacitance and conductance sensors showed that a set of stochastic features (amplitude and linear prediction coefficients) is uniquely related to the individual phase flow rates. Using template matching, as the pattern recognition method, individual phase flow rates were predicted by identifying the best match to the measured feature vector from a calibration data base. Measurement accuracy was within ±10% with a confidence level of 90% was reported for each of the individual phase flow rates.

The work of Toral *et al* (1990) is an extension of Darwich's. They introduced an orifice plate to the horizontal spool piece set up mentioned above, to study its ability to produce effective features for multiphase flow classification. This led to the production of enhanced discriminability for the extracted features.

In addition to array of sensors (pressure, conductance and capacitance sensors) in the ESMER spool piece, Beg *et al* (1993) introduced a gamma densitometer unit and was used to predict flow regimes and individual phase flow rates in 76.2mm and 406.4mm diameter pipelines. From each sensor, 24 feature vectors were extracted, namely; mean, variance, minimum, maximum and a 20-bin amplitude histogram. Measurement prediction accuracies were within ±10% for the gamma densitometer and ±18% for the pressure sensor in horizontal gas and liquid flows.

Akartuna (1994) compared and contrasted the template matching classification technique with an MLP neural network trained with the SCG algorithm using two additional features to those originally studied by Darwich, namely slug frequency and slug length. He conducted experiments in the slug flow regime for both two and three-phase flows with the 50.8mm horizontal spool piece with strip type capacitance sensors and pressure transducers. The MLP neural network gave superior classification properties when features from the pressure and capacitance sensor were fused. He reported that 97% of water cut, 90% of gas velocity, and 90% of liquid velocity measurements were predicted to within ±10% relative error.

Cai (1995) developed a flow regime specific pattern recognition model using the Kohonen self-organising feature map to classify data point into different flow regimes thereafter used a separate MLP neural network to estimate flow rate for the different flow regimes. Cai used an F-ratio feature saliency technique to select an effective feature set. In terms of phase flow rate measurement accuracies of the multi-level hierarchical system, 100% of the oil-continuous test points and 95.2% of the water-continuous test points were reported to be within ±5%. While 99.3% of gas and 100% of liquid phase superficial velocities were predicted to within ±9%.

Using radially and axially mounted absolute and differential pressure transducers in 50.8, 76.2, and 101.6mm horizontal multiphase flows, Beg (1998) extended the work of Darwich. He introduced five new features by taking the Fourier transform of the log spectrum of the signals and two new features from the amplitude domain (mean and variance). Using template matching technique, Beg reported that 100% of liquid phase and 93% of gas phase measurement accuracy are within ±10% through cross-sensor feature fusion. He applied a method of scaling, based on the hydrodynamic coordinates and feature vectors, after comparing the feature maps for the different pipe sizes and noting that different turbulence characteristics were obtained for the same flow conditions. However, the accuracy of this scaling technique gave poorer results.

Toral *et al* (1998) and Wood (2002) documented the commercial version of the ESMER multiphase flow meter developed by the Imperial College pioneering researchers mentioned above. In these works, statistical features from three differential pressure sensors (one top axial, one bottom axial and another radially mounted), impedance sensors (axially mounted on top) and a temperature sensor were imputed into an MLP neural network. After training and validation using the cross-validation technique to avoid over-fitting, the network was then tested. The individual phase flow measurements accuracy of ±10% was achieved by the ESMER meter using test separators as the reference.

Several studies beside the ESMER development programme in the application of pattern recognition techniques in multiphase flow measurement have been carried. They are enumerated below.

Goudinakis (2004) worked on flow regime identification in a horizontal pipeline and an S-shaped riser for air-water flow employing features from capacitance sensors and pressure transducers as the input into an MLP neural network. The network classified the flow regimes as stratified smooth, stratified wavy, bubble and slug. He reported that the S-shaped system was determined to accommodate long sever slugging flow cycles up to 230s but in the horizontal system, the slugging cycles was just 10s. Goudinakis further reported that a delay window of 200 inputs, which is equivalent to 20s of data at a sampling frequency of 10 Hz, was required for the horizontal pipe regime classification whereas 100 inputs, which is equivalent to 100s of data at a sampling frequency of 1 Hz was enough to identify the S-shaped riser's flow pattern. This technique was deemed not to be suitable for practical applications owning to the excessive training time needed to classify the flow regimes.

Jama (2004) documented the work on wet gas flow metering with pattern recognition techniques. He used features extracted from the absolute and differential pressure signals of a Venturi meter as the input into a Bayesian MLP. Using cross-sensor data (amplitude features) fusion, the gas and liquid superficial velocities were predicted to within ±5% relative error for all the measurement points.

Blaney (2008) reported the use of a single gamma densitometer unit in conjunction with pattern recognition techniques, to determine both the phase volume fractions and velocities to yield the individual phase flow rates of vertically upward multiphase flows. He performed three phase experiments with a fast-sampling (250 Hz) gamma densitometer installed at the top of a 10.5 m high, 108.2 mm internal diameter, stainless-steel catenary riser in the Cranfield University multiphase flow test facility. Features derived from the caesium-137 radioisotope-based densitometer data was used as the input into two pattern recognition models; namely, a single feedforward multilayer perceptron and a multilayer hierarchical flow regime specific model. Measurement accuracies of ±10% were reported for the gas and liquid superficial velocities and water cut based on flow regime specific correlations.

In the work of Ibrahim (2009), the application of an MLP neural network to multiphase slug flow measurement in a horizontal pipeline was investigated. Air-oil-water three phase flow experiments using a horizontal spool piece comprising absolute pressure, differential pressure (mounted axially), gamma densitometer,

capacitance and conductivity sensors were conducted. Amplitude and frequency domain features were extracted from these sensors as well as slug length and slug frequency features and used as inputs to the neural network. Using cross-sensor feature fusion, superficial gas, superficial liquid velocity and water cut prediction were 98%, 100% and 98%, respectively within a target accuracy of ±5%.

Wylie *et al* (2006) documented the use of an electromagnetic cavity resonator based sensor to determine multiphase flow rates. They determine phase fractions by monitoring the shift in the resonant frequencies with different fluid properties utilising low power radio frequencies that were transmitted across a pipeline containing the multiphase flow. Artificial neural network was implemented to overcome the modelling complications as a result of subjecting the system to different flow velocities, temperatures, pressures and installations. Based on the experimental data presented, Wylie *et al* reported measurement accuracies of ±10% for phase fractions with 4% measurement repeatability.

Sheppard and Russell (1993) reported on the ability of a neural network to classify horizontal multiphase flow based on the response of a gamma densitometer. The neural network was trained on 12 time series covering a range of flow regimes with standard statistical parameters extracted from the raw signals as input. Initial evaluation of the model using unseen data from the 12 time series used to train the network gave gas and liquid flow rates to within a root mean square error (RMSE) of 13%. The classification accuracy was reduced to a RMSE of 15% when a second phase of analysis was undertaken using data from previously unseen flow rates.

Bishop and James (1993) and Bishop (1995) conducted experiments using three vertical and three horizontal dual-energy gamma densitometer beams installed in a parallel configuration across a pipe section. The pattern recognition model use the six path lengths measured by the gamma densitometers as input features and was trained (with the Quasi-Newton training algorithm) to output the volume fractions of the oil and water phases. The conclusion drawn was that a neural network modelling could provide a practical solution in determining component phase fractions from the gamma densitometer data.

Åbro *et al* (1999) employed an amercium-241 source and a multi-beam configuration densitometer in conjunction with neural networks to predict void fraction and flow regime using simulated data. The network used energy spectrum for the photon range 30 to 68 keV (i.e. 38 bins of 1 keV) as input, with void fractions and the flow regime as the output. When a single detector was positioned at 180° to the amercium-241 source, an average error of 15.8% was reported for the void fraction measurements with a standard error deviation of 8%. With a multi-detector configuration and energy spectrum at detector positions of 180°, 156°, and 140° as inputs, average void fraction errors of 3% and a standard error deviation of 4.2% was achieved.

2.5 Measurement Uncertainty Estimation

2.5.1 Measurement and Uncertainty

The purpose of measurement is to provide information about a quantity of interest – a measurand (the quantity subject to measurement). For example, the measurand might be the volume of an oil tanker, the pressure in a gas export pipeline, or the mass flow rate of condensate from a well. No measurement is exact. When a quantity is measured, the outcome depends on the measuring system, the measurement procedure, the skill of the operator, the environment, and other effects (Bell, 1999). Even if the quantity were to be measured several times, in the same way and in the same circumstances, a different measured value would in general be obtained each time, assuming that the measuring system has sufficient resolution to distinguish between the values.

The spread or dispersion of the measured values would relate to how well the measurement is made. Their average would provide an estimate of the true value of the quantity that generally would be more reliable than an individual measured value. The dispersion and the number of measured values would provide information relating to the average value as an estimate of the true value. However, this information would not generally be adequate.

In metrology, measurement uncertainty is a non-negative parameter characterizing the dispersion of the values attributed to a measured quantity. The uncertainty has a

probabilistic basis and reflects incomplete knowledge of the quantity. All measurements are subject to uncertainty and a measured value is only complete if it is accompanied by a statement of the associated uncertainty. Fractional uncertainty is the measurement uncertainty divided by the measured value.

There are two types of measurement error, systematic and random:

I. A systematic error (an estimate of which is known as a measurement bias) is associated with the fact that a measured value contains an offset. In general, a systematic error, regarded as a quantity, is a component of the error that remains constant or depends in a specific manner on some other quantity.

II. A random error is associated with the fact that when a measurement is repeated it will generally provide a measured value that is different from the previous value. It is random in that the next measured value cannot be predicted exactly from previous such values.

Flow is a derived measurement that is invariably obtained from a number of measurements with a functional relationship that must be taken into account when analysing the measurement uncertainty. These relationships are often complex and frequently the results are inputed into a larger measurement system for the allocation of oil and gas production and sales (Basil, 2008). In evaluating the uncertainty associated with the value of a measurand one needs both a model that reflects the interrelation of all input quantities that influence the measurand and knowledge about these influencing input quantities (Sommer and Siebert, 2006). There are two approaches as to how the uncertainty is estimated:

I. *Type A evaluation of uncertainty* by statistical analysis of a series of observations.

II. *Type B evaluation of uncertainty* by means other than statistical analysis of a series of observations (Johansen and Jackson, 2004).

The ISO *Guide to the Expression of Uncertainty in Measurement (GUM)* provides internationally agreed approaches for the evaluation and expression of measurement uncertainty (ISO, 1995). The *GUM* provides a way to express the perceived quality

of the result of a measurement. Rather than express the result by providing a best estimate of the measurand along with information about systematic and random error values (in the form of an "error analysis"), the *GUM* approach is to express the result of a measurement as a best estimate of the measurand along with an associated measurement uncertainty.

One of the basic premises of the *GUM* approach is that it is possible to characterize the quality of a measurement by accounting for both systematic and random errors on a comparable footing, and a method is provided for doing that. This method refines the information previously provided in an "error analysis", and puts it on a probabilistic basis through the concept of measurement uncertainty. Another basic premise of the *GUM* approach is that it is not possible to state how well the true value of the measurand is known, but only how well it is believed to be known.

Measurement uncertainty can therefore be described as a measure of how well one believes one knows the true value of the measurand. This uncertainty reflects the incomplete knowledge of the measurand. The notion of "belief" is an important one, since it moves metrology into a realm where results of measurement need to be considered and quantified in terms of probabilities that express degrees of belief. It provides a consistent and transferable evaluation of measurement uncertainty.

The *GUM* further describes the concept of interval that may be expected to encompass a large fraction (typically 95%) of the values that could reasonably be attributed to the measurand. This interval, known as a coverage interval, provides a meaningful quantitative indication of the quality of the result. It provides a basis for stating the conformity with tolerances or limits by providing a probability statement that allows for reasonable decision to be made.

2.5.1.1 Stages of Uncertainty Evaluation

The main stages of uncertainty evaluation are formulation, calculation, propagation and summarizing. The formulation stage constitutes:

I. Defining the output quantity Y (the measurand),

II. Identifying the input quantities X_i, on which Y depends,

III. Developing a measurement model relating Y of the input quantities X_i, and

IV. Assigning probability distributions (Gaussian, rectangular, etc), on the basis of available knowledge, to the input quantities (or a joint probability distribution to those input quantities that are not independent).

The calculation stage consists of propagating the probability distributions for the input quantities X_i, through the measurement model to obtain the probability distribution for the output quantity Y, and summarizing by using this distribution to obtain:

I. The expectation of Y, taken as an estimate y of Y,

II. The standard deviation of Y, taken as the standard uncertainty $u(y)$ associated with y, and

III. A coverage interval containing Y with a specified coverage probability.

The propagation stage of uncertainty evaluation is known as the propagation of distributions, various approaches for which are available, including:

I. The GUM uncertainty framework, constituting the application of the law of propagation of uncertainty, and the characterization of the output quantity Y by a Gaussian or a t-distribution,

II. Analytic methods, in which mathematical analysis is used to derive an algebraic form for the probability distribution for Y, and

III. A Monte Carlo method (Bernardo and Smith, 2000), in which an approximation to the distribution function for Y is established numerically by making random draws from the probability distributions of the input quantities, and evaluating the model at the resulting values.

For any particular uncertainty evaluation problem, approach (I), (II) or (III) (or some other approach) is used; (I) being generally approximate, (II) exact, and (III) providing a solution with a numerical accuracy that can be controlled.

2.5.1.2 Measurement Model, Inputs and Outputs

In establishing the basis for uncertainty evaluation, the measurement model must first be defined and the information on the model input quantities quantified. A measurement model converts a quantity value into the corresponding value of the measurand. There are many types of measurement in practice and therefore many models. In general there are often several different quantities, for example temperature, humidity and displacement that contribute to the definition of the measurand, that need to be measured.

Irrespective of the field of application, the measurand or output can rarely be measured directly, instead it is determined from a number of contributions or input quantities which are themselves measurements or derived from other measurements or further information. The measurement model is then the fundamental relationship between the output quantity (*Y)* and the input quantities X_i given by:

Eqn. 2.82

The model function (*F)*, which can be a mathematical formula or a physical law, accounts for sources of variability and also include corrections for systematic effects (Papadopoulos, 2000). Correction terms should be included in the measurement model when the conditions of measurement are not exactly as stipulated. These terms correspond to systematic errors. Given an estimate of a correction term, the relevant quantity should be corrected by this estimate. There will be an uncertainty associated with the estimate, even if the estimate is zero, as is often the case.

As well as raw data representing measured values, there is another form of data that is frequently needed in a measurement model. Some such data relate to quantities representing physical constants, each of which is known imperfectly. Examples are material constants such as modulus of elasticity and specific heat. The items required by a measurement model to define a measurand are known as input quantities in a measurement model.

2.5.2 Conventional Uncertainty Estimation

An estimate of the measurand or output quantity Y, denoted by y, is obtained from Equation 2.83 using input estimates $x_1, x_2 . . . x_N$ for the values of the N input quantities $X_1, X_2 . . . X_N$. Thus, the output estimate y, which is the result of the measurement, is given by:

Eqn. 2.83

The true values of the input quantities $X_1,..., X_N$ are unknown. In the GUM approach $X_1,..., X_N$ are characterized by probability distributions and treated mathematically as random variables. These distributions describe the respective probabilities of their true values lying in different intervals, and are assigned based on available knowledge. Sometimes, some or all input quantities are interrelated and the relevant distributions, which are known as joint, apply to these quantities taken together.

The use of available knowledge to establish a probability distribution to characterize each quantity of interest applies to the X_i and also to Y. In the latter case, the characterizing probability distribution for Y is determined by the measurement model together with the probability distributions for the X_i. The determination of the probability distribution for Y from this information is known as the *propagation of distributions* (ISO, 2008).

Figure 2-38 depicts the measurement function $Y = X_1 + X_2$ in the case where X_1 and X_2 are each characterized by a (different) rectangular, or uniform, probability distribution. Y has a symmetric trapezoidal probability distribution in this case.

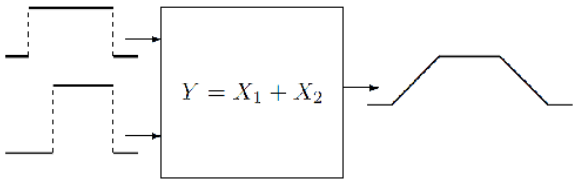

Figure 2-38 Propagation of Distributions

Once the input quantities $X_1,..., X_N$ have been characterized by appropriate probability distributions, and the measurement model has been developed, the probability distribution for the measurand Y is fully specified in terms of this

information. In particular, the expectation of Y is used as the estimate of Y, and the standard deviation of Y as the standard uncertainty associated with this estimate. Often an interval containing Y with a specified probability is required. Such an interval, a coverage interval, can be deduced from the probability distribution for Y. The specified probability is known as the coverage probability. For a given coverage probability, there is more than one coverage interval (Weise and Wöger, 1992).

In conventional uncertainty analysis, the aim is to combine all the sources of uncertainty (systematic and random) into the test results. This is done in each case by determining the sensitivity of the test results to uncertainty in each source by partial differentiation or other numerical means. The combined standard uncertainty of the measurement result y, designated by $u_c(y)$ and taken to represent the estimated standard deviation of the result, is the positive square root of the estimated variance $u_c^2(y)$ obtained from

— —— Eqn. 2.84

Equation 2.84 is based on a first-order Taylor series approximation of the measurement Equation 2.83 and is referred to as the law of propagation of uncertainty. The partial derivatives of f are called the sensitivity coefficients, which give the effects of each input quantity on the final result (or the sensitivity of the output quantity to each input quantity); $u(x_i)$ is the standard uncertainty associated with the input estimate x_i; and $u(x_i, x_j)$ is the estimated covariance associated with x_i and x_j.

The term, expanded uncertainty, $U(y,)$ is used in the GUM to express the percentage confidence interval about the measurement result within which the true value of the measurand is believed to lie and is given by:

Eqn. 2.85

where t is the coverage factor. For a normal distribution measurement, confidence interval is found by multiplying the standard deviation by t, as shown in Table 2-4

Table 2-4 Confidence Intervals with their Associated Coverage Factors

Confidence Interval (%)	Coverage Factor, t	
68	1.00	One standard deviation (SD)
90	1.65	
95	1.96	Taken as two SD by convection
99	2.58	

2.5.3 Monte Carlo Simulation Method

Simulation is generally defined as the process of replication of the real world based on a set of assumptions and conceived models of reality (Nicolis, 1995). In this context, Monte Carlo Simulation (MCS) is a procedure in which random numbers are generated according to probabilities assumed to be associated with a source of uncertainty. In other words, they are a class of computational algorithms that rely on repeated random sampling to compute their results. Because of their reliance on repeated computation and random or pseudo-random numbers, MCS methods are best done using a computer thus enabling the determination of the propagation of uncertainties of complex systems including many which cannot be found readily by convectional analytical means (Coughlan *et al*, 1999). The MCS method of estimating uncertainty, which is fully compatible with the *GUM,* entails evaluating the uncertainty of a measurement using a mathematical model of the measurement and the law of propagation of uncertainty (Basil and Jamieson, 1998). Monte Carlo Simulation methods has been applied to measurement system uncertainties with many claimed advantages, it takes account of all dependencies and propagates uncertainty automatically eliminating the need to analyse the sensitivity of complex calculations (Papadopoulos and Yeung, 2001).

In many applications of Monte Carlo, the process is simulated directly without necessarily deriving the differential equations that describe the behaviour of the system. That is to say, complex partial differentiations to determine the sensitivity coefficients are not necessary. It also takes care of input covariance or dependencies automatically. The only requirement is that the physical (or mathematical) system is described by probability density function (PDF) and that a PDF is associated with each of the input quantities. Since the PDF for an output quantity (measurand) can be derived from the input PDFs, then from this output

PDF, an interval can be determine that contains the value of the measurand with a specific probability (Cox et al, 2001). When applied to uncertainty estimation, random numbers are used to randomly sample parameters' uncertainty distribution space instead of mean values used in conventional uncertainty estimation methods. Such an analysis is closer to the underlying physics of the actual measurement processes that are probabilistic in nature (Basil *et al*, 2001).

The primary components of a Monte Carlo simulation method include the following (Allen *et al*, 1995):

- *Probability distribution functions (PDFs):* the inputs must be described by a set of PDFs.
- *Random number generator:* a source of random numbers evenly distributed on the unit interval must be available.
- *Sampling rule:* a prescription for sampling from the specified PDFs, assuming the availability of random numbers on the unit interval, must be given.
- *Scoring (or tallying):* the outcomes must be accumulated into overall tallies or scores for the quantities of interest.
- *Error estimation:* an estimate of the statistical error (variance) as a function of the number of trials and other quantities must be determined.
- *Variance reduction techniques:* methods for reducing the variance in the estimated solution to reduce the computational time for Monte Carlo simulation.
- *Parallelization and vectorization:* algorithms to allow Monte Carlo methods to be implemented efficiently on advanced computer architectures.

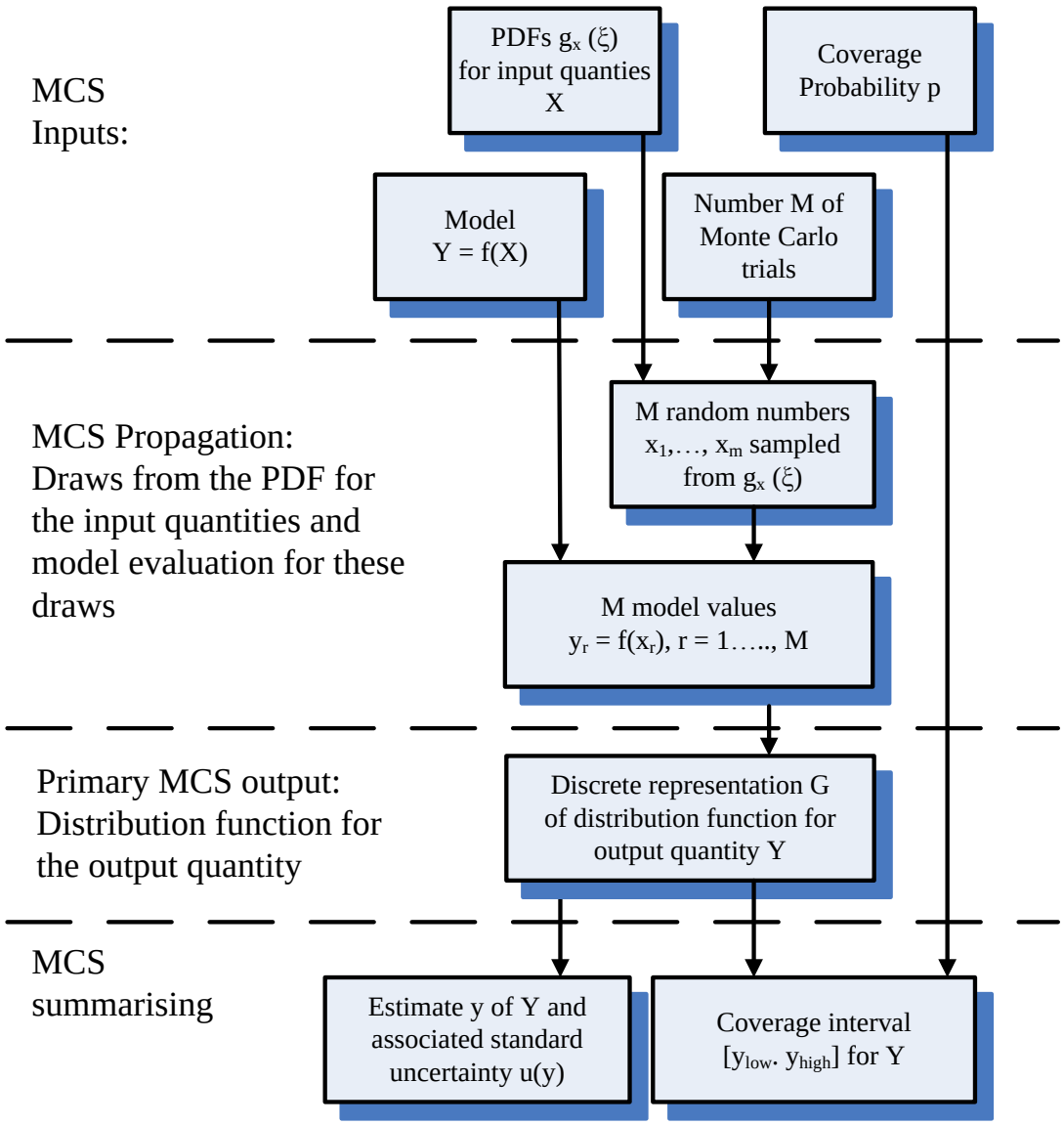

Figure 2-39 The Propagation and Summarising stages in Uncertainty Evaluation Using MCS (ISO, 2006)

As illustrated in Figure 2-39, the basic idea of this method is to draw random deviates from the PDFs, g_x *(ξ)* and to propagate these deviates through the model to yield random deviates distribution as *G* (*ISO*, 1995). Repeating this many times, an empirical distribution of *G* is obtained which is used to determine the estimate and its associated standard uncertainty as well as coverage intervals (*ISO*, 2008; Cox and Siebert, 2006; and Wübbeler *et al,* 2008). According to Wübbeler *et al* (2008), the number of trials should be sufficiently large, e.g. greater than 10^6 to ensure that the random error inherent in the results of g_x *(ξ)* is significantly reduced.

2.6 Chapter Summary

This chapter presents a comprehensive review of literature relevant to the subject matter. It addresses such topics like: fundamentals of multiphase flow, multiphase flow measurement, gamma radiation methods, pattern recognition techniques, and measurement uncertainty.

From the literature, it was ascertained that no single commercial multiphase meter is able to meet all the requirements of the oil and gas industry in spite of the advances in multiphase metering technology. This justifies the need for further development of MPFMs. The pattern recognition approach for clamp-on multiphase measurement employed in this research study provides one means for meeting this need.

The key findings are:

- Existing technologies for multiphase flow metering do not facilitate installation without breaking into the pipe.
- Pattern recognition techniques using feature extraction have proved successful in related fields (*Darwich, 1989; Cai, 1995; Jama, 2004; Blaney, 2008; and Ibrahim, 2009*).
- A single gamma densitometer unit has never been examined as complete metering package in horizontal multiphase flows.
- Previous pattern recognition studies were based on the assumption that horizontal flow has more features than vertical flow, thus better prediction results.
- To date, no work demonstrating this assertion has been published in the literature.

CHAPTER THREE

3. EXPERIMENTAL SETUP AND DATA ACQUISITION

This chapter describes the general features of the experimental rig and outlines the instrumentation used, data acquisition and processing and sensor calibration. Details of the experimental campaign are also presented.

Two and three phase experiments were conducted in the Multiphase Flow Laboratory of the Department of Offshore, Process and Energy Engineering of Cranfield University. Air-water, air-oil, and oil-water two phase and air-oil-water three phase data in the vertical and horizontal pipe orientation were collected and used to produce flow regime maps, void fraction and density estimation, phase inversion analysis and to predict flow rates using pattern recognition models.

3.1 Cranfield University Multiphase Flow Test Facility

The multiphase test facility at Cranfield University is used for flow assurance, multiphase metering and control systems research. It is a fully automated high pressure test facility designed to supply a controlled and measured amount of oil, water and air mixture from the flow metering area into the test area and finally into the phase separation area where the oil, water and air are separated. After separation in a horizontal three-phase gravity separator, the oil and water are cleaned in their respective coalescers before returning to their storage tanks while the air is exhausted into the atmosphere.

The test facility can be divided into four areas – the Fluid Supply and Metering Area, the Valve Manifold Area, the Test Area and the Separation Area. This facility is controlled by DeltaV, which is a Fieldbus-based Supervisory, Control and Data Acquisition (SCADA) system supplied by Emerson Process Management. Figure 3-1 shows the schematic of the multiphase test facility.

3.1.1 Fluid Supply and Metering

Air is supplied from a bank of two compressors (Atlas Copco Electonikon GA75 compressor (C01 and C02)), connected in parallel. When both compressors are

running in parallel, a maximum air flow rate of 1410 m^3/h FAD (Free Air Delivery) at 7 barg can be supplied. The air from the two compressors is accumulated in a large air receiver (R300) to reduce the pressure fluctuation from the compressor. Air from the receiver passes through a bank of three filters (coarse, medium and fine) where debris and condensates that are present in the air are stripped off and then through a cooler before it goes into the flow meters.

Water is supplied from a 12.5 m^3 capacity water tank (T100), and oil is supplied from a bounded oil tank (T200) of similar capacity. The water and oil are supplied into the flow loop by two identical multistage Grundfos CR90-5 pumps (P01 & P02). A maximum flow rate of 100 m^3/h at 10 barg can be supplied by each of them. Startup, speed control and shutdown of these two pumps are achieved remotely using the DeltaV control system.

The flow rates of the air, water and oil are regulated by their respective control valves. The air is metered by a bank of two Rosemount Mass Probar flow meters of 12.7mm and 25.4mm diameter respectively. The smaller air flow meter measures the lower air flow rate from 0 to 0.028 Sm^3/s while the larger meters the higher air flow rate from 0.028 to 1.181 Sm^3/s (subject to compressor capacity).The standard reference condition for the air flow rate is 15˚C and 101.325KPa as defined by the International Organization for Standardization (ISO). The water flow rate is metered by a Rosemount 8742 Magnetic flow meter (up to 1 kg/s) and a Foxboro CFT50 Coriolis meter (up to 10 kg/s) while the oil flow rate is metered by a Micro Motion Mass flow meter (up to 1 kg/s) and a Foxboro CFT50 Coriolis meter (up to 10 kg/s).

In addition, there is a gas injection point close to the Catenary riser base. It consists of four 12.7 mm copper tubing mounted radially to the flow loops.

Rustlick dielectric oil EDM-250 which has properties similar to condensate (light hydrocarbon liquid) is the oil used in the test facility. It has a favourable air release characteristics, good water separation properties, thermal and oxidation stability and environmental safety factor. The physical and chemical properties are listed in Table 3-1

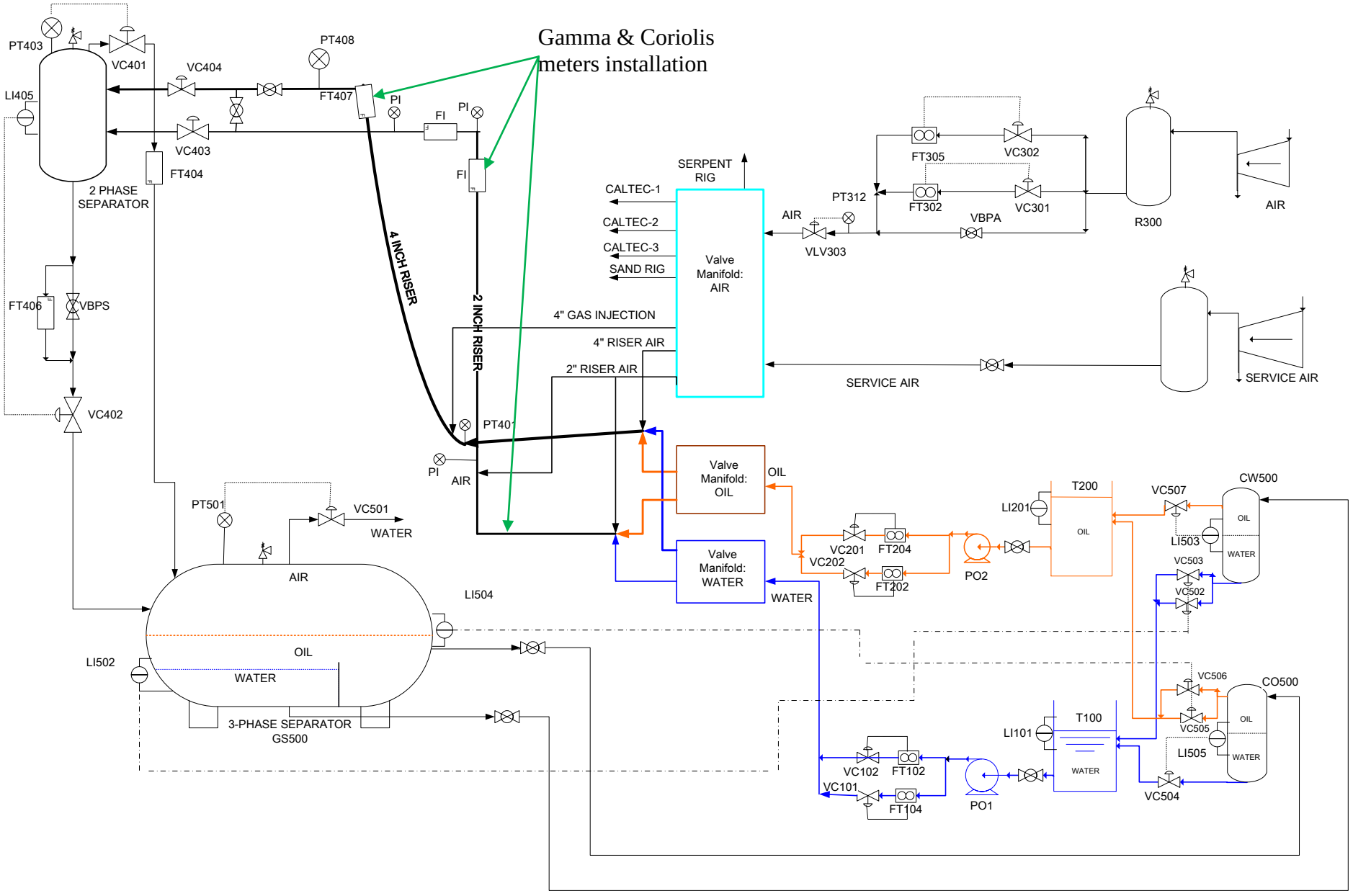

Figure 3-1 Cranfield University Three-Phase Test Facilities showing 101.6mm Catenary Riser and 50.8mm Vertical Riser (Cao and Yeung, 2009)

Table 3-1 Typical Properties of Rustlick EDM-250

Property	Value
Viscosity, cSt (at 40˚C)	2.7
Boiling Point, ˚C	243
Specific Gravity	0.81
Flash Point ˚C (Method)	93

3.1.2 Valve Manifold Section

Between the Fluid Supply and Metering Area and Test Area, is the Valve Manifold Area. It is designed to distribute fluids to various test rigs. The main purposes of the Valve Manifold Area are as follows:

- Supplying water to the 101.6mm or 50.8mm flow loops exclusively;
- Supplying oil to the 101.6mm or 50.8mm flow loop exclusively;
- Providing the accessibility of the main air supply to a variety rigs.

3.1.3 Test Section

The test area consists of a 101.6mm diameter flow loop and a 50.8mm diameter flow loop. The 101.6mm loop is a 55m long, 2° downward inclined pipeline joined to a catenary shaped riser with a vertical height of 10.5m. The 50.8mm loop is a 40m long horizontal pipeline, connected to a 10.5m height vertical riser. Both flow loops, which exit into a vertical two phase separator where the air and liquid are separated, is made of a combination of NB schedule 10 stainless steel sections and the clear Perspex sections (see Figure 3-1). The transparent Perspex sections help in visual observation of the multiphase fluid in the loops. The full specifications of the two riser loops are summarised in Table 3-2

Two Endress + Hauser Coriolis meters and two Neftemer gamma densitometers are installed on the 50.8mm flow loop – one set is installed in the horizontal section of the flow loop about 3m before the riser base and the other set at the top of the vertical riser. Whereas in the 101.6mm flow loop, only one set of Neftemer gamma densitometer and Endress + Hauser Coriolis meter is installed vertically at the top of

the catenary riser as shown in Figure 3-1. The riser base and the riser top pressures are metered by Rosemount pressure transducers (PT417) and (PT419) respectively.

Table 3-2 Specification of the 50.8mm and 101.6mm Riser Loops (Cao and Yeung, 2009)

Parameters	101.6mm Flow Loop	50.8mm Flow Loop
Diameter of Flow Loop & Riser	101.6mm NB Schedule 10	50.8mm NB Schedule 10
Internal Diameter of Flow Loop	108.2mm	54mm
Length of Flow Loop	55m	40m
Inclination of Flow Loop	2° Downward Inclined	2° Downward Inclined
Shape of Riser	Catenary	Vertical
Pressure Rating of Flow Loop	20 barg	20 barg
Temperature Rating of Test Facility	0 - 80°C	

3.1.4 Separation Area

Air, water and oil are gravity separated in the horizontal three-phase separator (GS500). The pressure, oil/water interface level and gas/liquid interface level are controlled by means of a pressure (PRC501) controller and two level controllers (LIC502 and LIC504), managed by the DeltaV control system.

After separation and cleaning in the three-phase separator air is exhausted into the atmosphere. Water and oil from the three-phase separator enter their respective coalescers (CW500 and CO500), where the liquids are further cleaned before returning to their individual storage tanks.

3.1.5 Reference Instrumentation

The multiphase flow facility is equipped with a state-of-the-art process control and management system, the DeltaV automation system from Emerson Process Management. All instrumentation in the multiphase flow test facility is interfaced via Fieldbus and PROFIBUS with the DeltaV automation system which is configured to record instrument output values at a frequency of 1Hz. All data are stored in the

DeltaV historian from where it could be downloaded after experimental work for further analysis or reference purposes.

Reference measurements were taken from the inlet delivery instrumentation and, where appropriate, these values were corrected using pressure and temperature data from the test sections to yield corrected values corresponding to the fluid flow rates at the point of the measurement. The multiphase flow test facility fluid delivery and test section instrumentation are shown in Table 3-3

Table 3-3 Three Phase Facility Reference Instrumentation

Tag	Description	Details	Range
FIR102	Inlet Water Flow Meter (high flow rate)	Coriolis – Foxboro CFS 20	0.120 – 11.6 kg/s
FIR104	Inlet Water Flow Meter (low flow rate)	Electromagnetic – Rosemount 8742	0.005 – 5.0 kg/s
FIR202	Inlet Oil Flow Meter (high flow rate)	Coriolis – Foxboro CFS 20	0.120 – 11.6 kg/s
FIR204	Inlet Oil Flow Meter (low flow rate)	Coriolis – Micro Motion CF3M	0.02 – 3 kg/s
FIR302	Inlet Air Flow Meter (high flow rate)	Differential Pressure - Rosemount Mass Probar	0.028 – 1.181 Sm^3/s
FIR305	Inlet Air Flow Meter (low flow rate)	Differential Pressure – Rosemount Mass Probar	0 – 0.028 Sm^3/s
PIRC403	Riser Top Pressure Transducer	Rosemount 3051	0 – 7 barg
PIR401	Riser Base Pressure Transducer	Rosemount 3051	0 – 7 barg
PIR312	Air Flow Line Pressure Transducer	Rosemount 3051	0 – 7 barg
TIR101	Air Flow Line Temperature Transducer	Rosemount 3244MV	0 – 100 ˚C

3.2 Data Acquisition System

Experimental data were obtained through three separate data acquisition systems using three stand-alone PCs namely: Delta V, LABVIEW, and Neftemer Ltd proprietary data processing unit. The Delta V plant automation system was used to control the test facility delivery flows and maintains steady state conditions during data collection operations. Figure 3-2 presents the graphic user interface of the Delta V system. Signals from the Coriolis meters and pressure transducers installed on the 50.8mm rig were obtained through a National Instruments data acquisition unit. This

is a multifunctional data acquisition unit with multiple input channels. A custom-build LABVIEW program installed on a Pentium IV personal computer is used in acquiring, processing and storing of all the data. This program is made up of three subdivisions: data acquisition, viewing and storing. The raw data is read from the channels in the form of output sensor voltages and then converted into engineering units. To achieve this, all sensors were previously individually calibrated to obtain their gains and zeros, using the expression given below:

—— Eqn. 3.1

where Q is the physical variable such as pressure being measured, v is the value of the voltage measured at zero value of the physical variable, v_f is the final voltage measured at a particular value of the physical variable and s is the gain or slope. The acquired data, while being written and saved in text files, is displayed in real time numerically and graphically. The saved files can be exported to a spreadsheet or MATLAB for further analysis.

Neftemer Ltd proprietary data acquisition system comprise of a stand-alone data processing unit (DPU). The core of this DPU is an ICP I-7188D programmable logic controller (PLC) where the raw densitometer signal is processed into gamma count signal. The DPU is connected to a dedicated PC (a 2.66 GHz Intel Core 2 Duo desktop system with 1.96 GB of RAM) through a RS-232 serial connection. The signals, sampled at 250 Hz, are stored in two separate files: one for the high-energy (hard) counts and the other for the low-energy (soft) gamma counts. The raw data files can be exported into MATLAB for further processing.

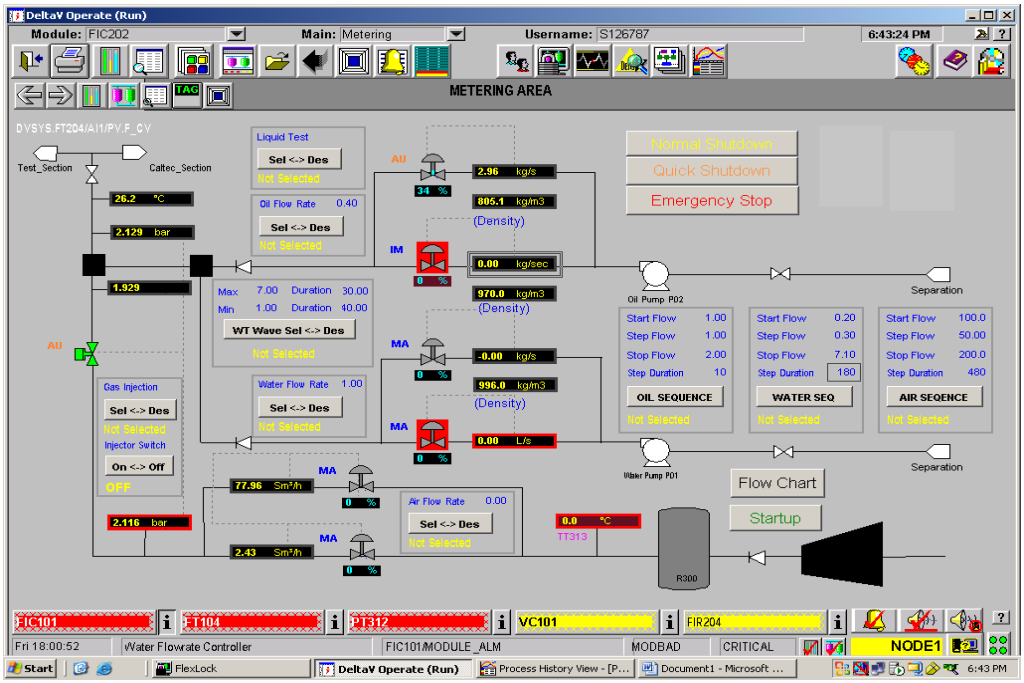

Figure 3-2 Graphic User Interface of the Delta V Plant Automation System

3.3 Instrumentation

The two main sensors used in this work are Endress and Hauser Coriolis meter and Neftemer Ltd gamma densitometer.

3.3.1 Coriolis Mass Flow Meter

If a moving mass is subjected to an oscillation perpendicular to its direction of movement, Coriolis forces occur depending on the mass flow. A Coriolis mass flow meter has oscillating measuring tubes to precisely achieve this effect. Coriolis forces are generated when a fluid (= mass) flows through these oscillating tubes. Sensors at the inlet and outlet ends register the resultant phase shift in the tube's oscillation geometry. A processor analyzes this information and uses it to compute the rate of mass flow. The oscillation frequency of the measuring tubes themselves, moreover, is a direct measure of the fluids' density. The temperature of the measuring tube is also registered for compensating thermal influences. This signal corresponds to the process temperature and is also available as an output signal. The Endress and Hauser (E&H) Coriolis mass flow meter (see Figure 3-4) utilised in this experiment is the Promass 83F. It has a good linearity property and a wide operating range: fluid

temperatures (up to +350 °C); process pressures (up to 100 bar); and mass flow measurement (up to 2200 t/hr).

3.3.1.1 Flow Rate Measurement

The measuring principle of the E&H Coriolis meter is based on the controlled generation of Coriolis forces. These forces are always present when both translational and rotational movements are superimposed on a system. The amplitude of the Coriolis force depends on the moving mass, its velocity in the system, and thus on the mass flow according to the equation below:

Eqn. 3.2

where F_c is the Coriolis force, Δm is the mass of the moving fluid, v is the radial velocity in the rotating or oscillating system and ω is the angular velocity.

Instead of a constant angular velocity the E&H sensor uses oscillation. This causes the tube through which the fluid is flowing to oscillate. The Coriolis forces produced at the measuring tubes induces a phase shift in the tube oscillations as illustrated in Figure 3-3:

- If there is zero flow, i.e. when the fluid is in static condition, the oscillation measured at points A and B has the same phase, and thus there is no phase difference (1).
- Mass flow causes deceleration of the oscillation at the inlet of the tubes (2) and acceleration at the outlet (3).

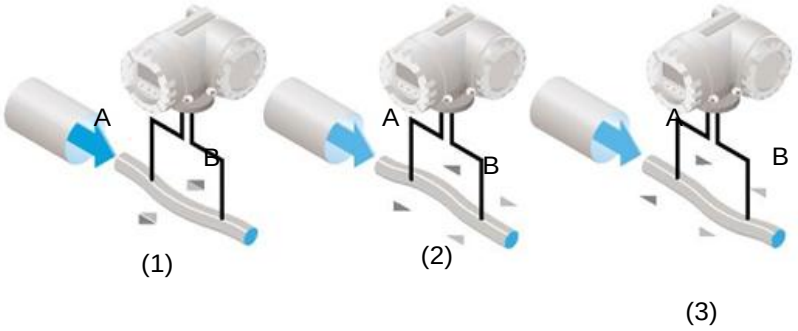

Figure 3-3 Operating Principle of the E&H Coriolis Mass Flow Meter

The phase difference (A-B) increases with increasing mass flow. Electrodynamic sensors register the tube oscillations at the inlet and outlet. A patented ITBTM (Intrinsic Tube Balance) system ensures balance and stability for the meter by creating a counterweight that runs parallel to the measuring tube. This counterweight oscillates in anti-phase to the measuring tubes and thus creates a balanced system, thus providing accurate measurements over a wide range of process and environmental conditions. The measuring principle operates independently of temperature, pressure, viscosity, conductivity and flow profile (Emerson, 2011).

Figure 3-4 Endress and Hauser Coriolis Mass Flow Meter

3.3.1.2 Density Measurement

The measuring tube is continuously excited at its resonance frequency. A change in the mass and thus the density of the oscillating system (comprising the measuring tube and fluid) results in a corresponding, automatic adjustment in the oscillation frequency. Resonance frequency is thus a function of fluid density. The microprocessor utilizes this relationship to obtain and output a density signal.

3.3.1.3 Temperature Measurement

The temperature of the measuring tube is determined in order to calculate the compensation factor due to temperature effects. This signal corresponds to the process temperature and is also available as an output.

3.3.2 Gamma Densitometer

The gamma densitometer supplied by Neftemer Ltd consists of a lead-filled source housing, a detector unit, and a data processing box. The gamma source housing and the detector are mounted directly opposite each other across the pipe with the aid of a mounting bracket, Figure 3-5.

The densitometer was installed in an enclosed area visibly delineated as containing radioactive material with access restricted to only trained personnel. Operation of a mechanical shutter at the side of the source block (marked ‘ON’ and ‘OFF’ as can been seen in Figure 3-5) enabled the gamma source to be moved between its safe ‘OFF’ and active ‘ON’ positions. At all times, a large colour coded panel located in the enclosed area indicated whether the gamma source was in its ‘active’ open (RED) or ‘dormant’ closed (GREEN) position. Throughout the experimental campaigns, the source was left in its active position to ensure source positioning was identical for all experiments.

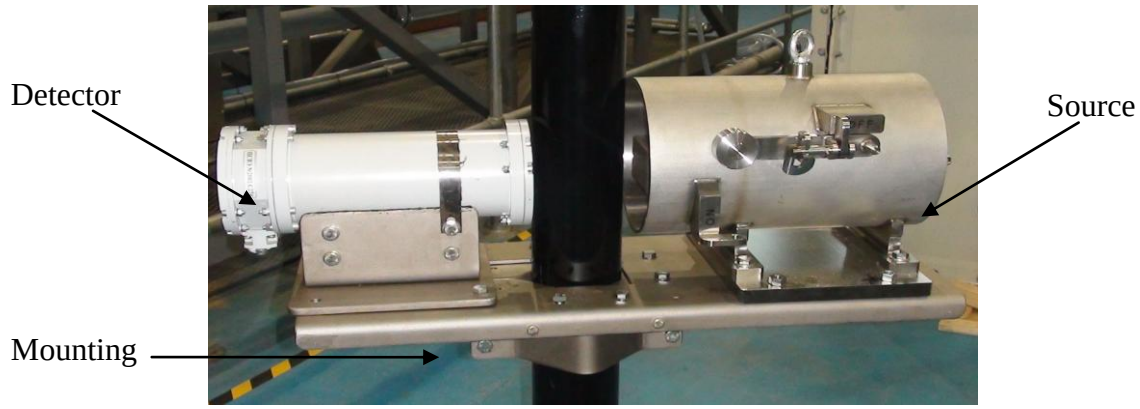

Figure 3-5 Neftemer Gamma Densitometer

3.3.2.1 Gamma-Source Housing

The gamma-source housing consists of an outer casing fabricated from stainless steel. This casing adds mechanical strength and rigidity to the lead-filled internals that contains a gamma radionuclide source capsule surrounded by a lead body to prevent the gamma radiation emitted by the source from escaping into the surrounding environment. A collimator designed to limit the size and angle of spread of the gamma rays, is built into the housing to provide an outlet that produces a cone

of beam having uniform physical properties in all directions with an angle of 6 degree to be directed across the diameter of the pipeline. Brass discs of various thicknesses could be inserted in the collimated beam path to control the intensity of the gamma radiation that is passing through, taking into account the size and thickness of the installation pipe and the strength of the source.

The nucleus of the 6.6 GBq caesium-137 radionuclide undergoes radioactive decay through the mechanism depicted in Figure 3-6(Prepost, 2001).

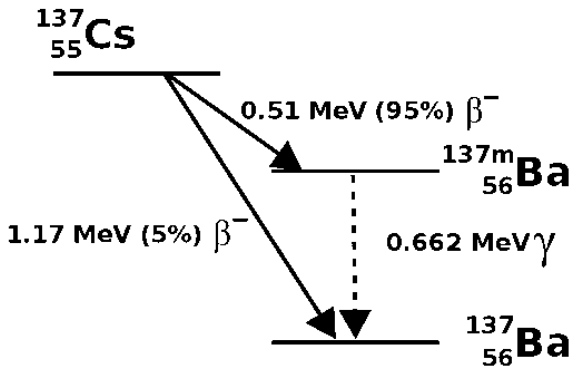

Figure 3-6 Caesium-137 Decay

It emits an electron (β) and a neutrino. As a result, its nuclear charge increases from 55 to 56 by changing a neutron into a proton. From Figure 3-6, 95% of the decays result in only 0.5 MeV being transferred to the electron and neutrino, leaving the barium-137 in a metastable, excited state. This will further decay by either emitting a 0.662 MeV gamma or by 'internally converting' the gamma before it leaves the barium atom and ejecting a K-shell electron instead.

Figure 3-7 is the caesium-137 spectrum plot obtained during calibration of the Neftemer gamma densitometer unit clamped on to an empty pipeline. The x-axis of the spectrum plot represents the channels from the multiple channel analyser used to classify the gamma photon energy distribution, where the channel number is directly proportional to the gamma photon energy. The y-axis represents the number of counts per second. From the plot, it is noted that the caesium-137 source emits a wide range of photon energies. The Neftemer unit exploits the direct high-energy 0.55 – 0.94 MeV photons (subsequently referred to as the hard spectrum) and the lower energy 0.1 – 0.55MeV Compton scattered range (subsequently referred to as the soft spectrum) for multiphase flow measurement.

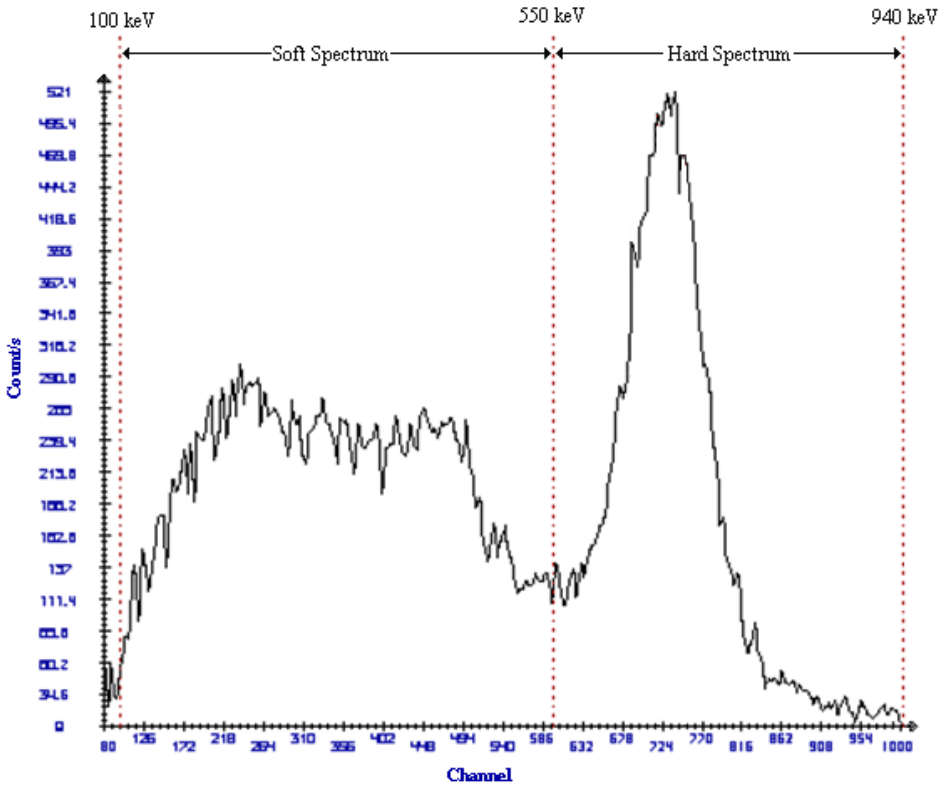

Figure 3-7 Measured Caesium-137 Spectrum

3.3.2.2 Gamma-Detection Unit

Four key components make up the gamma-detection unit; namely, scintillation crystals, photomultiplier tube (PMT), amplifier electronics and two single channel analysers (SCA), as diagrammatically depicted in Figure 3-8. It also contains a temperature regulating device that controls the detector internal temperature to ensure that it does not fall below 20 ºC; thus, minimising the influence of temperature fluctuation on the detection electronics.

The scintillation crystals are sodium iodide (NaI) crystals doped with thallium and is contained in a 30mm × 60mm tube in gamma-detector unit. These crystals produce a pulse of visible light with an energy proportional to that of the incident gamma photon and are detected by a FEU-115M photomultiplier which converts the light pulses into voltage pulses of proportional amplitudes. Propriety electronic circuits are used to amplify and condition the voltage pulses which are then passed on to channel analysers for classification.

The single-channel analysers (SCAs) effectively act as counters of the voltage pulses. The SCAs are setup to measure the gamma count of the 0.50 – 0.94 MeV hard energy spectrum and the gamma count for all photon energies of interest: 0.1 – 0.94 MeV. The soft energy spectrum count is the difference between the two measured ranges. The accuracy of the gamma densitometer count measurements is quoted as ±0.5% by the manufacturer, Neftemer (UK) Ltd.

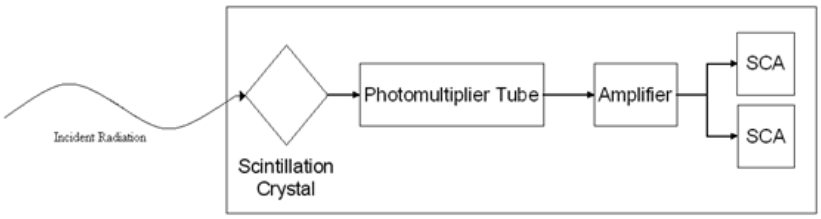

Figure 3-8 Key Components of Gamma Detection Unit

3.3.2.3 Installation and Calibration

The gamma-source housing and detection unit are mounted diametrically opposite each other on a vertical or horizontal pipe section using a clamp-on mounting bracket and positioned such that the source and detection units are aligned with the centre of the pipe as shown in Figure 3-9 (All dimensions are in millimetre). The clearance between the source housing and the pipe wall should be approximately 70mm and that between the detector and the pipe wall should be approximately 10mm. After installing the densitometer assembly, Neftemer Ltd propriety software is used to produce a pulse height spectrum. The caesium-137 pulse height spectrum detected is then analysed to ensure the installation was successful.

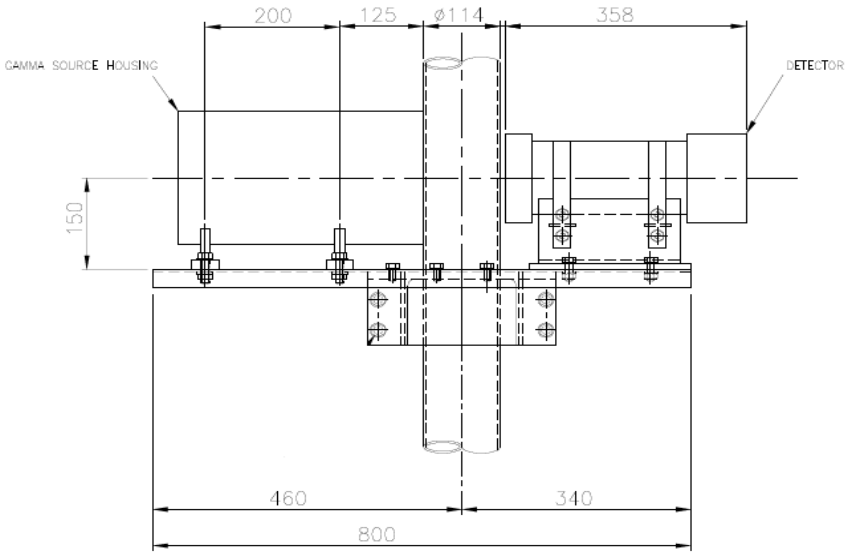

Figure 3-9 Gamma Densitometer Assembly

The Assembly may be re-adjusted if the characteristic features associated with a caesium-137 spectrum as shown in Figure 3-7 are not present in the detected spectrum.

Calibration gamma count values for the different test fluids (air, oil and water) were obtained in static conditions in the multiphase flow facility before the commencement of the experimental campaign. The densitometer measurement is initiated and gamma count collected for one hour when the test section is completely filled with each fluid in static conditions. The densitometer has a high sampling rate of 250Hz. Thus every four millisecond a gamma count value is registered. The average gamma count for the two energy levels and the corresponding mass attenuation coefficients of the test fluids are summarised in Table 3-4. The linear attenuation coefficient of air (at 1bar) is taken to be zero.

Table 3-4 Average Gamma Count and Attenuation Coefficients for Test Fluids (the gamma count values are one hour average)

	Average Gamma Count			Linear Attenuation Coefficient (m^{-1})		
	Air	Water	Oil	Air	Water	Oil
Hard	409.19	176.96	203.54	0	8.21	6.82
Soft	826.07	455.35	508.89	0	5.85	4.75

The higher linear attenuation coefficient for water, for both energy levels, demonstrates that the water attenuates the gamma rays to a greater degree than the oil due to its higher density. Though the ratio of attenuation imposed by the water and oil phases differ for the two energy levels; that is 1.203 and 1.232 for the hard and soft spectrums respectively. A plot of the mean gamma counts versus test fluid densities for the calibration experiments are shown in Figure 3-10.

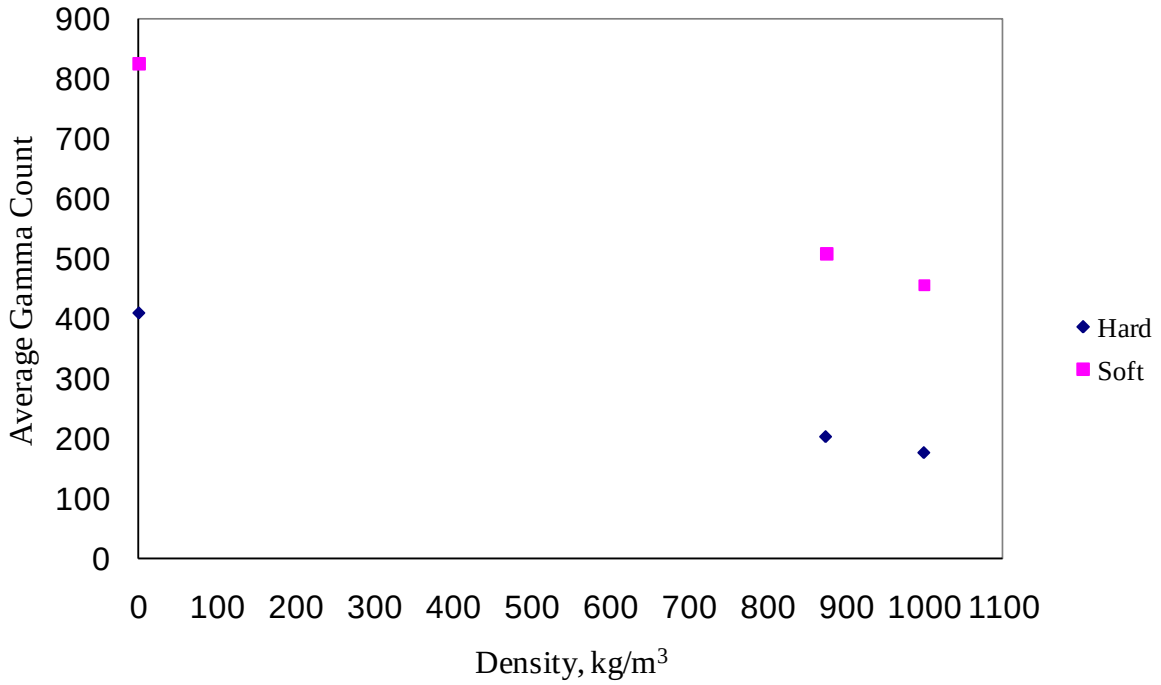

Figure 3-10 Gamma Attenuation as a Function of Material Density

The gamma densitometer displayed a linear decrease in gamma count with increasing test fluid density for both the hard and soft signals. The hard and soft energy gamma counts experienced differing rates of attenuation with increasing density. This expected discriminatory response to test fluids of differing densities from the caesium-137 gamma densitometer showed that it was functioning accurately to instil confidence in the reliability of the instrument for data analysis purposes.

3.3.2.4 Management of Radiation Work and Safety

All life is constantly exposed to various forms of radiation, which are emitted from natural and man-made sources. Radiation is an energy transfer from one place to another in waveform, and some of its effects are essential to the existence of life on

earth. The consequences of the transfer of radiated energy to living organisms are biological effects, many of which are useful and many more injurious.

In compliance with Heath and Safety legislation, radioactivity levels around the installation are monitored closely by measuring the dose-rate around the source each month in order to check the presence of enhanced levels of radiation exposure within and beyond the confines of the Controlled and Supervised Areas and to check for leakage beams emerging from the source housing. Figure 3-11 shows the measurement locations and their relative distances from the source-housing. The working area is approximately 3 meters away from location 4.

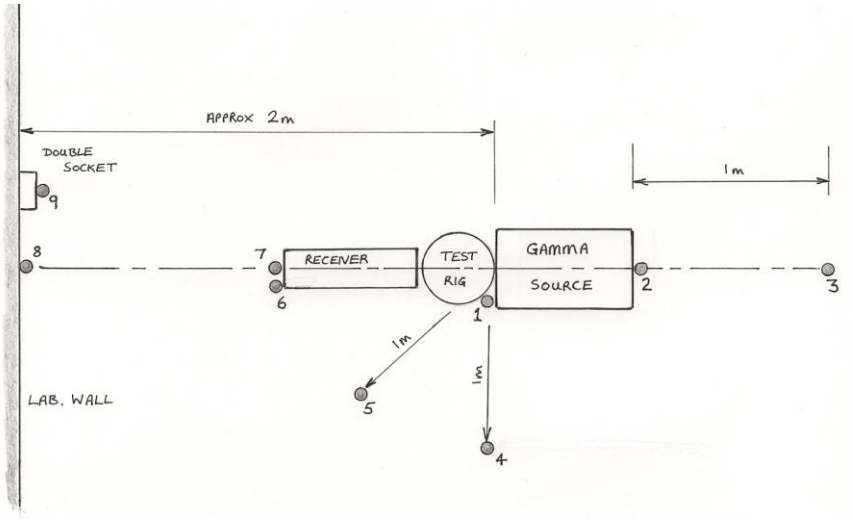

Figure 3-11 Radiation Level Measurement Locations

First the background radiation level, taken in the centre of the lab, was <0.2 µSv/hr. Then additional readings were taken around the installation with the source open and close. The results are summarised in Table 3-5.

Table 3-5 Radiation Level Measurements in µSv/hr

Shutter Position	Location								
	1	2	3	4	5	6	7	8	9
Source Closed	0.5	2.0	0.25	N/A	N/A	N/A	N/A	N/A	0.15
Source Open	18.0	2.0	0.25	0.3	0.8	2.0	12.0	2.0	0.7

The unit of effective dose is the Sievert (Sv). The permitted exposure level for an employee is up to 7.5 µSv/hr (with exceptions) for an 8 hour day. The maximum

effective dose for radiological workers is set at 20 mSv per year (whole body dose). This figure is averaged over a 5-year period and no single year can exceed 50 mSv. The installation radiation levels and control measures met the Environment Agency and Health Protection Agency criteria. Yet, personal thermoluminescent dosimeters (TLD) were worn at all time in the laboratory to record exposure when working with the densitometer thereby ensuring that personnel exposure did not breach the specified limits. These dosimetry badges are subsequently sent to a special laboratory for analysis every three months and the results kept for 50yrs.

3.3.2.5 Signal Characteristics

In gamma ray detection systems, measurement time is very important due to the random and discrete nature of radioactivity. As a result, gamma count values are affected by statistical fluctuations (Thiyagarajan *et al*, 1991). These changes in value can be ameliorated by longer measurement periods. That is the longer the measurement time the lower the statistical errors. The signal characteristics of the gamma densitometer has been analysed in order to determine the optimal data collection period. Blaney (2008) stated that taking a measurement time of 20 minutes for static fluid test will enable sufficient stabilisation in the mean gamma count values (±0.01% change in the mean) representative of the fluid condition. Whereas for dynamic flow in steady state, he found that the time taken to attain a stable value (±0.015% change in the mean) is relatively low for low GVF data points (16 minutes for a GVF of 23%); whereas, high GVF data points required a longer time to establish the prescribed level of stability (35 minutes for GVF of 89%).

Since the high-energy (hard) gamma count was less subjected to statistical fluctuation due to its narrower window range and larger transmission rate when compared with the low-energy (soft) gamma count, it was exploited in subsequent statistical analyses of the signals.

For this present work, a measurement time of five minutes was adopted for all experiments in 50.8mm test rig due to test rig availability, time constraints and the sheer volume of experimental test points to be covered. In addition, a ±0.2% change in the mean of the gamma count in five minutes was deemed to be a sufficient stabilization for experimental purposes (see Figure 3-12 and Figure 3-13).

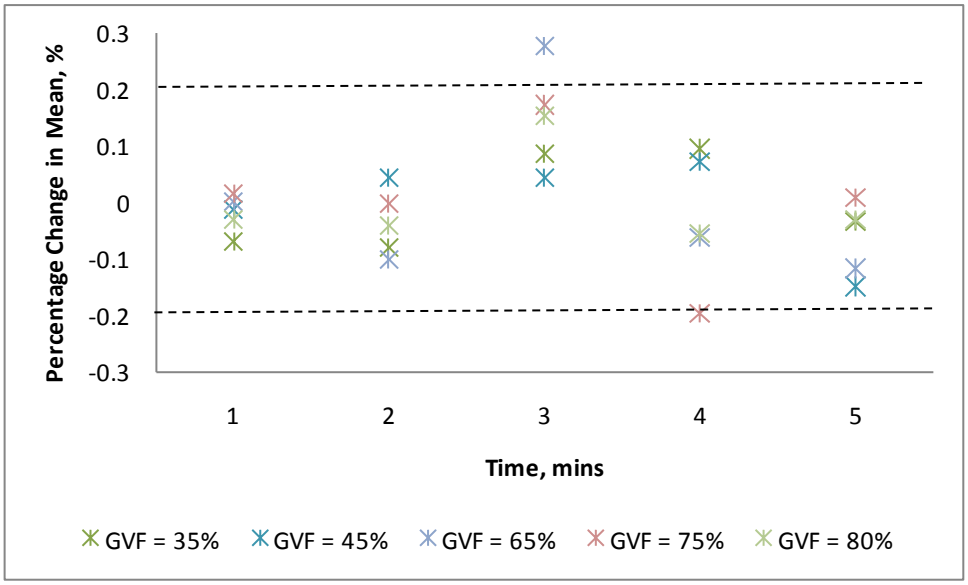

Figure 3-12 Hard Energy Count Stability for Horizontal Multiphase Flow Tests

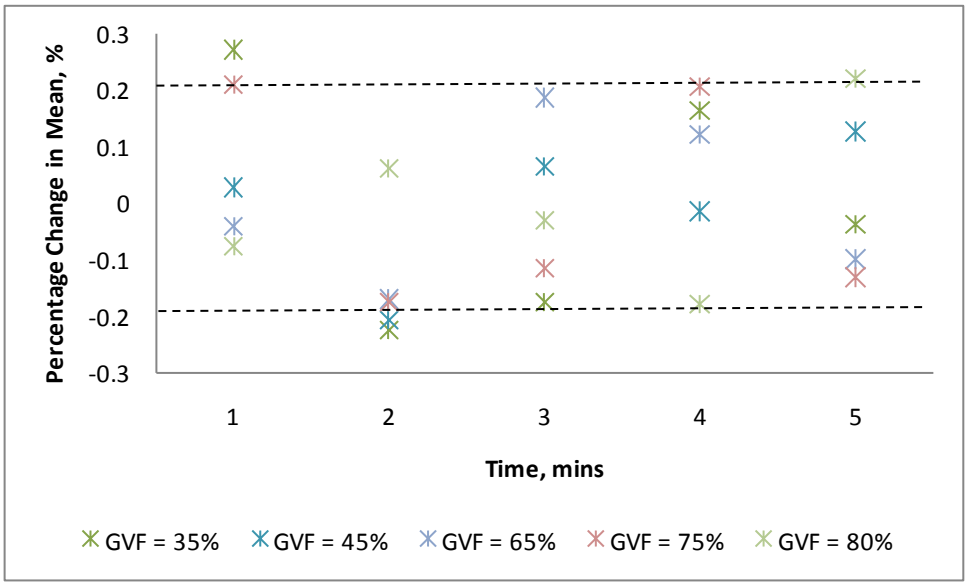

Figure 3-13 Hard Energy Count Stability for Vertical Multiphase Flow Tests

3.4 Test Matrix

The operation of the Cranfield multiphase test facility is automated. Further details of the operating procedure can be found in Cao and Yeung, (2009). This facility was operated in two different modes:

I. Air was injected at the riser base.

II. Air was delivered into the flow loop at the mixing section.

From the above configuration, the entrance effect on the flow patterns in vertical riser and their transition could be studied. The desired flow rates are set through the DeltaV plant management system. The real time graphical display of the DeltaV system allows the user/operator to closely monitor the parameters until the targeted set point is achieved. For each test condition, a waiting time of ten minutes was established in order to allow the flow to stabilise after which data collection was started. The data acquisition duration for each experimental run was five minutes at a frequency of 1 Hz, 100 Hz, and 250 Hz for Delta V, LABVIEW, and Neftemer data acquisition systems respectively.

The test conditions are given in terms of the superficial gas and liquid velocities and water cut. The gas velocities were corrected for pressure and temperature to account for conditions at the test sections. The difference between the water and oil phase velocity was assumed to be negligible, thus their velocities were represented by a common total liquid velocity. Air-water, air-oil, and oil-water two phase flows and air-oil-water three phase flow conditions employed in the study are summarised below.

3.4.1 50.8mm Flow Loop

A total of 372 test runs were conducted covering a range that is typical of operating conditions in the oil and gas industry. Table 3-6 and Table 3-7 summaries the ranges of the experimental parameters covered.

Table 3-6 Horizontal Configuration Experimental Range

Parameters	Range
Gas Superficial Velocities, m/s	0.27 – 11.59
Oil Superficial Velocities, m/s	0.61 – 2.75
Water Superficial Velocities, m/s	0.10 – 3.47
Water Cut, %	0 – 100
Pressure, barg	2.32 – 6.21
Temperature, ˚C	17.30 – 33.07

Table 3-7 Vertical Configuration Experimental Range

Parameters	Range
Gas Superficial Velocities, m/s	0.76 – 27.70
Oil Superficial Velocities, m/s	0.61 – 2.75
Water Superficial Velocities, m/s	0.10 – 3.47
Water Cut %	0 – 100
Pressure, barg	1.02 – 2.77
Temperature, ˚C	17.30 – 33.07

3.4.2 101.6mm Flow Loop

The air-water two phase experiments carried out in the 101.6mm diameter flow loop were mainly in the bubble, slug and churn flow regimes and consisted of 260 experimental data points with water superficial velocities from 0.12 to 0.85 m/s and gas superficial velocities from 0.15 to 3.09 m/s.

3.5 Chapter Summary

In this chapter, details of the Cranfield University Multiphase Test Facility have been presented. This facility is used for flow assurance, multiphase metering and control systems research. The two flow loops used in this study as well as the working fluids and their supply circuits were described. Details of instrumentation used were presented and how data were acquired from these instruments was discussed. The methodology adopted to perform experiments was discussed in detail, operating ranges defined and signal characteristics summarized.

Lastly, details of the procedures and equipment to measure and monitor radiation, assess risks and ensure the safety of the work area were presented. It was shown that the legal requirements on health and safety regulations in the management of radiation protection were fully met.

CHAPTER FOUR

4. EXPERIMENTAL RESULTS

The current chapter discusses the various results obtained from the Cranfield Multiphase test facility and a field data. They include flow pattern characterisation, flow regime maps and the effects of inlet conditions on three phase flows in the vertical riser. Also presented in this chapter are the evaluation of void fraction correlations (drift-flux model) against the experimental data, uncertainty estimation in phase fraction measurement, performance assessment of Coriolis and Gamma density measurements, phase inversion and analysis of a real field data.

4.1 Flow Pattern Characterization

The flow patterns described below were determined visually (where possible) and by the analysis of the probability mass function (PMF) from the raw signal of the gamma densitometer. PMF is a function that provides the probability for each value of the random variable. Mathematically, the probability mass function, $f(X)$ of a discrete random variable X is given by $f(X) = P(X = x)$ for all x.

The use of visual observation for determining flow patterns has the disadvantage of being subjective and can lead to differences in the interpretation of flow patterns. However, since each flow pattern had a characteristic signal trace, the use of PMF and raw signal analysis gives a simple quantitative means for the determination of flow patterns and was, therefore considered desirable (Kellessidis and Dukler, 1988; Mi *et al*, 2001; Blaney and Yeung, 2007; Ali, 2009).

Figure 4-1 shows the PMF plots generated from the gamma densitometer response to the flow behaviour at the top of the 50.8mm vertical riser at 20% water cut and 0.92 m/s superficial liquid velocity. In Figure 4-1 (a), there is a high proportion of low gamma counts because of the high fluid density, with a narrow band observed for counts between 180 and 220 caused by the passage of relatively small quantities of gas indicative of a bubble regime. As the superficial gas velocity is increased, the basic bubble flow PMF shape is conserved but a second peak starts developing, Figure 4-1 (b). This indicates a transition boundary between bubble and slug regime.

With the same liquid loading but a higher gas flow rate, the PMF geometry is distinctly different with a twin peak as shown in Figure 4-2 (a) and (b). A smaller proportion of the low counts are obtained which formed the dominant peak structure. The increased gas content enables a higher proportion of counts in the range of 180 to 240 and the formation of a second peak structure, Figure 4-2 (a). The reverse is the case with Figure 4-2 (b); here the more prominent peak is in the high gamma count range and a smaller peak in the low count region due to further increase in the gas flow rate. Two-peaked PMF have been shown to be characteristic of slug type flows with one peak representative of the passage of liquid slug body and the other, the gas dominated film body. Figure 4-3 (a) represents the PMF for a gas dominated multiphase flow. The PMF geometry is somewhat different from the previous one as the main peak is shifting towards the high count range. However, the liquid loading is still sufficient to produce a significant proportion of lower counts, giving rise to a second smaller peak. At a very high superficial gas velocity, a distribution showing a single dominant peak in the high count region (180 to 240) indicating a churn flow regime is observed, Figure 4-3 (b).

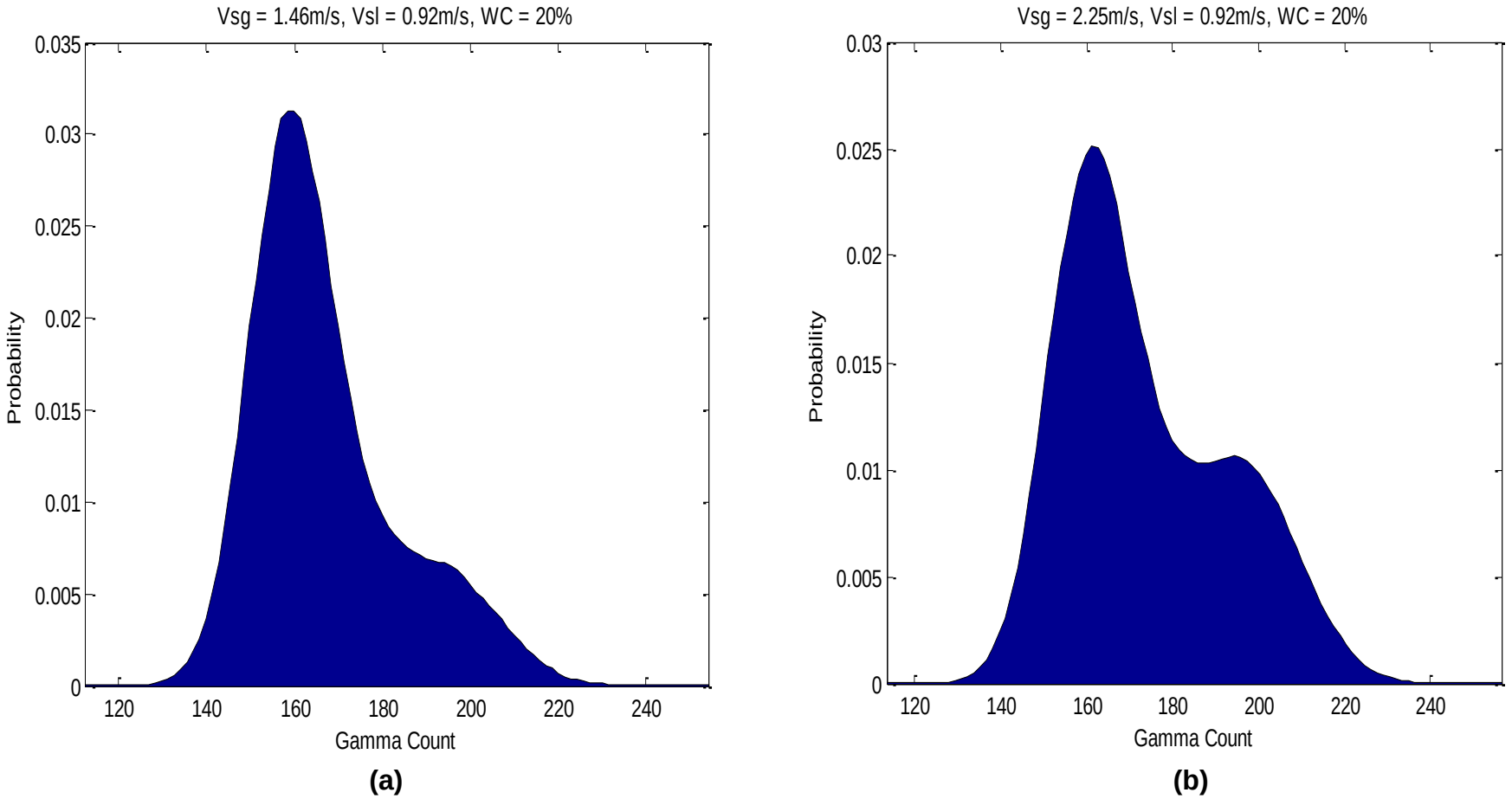

Figure 4-1 PMF Plots of the Gamma Densitometer Signals at a WC of 20% and Vsl = 0.92 m/s for (a) Vsg = 1.46m/s and (b) Vsg = 2.25m/s

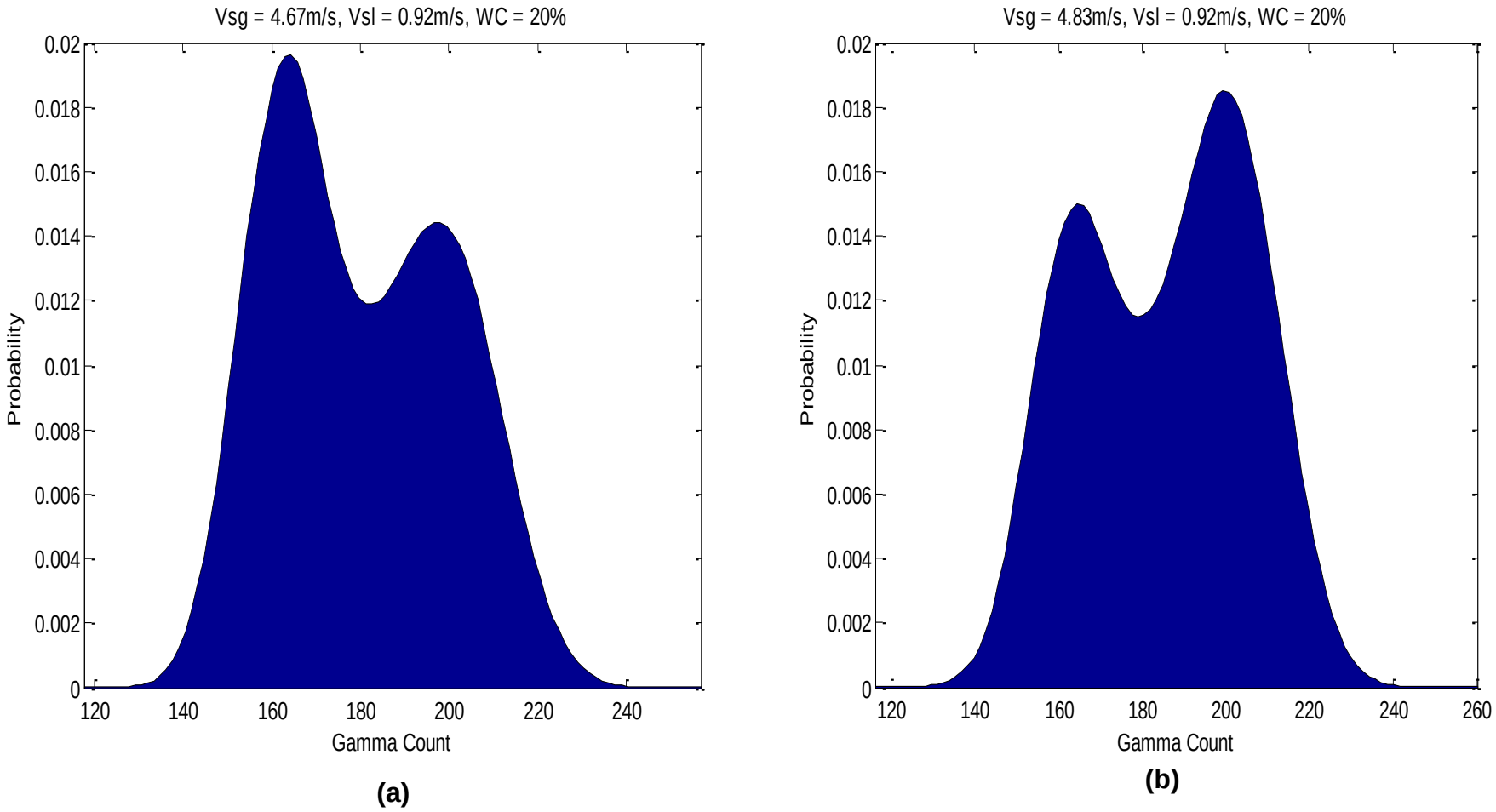

Figure 4-2 PMF Plots of the Gamma Densitometer Signals at a WC of 20% and Vsl = 0.92 m/s for (a) Vsg = 4.67m/s and (b) Vsg = 4.83m/s

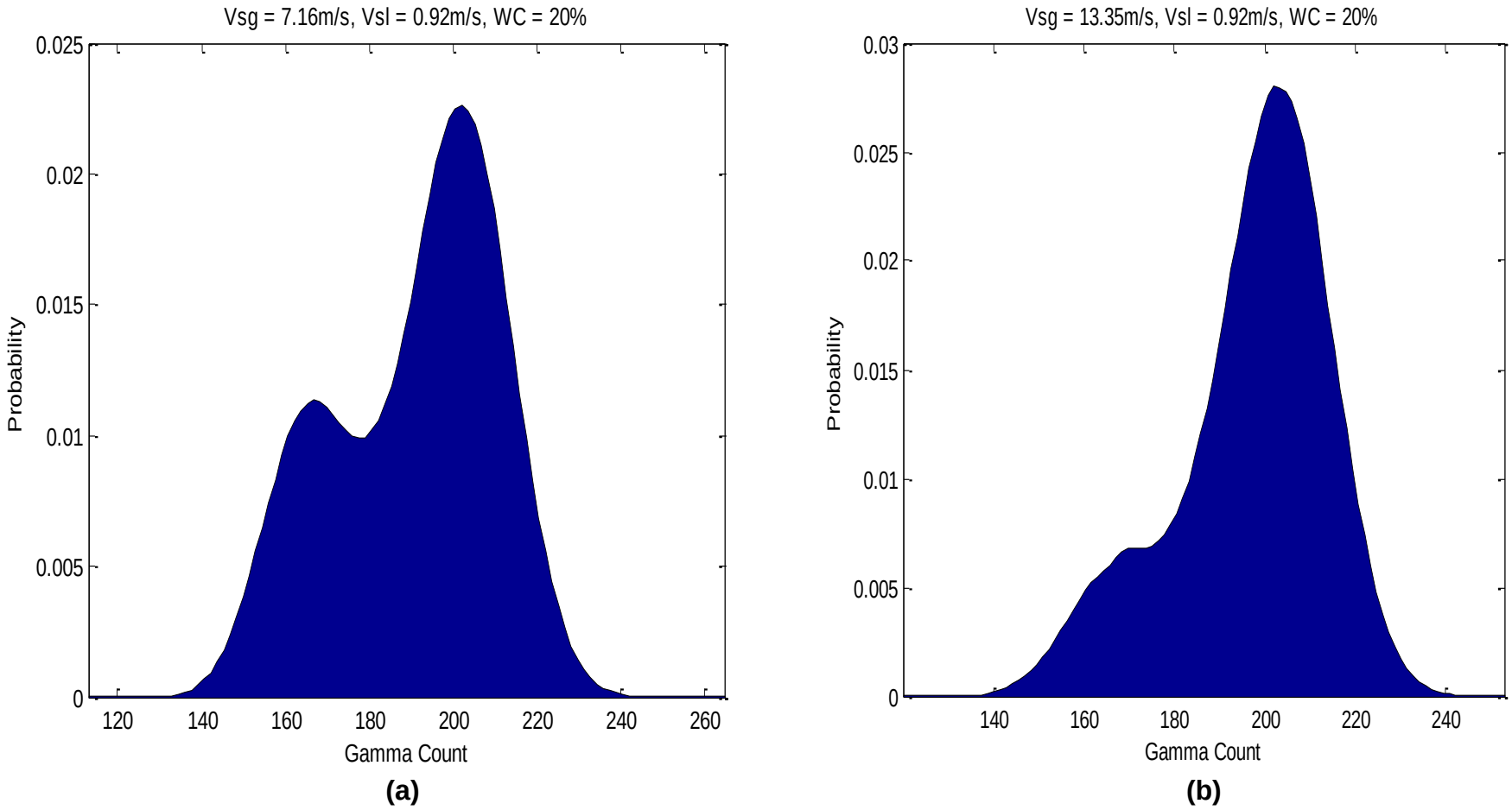

Figure 4-3 PMF Plots of the Gamma Densitometer Signals at a WC of 20% and Vsl = 0.92 m/s for (a) Vsg = 7.16m/s and (b) Vsg = 13.35m/s

Since the gamma densitometer installation location in the riser does not facilitate visual identification of flow regimes, the flow regimes classifications inferred from PMF and raw signal analysis were compared with the generic flow regime maps of Dykesteen *et al*, (2005). Though there are transparent sections in the riser for virtual observation. From the analysis of the full data and the void fraction PMF distribution, agreement with published flow regime maps was found to be good and gives a reliable indication of the test point flow regime. However, data points located near to the generic flow regime map boundaries exhibited properties of both bubble, slug and annular/churn flow regimes and could not be objectively classified.

4.2 Flow Regime Maps

The knowledge of pressure drop and stability characteristics of the flow in subsea flow lines and risers are important to the efficient operation of offshore production installations, and they depend ultimately on the flow regime that occur. Thus an important aspect of this work is the generation of the flow regime map.

Below are the flow regime maps plotted in terms of superficial gas and liquid velocities on the axes based on the void fraction PMF distribution of the gamma densitometer signals. The flow characteristics observed in this study are within bubble, bubble-slug transition, slug, slug-churn/wave transition and churn/wave flows. Comparing the horizontal and vertical experimental flow maps, it is interesting to observe that some test points that are identified as slug in the horizontal section of the flow loop were identified as bubble in the vertical section. This is as a result of hydrodynamic slugging effect and high riser base pressure in the horizontal, but as the mixture flows up the vertical riser, pressure is reduced and the air coalesce giving rise to bubbly flow. It was also observed that the transition boundary between slug and wave/churn were pretty the same for both the horizontal and vertical configurations, Figure 4-4. Similar behaviour is observed for air-water mixtures, Figure 4-5.

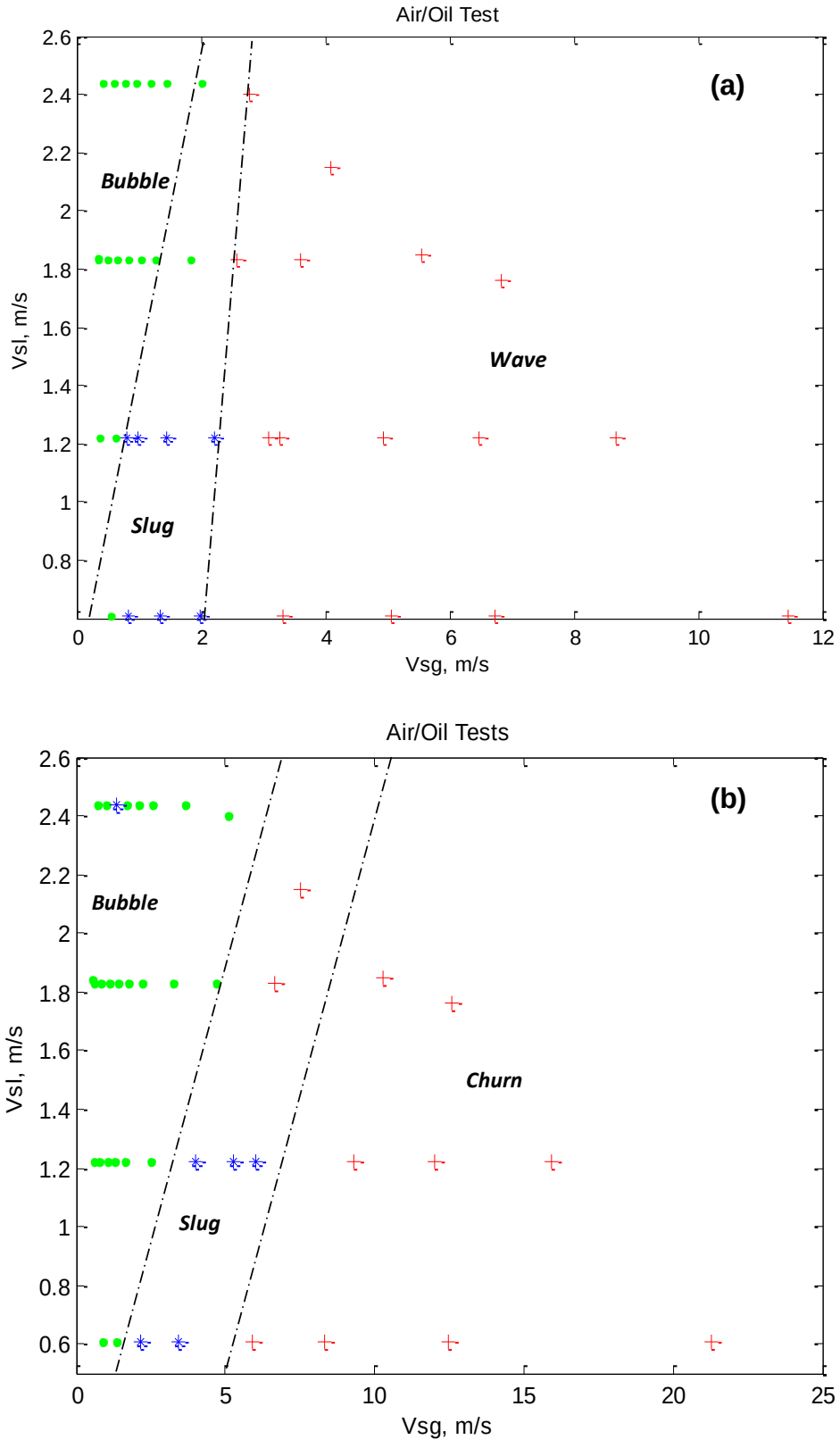

Figure 4-4 50.8mm Flow Loop Regime Maps for Air-Oil Two Phase Tests in the (a) Horizontal and (b) Vertical Configuration

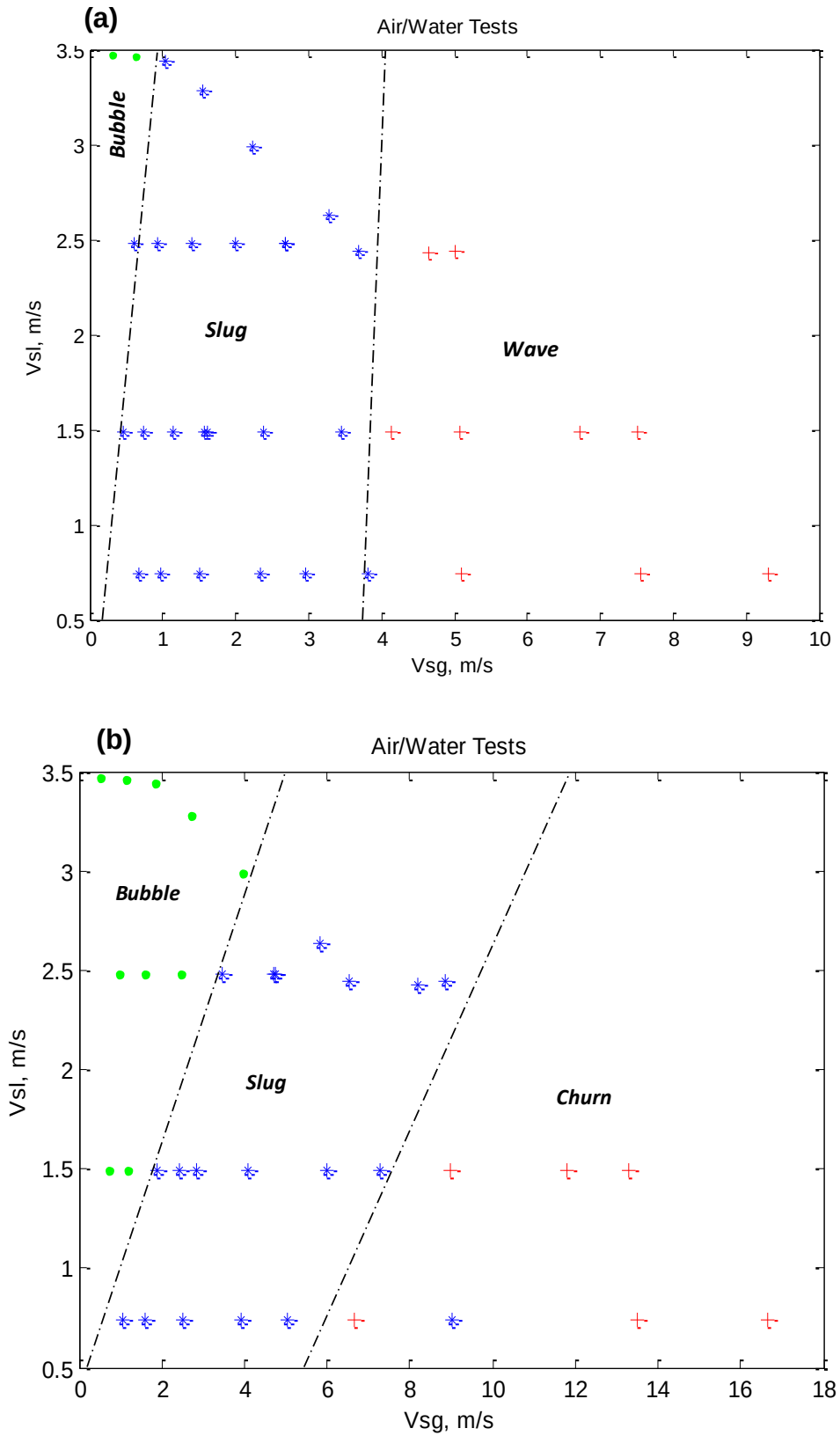

Figure 4-5 50.8mm Flow Loop Regime Maps for Air-Water Two Phase Tests in the (a) Horizontal and (b) Vertical Configuration

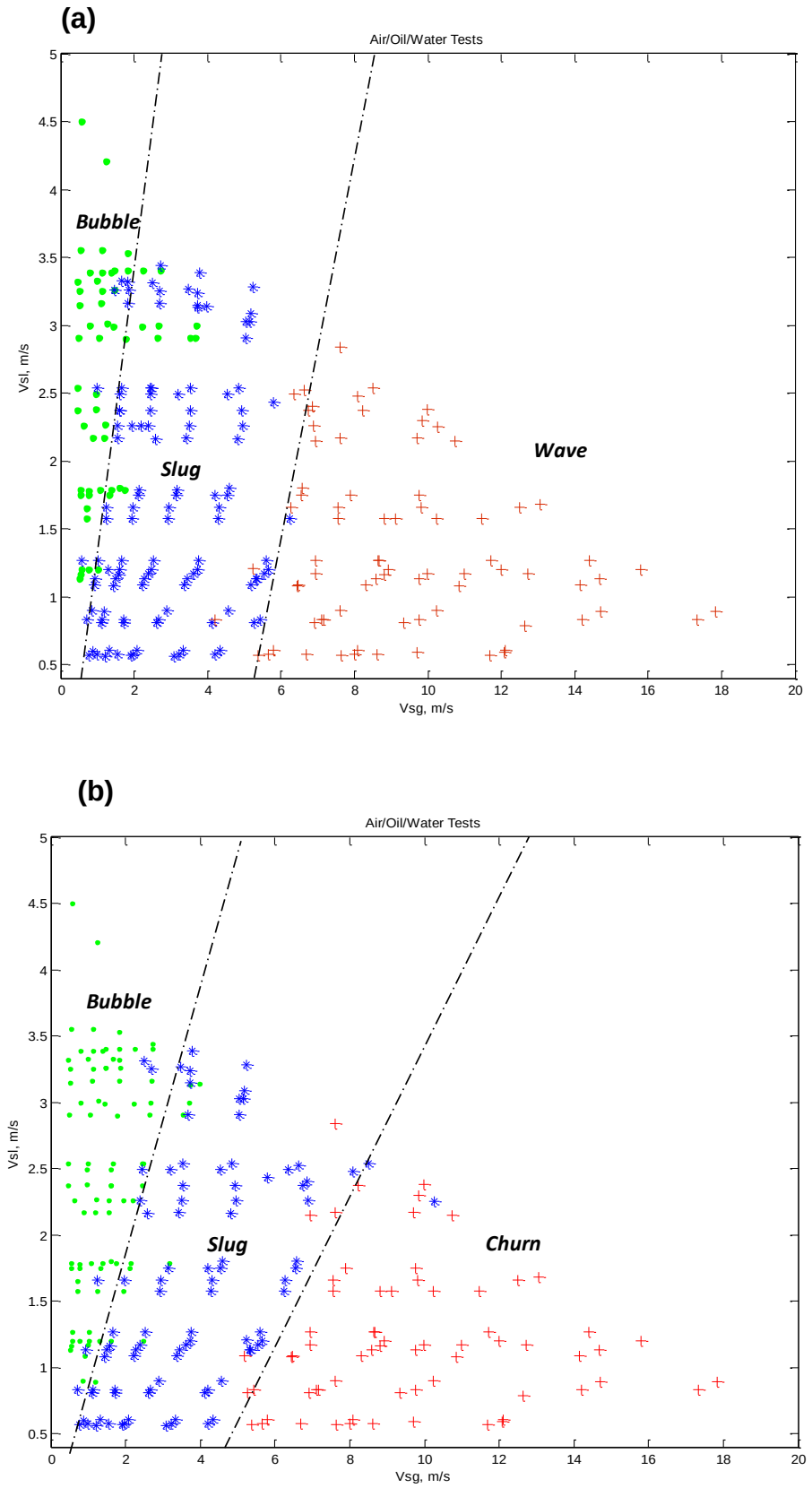

Figure 4-6 50.8mm Flow loop Regime Maps for Air-Oil-Water Three Phase Tests for WC of 10% – 95%in the (a) Horizontal and (b) Vertical Configuration

In three-phase stratified flows one can have a dispersed mixture of the immiscible liquid phases. Moreover, oil-based flow regimes bring a new variety of flow regimes that do not occur in water-based three-phase flow. This fact makes Açikgöz *et al* (1992) to propose new terminology for these flow regimes in an attempt to classify horizontal three-phase flow regimes.

In Figure 4-6, the vertical axes represent the total liquid (i.e. oil plus water) superficial velocity. The water cut ranges from 10% to 95% From this plots it is seen that the transition boundaries is quite different for both the horizontal and vertical pipes. This is attributed to the many possible transport properties of three-phase fluid mixtures in addition to pressure and hydrodynamic effects. The transition boundaries are very important regions of any flow regime map. In three-phase flows, transition boundaries exist at which there is a transition of the base fluid (that is the continuous phase) making the quantification of three-phase flow regime boundaries a challenging task. To this end, the plot presented in Figure 4.6 makes a good contribution to our understanding of horizontal and vertical three-phase flow regimes.

4.3 Effect of Air Inlet Condition on Flow Patterns in Vertical Riser

The examination of the effect of upstream conditions on flow patterns in the vertical riser was carried out as part of the objective of this work. The experiments were conducted with two different air inlet conditions, that is: (i) the upstream horizontal flowline mixing point and (ii) riser base gas injection in the 50.8mm test rig. In other words, the former corresponds to the introduction of air into the oil-water flow at the inlet of the flowline prior to the riser base whereas the later refers to the continuous injection of air directly at the base of the riser. Only selected results of the experiments under these two different inlet conditions are presented here.

The flow characteristics observed for the riser base gas injection condition at 0.46m/s superficial liquid velocity and 20% water cut were that of bubble flow whereas slug flow condition was observed when the same condition of gas was introduced upstream at the mixing section as can be seen from the shape of the PMFs in Figure 4-7. On increasing the gas superficial velocity from 1.55m/s to 2.34m/s at the same liquid loading, the flow pattern changes to what is referred to by some researchers as agitated bubbly flow or bubble to slug transition for the riser

base gas injection condition. However, a fully develop slug flow, depicted by two-peak PMF, was observed for the other gas inlet condition as illustrated in Figure 4-8.

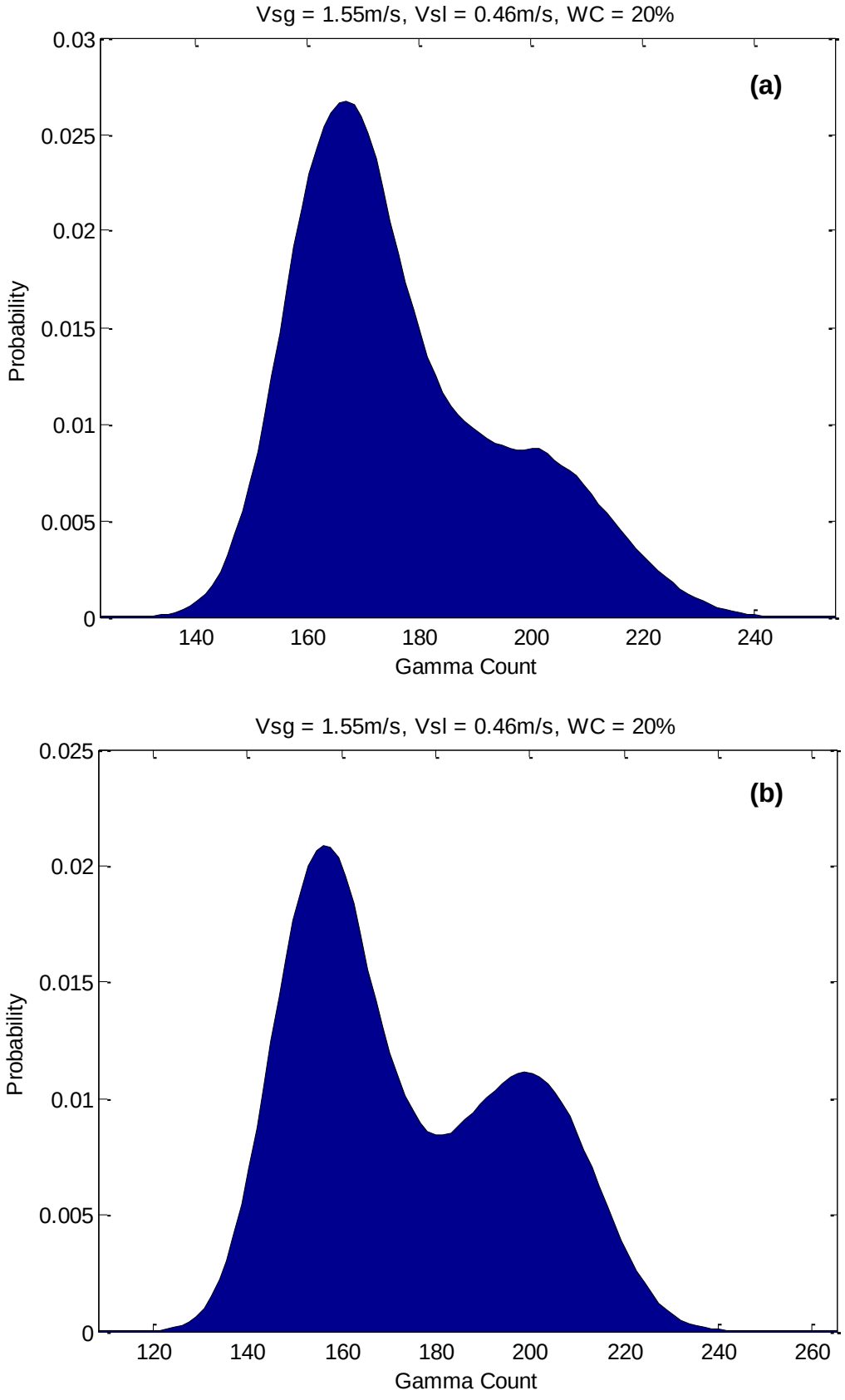

Figure 4-7 Gas Inlet Condition Effects at (a) Riser Base Injection and (b) Upstream Flowline Mixing for Vsg = 1.55m/s, Vsl = 0.46m/s and WC = 20%

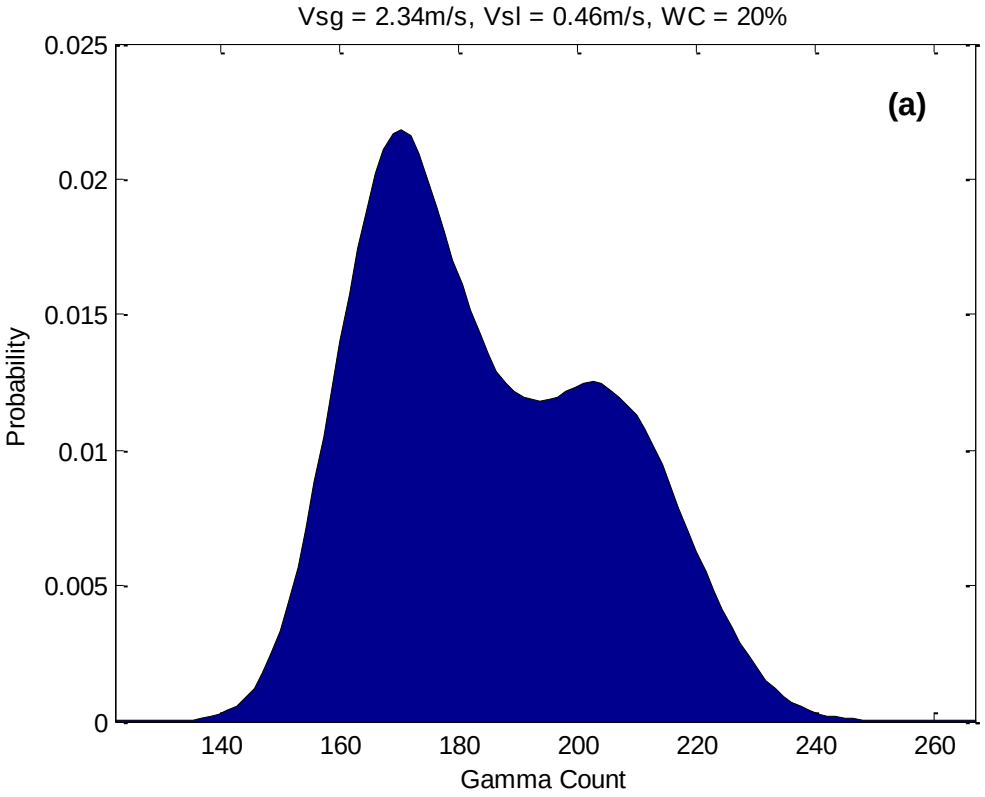

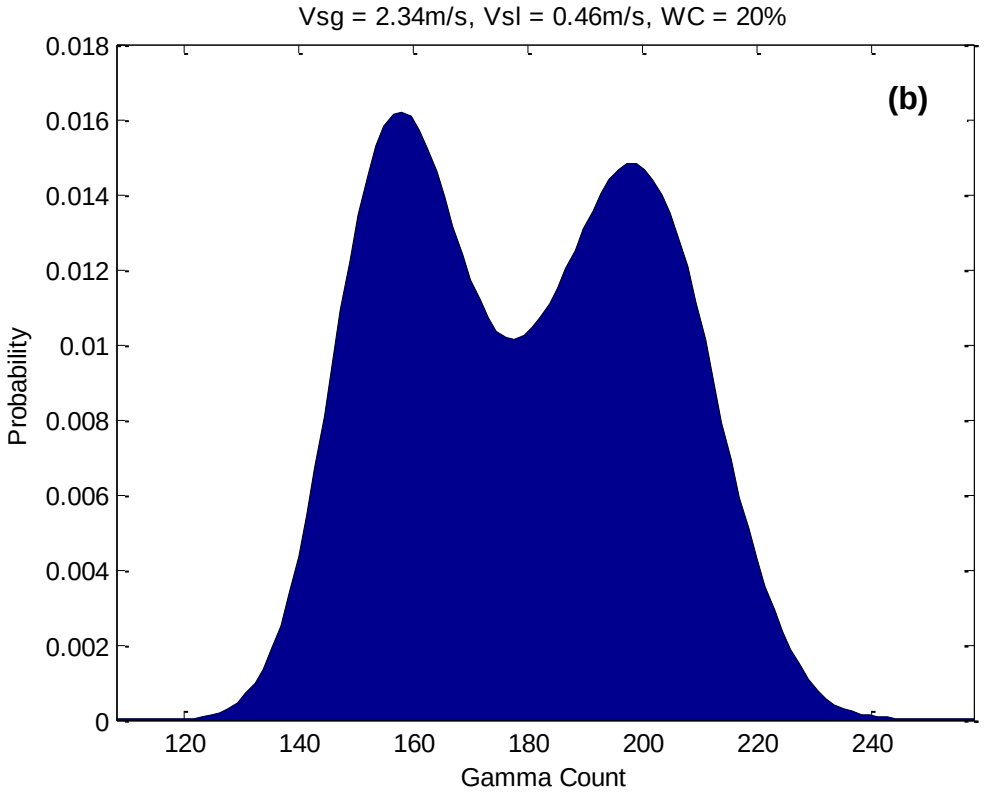

Figure 4-8 Gas Inlet Condition Effects at (a) Riser Base Injection and (b) Upstream Flowline Mixing for Vsg = 2.34m/s, Vsl = 0.46m/s and WC = 20%

Figure 4-9 to Figure 4-11 contain the probability mass function plots with (a) representing the riser base gas injection condition and (b) the upstream horizontal flowline mixing point at a higher liquid phase water cut of 40%. At low air superficial velocity (0.83m/s) a thin distinct peak in the low gamma count region implies the presence of smaller quantity of the gaseous phase or bubble flow, Figure 4-9. Upon increasing the air superficial velocity (1.40m/s) at this high water cut, a second peak begins to develop indicating an agitated bubble flow or bubble-slug transition (since the second peak is not fully developed) as can be seen from Figure 4-10. In these conditions the flow characteristics tend to transit toward slug flow regime as noticed from the broadening of the distribution due to large bubble sizes with increasing mixture density caused by the high water cut. This is attributed to a decrease in the effective viscosity with increasing water cut. Further increases in air superficial velocity (2.18m/s) transform the flow to developing slug for the riser base gas injection and a fully developed slug for the upstream horizontal mixing point as indicated by the twin peak distribution, Figure 4-11.

From the foregoing, it is deduced that no inlet conditions (that is riser base gas injection and upstream horizontal flowline mixing point) effects was observed at low gas throughput as similar flow pattern were encountered. However at higher air and water superficial velocities it was observed that the two inlet configuration exhibited dissimilar flow regimes, e.g., agitated bubble for one and fully developed slug for the other at the same experimental conditions. This dissimilarity is due to the effect of hydrodynamic slugging from the horizontal flowline influencing the vertical riser behaviour or some unstable processes in the flowline-riser system.

This finding shows that, for multiphase phase meters that are flow regime dependent, there will be some measurement implication. For example, in applications that utilizes gas-lift or gas injection, the location of the injection point will impact on the measurement results of a multiphase meter that is flow regime-dependent.

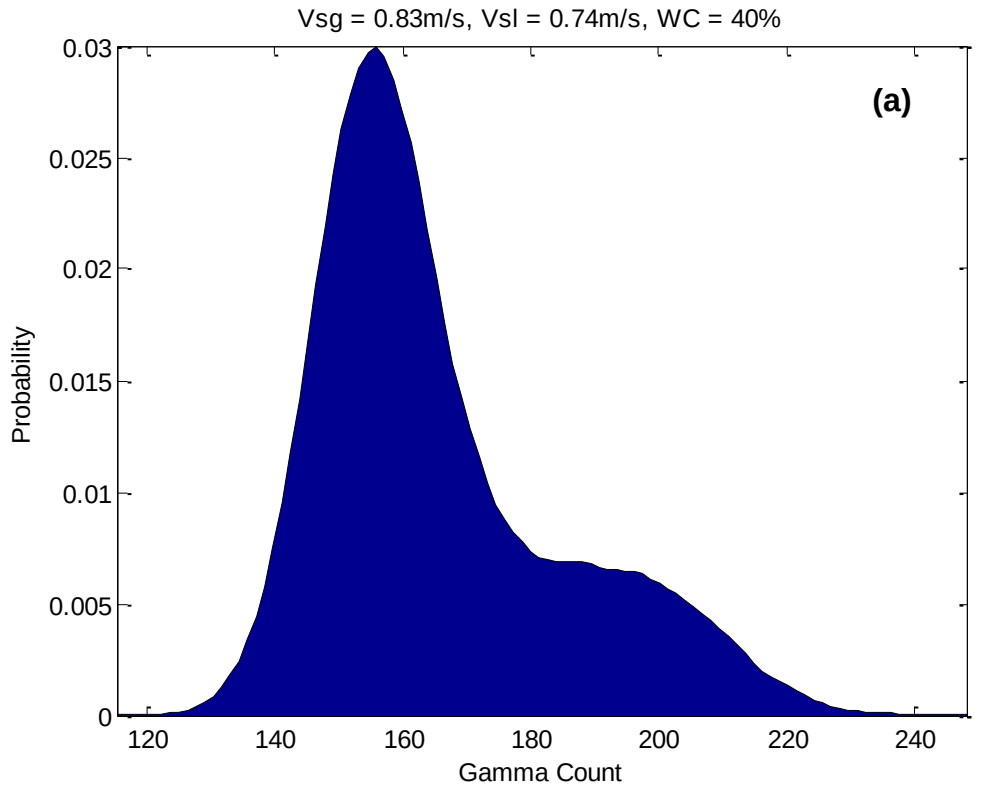

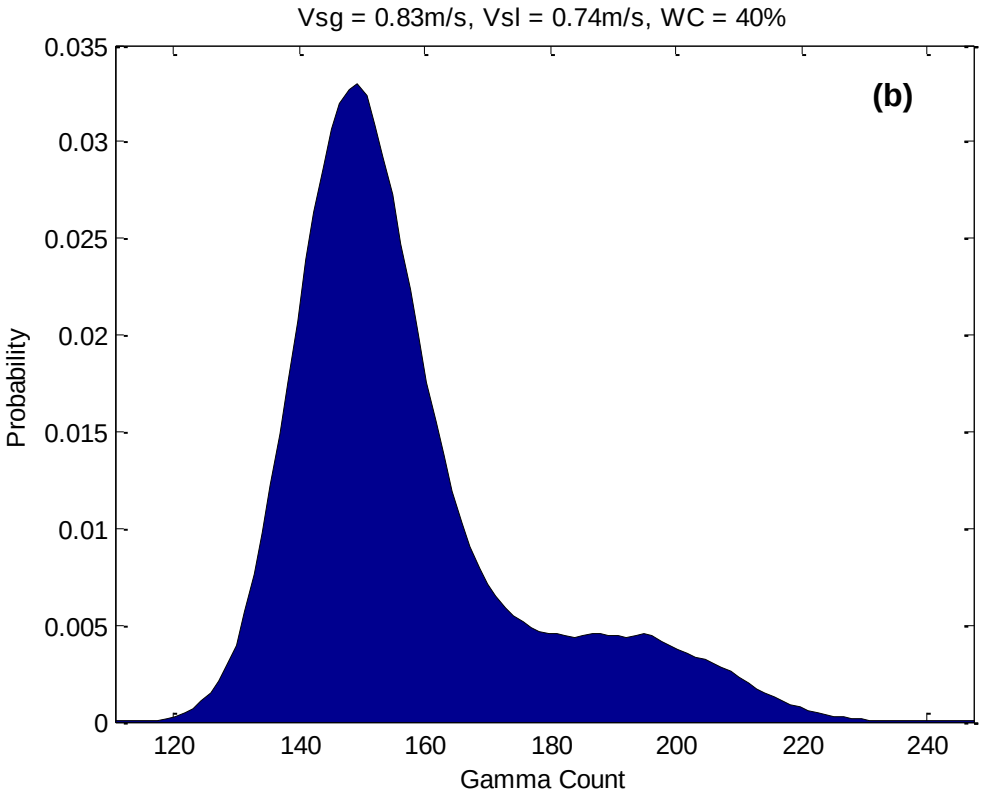

Figure 4-9 Gas Inlet Condition Effects at (a) Riser Base Injection and (b) Upstream Flowline Mixing for Vsg = 0.83m/s, Vsl = 0.74m/s and WC = 40%

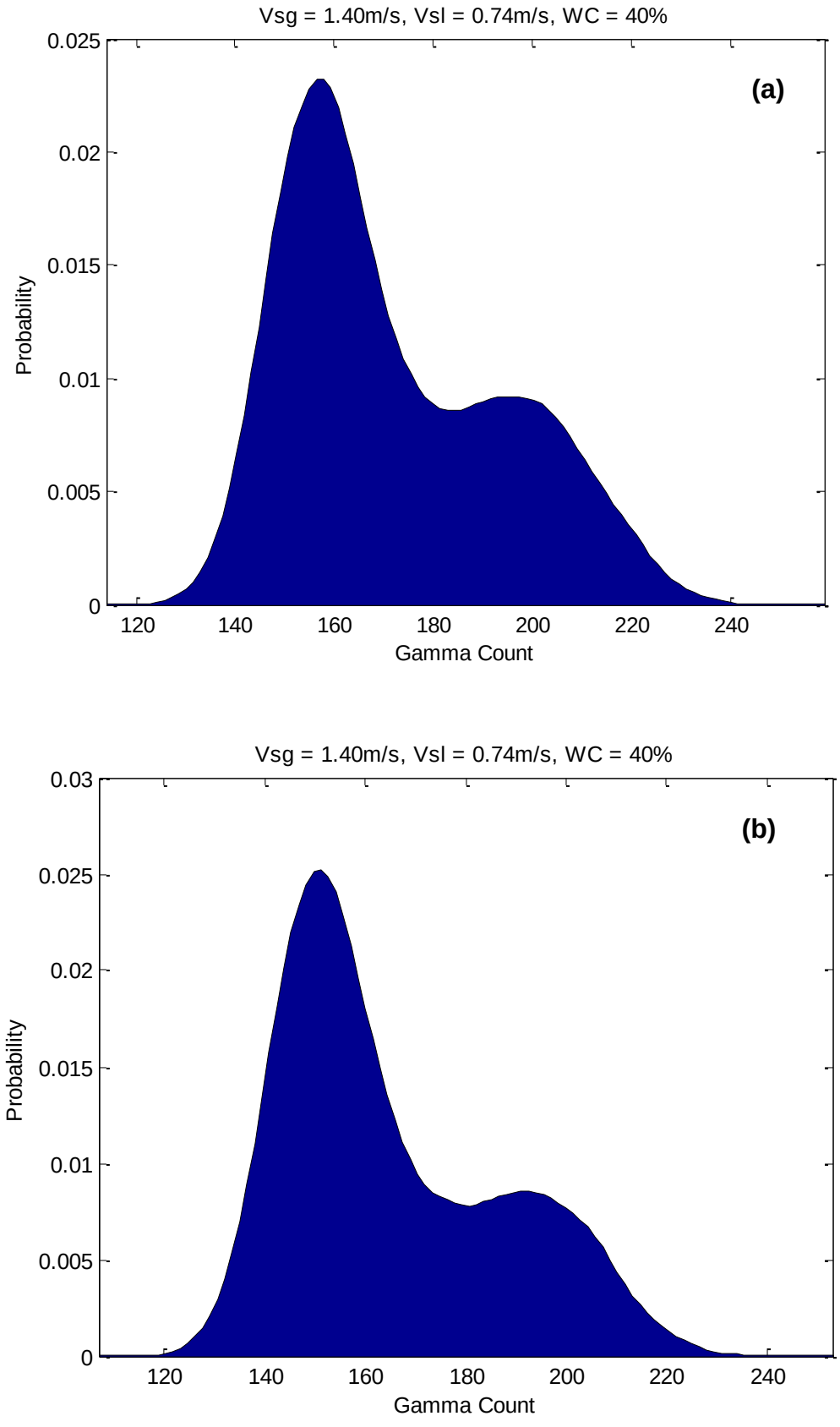

Figure 4-10 Gas Inlet Condition Effects at (a) Riser Base Injection and (b) Upstream Flowline Mixing for Vsg = 1.40m/s, Vsl = 0.74m/s and WC = 40%

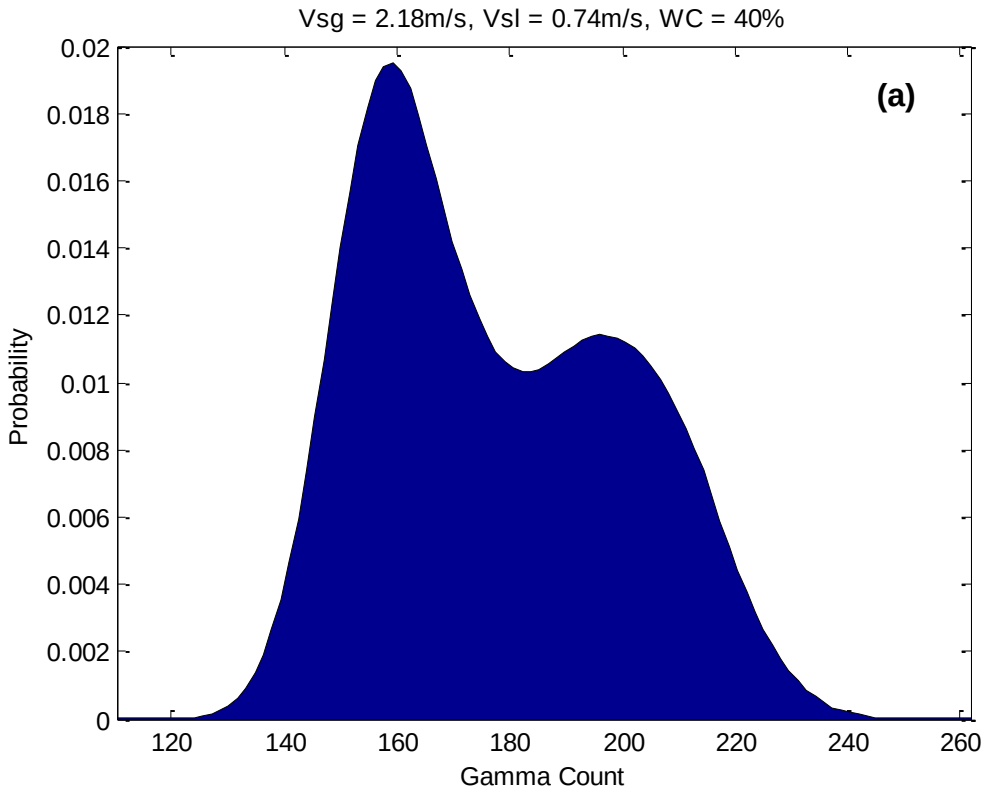

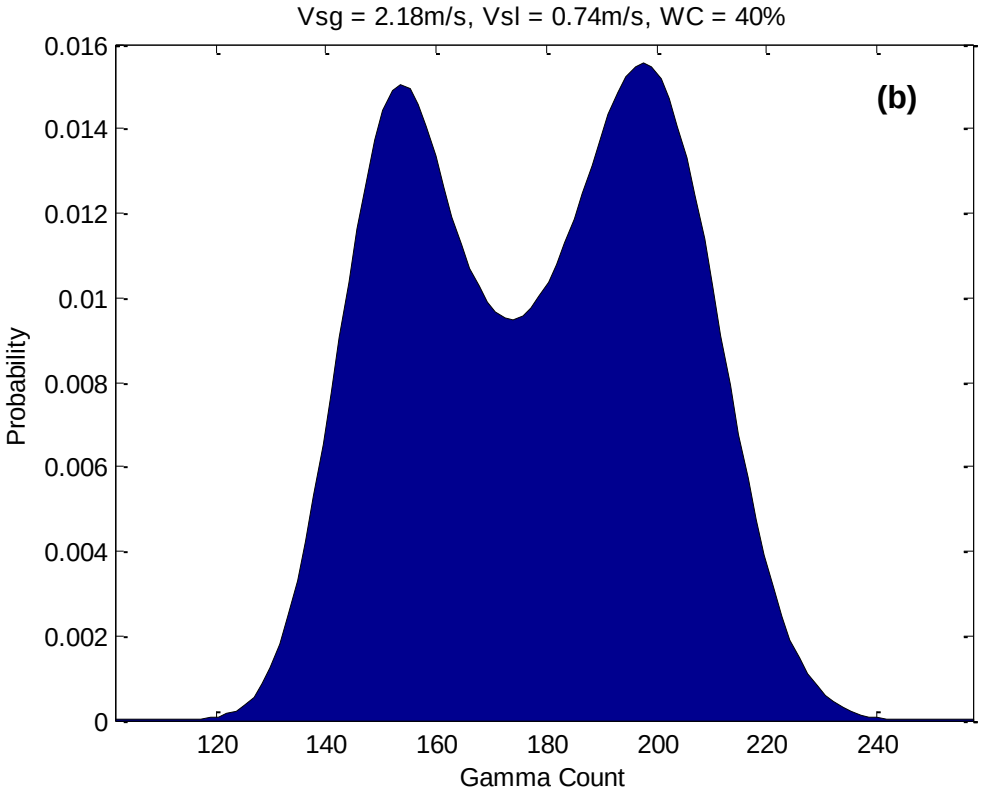

Figure 4-11 Gas Inlet Condition Effects at (a) Riser Base Injection and (b) Upstream Flowline Mixing for Vsg = 2.18m/s, Vsl = 0.74m/s and WC = 40%

4.4 Drift-Flux Model for Two-Phase Flow Analysis

The void fraction is an important variable in describing multiphase flows, as it is required to predict the heat and mass transfer coefficients and the pressure drop in a pipe. It also gives an indication of the prevalent flow regime. The purpose of this section is to correlate the measured void fractions from the gamma densitometer and to account for slip in the multiphase flow using the drift-flux model.

A general transient two-phase flow problem can be formulated by using a two-fluid model or a drift-flux model, depending on the degree of the dynamic coupling between the phases. The drift-flux model, which is an approximate formulation in comparison with the more rigorous two-fluid formulation, takes into account the relative motion between phases as a constitutive relation. Its ability to account for the slip between the fluids gives it an advantage over homogeneous non-slip models. This property allows the drift-flux model to represent different velocities of different phases flowing in the flowline or wellbore. Owing to its simplicity and applicability to a wide range of two-phase flow problems of practical interest, the drift-flux model is of considerable importance (Goda *et al*, 2003). In view of the practical importance of the drift-flux model for two-phase flow analysis, it has been studied extensively and utilized in solving many engineering problems involving two-phase flow dynamics (Hibiki and Ishii, 2003a; Hibiki and Ishii, 2003b). The model is found to predict such two phase characteristics like void fraction (Ali, 2009). On account of the importance of the drift-flux model in predicting two phase flow characteristics, the drift-flux parameters, which are the distribution parameter (C_o) and the drift velocity of the gas phase (U_g) were calculated for the air-oil and air-water two phase experimental data for both horizontal and vertical flows.

4.4.1 The Drift-Flux Relations

The drift-flux model, as proposed by Zuber and Findlay (1965), is based on the assumption that the mean void fraction occurring in two-phase gas liquid flows is as a result of two different phenomena. These are the radial heterogeneities (of void fraction and velocities) due to transverse forces, and the relative velocity between the phases, due to axial forces, (Guet *et al*, 2004). The effects of these two contributions are then taken into account by two parameters, i.e., the distribution pa-

rameter C_o and the drift velocity of the gas phase U_g. The drift-flux model is then given by:

— Eqn. 4.1

where V_{sg} is the superficial gas velocity, V_m is the average mixture velocity ($V_m = V_{sg} + V_{sl}$), α is the mean void fraction and U_g is the weighted mean drift velocity. The drift-flux model is often applied to predict the mean void fraction α from the known superficial gas and liquid velocities and by using appropriate models for C_o and U_g. The mean void fraction resulting from any given flow rates of gas and liquid has a direct relationship with the gravitational pressure drop ($\delta P/\delta z$) through the mixture density (ρ_m) as given by Equation 4.2 and 4.3.

Eqn. 4.2

— Eqn. 4.3

where g is the force of gravity.

The drift velocity can be defined by the slip velocity, V_{slip}, between the gas and the mixture is related to this slip velocity in the following way:

Eqn. 4.4

However the void-fraction weighted mean drift velocity, as used in the drift -flux model, is given by:

— Eqn. 4.5

where the symbol represents the void fraction weighting procedure applied to and represents the area-average value of . According to Guet *et al*, (2004) this average drift velocity is often taken as the rise velocity of a single bubble in an infinite medium, U_t. The slip velocity is generally correlated to the terminal velocity of a single bubble and the local void fraction.

From the literature, distribution parameter can range from 1.0 to 1.5 for bubbly and slug flow regimes (Alkaya, 2002). However, at high gas superficial velocities the flow becomes more homogeneous and the profile flattens out, resulting in (C_o) approaching 1.0. In other words, as the gas void fraction approaches 1.0 (C_o) must approach 1.0.

Figure 4-12 to Figure 4-15 is a plot of V_{sg}/α against V_m showing the results for the individual flow regime for air-water and air-oil experiments in the vertical as well as the horizontal orientation. The distribution parameter (C_o) and the drift velocity of the gas phase (U_g) are flow regime dependent, so data plotted for each of these are according to the flow regime as predicted by the probability mass function plots discussed earlier. From these plots, the y-axis intercept represent the drift velocity of the gas phase (U_g) whereas the slope of the best-fit line represents the distribution parameter (C_o). The drift velocity of the gas phase (U_g) is the local relative velocity effect while the distribution parameter (C_o) quantifies the degree of flow uniformity since it represents the global effect due to radial non-uniform void and velocity profiles.

A curve fitting method is then used to obtain approximate values of (C_o) (the slope of these plots) and (U_g) (the intercept of these plots) from the experimental data.

Table 4-1 Experimental Drift-Flux Parameters for Different Flow Regimes in Vertical Flows

Flow Regime	Bubble	Slug	Churn
Air-Water Experiments			
Distribution Parameter, C_o(-)	0.989	1.123	1.049
Drift Velocity, U_g(m/s)	2.061	0.866	1.482
Air-Oil Experiments			
Distribution Parameter, C_o(-)	0.993	1.049	0.989
Drift Velocity, U_g(m/s)	1.964	1.132	2.127

Table 4-2 Experimental Drift-Flux Parameters for Different Flow Regimes in Horizontal Flows

Flow Regime	Bubble	Slug	Wave
Air-Water Experiments			
Distribution Parameter, C_o(-)	3.138	0.934	1.155
Drift Velocity, U_g(m/s)	-9.723	0.251	-0.366
Air-Oil Experiments			
Distribution Parameter, C_o(-)	0.826	1.047	1.077
Drift Velocity, U_g(m/s)	0.676	0.289	-0.049

The values for the distribution parameter (C_o) and the drift velocity of the gas phase (U_g) obtained from Figure 4-12 to Figure 4-15 are presented in Table 4-1 and Table 4-2 for vertical and horizontal flows respectively.

From Figure 4-12(a) and Figure 4-13(a), it observed that all the data points for bubble flow regime in both air-water and air-oil tests do not lie on a straight line. This behaviour is consistent with the work of Hibiki and Ishii (2003a) for 50.8mm diameter vertical pipe experiments in which they suggested that the scatter in the data points is as a result of the turbulence caused by the bubbles being dominant and influencing the flow field. Similar behaviour is also seen in the horizontal air-oil tests for this flow regime while for the air-water horizontal tests (see Figure 4-14(a)) the extremely limited data (just two data point) for this flow regime makes the plot appear to be in a straight line, and Figure 4-15(a). For the vertical flow at higher and intermediate mixture velocities, it can be seen that the data points tend to converge into a straight line for all the flow regimes as shown in Figure 4-12(b&c) and Figure 4-13(b&c). Ali (2009) suggested that this behaviour, which is also found in large diameter upward flow, is due to the insignificant recirculation and similar drift velocity among all the flow regimes. In other words, a total suppression of localised recirculation with increased superficial gas velocity. In the case of the of the slug and wave flow regime for the horizontal flow, the data does not lie on a straight line, Figure 4-14(b&c) and Figure 4-15(b&c). These results is consistent with the findings of Franca and Lahey Jr (1992) wherein they showed that horizontal two-phase flows can be well-correlated using the drift flux model.

According to Franca and Lahey Jr (1992), the drift velocity in vertical flows results from a balance between the local interfacial drag and the buoyancy on the dispersed phase. This is not the case for horizontal flows. The drift velocity in these flows is related to the phase distribution and to the local slip resulting from the lateral and axial pressure gradients. Thus the drift velocity can be significant as seen from Table 4-2 (bubble and slug regime) and as such should not be ignored even when the buoyancy effects are negligible. Moreover, in separated horizontal flows the structure of the interface determines the drift-flux parameters (Franca and Lahey Jr, 1992). Thus it is seen that for horizontal flows the drift velocity is not normally zero as was erroneously assumed by many previous authors.

The results of this current study were compared with the previous drift flux studies conducted on vertical and horizontal small diameter pipes and detailed in Table 4-3.

Table 4-3 Comparison of Drift Flux Parameters

	Franca and Lahey Jr (1992)		Hibiki, T. and Ishii, M. (2003a)		Hibiki, T. and Ishii, M. (2003a)		Current Work	
Internal Diameter (mm)	19		50.8		102		50.8	
Fluid	Air-Oil-Water		Various		Various		Air-Oil and Air-Water	
Pipe Orientation	Horizontal		Vertical		Vertical		Horizontal and Vertical	
Distribution Parameter, C_o (-)	Plug	≈1	Bubbly	1.19	Bubbly	1.18	Bubbly	0.99*; 0.83[a]
	Slug	1.2	Slug	1.19	Slug	1.18	Slug	1.05*; 1.05[a]
	Wave/ Annular	≈1	Churn	1.19	Churn	1.18	Churn/ Wave	0.99*; 1.08[a]
Drift Velocity, U_g (m/s)	Plug	0.16	Bubbly	0.12	Bubbly	0.12	Bubbly	1.96*; 0.68[a]
	Slug	-0.2	Slug	0.25	Slug	0.35	Slug	1.13*; 0.23[a]
	Wave/ Annular	0.2 (for V_{sl} = 0.005 m/s) 2.7 for (V_{sl} = 0.27 m/s)	Churn	0.23	Churn	0.23	Churn/ Wave	2.13*; 0.05[a]
** for vertical data and [a]for horizontal data*								

Since the drift-flux model relates the gas-liquid velocity difference to the drift flux (or 'drift velocity') of the gas relative to the liquid, it can be seen from Table 4-3 that, the drift velocities for the vertical flows are higher than that of the horizontal. This is due to slip. The drift velocities for both the vertical and horizontal flow generally decreases from bubbly to slug to churn/wave, thereby corroborating the fact that phase slip decreases at higher gas and liquid superficial velocities.

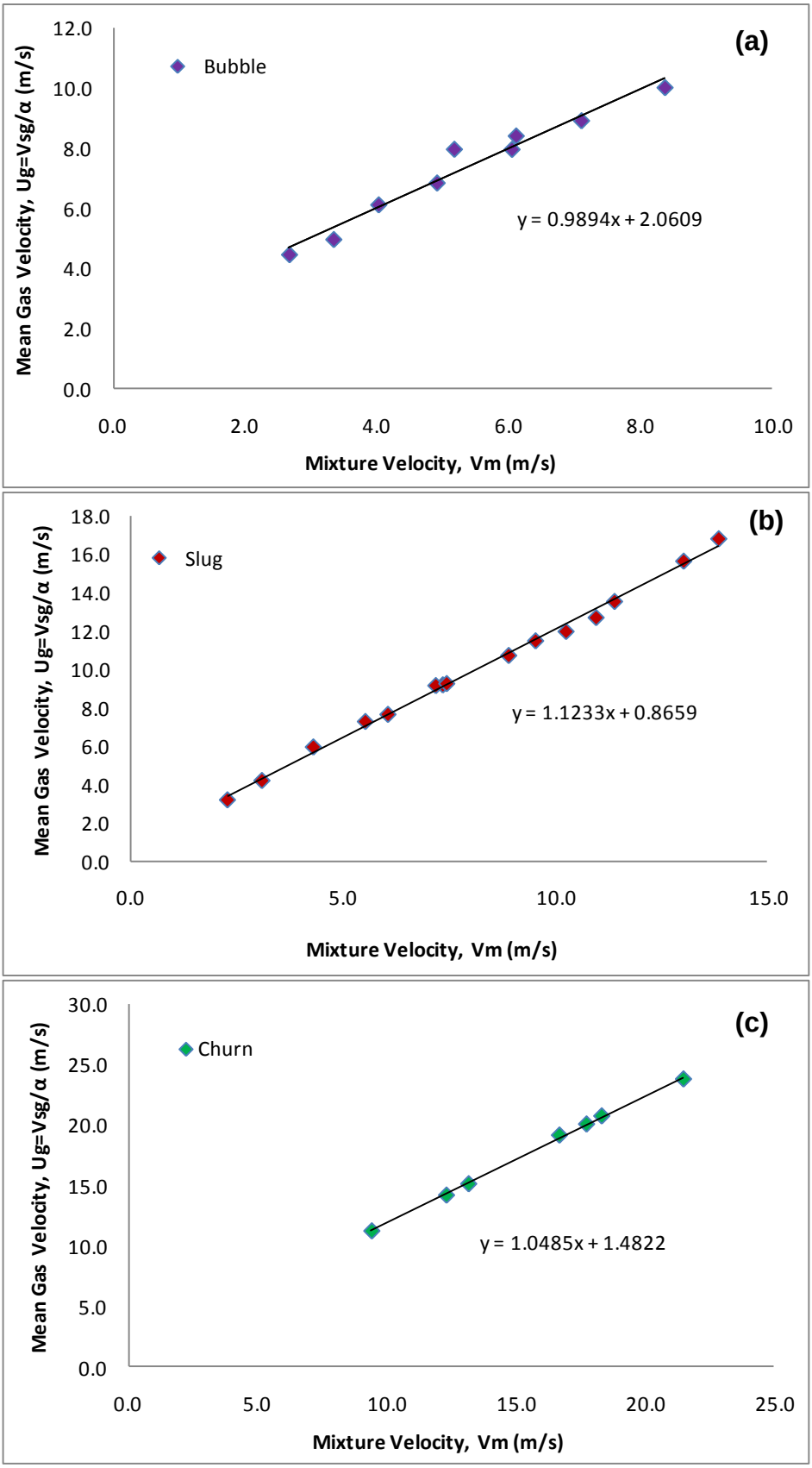

Figure 4-12 Experimental Drift-Flux Relationship in (a) Bubble Flow, (b) Slug flow and (c) Churn Flow Regimes for Air-Water Vertical Tests

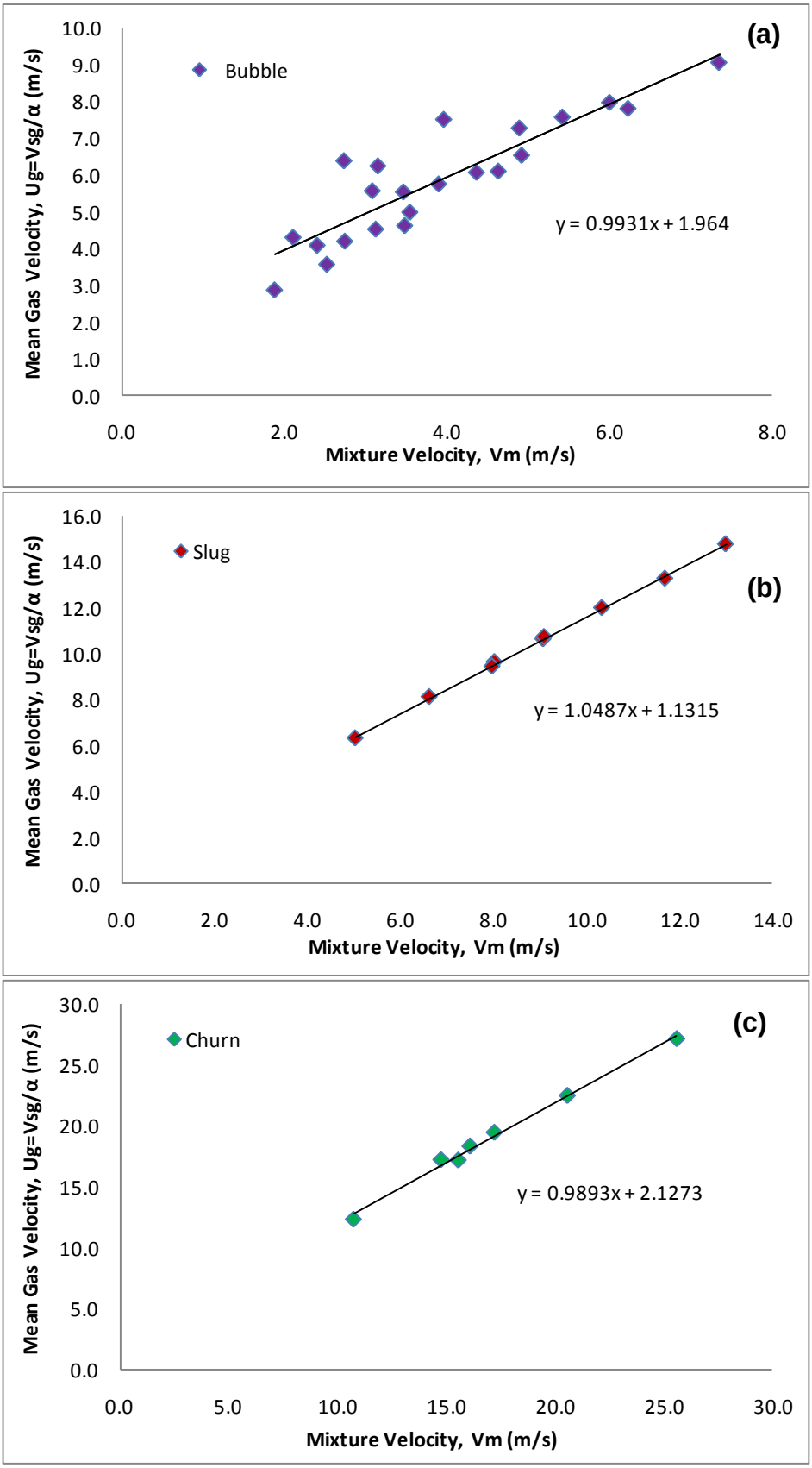

Figure 4-13 Experimental Drift-Flux Relationship in (a) Bubble Flow, (b) Slug flow and (c) Churn Flow Regimes for Air-Oil Vertical Tests

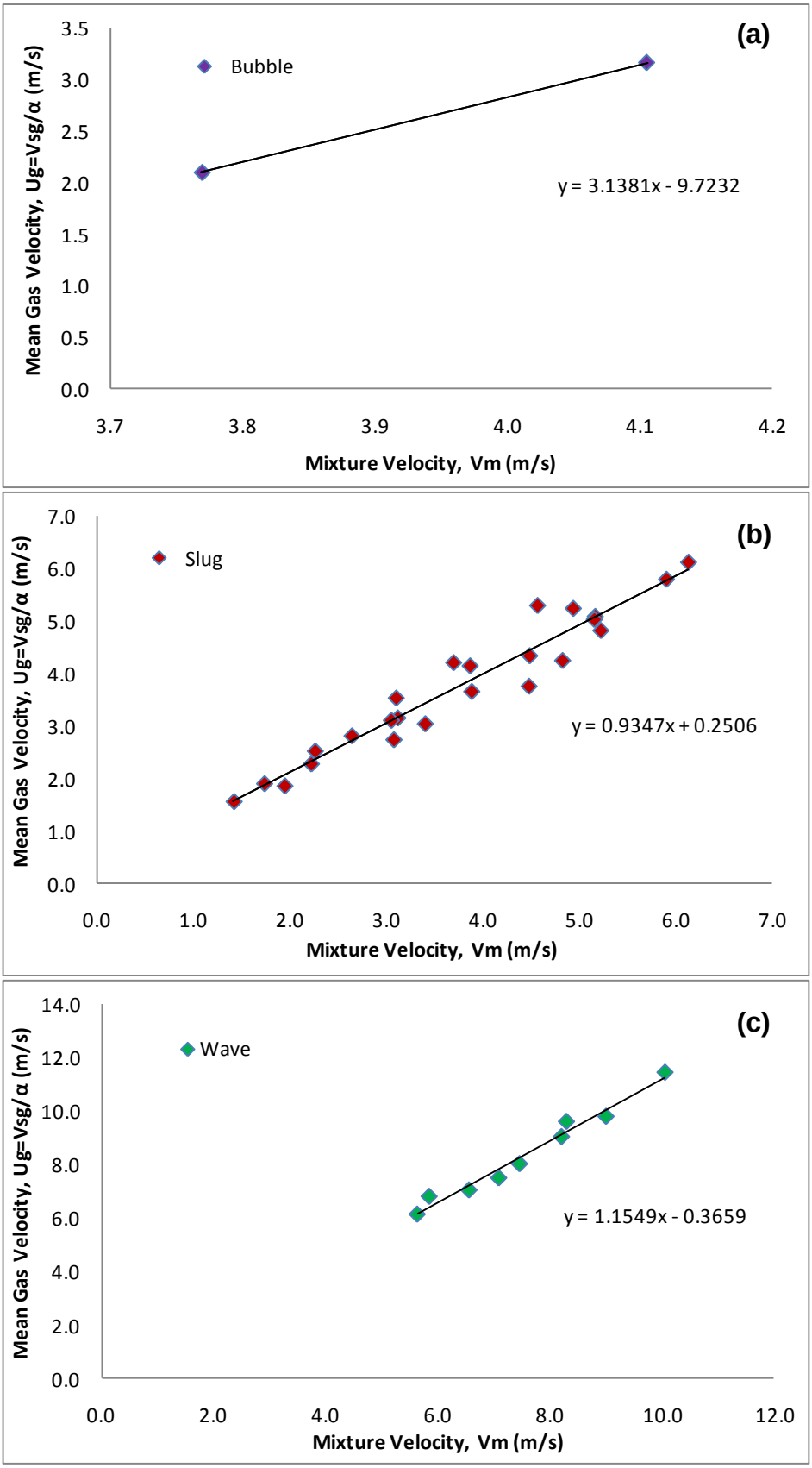

Figure 4-14 Experimental Drift-Flux Relationship in (a) Bubble Flow, (b) Slug flow and (c) Wave Flow Regimes for Air-Water Horizontal Tests

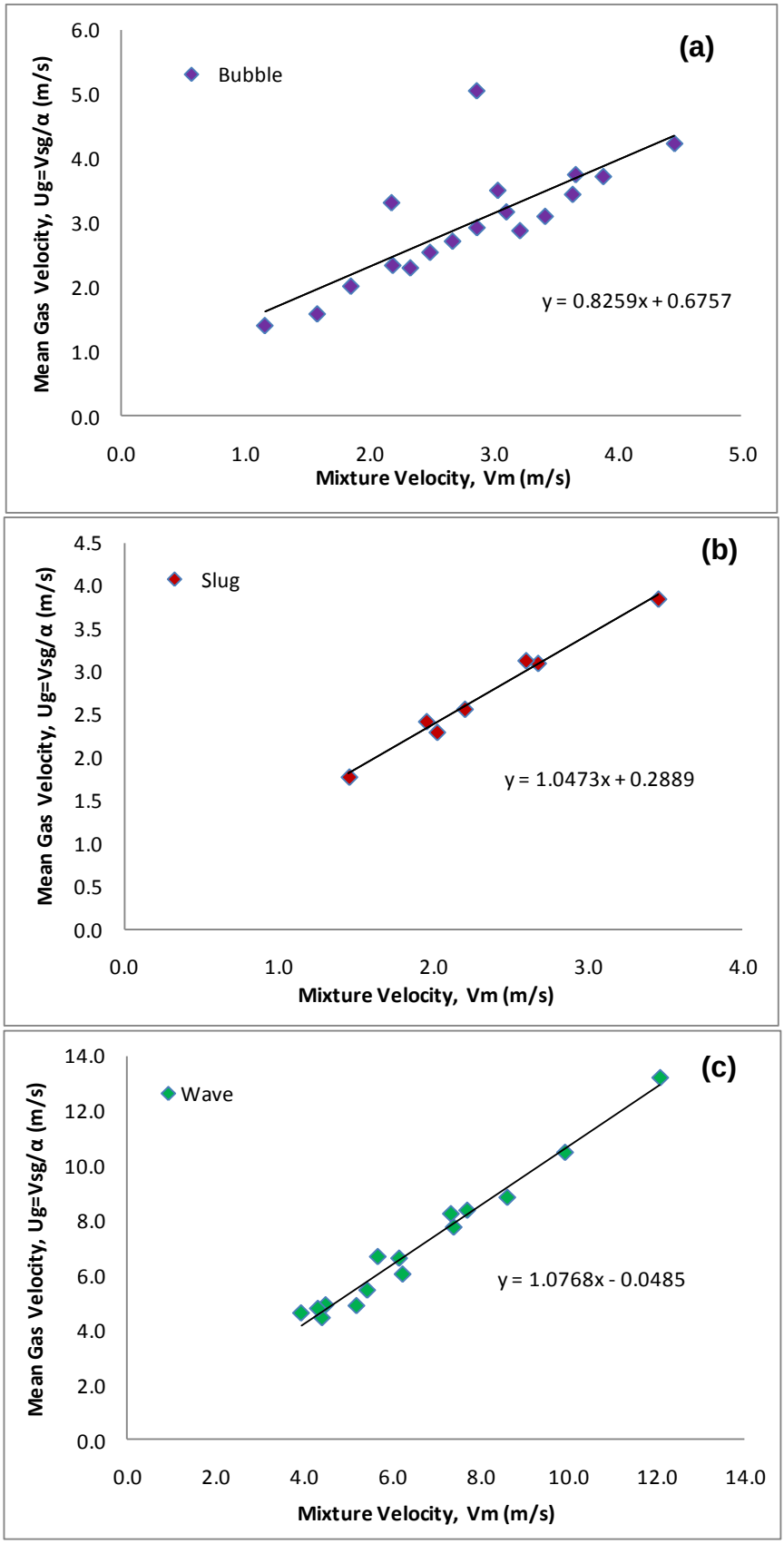

Figure 4-15 Experimental Drift-Flux Relationship in (a) Bubble Flow, (b) Slug flow and (c) Wave Flow Regimes for Air-Oil Horizontal Tests

4.5 Comparative Performance Assessment of Coriolis and Gamma Density Measurements

A comparative performance assessment study of the density measurement for the Coriolis meter and the gamma densitometer was conducted for both two and three phase flows in horizontal as well as vertical pipe orientation. The results are presented in this section.

4.5.1 Coriolis Density Measurements

The Coriolis meter shows a good response in terms of mixture density for liquid-liquid two phase and air-liquid three phase flows up to certain gas volume fraction (GVF). As expected, the mixture density decreases with increase GVF as can be seen from Figure 4-16 and Figure 4-17. It was observed from the data set that the horizontal orientation gave superior response when compare to the vertical.

Henry *et al* (2006) states that factors affecting Coriolis meter measurement errors are GVF, flow tube orientation, flow tube geometry, process fluid viscosity and other properties. The normalised error of the density difference between the theoretical mixture density at the test section and the measured density from the Coriolis meter was plotted against gas volume fraction, and shown in Figure 4-18. The normalised error refers to the division of each density difference a by the maximum density difference in order to cancel out the effect this maximum has on the data, thus allowing underlying characteristics of the data sets to be compared The normalised error was found to increase with increasing with GVF and water cut. This finding is in agreement with the work of Anklin *et al* (2006) wherein they suggested that this error, known as ‘bubble’ effect, is due to the relative motion of gas bubbles in the liquid phase. It is also noticed that majority of the normalised error are positive indicating that the Coriolis density readings were lower than the theoretical ones for these points. This is due to the effect of slip between liquid and gas. The lighter gas phase will normally move much faster than the liquid phase thereby leading to lower measured void fractions.

In terms of orientation effects, there was more scatter in the normalised error data in the vertical than in the horizontal, especially at high GVFs. For example at 8% water

cut, the normalised error varies as much as 10% between the horizontal and the vertical readings while at a higher water cut of 70%, the normalised error varies as much as 20%. Although the cause of this pattern of error is poorly understood at present, it is recommended, based on this experimental data, that where practical, horizontal orientation is the preferred orientation.

4.5.2 Gamma Density Measurements

Figure 4-19 and Figure 4-20 show the response of the gamma densitometer to the multiphase flow density as the GVF increases, for horizontal as well as vertical flows. It was observed that the density decreases in a linear fashion with increasing gas volume fraction. Similar trends were also obtained for both the two phase and three phase flow; however, it is interesting to note also that the data trend in the horizontal was better than that of the vertical for these experiments.

With reference to the theoretical mixture density at the test section, it was found that the normalised error increases with increasing GVF but in a smaller range when compared with those of the Coriolis meter, Figure 4-21. Again the effect of phase slip in the vertical flow is seen because the gamma densitometer gives a lower void fraction measurement. This position is further highlighted in that the gamma densitometer mounted horizontally has a normalised error of ±1 compare to that of the vertical with a normalised error of ±2

The mixture density calculated from the hard gamma count was also compared with that from the soft gamma count and shown in Figure 4-22. The experimental results showed that the disparity in the density measurements between the hard and soft gamma signal exhibits a linear correlation with increasing GVF for the horizontal orientation but no such trend was seen for the vertical. In addition the hard-soft density difference was much higher in the vertical orientation than in the horizontal especially at high GVFs. These findings suggest that there will be higher measurement errors caused as a result of phase slip if the vertical gamma mixture density is utilised in computing three phase flow rates. As such appropriate slip correction models need to be developed to account for these errors in real field measurement.

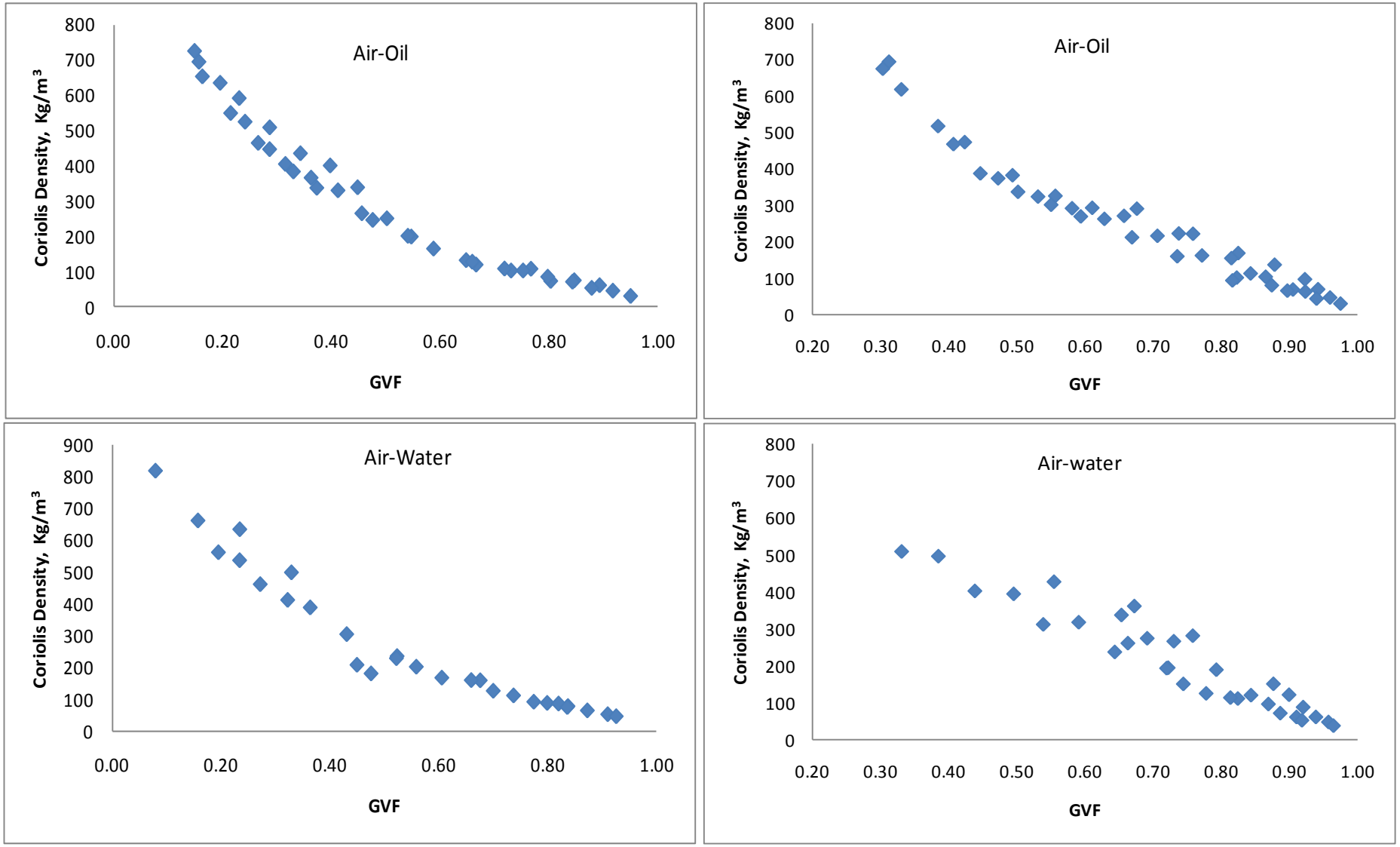

(a) (b)

Figure 4-16 Density Measurements of the Coriolis Meter in (a) Horizontal and (b) Vertical Pipe Orientation for Two Phase Flow

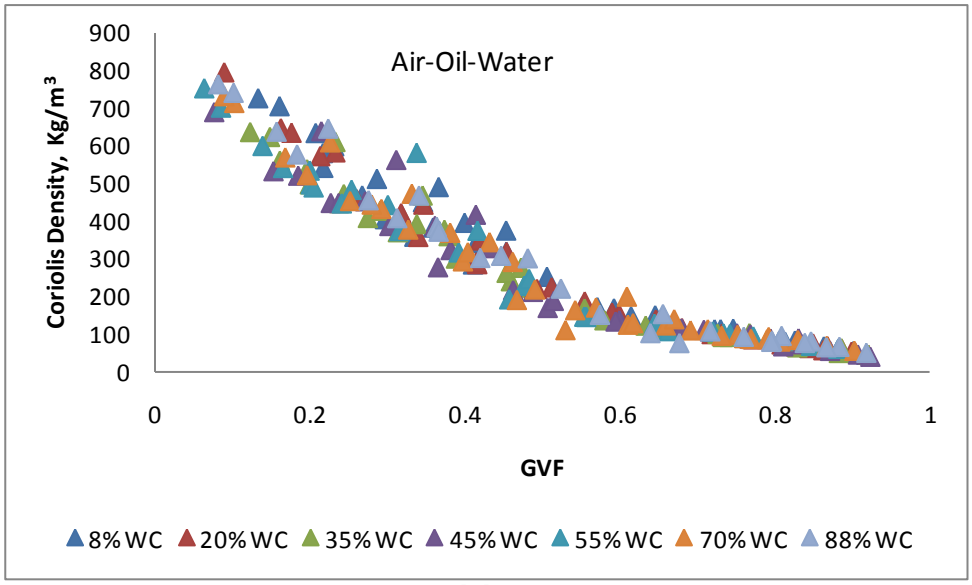

(a)

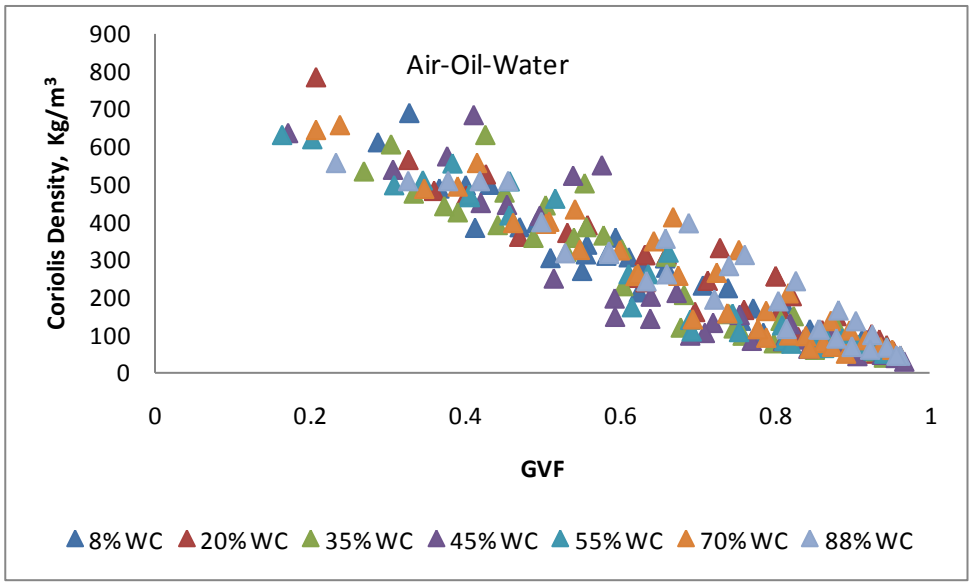

(b)

Figure 4-17 Density Measurements of the Coriolis Meter in (a) Horizontal and (b) Vertical Pipe Orientation for Three Phase Flow

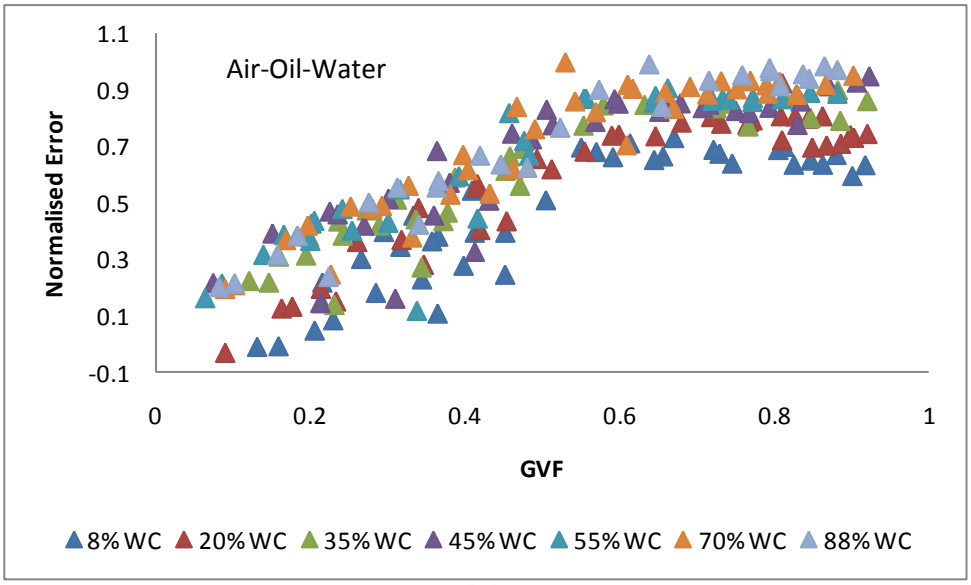

(a)

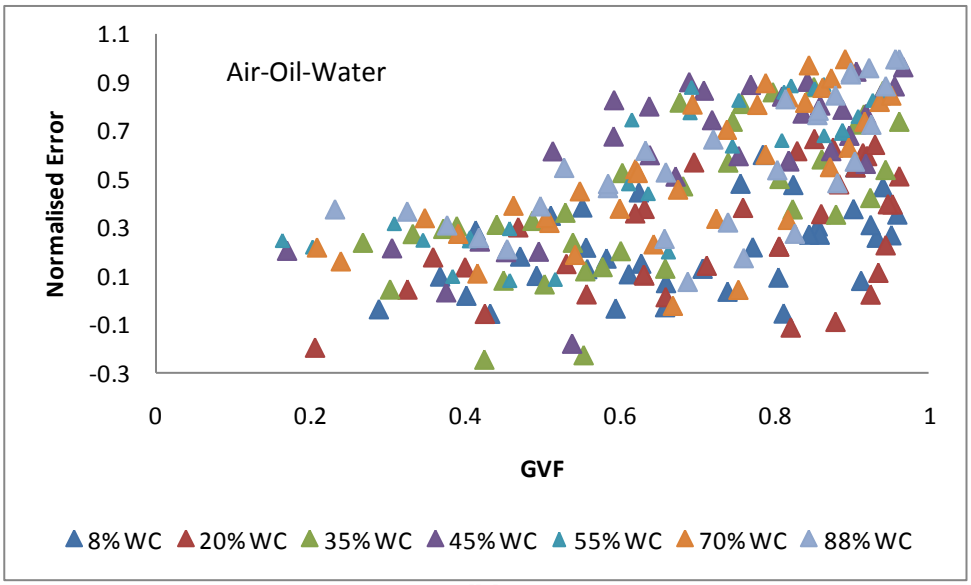

(b)

Figure 4-18 Normalised Density Error of the Coriolis Meter in (a) Horizontal and (b) Vertical Pipe Orientation for Three Phase Flow

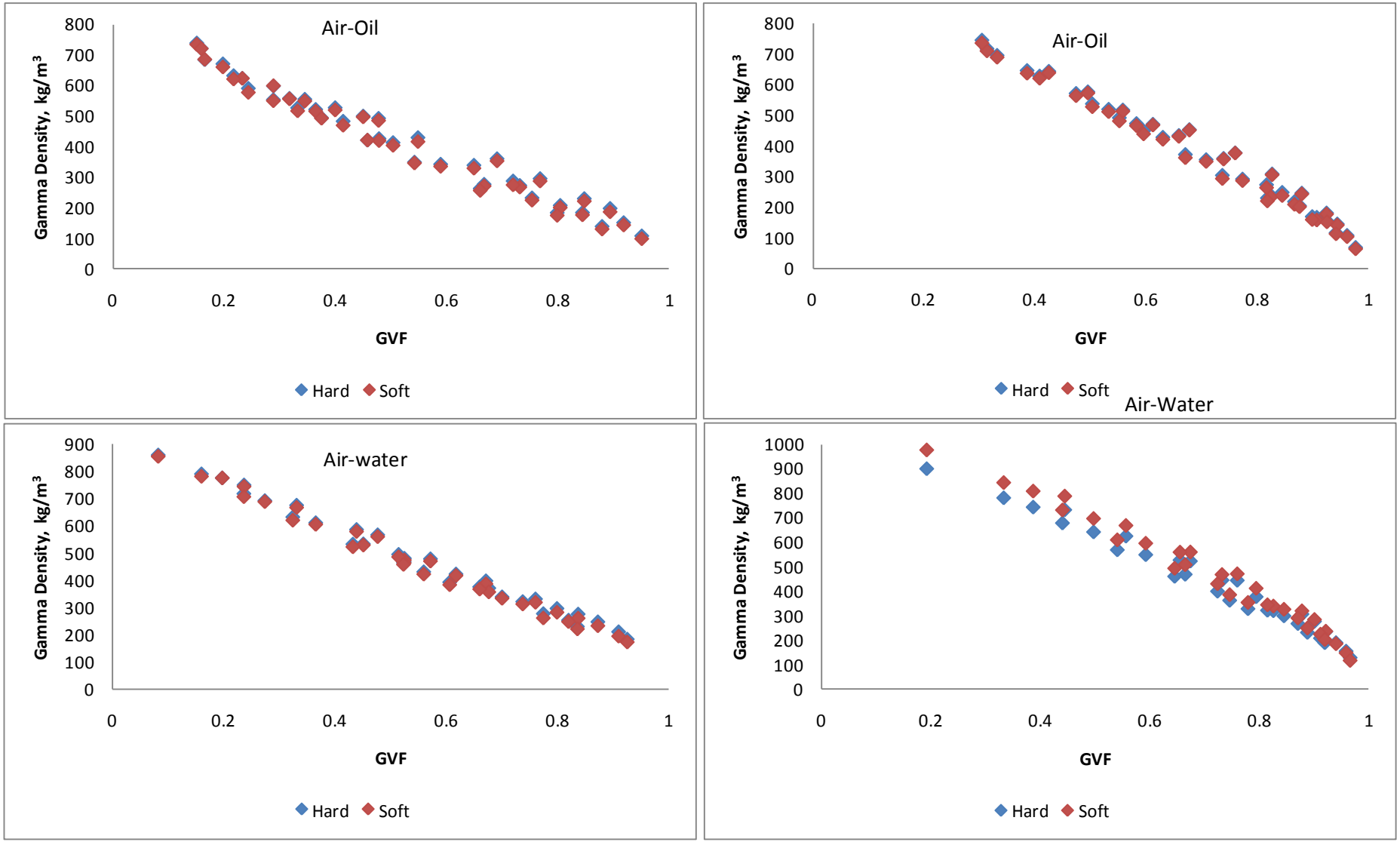

(a) **(b)**

Figure 4-19 Density Measurements of the Gamma Densitometer in (a) Horizontal and (b) Vertical Pipe Orientation for Two Phase Flow

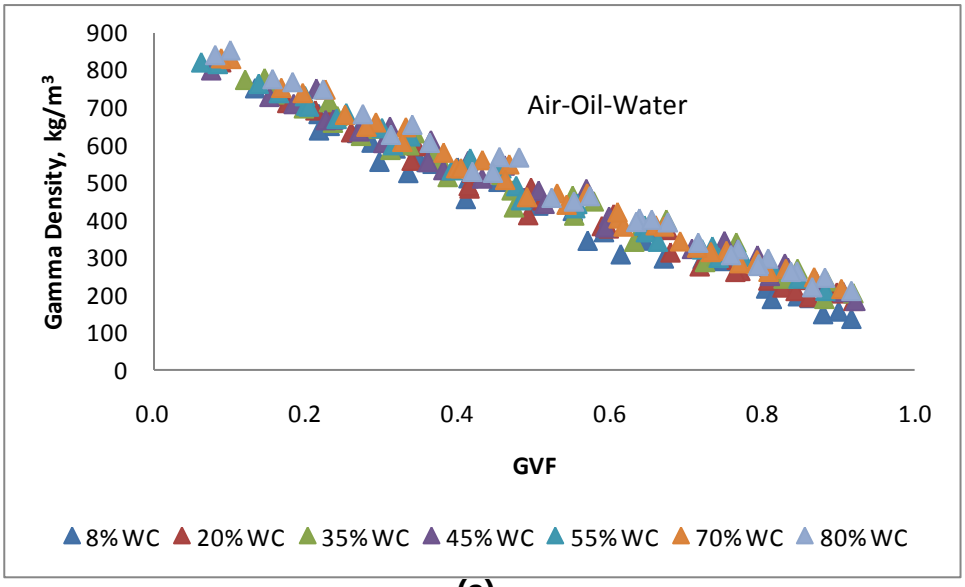

(a)

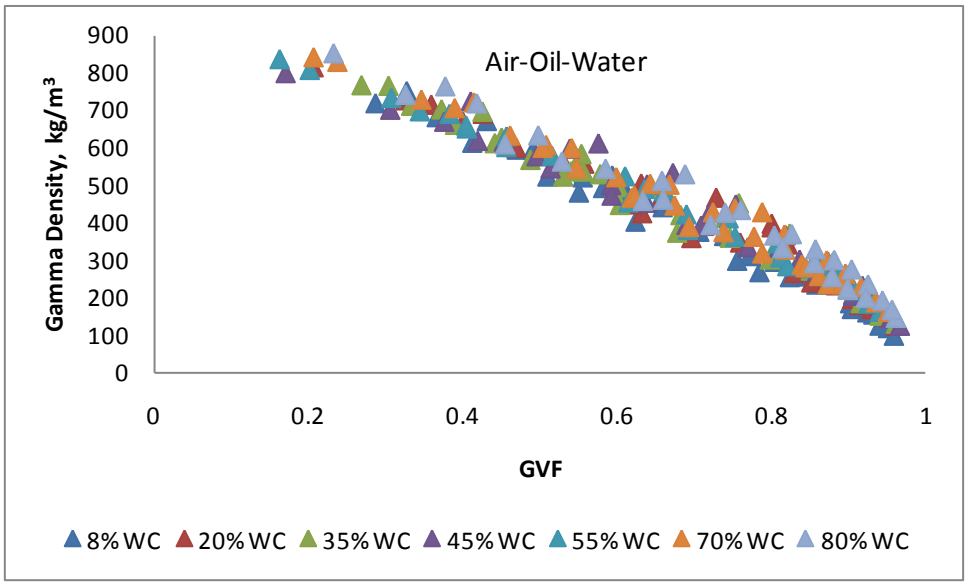

(b)

Figure 4-20 Density Measurements of the Gamma Densitometer in (a) Horizontal and (b) Vertical Pipe Orientation for Three Phase Flow

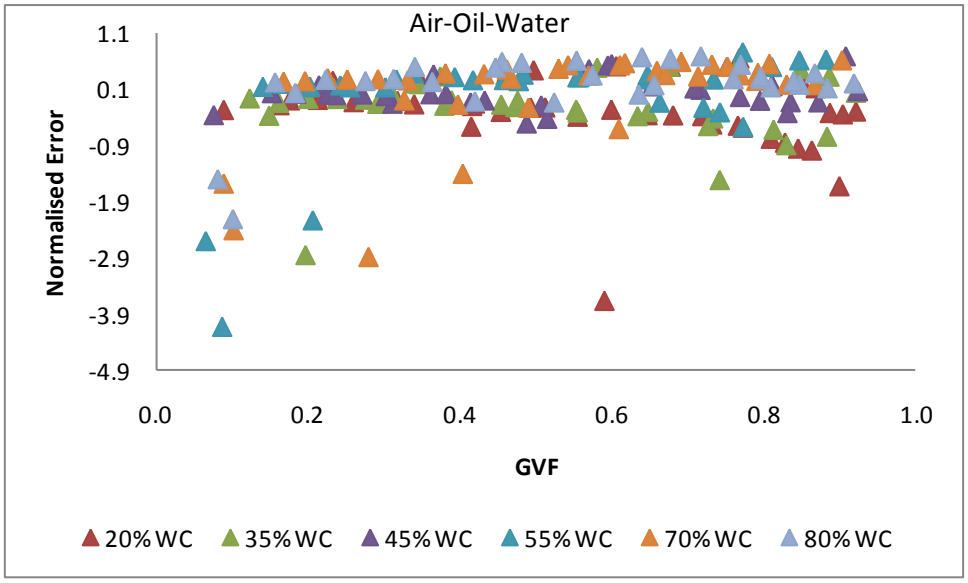

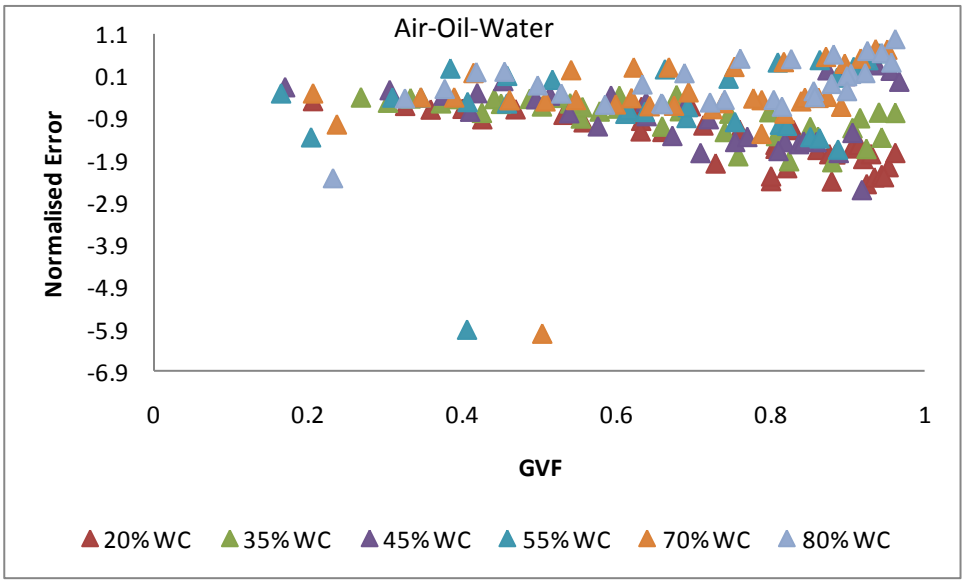

Figure 4-21 Normalised Density Error of the Gamma Densitometer in (a) Horizontal and (b) Vertical Pipe Orientation for Three Phase Flow

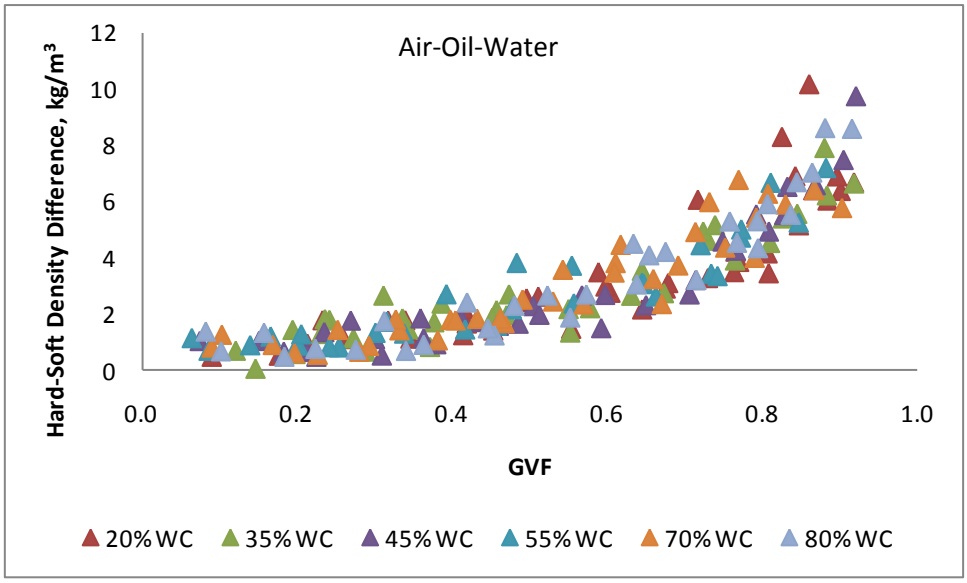

(a)

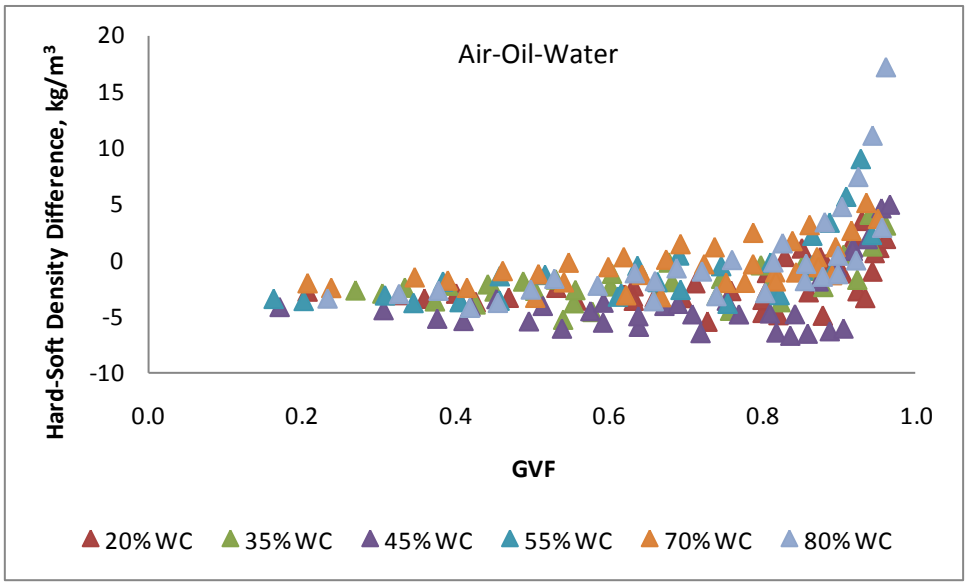

(b)

Figure 4-22 Hard-Soft Density Difference of the Gamma Densitometer in (a) Horizontal and (b) Vertical Pipe Orientation for Three Phase Flow

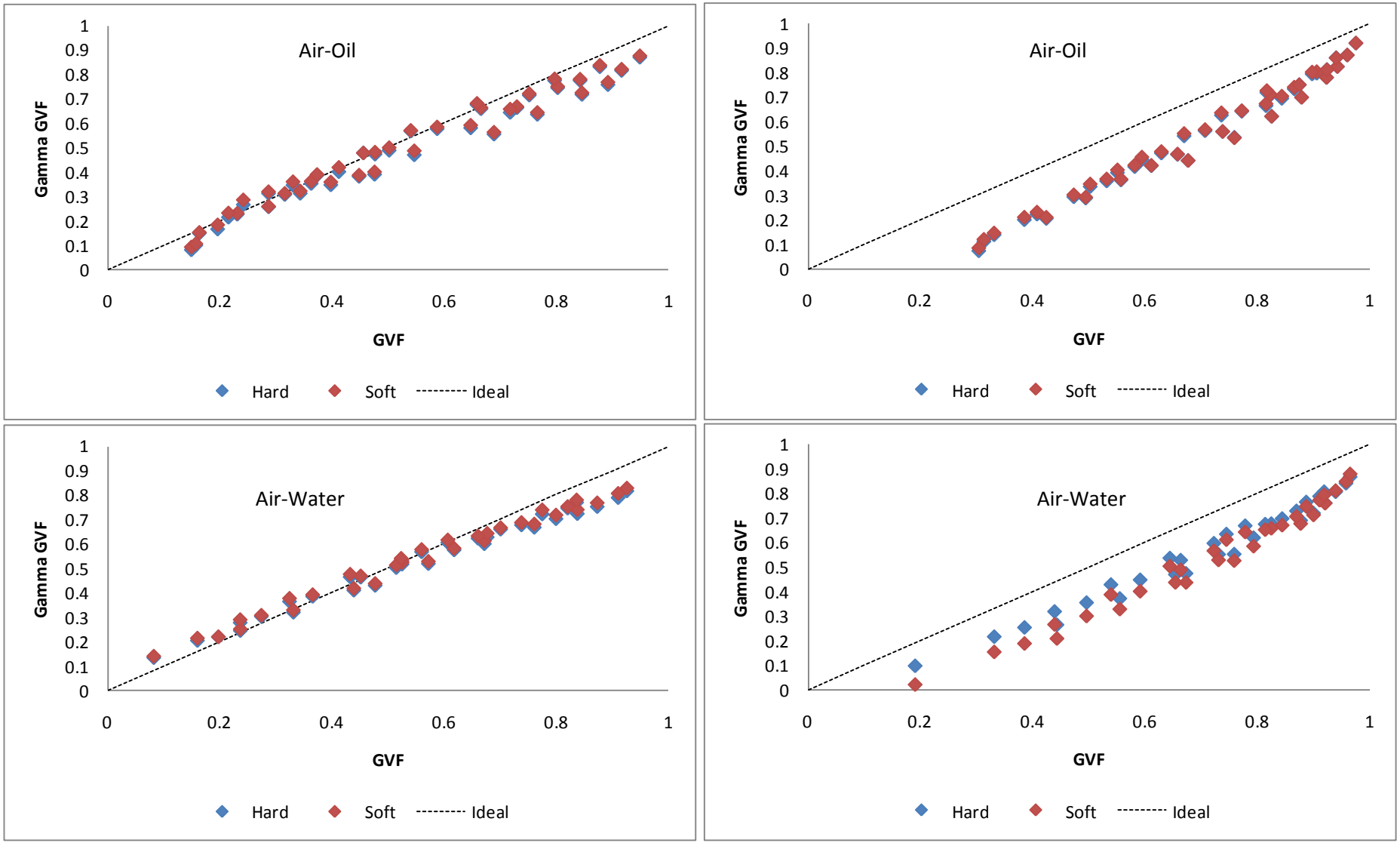

(a) **(b)**

Figure 4-23 Resolution of Air Phase Fractions Using the Hard and Soft Energy Signal for (a) Horizontal and (b) Vertical Pipe Orientation

Resolution of the gas phase fraction from the data generated by the gamma densitometer response to a series of horizontal and vertical multiphase flows employing the Beer-Lambert's Law of Attenuation was carried out. The deviation of measured gas phase fractions from the test facility reference values are illustrated in Figure 4-23, wherein it was observed that the gas phase volume fractions were fairly well predicted up to about 70% input GVF for the air-oil and air-water horizontal flows. Thereafter the gamma densitometer under predicts the GVF. This is envisaged because as the gas throughput increases, the slip between the gas and liquid phase increases also. Significant deviations were encountered in the gas component fraction calculation in the vertical pipe orientations where the GVF was under predicted for the range of the data points covered in the air-oil and air-water two phase flows experiments. This is due mainly to phase slip. The sensor's limited view of the pipe cross-section and the different flow regimes are thought to be the other sources of these deviation, (Arubi and Yeung, 2010).

4.5.3 Coriolis-Gamma Density Measurement Comparison

As explained in Section 4.5.1, density measurement from the Coriolis meter becomes unreliable when subjected to gas-liquid flow. Hence for an objective comparison between Coriolis and the Gamma densitometer, only oil-water flow data was employed. Oil-water mixture densities calculated from both hard and soft gamma counts were compared with those obtained from the Coriolis meter. The mixture densities obtained from the Coriolis meter and the Gamma densitometer correlate quite well in both horizontal and vertical orientation as illustrated in Figure 4-24. In addition, it was found out that the oil-water mixture densities obtained from Coriolis meter and Gamma Densitometer are very close with the percentage difference of ±0.5%, Figure 4-25. This shows that Coriolis meters give accurate density measurements in immiscible liquid-liquid flows. The Gamma mixture density was used as the reference therefore, negative difference depicts that Coriolis density is greater while positive difference depicts Gamma density is greater. Furthermore, in terms of orientation effects, no discernable trend was observed when this percent difference was plotted against water cut. Yet when this difference in densities measurement between the Coriolis and the Gamma meter is analysed with respect to input total flow rate, it was found that at lower input flow rates, the gamma density

is slightly higher than that of the Coriolis (depicted by positive percentage difference values), while at higher input flow rates, the reverse is the case (depicted by negative percentage difference values) as shown in Figure 4-26. This could be as result of the fact that Coriolis meter performance increases with higher mass flow and increased line pressure, (Anklin *et al,* 2006).

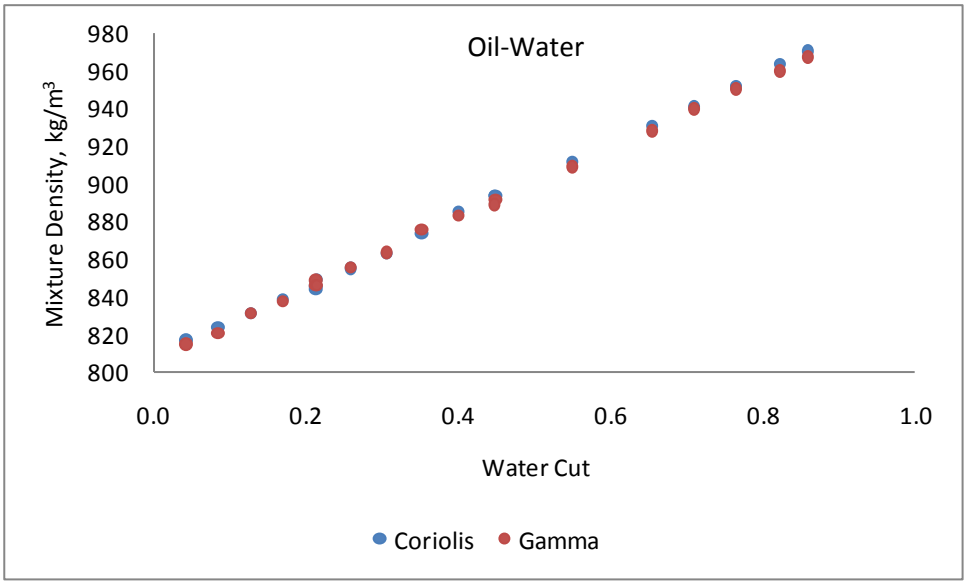

(a)

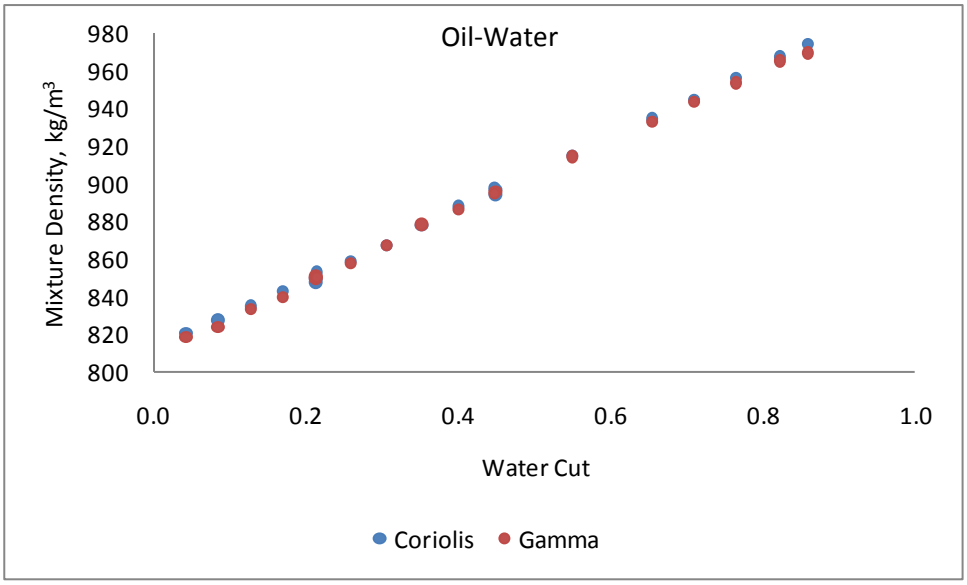

(b)

Figure 4-24 Correlations between Coriolis and Gamma Densities for Liquid-Liquid Flow in (a) Horizontal and (b) Vertical Pipe Orientation

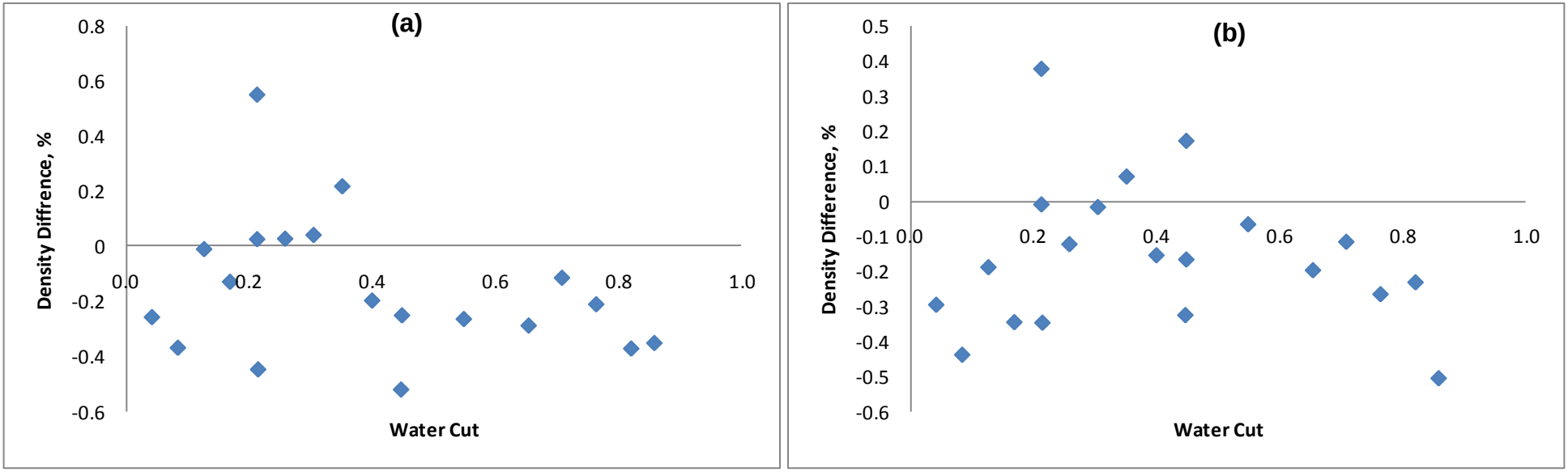

Figure 4-25 Percentage Difference between Coriolis and Gamma Mixture Densities for Liquid-Liquid Flow versus Input Water Cut for (a) Horizontal and (b) Vertical Orientation

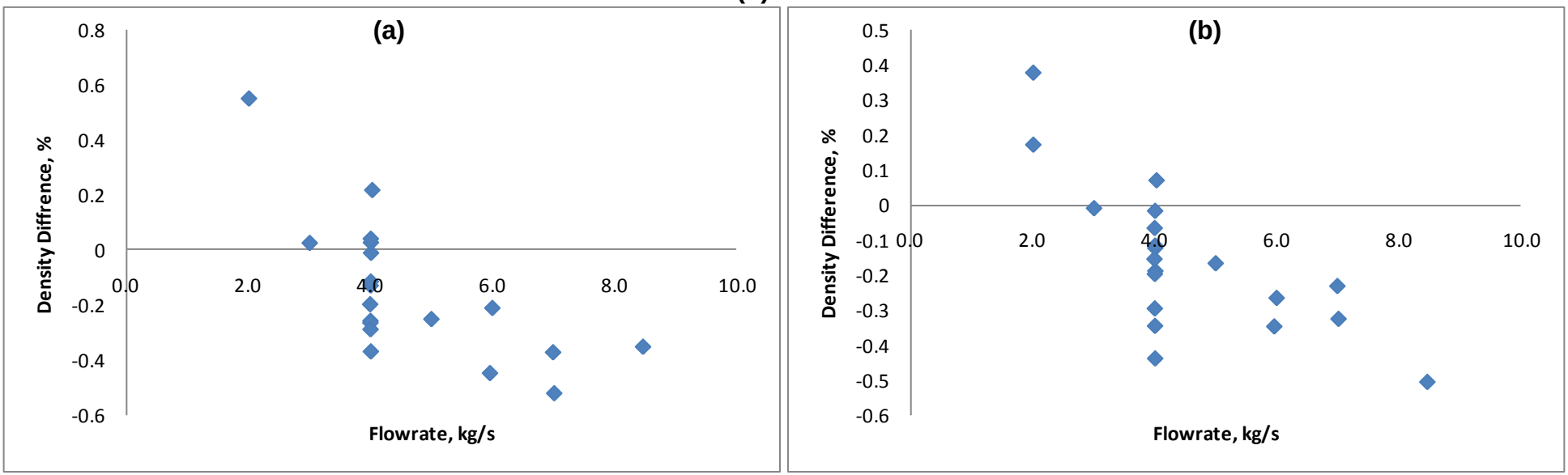

Figure 4-26 Densities Difference between Coriolis and Gamma Mixture Densities for Liquid-Liquid Flow versus Input Flowrate for (a) Horizontal and (b) Vertical Orientation

4.6 Phase Fraction Uncertainty Estimation

Measurement uncertainty estimation using Monte Carlo Simulation (MCS) was conducted to investigate the density fluctuation characteristics induced by the passage of blob of different diameters and shapes at varying velocities to determine the uncertainty associated with the phase fraction measurement. In undertaking this work, the ultimate resolution of the gamma detection unit was quantified and its limitations defined.

4.6.1 Experimental Apparatus and Procedure

For this work, flow patterns similar to those found in oil-water two-phase flow were modelled by inserting 'blobs' of polyvinyl chloride, PVC, (Density = 1300kg/m^3) in spherical, cylindrical and bullet shapes (see Figure 4-27) in static water. As the experiments were static, it means the void fraction and flow regime were constant, thereby providing reliable references. The outer diameter of the 'blobs' ranges from 20mm to 70mm and are 100mm in length (for the cylindrical and bullet shapes). Gamma count data for 180 experimental test points were collected. Each test point involved the programming of an electric stepper motor for a given velocity and blob diameter.

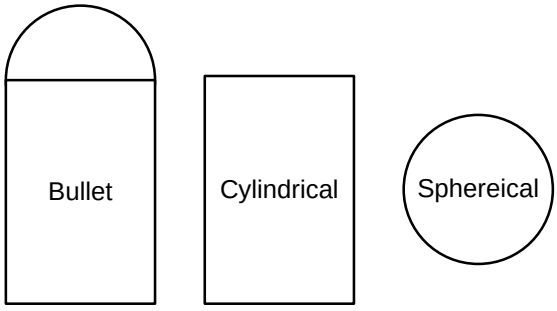

Figure 4-27 Geometry of Flow Structures

The experimental setup is illustrated in Figure 4-28. It consists of an electric stepper motor that is programmed to control the speed of the blob. The blobs are attached to the stepper motor by means of a thin fishing line. A gamma densitometer comprising of the gamma source and the detector unit is installed diametrically opposite each other on a pipe section filled with water. On initiation, the stepper motor pulls the blob up the column of static water and passes the measurement section of the

densitometer, stop and ramps down ready for another run. Gamma count recording was commenced as soon the stepper motor starts running and terminated when the blob has passed the measurement section of the densitometer. The number, shape, length, distribution and velocity of these blobs were varied to approximate a range of flow regimes (slug, bubble, annular) in order to provide a comprehensive response database.

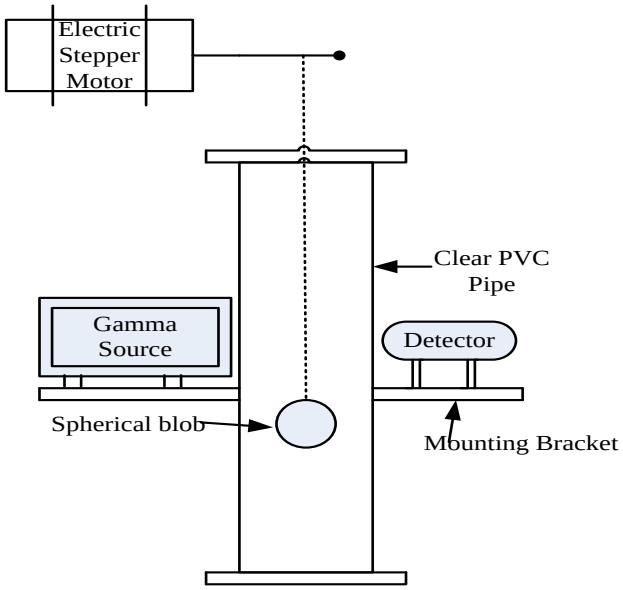

Figure 4-28 Experimental Setup

4.6.2 Phase Fraction Measurement

The principle of gamma-ray attenuation technique is based on the experimentally observed fact that the intensity of the gamma beam decreases exponentially as it passes through matter (Beer-Lambert law). In this study, the gamma densitometer is operated in the count mode and the measured intensities are represented by counting rates. For two-phase flow, the phase fraction can be obtained by:

$$\frac{\quad}{\quad} \qquad \text{Eqn. 4.6}$$

where I_w and I_{blob} corresponds to 100 % water and 100% blob respectively and are used as calibration values. I_{mix} is the measured intensity which depends on the amount of water and blob in the flow. The main limitations of directly applying this law is that it does not take into account the circular geometry of the pipe, the

prevailing flow regime or the presence of phase slip; thus, the theoretical phase fractions could contain significant errors depending on the flow conditions.

The fluid composition as 'seen' by the sensor can vary significantly from the actual composition, depending on the position of the 'blob', as illustrated in Figure 4-29.

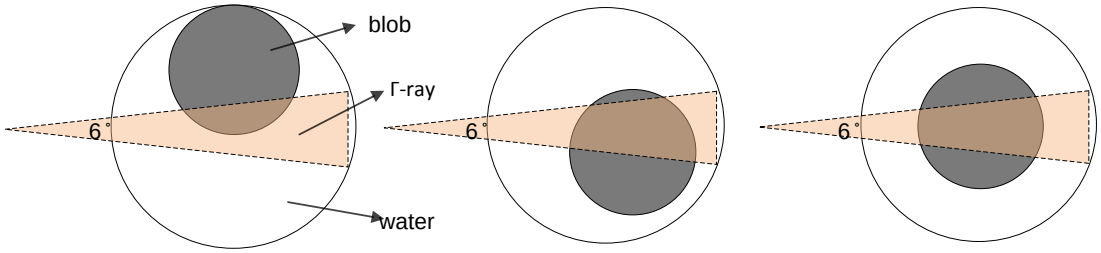

Figure 4-29 Gamma Densitometer View of the 'Blob'-Water Mixture

The theoretical phase fraction is based on the geometry describing the volume that is defined by the radiation beam and the detector area, i.e. measurement volume. For densitometers with parallel radiation beam, an expression for the theoretical phase fraction, (α_t) in the measurement volume of annular flows can be found as:

– Eqn. 4.7

whereas the actual or true phase fraction (α_c) for annular flow is calculated using Equation 4.7, where R is the total radius of the flow and r is the radius of the gas core (Åbro and Johansen, 1999).

— Eqn. 4.8

For the bullet shaped blobs, the measured fractions are slightly overestimated when compared with the theoretical fractions, Figure 4-30. This is consistent with published works for annular flow regime (simulated by the bullet-shaped blobs in this case). If extrapolated to the limits, there will be no deviations between the measured fraction and the calculated fraction because it will be single phase and the flow in the measurement volume will be representative of the flow over the entire pipe cross-section. Figure 4-31 plots the measured phase fraction against the true phase fraction.

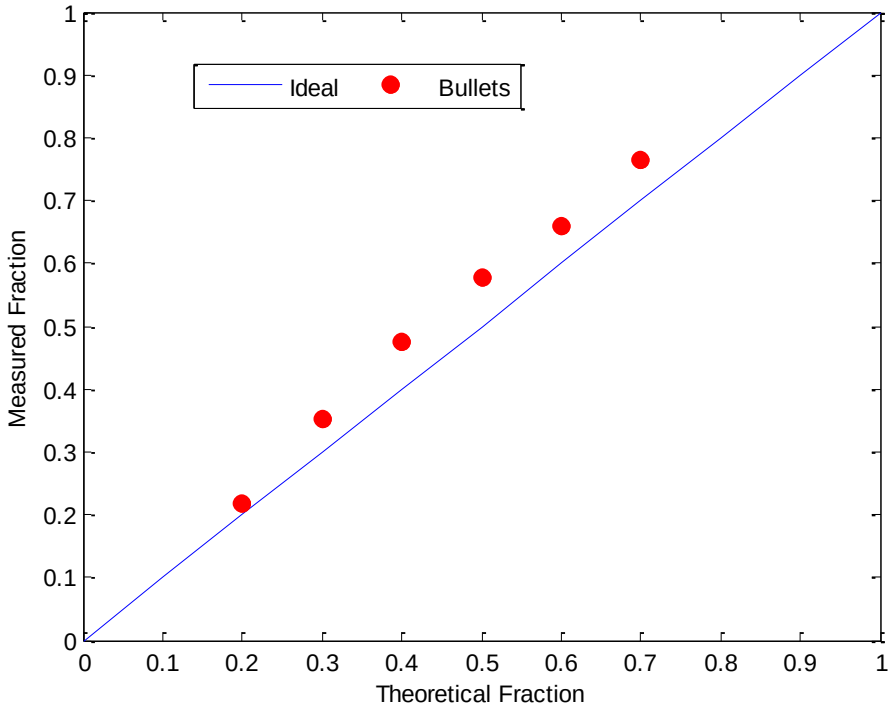

Figure 4-30 Blob-Water Tests Component Fractions: Measured Void Fraction versus Theoretical Void Fraction

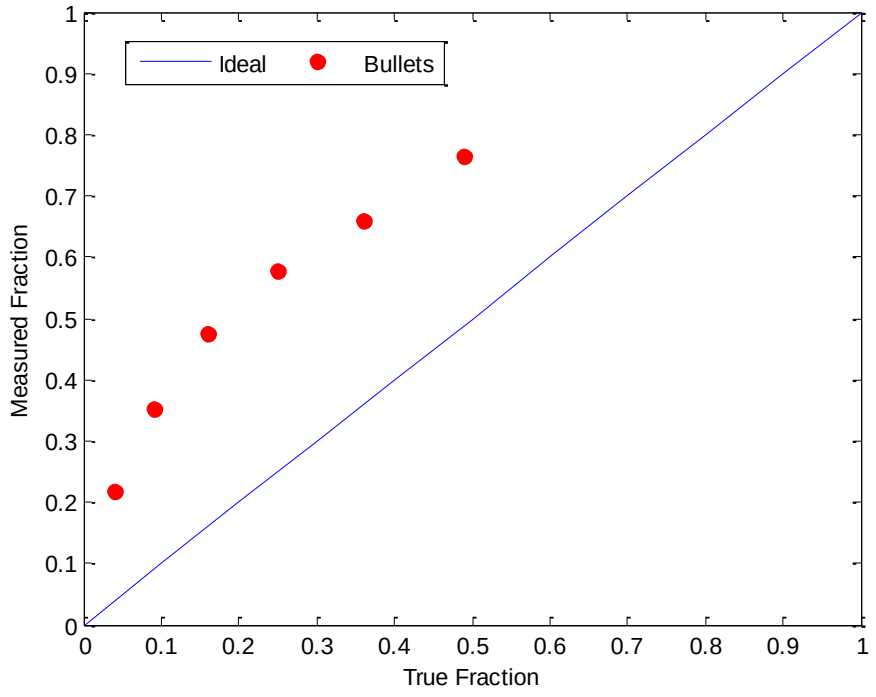

Figure 4-31 Blob-Water Tests Component Fractions: Measured Void Fraction versus True Void Fraction

Figure 4-32 shows the resulting probability density function (PDF) for the phase fraction measurement using Equation 4.6 as the model function by Monte Carlo simulation (MCS). Similar distributions were obtained for other test points. Each input term is simulated by generating random numbers from the distribution of the I_{mix}, I_w and I_{blob} using their mean and standard deviation as described in Section 2.5.3. The numbers of trials were 10^7 and were found to be sufficiently large for these experiments. The MCS uncertainty values given in Table 4-4 are standard uncertainty and are defined as one standard deviation (σ) of the average all the observed values. That is, there is a 68.3% probability that the measured value of the input quantity will be within the confidence interval from -σ to +σ.

The large uncertainties obtained in this case are as a result of the fact that all radioisotope intensity measurements are subject to statistical fluctuation in the number of counts due to the random nature of photon or particle emission. This statistical error does propagate and influences the accuracy of these measurements.

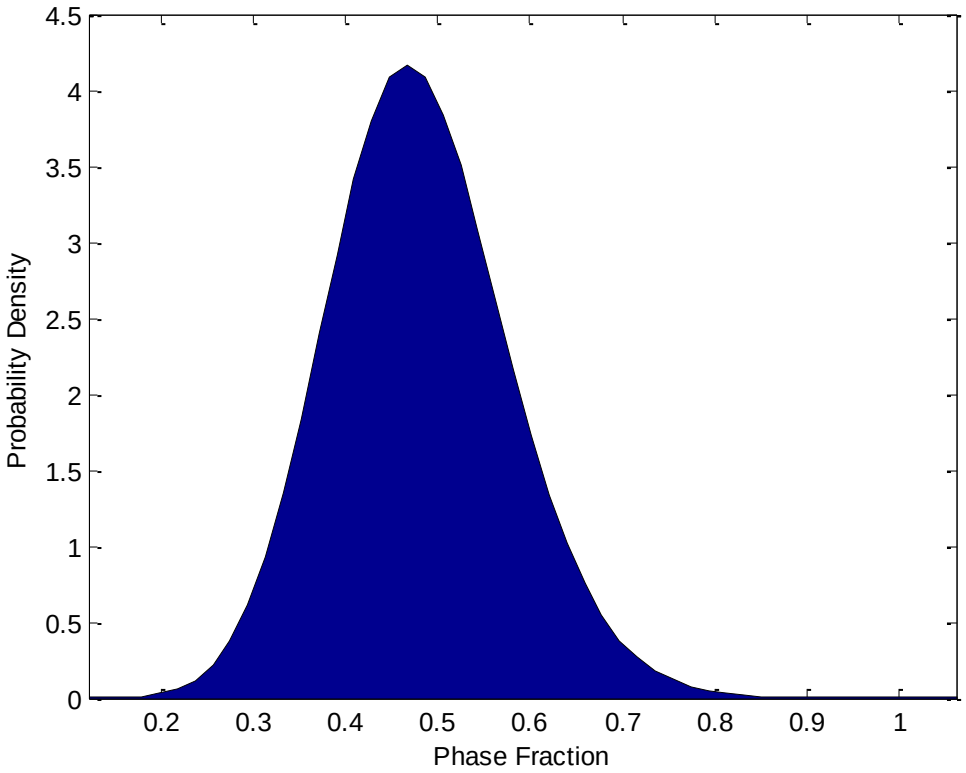

Figure 4-32 MCS Uncertainty Evaluation for Phase Fraction (40mm Bullet-Shaped Blob)

Table 4-4 MCS Uncertainty Evaluation for Phase Fraction (Bullet-Shaped blobs)

		Phase Fractions (measured)	MCS Phase Fractions	MCS Uncertainty @ 1σ
Bullets	20mm	0.217	0.221	0.088
	30mm	0.351	0.355	0.095
	40mm	0.475	0.480	0.097
	50mm	0.577	0.582	0.102
	60mm	0.658	0.663	0.106
	70mm	0.765	0.770	0.111

4.7 Phase Inversion

In gas-liquid or liquid-liquid dispersed flow systems, depending on the operational conditions, either of the two fluids involved can make up the continuous phase. Phase inversion refers to a phenomenon where the dispersed phase spontaneously becomes the continuous and vice versa. According to Brauner and Ullmann (2002), the inversion point is usually defined as the critical volume fraction of the dispersed phase above which this phase will become the continuous phase. Such phenomenon is commonly encountered in the process, nuclear and petroleum industries. In oil and gas production, oil extraction is often accompanied by a high water throughput because of the presence of water in oil well or injection of water into the reservoir for secondary recovery purposes and/or reservoir pressure maintenance schemes. The effect of the water phase with respect to the pressure gradient is of particular importance for oilfields operating at high water cuts and low wellhead pressure. Depending on which phase is continuous and which is dispersed, the pressure gradient in either case can be quite different, thus it is very important to predict the occurrence of phase inversion. In addition, this transition is usually associated with an abrupt change in the rates of momentum, heat and mass transfer between the continuous and dispersed phases and between the dispersion and the system solid boundaries. Therefore phase inversion is a major factor to be considered in the design of oil-water pipelines, since the rheological characteristics of the dispersion and the associated pressure drop change abruptly and significantly at or near the phase inversion point (Bonizzi and Issa, 2003; Descamps *et al*, 2007; and Xu *et al*, 2010). Furthermore, the rate of flowline corrosion is determined to a large extent by which of the phases that wets it.

However, the intricate mechanisms responsible for phase inversion and the effect of physical and geometrical parameters on it are not well understood yet. In this work, efforts have been made to identify the phase inversion point and frictional pressure gradient effects for air-oil-water flow through a 10.5m vertical riser in several different flow regimes.

4.7.1 Pressure Gradient

The pressure drop in a channel or conduit can be expressed by the Equation 4.8 if the flow is assumed to be one-dimensional flow and the pressure gradient in the system is constant, (Munson *et al*, 1994):

— Eqn. 4.8

where *ΔP* is the pressure difference of the two-phase mixture between two points in the channel/conduit, *ΔL* is the distance between theses point and *dP/dL* is the pressure gradient in the channel/conduit . From Equation 4.9, the total pressure gradient is seen as a superposition of three components due to the mixture acceleration, friction and gravity:

— — — — Eqn. 4.9

The first component of the pressure gradient in Equation 4.9, the acceleration component, is usually neglected for adiabatic flows in both horizontal and vertical pipes because its effect is very small, typically less than 1% (ESDU, 2004).

In Figure 4-33, the total pressure gradient measured for three different mixture velocities (1.5, 3.0 and 6.0m/s) at various GVF is plotted as a function of the water fraction. For the mixture velocity of U_m = 1.5 m/s there are five values for the gas-volume fraction (GVF = 65, 80, 85, 90, and 95%); for the mixture velocity of U_m = 3.0 m/s there are four values for the gas-volume fraction (GVF = 40, 65, 70 and 85%) while for the mixture velocity of U_m = 6.0 m/s there also five values for the gas-volume fraction (GVF = 40, 45, 50, 60 and 70%). As can be seen from the plot, GVF has a significant influence on the pressure drop over the riser. The pressure drop decreases with increasing GVF.

Form the data presented in Figure 4-33, phase inversion takes place at a water fraction of about 45%. It is evident from the plots that the pressure drop peak during phase inversion and is more strongly enhanced at high mixture velocities than at low velocities. At constant gas flow rate and increasing liquid mixture velocity, the pressure gradient increases because of a higher friction. At constant liquid mixture velocity and increasing gas superficial velocity, the pressure gradient is reduced, due to the lower gravitational pressure drop over the pipe when more gas is present.

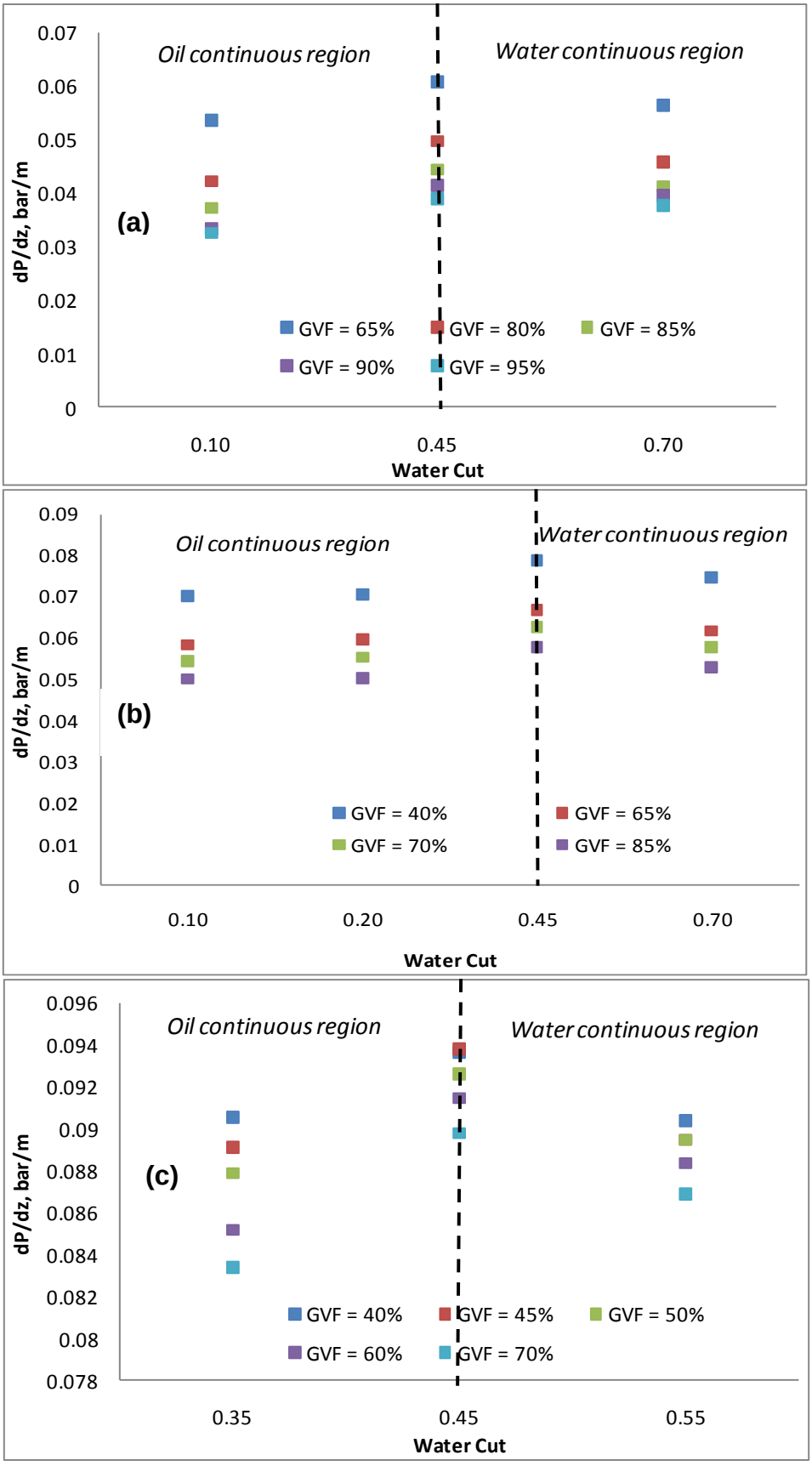

Figure 4-33 Total Pressure Gradient as a Function of Water Fraction for Air-Oil–Water Flow for a Mixture Velocity of (a) 1.5m/s, (b) 3.0m/s and 6.0m/s

4.8 Real Field Data Analysis

Multiphase flow meters are installed in facilities to help operators and energy companies to optimise production and manage these facilities. Currently multiphase flow meters are tested and validated under laboratory conditions before they are deployed to the field. There is little real field data available in the public domain. A 12 days worth of high frequency data using Neftemer densitometer installed on a platform owned by a major international oil company in Brazil was recently acquired by Cranfield University.

4.8.1 Monitoring Well Performance

It is necessary to keep track of the gas, oil, and water production from each well to be able to manage the reserves properly, evaluate where further reserve potential may be found, and diagnose well problems as quickly as possible. Proper allocation of income also requires knowledge daily production rates as the royalty or working interest ownership may be different for each well. In facilities that handle production from many wells, each well is routed through the test manifold on a periodic basis for testing. Total production from the facility is then allocated back to the individual wells on the basis of these well tests. Therefore testing a well is a key factor for monitoring performance.

Traditionally the industry uses conventional fixed/mobile test separators or mobile multiphase meters assemblies for well testing. These tests are periodic and normally lasted for a day or two as it is thought that production from wells is stable over this period and that switching wells into testing mode does not affect their production. These assumptions are seldom valid: as recent experience has shown that production from a well could be very chaotic and unstable in terms of gas flow rate, oil flow rate and water-in-liquid ratio. This could be more so due to higher water cuts as the field matures, more wells being drilling, and fluctuation in field production requirements.

Figure 4-34 is a plot of a well test data showing a combined mixture density (on the left vertical axis) and liquid flow rate (right vertical axis) versus time (on the horizontal axis) for a 24hr period for two different days. These data is part of the 12 days high

frequency data obtained from *Well X* in offshore Brazil using Neftemer gamma densitometer. From Figure 4-34a, it can be seen that the behaviour of the well is stable for some period of time and becomes chaotic at other times (Figure 4-34b). Probability mass function plots for periods of stable shows consistent shape that denotes a homogeneous mixture irrespective of the duration of the test data as shown in Figure 4-35. Hourly PMFs plots for periods of unstable flow for this same *Well X* yielded a variety of shapes denoting different flow regime due to fluctuating gas and liquid flow rates, depicted in Figure 4-36.

Looking at Figure 4-36 from the first row, a flow structure that is dominated by high liquid content is noted; since the peak of the PMF is in the low gamma count region. This is the first hour of the data. For the second hour, there is sudden influx of gas through the system because the peak of the PMF has shifted rightwards into high gamma count region. This situation continues for the next two hours. As more liquid is produced, the mixture attained homogeneous flow as depicted by the PMF at the fifth hour and remain in this state for the next three hours. Thereafter the gas content of the flow increases and causes the flow to become more chaotic giving rise to churn flow regime. Then the liquid flow rate catches up with that of the gas, giving rise to a homogenous flow again.

From the analysis above, it is clear that there is need to continuously monitor oil and gas wells. Such a practice will help petroleum production engineers to better manage the interface between the reservoir and the well, including design of downhole flow control and monitoring equipment; evaluate artificial lift methods; properly size surface equipment and ultimately optimise of production and injection rates.

Thus there is need to continuously monitor wells as a key to optimising production and this requires inexpensive per well monitoring utilizing multiphase flow meters. This will give a considerable economical savings in the long run in addition to wellhead flow measurement information.

In another light, there will be some implications on the in-situ performance and calibration of multiphase flow meters as a result of this unstable production behaviour of some wells. If a multiphase flow meter is calibrated in the field with reference to test separator measurements when the flow was stable, then when the

flow becomes unstable, frequent re-appraisal will be necessary. That is, where variations are found to have occurred, some mechanism for changing calibration constants and accounting for historical deviations must be implemented.

Calibration of multiphase flow meters is another problem which has not yet been fully addressed. The practice of using test separators as calibration devices is not universally accepted yet, because the order of uncertainty in a test separator is similar to that for a multiphase flow meter. It is pertinent to note that no satisfactory method of checking velocity measurement has yet been proposed, however for phase fraction measurements, most installations currently have a section in their facility that enables the meter section to be filled with gas or liquid in order to check the end point calibrations of the phase fraction measurement sensors (e.g. gamma densitometers).

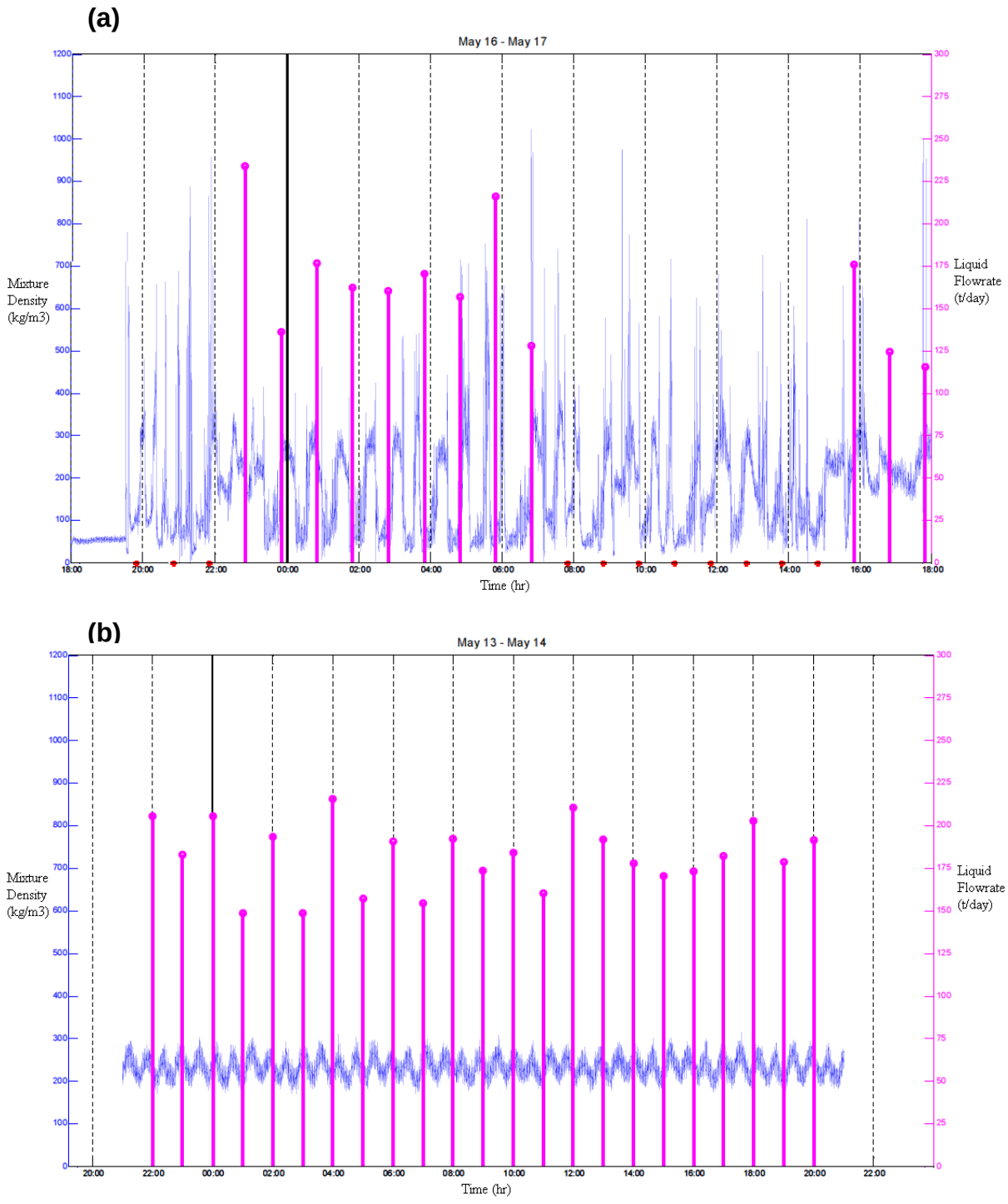

Figure 4-34 Well Performance Monitoring for Well X for Different Days; (a) 13–14th/05/2010 and (b) 16–17th/05/2010 (Courtesy: Neftemer Ltd)

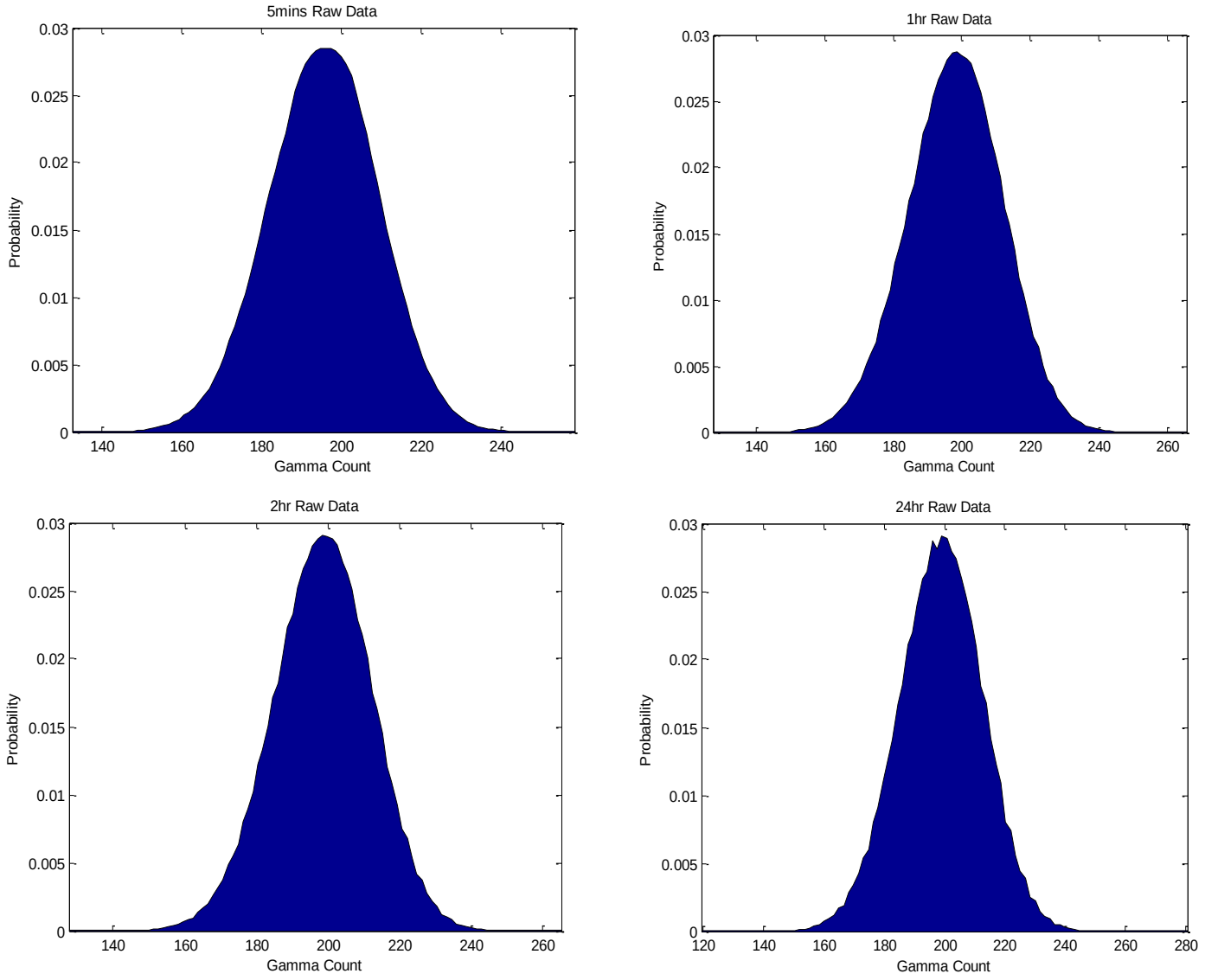

Figure 4-35 PMFs Plot for Well X during Stable Production Periods: 13–14th/05/2010

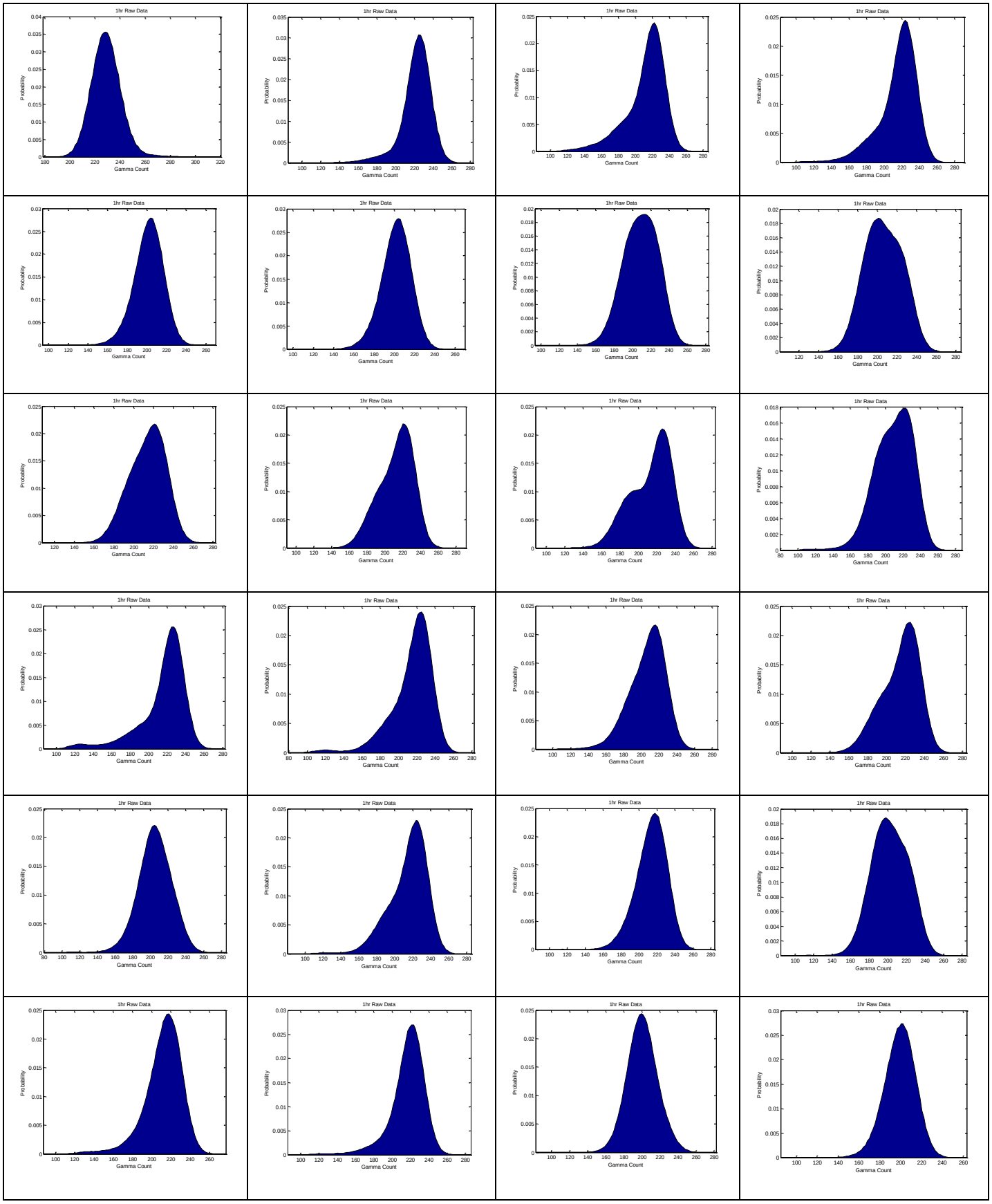

Figure 4-36 Hourly PMFs Plot for Well X during Unstable Production Periods: 16–17th/05/2010

4.9 Chapter Summary

In this chapter, the experimental flow pattern maps were developed based on the identification of the flow regimes from probability mass function plots in a similar manner to Matsui (1984), Mi et al, (1998) and Lee et al (2008). For all experiments, under the air-liquid, or air-liquid-liquid superficial velocity range covered, three different flow patterns were detected in the vertical test section namely bubble, slug and churn flow. While in horizontal test section bubble, slug and wave flows were detected.

The effect of upstream conditions on flow patterns in the vertical riser was investigated by varying the air inlet configuration. The experiments were conducted with two different air inlet conditions, that is: (i) the upstream horizontal flowline mixing point and (ii) riser base gas injection in the 50.8mm test rig. In other words, the former corresponds to the introduction of air into the oil-water flow at the inlet of the flowline prior to the riser base whereas the later refers to the continuous injection of air directly at the base of the riser.

It was deduced that no inlet conditions effects was observed at low gas throughput as similar flow pattern were encountered. However at higher air and water superficial velocities it was observed that the two inlet configuration exhibited dissimilar flow regimes, e.g., agitated bubble for one and fully developed slug for the other at the same experimental conditions. This dissimilarity is attributable to the effect of hydrodynamic slugging from the horizontal flowline influencing the vertical riser behaviour or some unstable processes in the flowline-riser system. This finding shows that, for multiphase meters that are flow regime dependent, there will be some measurement implication.

From the drift flux analysis results, it found that the values of the drift velocities and distribution parameters in vertical as well as the horizontal flows are in good agreement with the values obtained in the literature. It was also shown that the drift velocity in horizontal flows is not normally zero but substantially lower than those of the vertical.

A comparative performance assessment study of the density measurement for the Coriolis meter and the gamma densitometer was conducted for both two and three phase flows in horizontal as well as vertical pipe orientations. Density measurements from the Coriolis meter was excellent in liquid-liquid flow and correlates well with those of the gamma densitometer but becomes unreliable when subjected to gas-liquid flow due to the relative motion of gas bubbles in the liquid phase also known as the 'bubble effect'. It was also observed that, due to the disparity between the phase fraction computed from the hard gamma count and that of the soft gamma count, there will be high inaccuracies in the measurement due to phase slip if the vertical gamma mixture density is utilised in computing three phase flow rates.

Phase fraction measurement uncertainty was investigated using Monte Carlo simulation method. MCS was used because the measurement from the detector is a combination of effects e.g. the gamma source, fluid density etc, which readily propagates through the entire measurement system. All these effects are highly nonlinear in combination. The phase fraction measurement uncertainty was found to be high.

Efforts were made to identify the phase inversion point and frictional pressure gradient effects for air-oil-water flow in the 10.5m vertical riser in different flow patterns. It was found that phase inversion always takes place at a water fraction of about 45% and that pressure drop peak at this point for this set of experiments. At constant gas flow rate and increasing liquid mixture velocity, the pressure gradient increases because of a higher friction. Whereas at constant liquid mixture velocity and increasing gas superficial velocity, the pressure gradient is reduced, due to the lower gravitational pressure drop over the pipe when more gas is present.

Analysis of a real field production data showed that assumptions made in well testing is not always valid because production from a well could be very chaotic and unstable for a variety of reasons. PMFs plots of the field data revealed that the behaviour of this well is stable for some period of time and becomes chaotic at other times. This analysis reiterates the need for continuous monitoring of well performance for better reservoir management and highlights concerns regarding in-situ calibration and performance of multiphase flow meters.

CHAPTER FIVE

5. SIGNAL ANALYSIS

This chapter presents details of the Gamma densitometer response to different multiphase flow conditions (air-water two phase flows in the 101.6mm test rig and air-oil-water three phase flow in the 50.6mm test rig as described in ***Chapter 3****), signal analysis in the time and frequency domain and orientation effects on the sensor response*.

5.1 Time Domain Analysis

5.1.1 Sensor Response to Flow Conditions

Figure 5-1 to Figure 5-4 are time domain representations of the gamma response when subjected to the passage of different multiphase flow conditions. It is evident from these plots that the sensor responded well to the prevailing flow conditions depicted by the various peaks and troughs in the amplitude of the time varying signal traces due to mixture density fluctuations in the multiphase flow.

For high mixture density flow conditions, the number of gamma photons absorbed by the fluid increases so the magnitude of the output signal of the densitometer decreases accordingly. In the same way, for low fluid density conditions, the number of photons detected increases so the magnitude of the gamma count increases.

Analysing a thirty seconds snapshot of the raw signal traces gives a useful visual indication of the flow behaviour in the horizontal and vertical flowline. The first case in Figure 5-1 represents a multiphase system having air-oil superficial velocity of 1.10 and 2.44m/s respectively. For this flow condition, there are sharp and very narrow peaks in the amplitude of the signal. With an increase in the gas flow rate and a decrease in liquid flow rate (V_{sg} = 3.42m/s and V_{sl} = 1.22m/s), distinct peaks and troughs are produced by the passing gas and liquid structures as illustrated in Figure 5-2. This is typical of a slugging system. A further increase in the gas superficial velocity with the same liquid loading (V_{sg} = 5.40m/s and V_{sl} = 1.22m/s) leads to a higher frequency slugging regime as shown in Figure 5-3.Figure 5-4, (V_{sg}

= 12.9m/s and V_{sl} = 1.85m/s) is indicative of chaotic flow behaviour wherein the gas and liquid structures shows no discernable pattern as is the case of churn flow. These peaks represent the passage of gas structures through the measurement section of the flowline. Larger gas bubbles or the passage of more than one gaseous structure in close proximity to each other will induce a wider peak inferring a high local gas void fraction. Thus peak width provides an indication of the gas structure length in the axial direction.

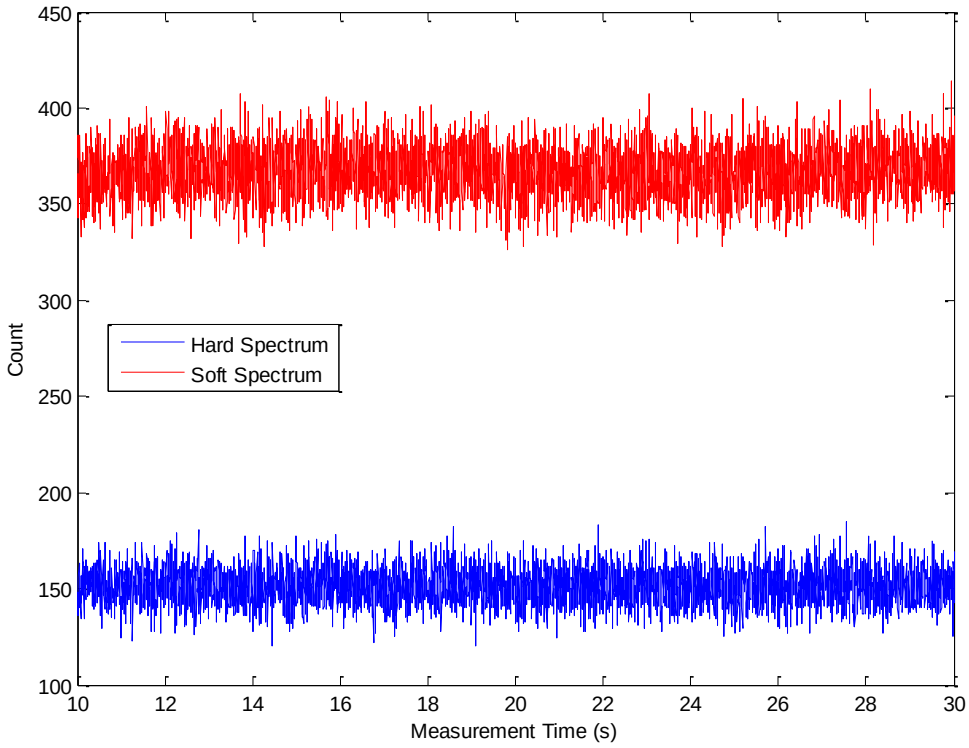

Figure 5-1 Gamma Densitometer Response to Flow Conditions: Air-Oil Two Phase Flow at Vsl = 2.44m/s; Vsg = 1.10m/s

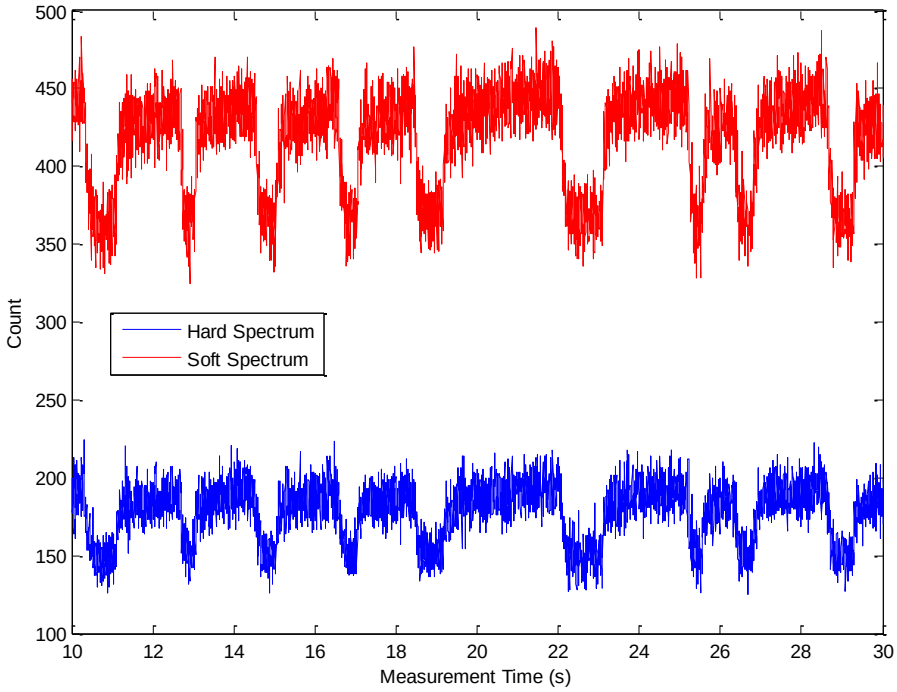

Figure 5-2 Gamma Densitometer Response to Flow Conditions: Air-Oil Two Phase Flow at Vsl = 1.22m/s; Vsg = 3.42m/s

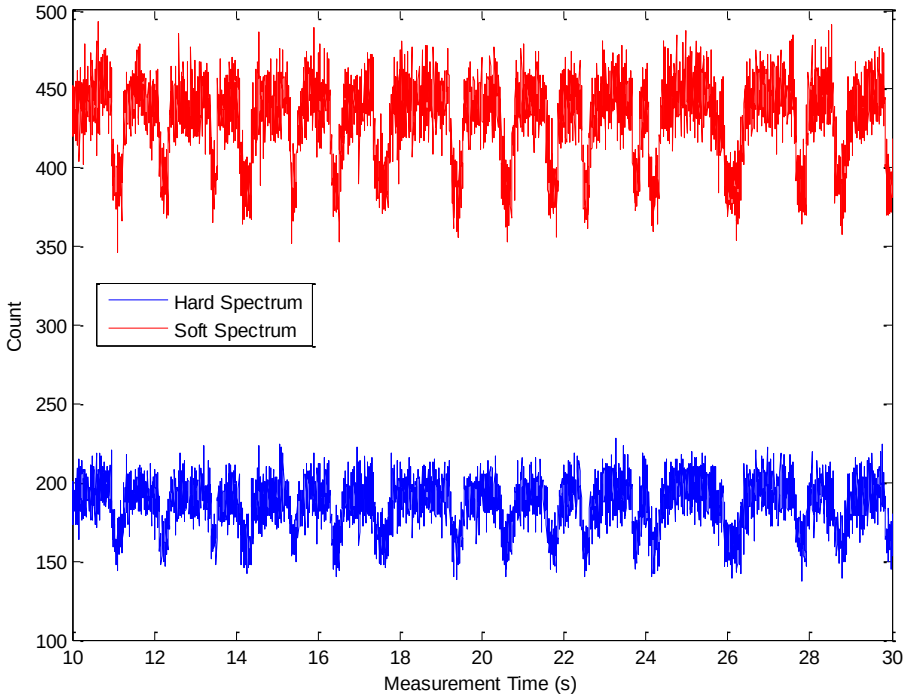

Figure 5-3 Gamma Densitometer Response to Flow Conditions: Air-Oil Two Phase Flow at Vsl = 1.22m/s; Vsg = 5.40m/s

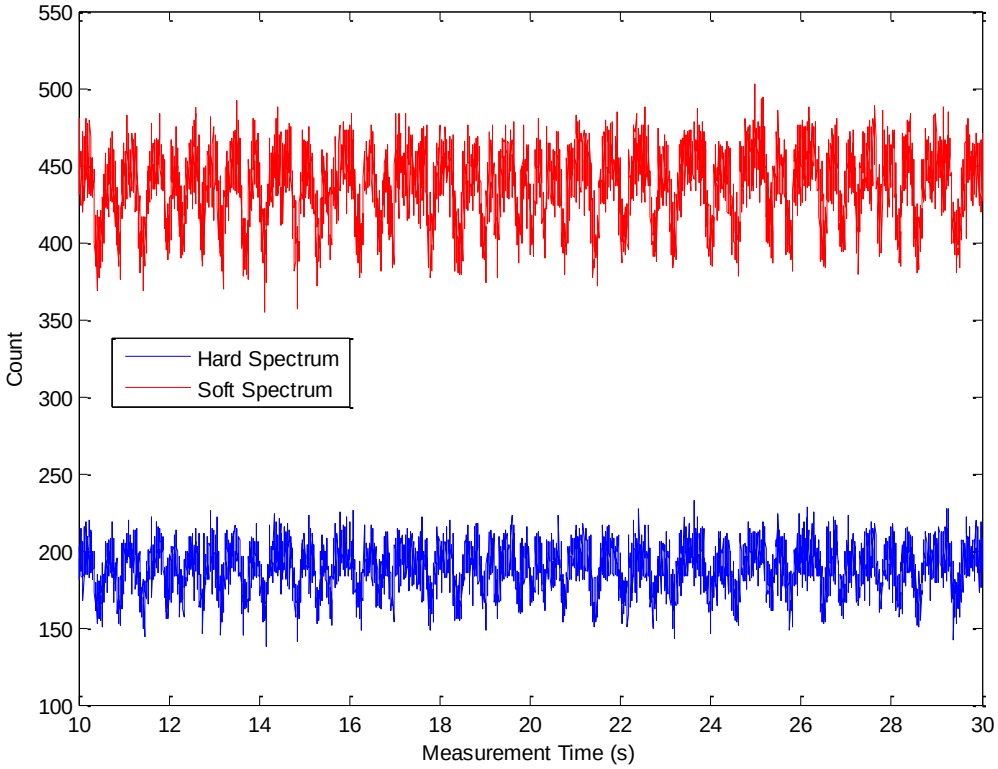

Figure 5-4 Gamma Densitometer Response to Flow Conditions: Air-Oil Two Phase Flow at Vsl = 1.85m/s; Vsg = 12.9m/s

Figure 5-5 shows the location of the test points described above on the air-oil two phase vertical flows using Taitel *et al* (1980) flow regime boundary.

Locating the points on a flow pattern map act as supplements to the analysis made on the raw signal traces. The time trace in Figure 5-1 have sharp, narrow peaks denoting the passage of small, discrete gas structures, identified as bubbly flow on the flow regime map. Figure 5-2 and Figure 5-3 shows higher and wider peaks that are characteristic of the passage of larger gas structures and were classified as slug flow on the map, while Figure 5-4 has peaks that are irregular in sizes. On the flow pattern map, they are identified as belonging to the churn flow regime.

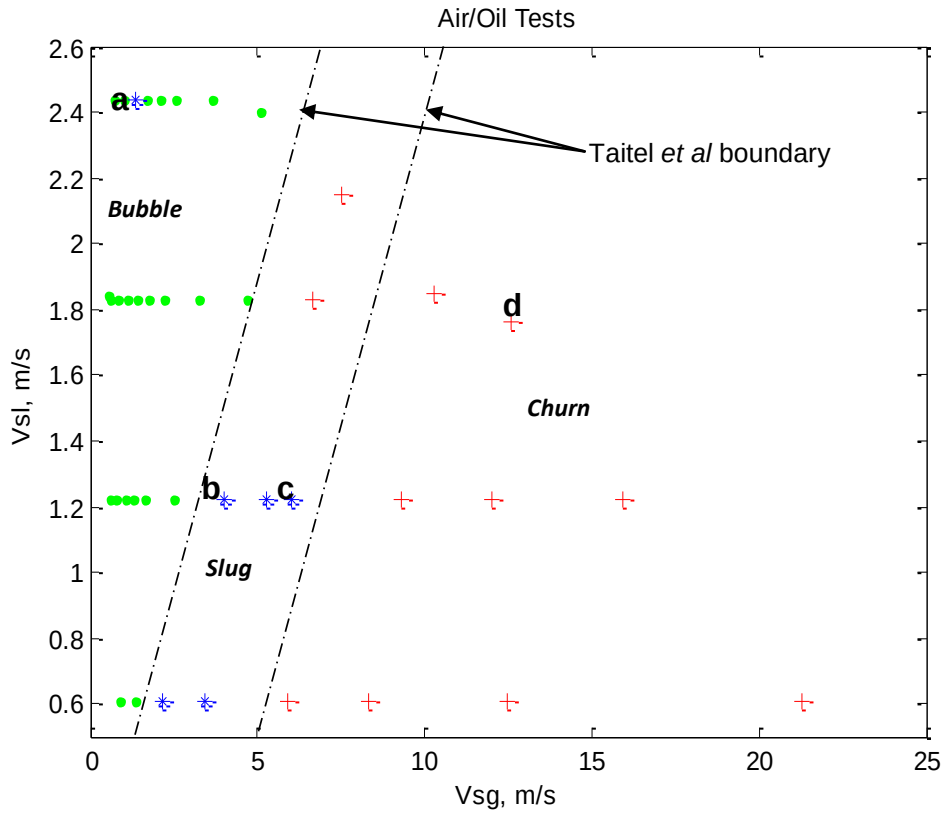

Figure 5-5 Test Points Locations on Air-Oil Vertical Flow Regime

Detailed examination of the entire experimental data in terms of amplitude, time and frequency features showed that the signal of each test data differs from its counterparts and correlates well with the Taitel *et al* flow regime map for vertical flow in a 51mm diameter flowline. Classification of the dominant flow regime for data points located close to the flow regime boundaries was not possible as features of both regimes were present. The inference from the sensor response analysis is that vital clues as to the characteristics of the multiphase flow present could be obtained through the extraction of appropriate features from the gamma count output signals; and correlating these with multiphase flow parameters.

5.1.2 Statistical Analysis

A number of statistical parameters were calculated from the transducers output signals to analyse their relationship with key multiphase flow characteristics. The parameters investigated are described in **Appendix C**. Statistical features such as the central moments, linear prediction coefficients (LPCs) and linear spectral frequencies were calculated from the hard gamma counts and plotted against gas

void fraction, Figure 5-6 and Figure 5-9. The average value (mean) of the gamma count was observed to increase with increasing GVF as a result of the decreasing mixture density, Figure 5-6(a). As one would expect, the lower the water cut, the higher the mean gamma count for all GVF values.

The standard deviation parameter increases with increasing GVF and water cut up to about 50% GVF. Thereafter, further increases in water cut and GVF resulted in a decreasing standard deviation, Figure 5-6(b). It is hypothesised that flow regime change may be responsible for this behaviour in the standard deviation.

The coefficient of skewness and kurtosis parameters are shown in Figure 5-6(c) and (d). The skewness exhibited a linear decrease with GVF up to about GVF of 80% while the kurtosis decreases linearly with the GVF until 50%. Thereafter further increases in GVF had led to an increase in both the skewness and the kurtosis. In general, the skewness decreased with increasing water cut whereas the kurtosis decreased with increasing water cut until 50% GVF and the reverse was the case thereafter, Figure 5-6(d). Again, flow regime change is hypothesised to be the source of this behaviour.

At water cut above 35%, it was observed that LPC1 and LPC2 increase with increasing GVF, Figure 5-7(a) and (b). At lower GVFs, LPC1 and LPC2 range are higher than at higher GVF. The magnitudes of the LPC1 and LPC2 values are a function of water cut.

The magnitude of LPC3 values was virtually unaffected by increasing the GVF but variation between different points with the same GVF but different water cut diminished as illustrated in Figure 5-7(c).

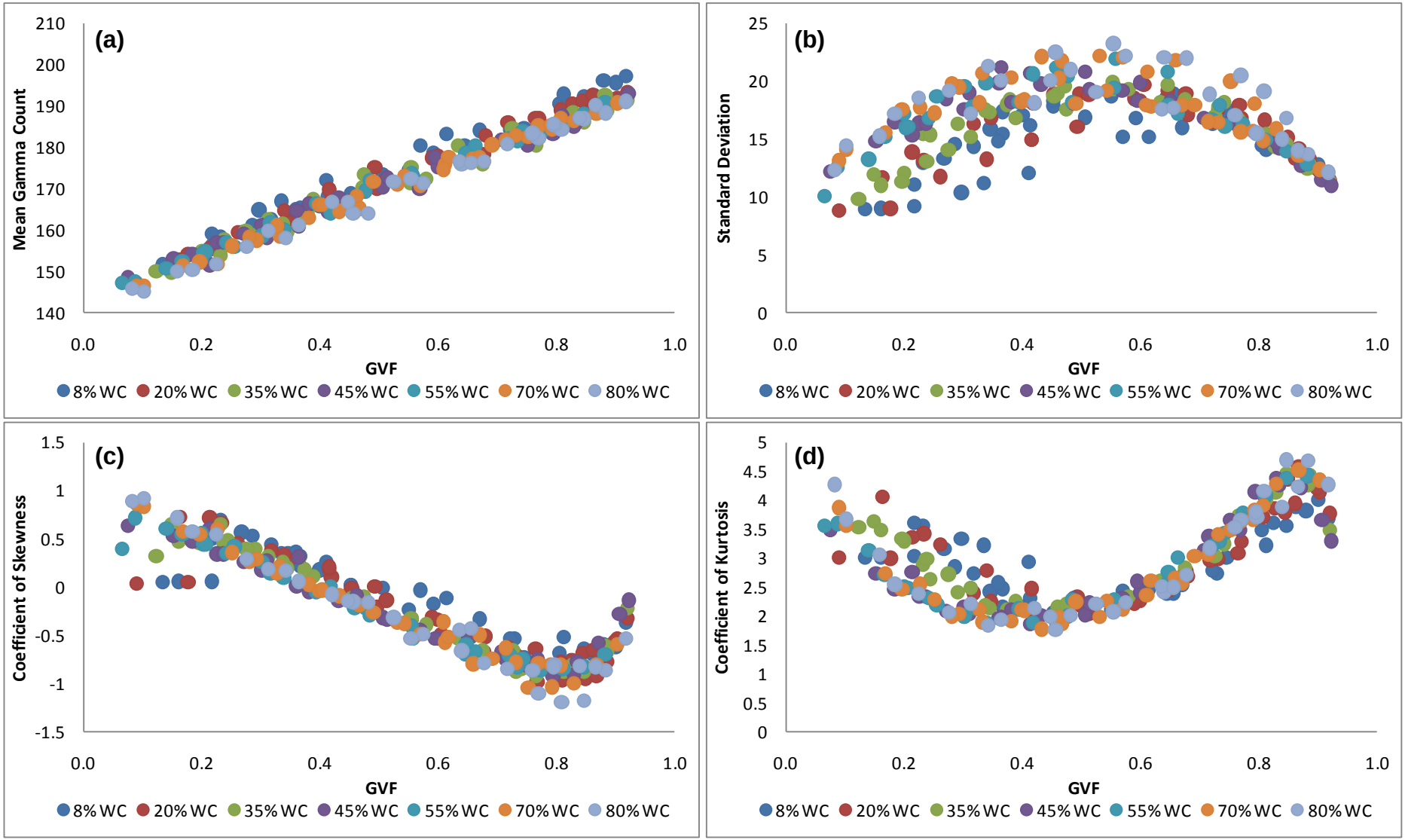

Figure 5-6 Scatter Plots of (a) Mean; (b) Standard Deviation; (c) Skewness and (d) Kurtosis versus Gas Void Fraction

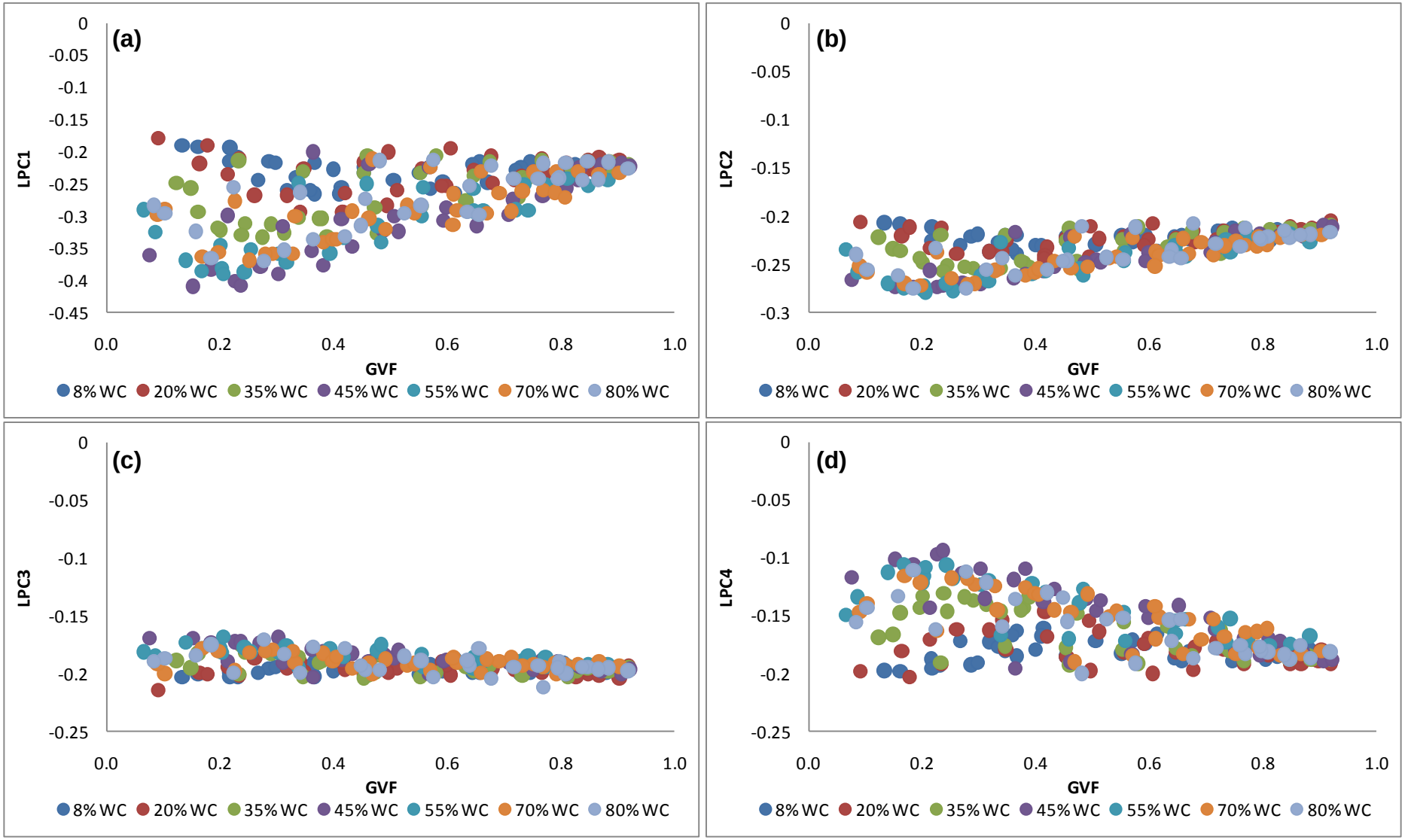

Figure 5-7 Scatter Plots of (a) LPC1; (b) LPC2; (c) LPC3 and (d) LPC4 versus Gas Void Fraction

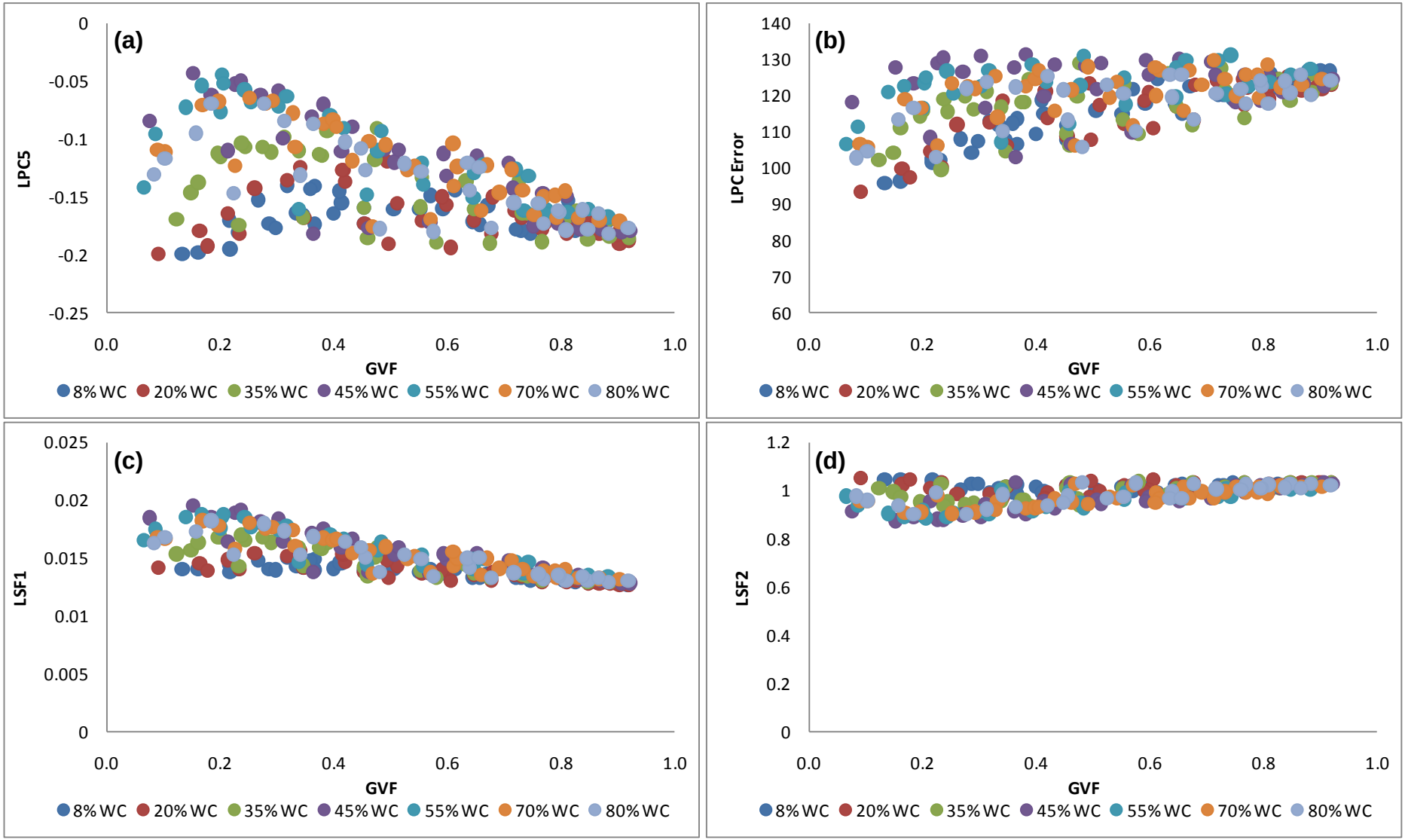

Figure 5-8 Scatter Plots of (a) LPC5; (b) LPC Error; (c) LSF1 and (d) LSF2 versus Gas Void Fraction

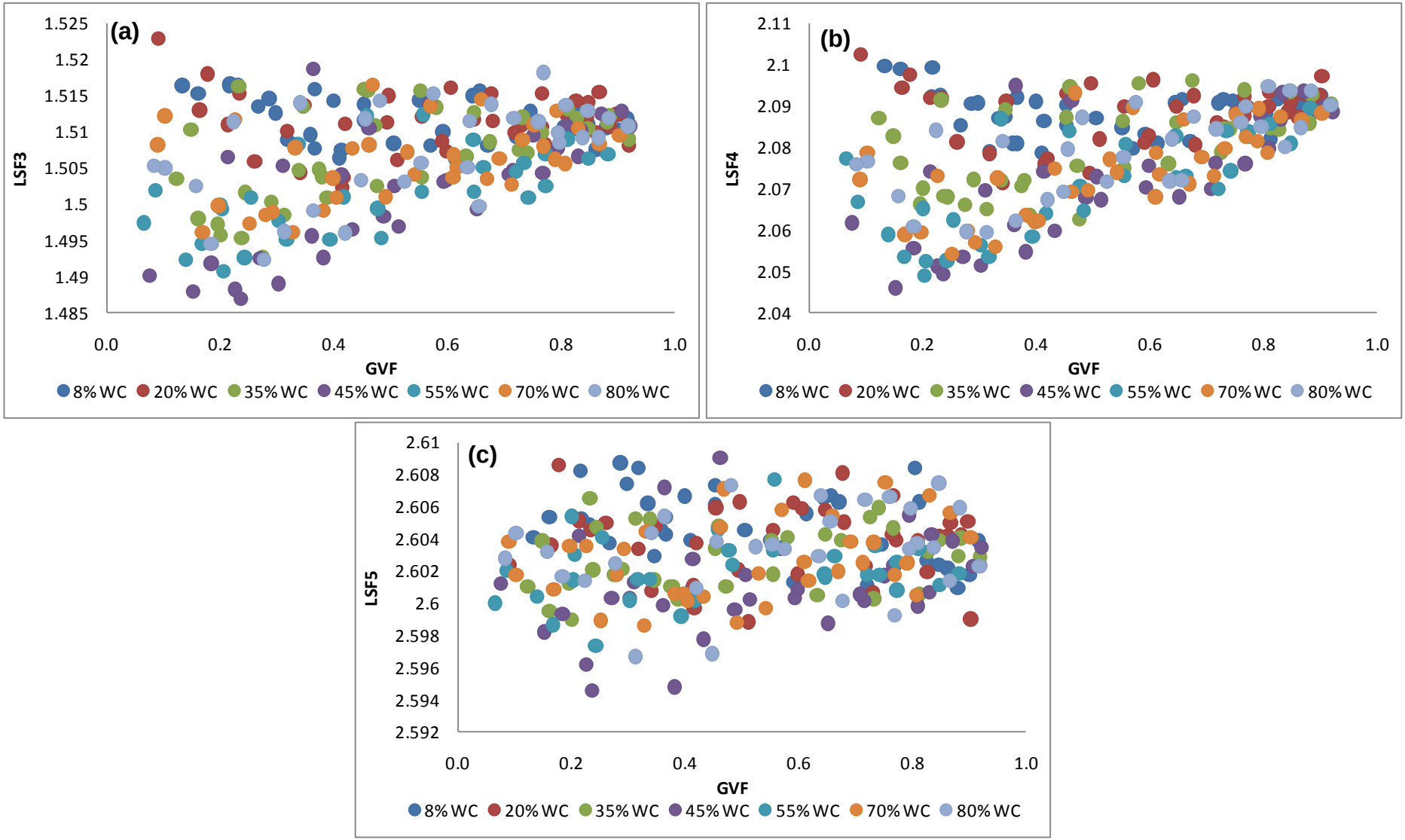

Figure 5-9 Scatter Plots of (a) LSF3; (b) LSF4; and (c) LSF5 versus Gas Void Fraction

LPC4 and LPC5 exhibited similar but reverse behaviour to that of LPC1 and LPC2, Figures 5.7 (d) and Figure 5-8(a). From Figure 5-8(b) the linear prediction coefficient error (E_R) increases in an approximate linear fashion with increasing GVF. Water cut influences the linear prediction error as large variations were observed in the E_R for GVF between 20 to 75%. Above this GVF, a significant decrease in the influence of water was observed.

The magnitude of the first line spectral frequency (LSF1) decreases with increasing GVF, Figure 5-8(c). Water cut was observed to have an influence in the LSF1 magnitude.

LSF2 and LSF5 demonstrated no detectable response to the multiphase flow with increasing GVF, Figure 5-8(d) and Figure 5-9(c).

The LSF3 and LSF4 coefficients decreased in magnitude with increasing GVF for water cuts above 35%, Figure 5-9(a) and (b). However below this water cut, no reasonable trend was observed. Also variation in the magnitude LSF3 and LSF4 was higher at lower GVF and narrows down as the GVF increases.

5.2 Frequency Domain Analysis

Power spectral density function (PSD) shows the strength of the variations (energy) of a signal as a function of frequency. In other words, it shows at which frequencies variations are strong and at which frequencies variations are weak. Spectral analysis is commonly used to reveal the periodicity in time-series signals. PSD is a frequency domain characteristic of a time series and is appropriate for the detection of frequency composition in a stochastic process (Xie *et al*, 2004). The power spectral density function $P_x(f)$ of a discrete-time signal $x(n)$ is defined as the Fourier transform of the autocorrelation sequence $R_x(k)$:

Eqn. 5.1

where f_s is the sampling frequency. Dynamic fluctuations are inherent in multiphase flow systems.

The time-varying raw signals of the gamma densitometer were analysed in the frequency domain. Figure 5-10 are examples of the PSDs for the flow regimes

encountered in the two phase air-oil horizontal flows. The power spectrum in the bubbly flow regime exhibits no clear peaks and no dominant frequency for this example. This could be so because the gas bubbles are finely dispersed in the liquid body. However as the gas flow rate is increased, a peak starts developing in the low frequency region, Figure 5-10Figure 5-10 Power Spectral Density of the Gamma Densitometer Responses in Horizontal Air-Oil Flows: (a) Bubble Flow, (b) Slug Flow and (c) Wave-Turbulent Flow

(aii). This may correspond to the frequency of gas bubbles of different size groups. In the slug flow regime, the lower-frequency peak becomes more dominant. This may represent the passing-by of large gas plugs with dimensions comparable to the pipe diameter, Figure 5-10(bi) and (bii). The power spectrum of wave flow regime shows several peaks spread over a wide frequency range from 0 to 5 Hz, Figure 5-10(ci) and (cii). These peaks may represent the coalescence and collisions of gas pockets.

Examination of the full data set revealed that the frequency components over 10 Hz do not contribute much to the power spectral density. From the above examples, it is concluded that the power spectral structure of each hydrodynamic regime in a gas-liquid flow is distinct, and therefore, could be used to identify the flow regimes based on their estimated gamma signal power spectral characteristics. However, care should be exercised especially for data points that are close to transition boundaries due to regime duality.

5.3 Chapter Summary

Signal analysis of the gamma densitometer response to a variety of multiphase flow conditions was undertaken. Time domain plots of the gamma counts gave a good visual indication of the gas and liquid phase distribution in the flow. A range of statistical features, mainly in amplitude, linear prediction coefficients and line spectral frequencies, were extracted from these signals and found to exhibit discriminatory trends with variation in flow condition. It was observed that no single feature could be used to conveniently describe all the multiphase phase flow conditions and that certain correlations were exhibited over a specific range of conditions.

Spectral analysis was used to reveal the periodicity in the time-series gamma signals. It was evident from the PSD plots that each hydrodynamic flow regime is

distinct, and therefore could be used to identify the prevalent flow regimes; however care should be exercised especially for data points that are close to transition boundaries due to regime duality.

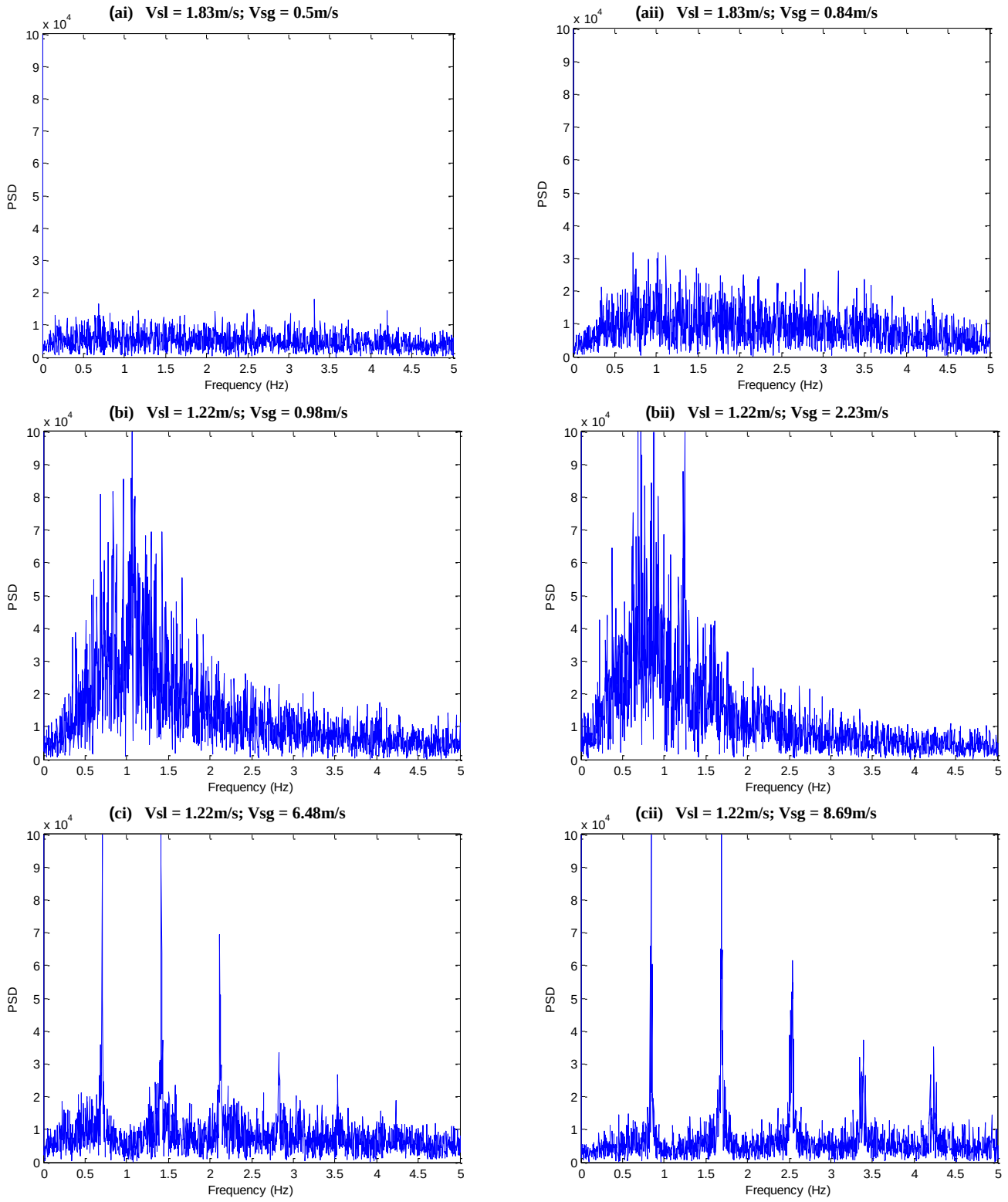

Figure 5-10 Power Spectral Density of the Gamma Densitometer Responses in Horizontal Air-Oil Flows: (a) Bubble Flow, (b) Slug Flow and (c) Wave-Turbulent Flow

CHAPTER SIX

6. PATTERN RECOGNITION TECHNIQUES

This chapter details the application of pattern recognition techniques to predict individual phase flow rates for both horizontal and vertical multiphase flows. Results of the single multilayer perceptron model and how sensors orientation affects the model predictions are also presented here.

An effective signal is a prerequisite to the success of any pattern recognition and modelling systems. In this study, derived features from the hard, soft energy and a combination of both energies of the gamma signals were used as input parameters. Feature sensitivity and strength from these signals were considered from the view point of flow rate identification, thus an objective criterion was used to assess the relationship between each input feature vector and the output vectors which are the superficial gas and liquid velocities and the liquid phase water cut.

6.1 Feature Extraction

Feature extraction, which is a technique used in reducing the dimensionality of raw data, was employed to represent the gamma densitometer data because previous studies in the application of pattern recognition techniques to multiphase metering had reported that the isolation of discriminatory information in the flow lies in efficient feature extraction (Akartuna, 1994; Cai, 1995; Jama, 2004; Blaney, 2008 and Ibrahim, 2009). Also the sheer volume of the data generated by the gamma densitometer (75,000-dimensional input space; i.e. 5 minutes × 60 seconds/minute × 250 Hz) could not be practically handled by a neural network system.

To this end, a number of features were extracted from the hard-energy, soft-energy gamma count and a combination of these energies in the time and frequency domain in order to reduce the dimensionality of the raw data. In our previous research work, all features have been subjected to contour profile analysis to establish their discriminability with respect to key multiphase flow parameters. Owning to the number of features selected for investigation, there was a vast number of possible input vector combinations. Literature review showed that an effective feature vector

permutation will be obtained through the combination of features from each of the information domains. Table 6-1 lists the features selected for examination. These features are described in details in **Appendix C**.

Table 6-1 Features Selected For Examination

		Information Domain			
Feature	**Symbol**	**Amplitude**	**LPC**	**LSF**	**ACF**
Mean Value	AV	✓			
Standard Deviation	SD	✓			
Coefficient of Skewness	CS	✓			
Coefficient of Kurtosis	CK	✓			
Signal Total Energy	E_T	✓			
Linear Prediction Coefficient 1	LPC1		✓		
Linear Prediction Coefficient 2	LPC2		✓		
Linear Prediction Coefficient 3	LPC3		✓		
Linear Prediction Coefficient 4	LPC4		✓		
Linear Prediction Coefficient 5	LPC5		✓		
Linear Prediction Error	E_R		✓		
Line Spectral Frequency 1	LSF1			✓	
Line Spectral Frequency 2	LSF2			✓	
Line Spectral Frequency 3	LSF3			✓	
Line Spectral Frequency 4	LSF4			✓	
Line Spectral Frequency 5	LSF5			✓	
ACF Coefficient at Minimum	ACF1				✓
ACF Lag Minimum	ACF2				✓
ACF Coefficient at Maximum	ACF3				✓
ACF Lag Maximum	ACF4				✓

In applications (Jama, 2004; Blaney, 2008 and Ibrahim, 2009) similar to this study, the dimensions of the raw data were significantly reduced by extracting features considered useful. Therefore, the use of principal component analysis (PCA) as a further dimensional reduction procedure is not recommended because it introduces great computational complexity without necessarily improving classification accuracy.

Thus only the zero mean and unit variance normalisation pre- and post-processing technique was applied to the input and output feature vectors in this study.

6.2 Features Selection

In using neural networks for classification and pattern recognition problems, some representative features must be presented to the network for training. Good features

are expected to result in a better performing network; however the task of selecting a set of meaningful and representative features is a difficult one. Only an exhaustive search can guarantee an optimal solution.

A number of feature selection techniques have been used by various researchers. These include the branch and bound algorithm, sequential forward and backward selection, sequential forward floating selection, fuzzy set theory and neural networks. The use of neural networks for feature selection is established and seems promising, since the ability to solve a task with a smaller number of features is evolved during training by integrating the processes of learning, feature extraction, feature selection, and classification (Verikas and Baccauskiene, 2002). Using neural network to select features is a special case of architecture pruning, whereby input features are pruned based on some saliency criteria aimed at removing less relevant features.

6.2.1 Neural Network Output Sensitivity-based Feature Ranking

The saliency (quality) of a given input feature is very important in pattern recognition especially when there are numerous features available to the neural network. Often it is assumed that all features are equally relevant but this is not the case as some features could be correlated, some scaled duplicates and others completely irrelevant for the classification process. This subsection presents the neural network output sensitivity based feature saliency measure that was used as the feature selection technique in this study.

After training the feedforward multilayer perceptron with the data set, a feature quality index is computed for every input feature p and then all the features are ranked according to the feature quality index (De *et al*, 1997). For each training data point x_i (i = 1, 2,...,Q), one of the features (x_{ip}) is set to zero. Let $x_i^{(p)}$ denotes this modified data point and o_i and $o_i^{(p)}$ the output vectors obtained from the network after the presentation of x_i and $x_i^{(p)}$ The feature quality index (FQI_P) is computed as shown below:

Eqn. 5.1

The larger the index, the more important the feature is. Some results from the use of this FQI_P saliency technique are presented here. The aim is to predict gas and liquid superficial velocities from the densitometer measurement. Sixteen features were extracted from the hard spectrum of the gamma signal response to the air-water two phase flow experiments carried out in the 101.6mm test rig. An MLP neural network was then constructed with 16 nodes in the input layer, 10 nodes in the hidden layer and 2 nodes in the output layer. The network is then trained, the FQI_P computed and the features ranked in terms of their effectiveness in predicting the gas and liquid superficial velocities. Table 6-2 shows the results.

Table 6-2 Ranking of Statistical Features Derived from the Hard Gamma Count Signal

S/N	Features	FQI	Ranking
1	Mean	642.09	1
2	Standard Deviation	282.11	5
3	Skewness	537.89	2
4	Kurtosis	442.44	3
5	Energy	119.37	9
6	LPC1	129.58	8
7	LPC2	436.44	4
8	LPC3	30.341	14
9	LPC4	31.086	13
10	LPC5	114.6	10
11	Residual Error	237.33	6
12	LSF1	211.1	7
13	LSF2	32.536	12
14	LSF3	32.634	11
15	LSF4	29.723	15
16	LSF5	12.998	16

It can be observed from the table that the mean has the highest FQI and was ranked first. This result is supported by Figure 5-6(a) which shows strong dependence of the mean of the gamma count on gas flow rate. In addition to the mean, skewness, kurtosis, and LPC2 also show relatively high values of FQI. On the other hand LSF5, LSF4 and LPC4 appear to be of little relevance in terms of flow rate prediction. After several trials, the first ten features were then selected because they gave a better generalisation and prediction performance.

6.3 Single Feedforward Multilayer Perceptron Model

Figure 6-1 shows a generic workflow of the main elements involved in the pattern recognition approach for multiphase flow metering carried out in this study.

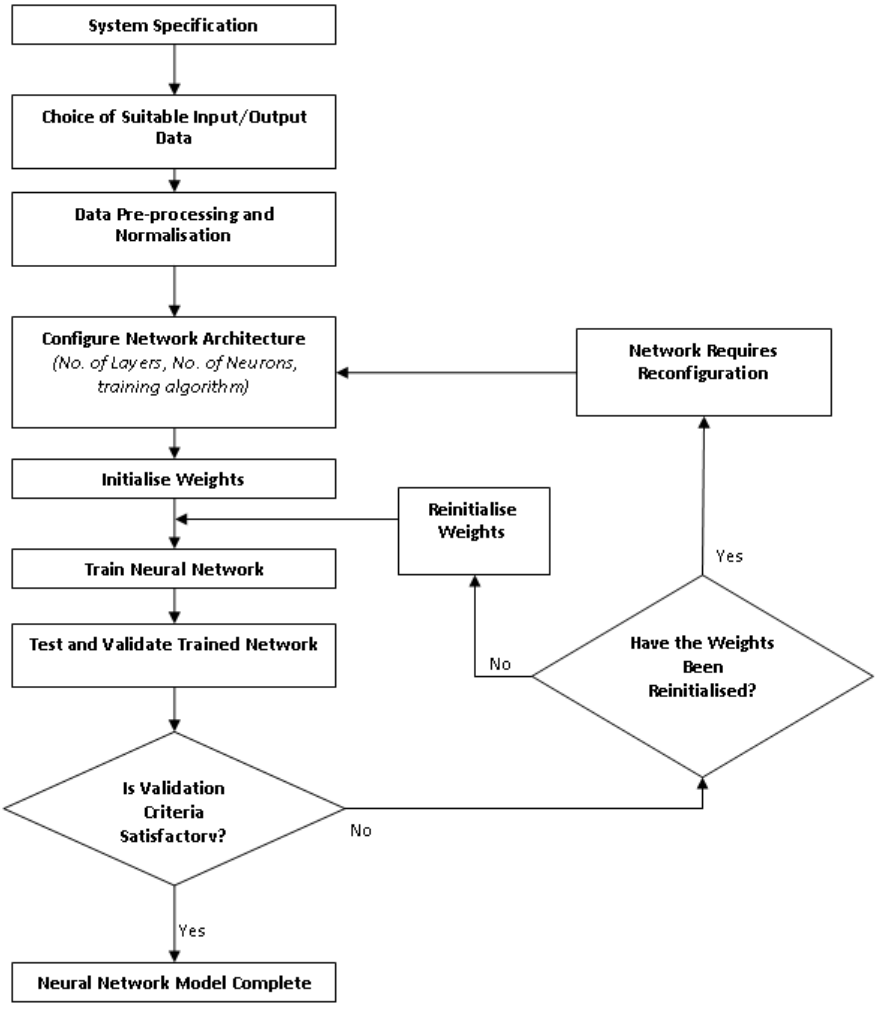

Figure 6-1 Neural Network System Identification Methodology

A feedforward multilayer perceptron (MLP) model was developed with the superficial gas velocity (V_{sg}), superficial liquid velocity (V_{sl}) and water cut (WC) as the output nodes as illustrated in Figure 6-2. The 260 experimental data of the air-water two phase flow (in the 50.8mm rig) and the 744 data points of the air-oil-water three phase flow (in the 101.6mm rig) were divided into training and test sets with two-third used for training the network and one-third for testing purposes. All input and target outputs for the network were pre-processed using the zero-mean unit-variance

(ZMUV) normalization technique in order to equalise the magnitude and dynamic range of each feature.

Prior to running the neural network simulation, the network architecture has to be determined, by specifying the number of hidden layers and the number of neurons in each layer. Recent work has revealed that optimal performance can only be achieved if the network architecture is chosen according to the peculiarity of the problem. This is so because a system cannot be modelled by a network with insufficient resources.

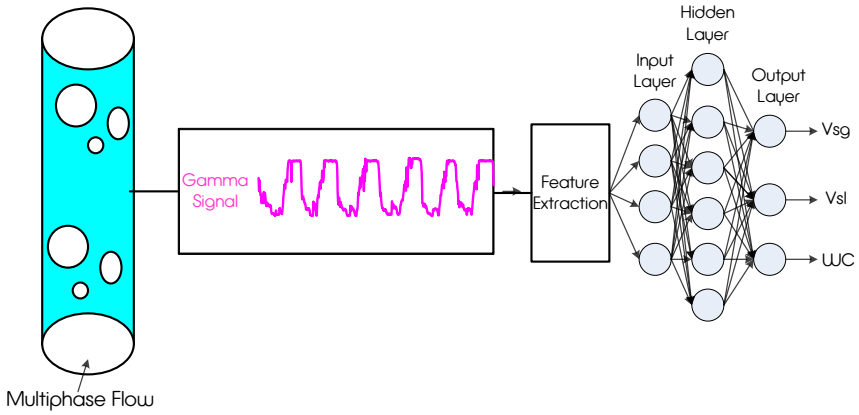

Figure 6-2 The MLP Neural Network Model Concept

Conversely an architecture that is too complex will require a very large training data set in order to specify all parameters in the network. After several trials, the final architecture was defined as [n – 12 – 2] for the air-water two phase flow data and [n – 14 – 3] for the air-oil-water three phase flow data. Where;

- n – is the number of input feature vectors (variable)
- 12 and 14 – are the number of neurons in the hidden layer (fixed)
- 2 and 3 – are the number of output neurons, i.e., one each for the target (fixed)

Batch training approach, whereby all the training data is fed into the network and the weights of the network updated only when the entire batch of the data has been processed, was utilised in this simulation. The process of training the network and adjusting its weights was repeated until a point sufficiently close to the minimum was

determined. This was achieved using the Bayesian regularisation with the Levenberg-Marquardt (LM) algorithm technique described in section 2.4

After training, the neural network model was assessed to evaluate its repeatability capabilities. The same training data set is presented to the trained neural network for testing. Figure 6-3 shows the repeatability results of the phase superficial velocities predicted by the MLP network against the target phase superficial velocities. Near perfect linear approximation was achieved demonstrating that the model developed exhibits good repeatability. It is pertinent to note here that a neural network training result only shows whether the learning process is successful. That is, an excellent performance of the network on the training data set does not guarantee a similar level of performance on the test data; though the test performance result should be comparable with that of the training with some degradation.

In order to get a quantitative comparison of the neural network performance, an error criterion, calculated as a relative error over the measurable flow range of each phase was established as given by Equation 6.3. The target accuracy for this work was set at ±5% for the air-water two phase flow data and ±10% for the air-oil-water three phase flow data for each of their target output.

$$\frac{\qquad}{\qquad} \qquad \text{Eqn. 6.3}$$

Where Y_m is measured variable, Y_a is the actual or reference measurement and ($Y_{max} - Y_{min}$) is the measurable range. This performance classification method has been widely used by several researchers, (Darwich, 1989; Akartuna, 1994; Cai, 1995; Jama, 2004; Blaney, 2008 and Ibrahim, 2009).

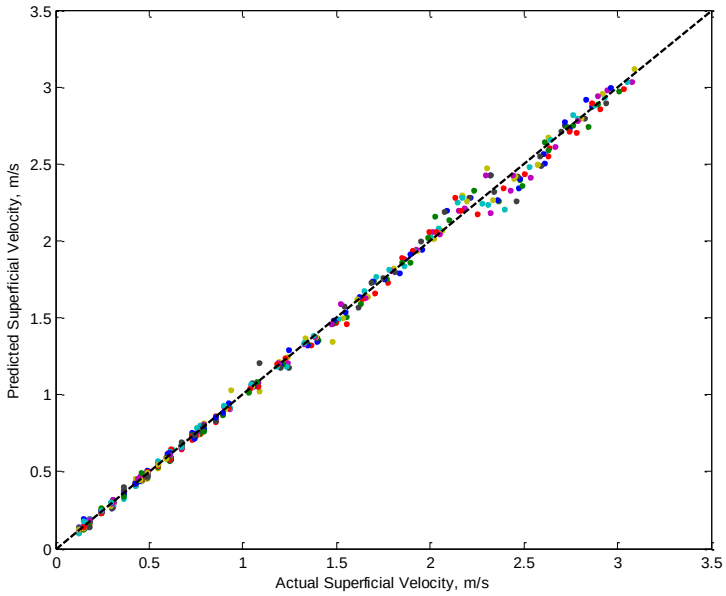

Figure 6-3 Performance for the Superficial Gas and Liquid Velocity (Training Results)

6.4 Multiphase Flow Measurement Results

Flow rate measurement results of the air-water two phase vertical flow (101.6mm test rig) obtained for both the gas and liquid superficial velocities with the gamma densitometer hard, soft and hard-soft combined signals are presented in Figures 6-4, 6-5.and 6-6 and are also shown Table 6-3 . At a measurement error band of ±10%, 100% of the data points were predicted correctly for both the gas and liquid superficial velocities for all the input features.

For the hard signal, and at an error band of ±5%, 91% of the test data points were correctly predicted for the gas superficial velocities and 80% for the liquid superficial velocities, Figure 6-4.

Prediction results for the soft gamma signal outperforms those of the hard signals at the ±5% error band as 95% of the test data points were correctly predicted for both the gas and liquid superficial velocities, Figure 6-5.

Combining features from both soft and hard gamma signal yielded results similar to those obtained with the soft gamma signals only. That is 95% of the test data points were predicted to within ±5% target value for the gas and liquid superficial velocities, Figure 6-6.

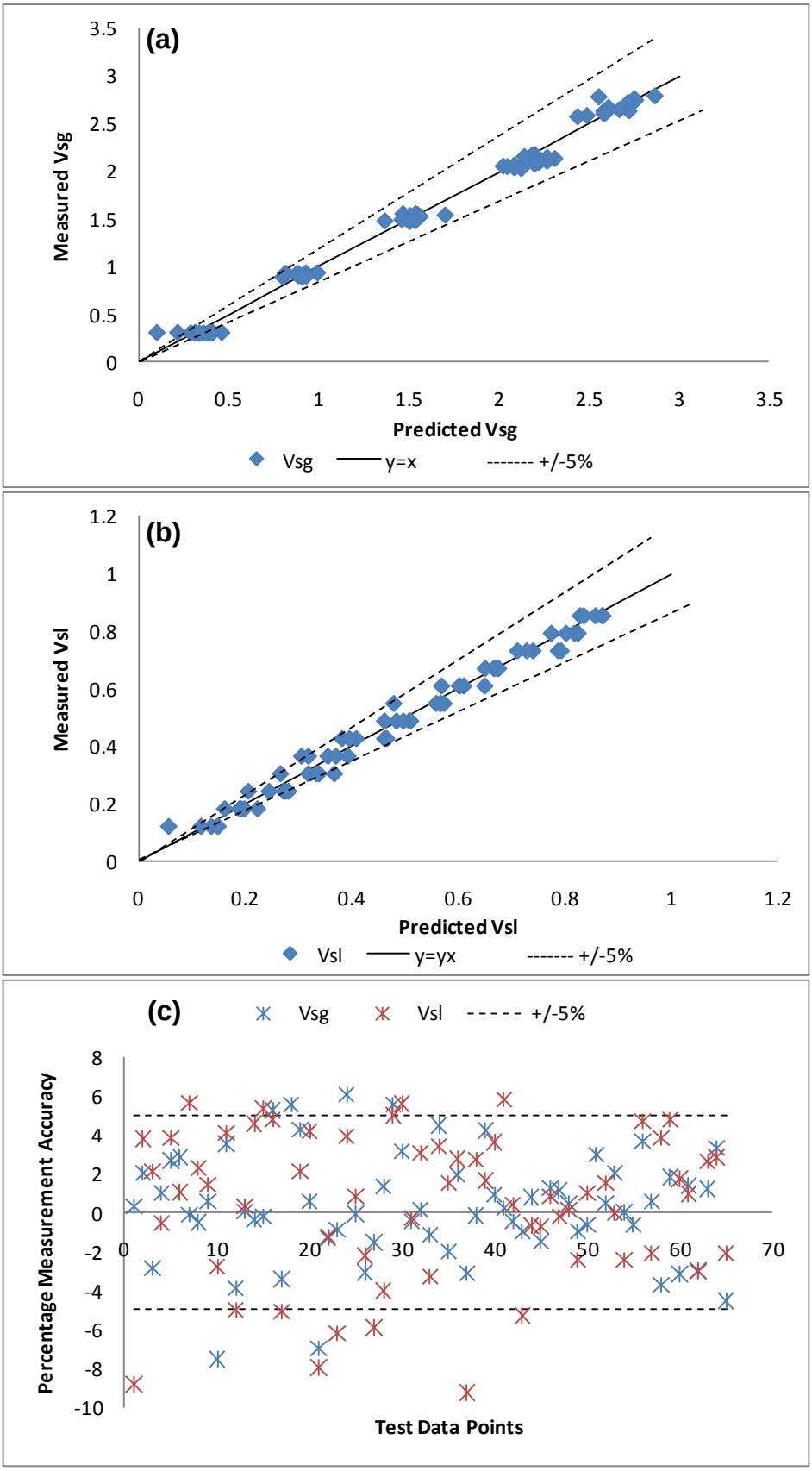

Figure 6-4 (a & b) Predicted versus Measured Vsg and Vsl; (c) Prediction Performance from the Hard Energy Features in Air-Water Vertical Flows (101.6mm Flow Loop)

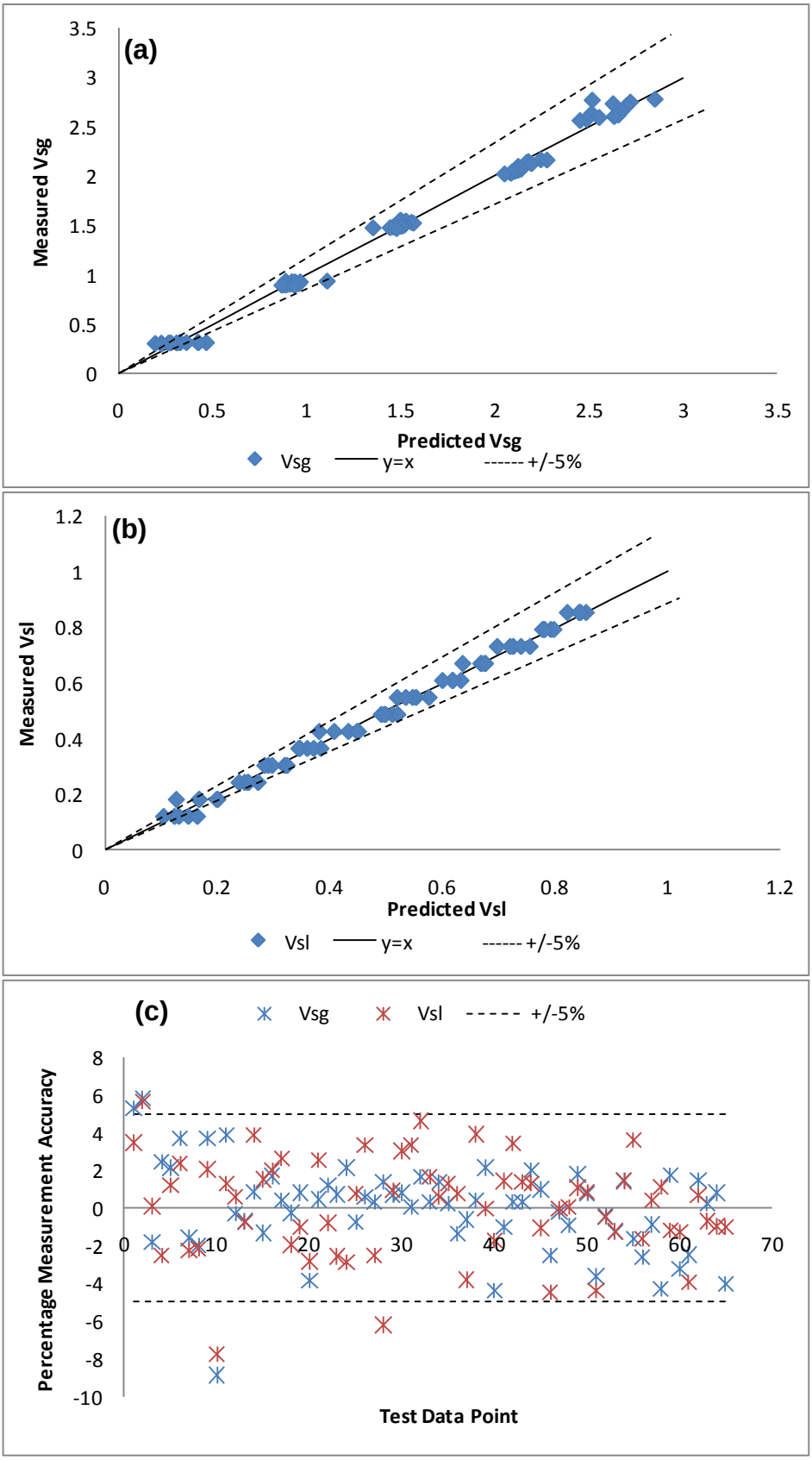

Figure 6-5 (a & b) Predicted versus Measured Vsg and Vsl; (c) Prediction Performance from the Soft Energy Features in Air-Water Vertical Flows (101.6mm Flow Loop)

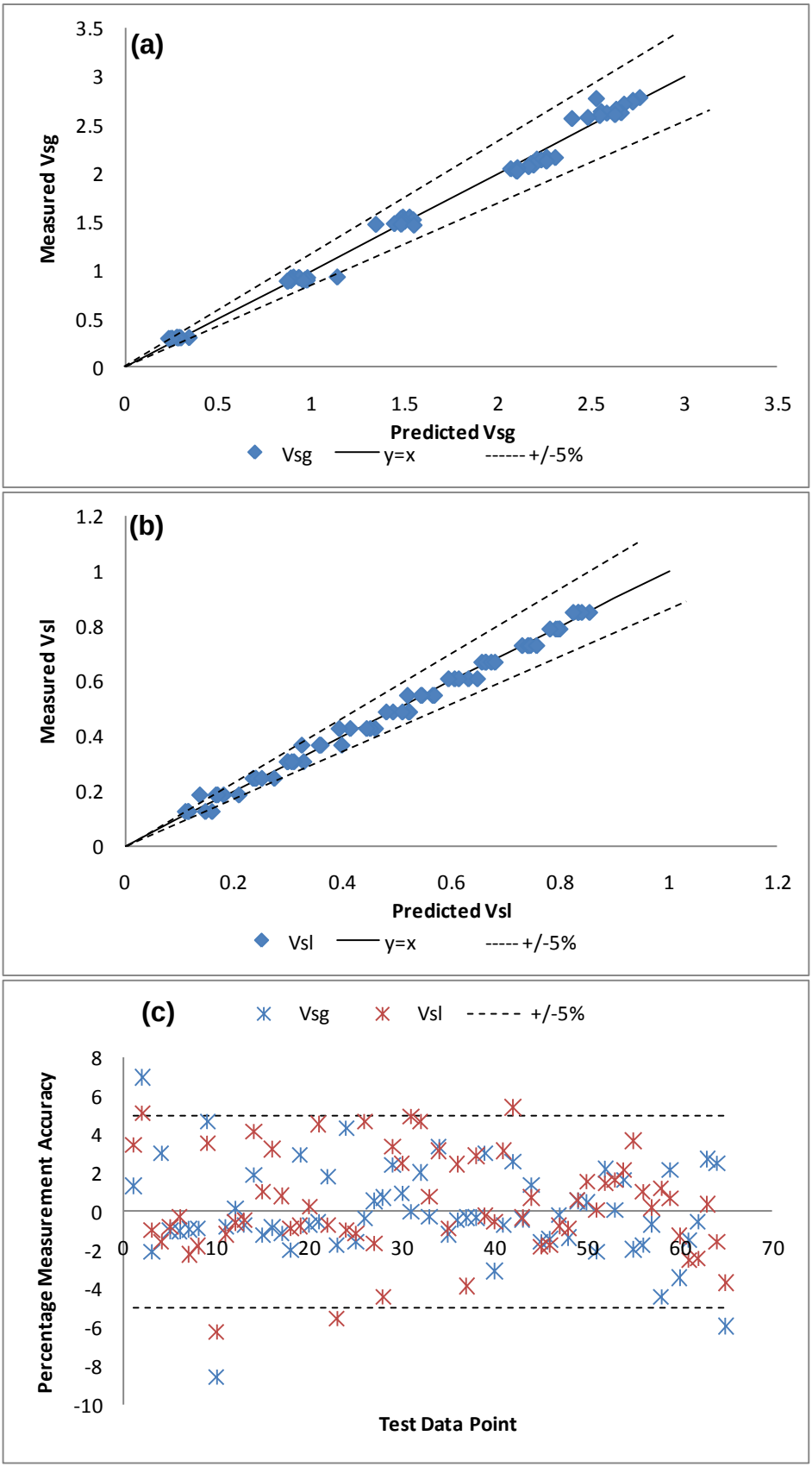

Figure 6-6 (a & b) Predicted versus Measured Vsg and Vsl; (c) Prediction Performance for the Combined Hard-Soft Energy Features in Air-Water Flows (101.6mm Flow Loop)

Flow rate and water cut measurement results of the air-oil-water three phase flows (50.8mm test rig) obtained with the gamma densitometer hard, soft and hard-soft combined signals are presented in Figure 6-7, Figure 6-9 and Figure 6-11 for the horizontal and Figure 6-13, Figure 6-15 and Figure 6-17 for the vertical. Table 6-4 contains a summary of the flow rates and water cut prediction performance. In general, the results from the gamma densitometer mounted in the horizontal orientation are much better than those got from the one mounted vertically. The soft gamma signal was generally better in predicting the superficial velocity. It is thought that the soft beam samples more of the flow. Also, it was observed that combining the hard and soft signals did not necessarily improve the prediction performance of the network.

The MLP neural network model exhibited good gas classification suggesting that the extracted features yielded good correlation with the multiphase flow gas and liquid phase properties across the measurement range studied and discrepancies in the correlations between flow regimes could be sufficiently modelled by a single neural network model.

However, with the current feature set, it is not possible to obtain satisfactory liquid phase water cut parameter predictions using only a single MLP neural network for the three phase flow data. It was anticipated that the liquid phase predictions would be less accurate when compared to those obtained for the gas phase. This is because the densitometer signal is dominated by the passage of gas structures. As such, the underlying features contained in the signals will be more predictive to the gas phase correlations than for those of the liquid phase. To this end, it is suggested that filtering the signals to remove the fluctuations caused by large gas structures, could lead to better prediction performance for the liquid phase parameters.

Table 6-3 Summary of Measurement Prediction Results for Air-Water Two Phase Flows in the 101.6mm Test Loop

SIGNAL	(E_R)		(E_R)	
	V_{sg}	V_{sl}	V_{sg}	V_{sl}
Hard Gamma	100	100	91	80
Soft Gamma	100	100	95	95
Hard-Soft Combined	100	100	95	95

Table 6-4 Summary of Measurement Prediction Results for Air-Oil-Water Three Phase Flows in the 50.8mm Test Loop

SIGNAL	HORIZONTAL (E_R)			VERTICAL (E_R)		
	V_{sg}	V_{sl}	WC	V_{sg}	V_{sl}	WC
Hard Gamma	95	80	42	90	67	43
Soft Gamma	95	73	41	91	70	42
Hard-Soft Combined	95	76	42	92	68	40

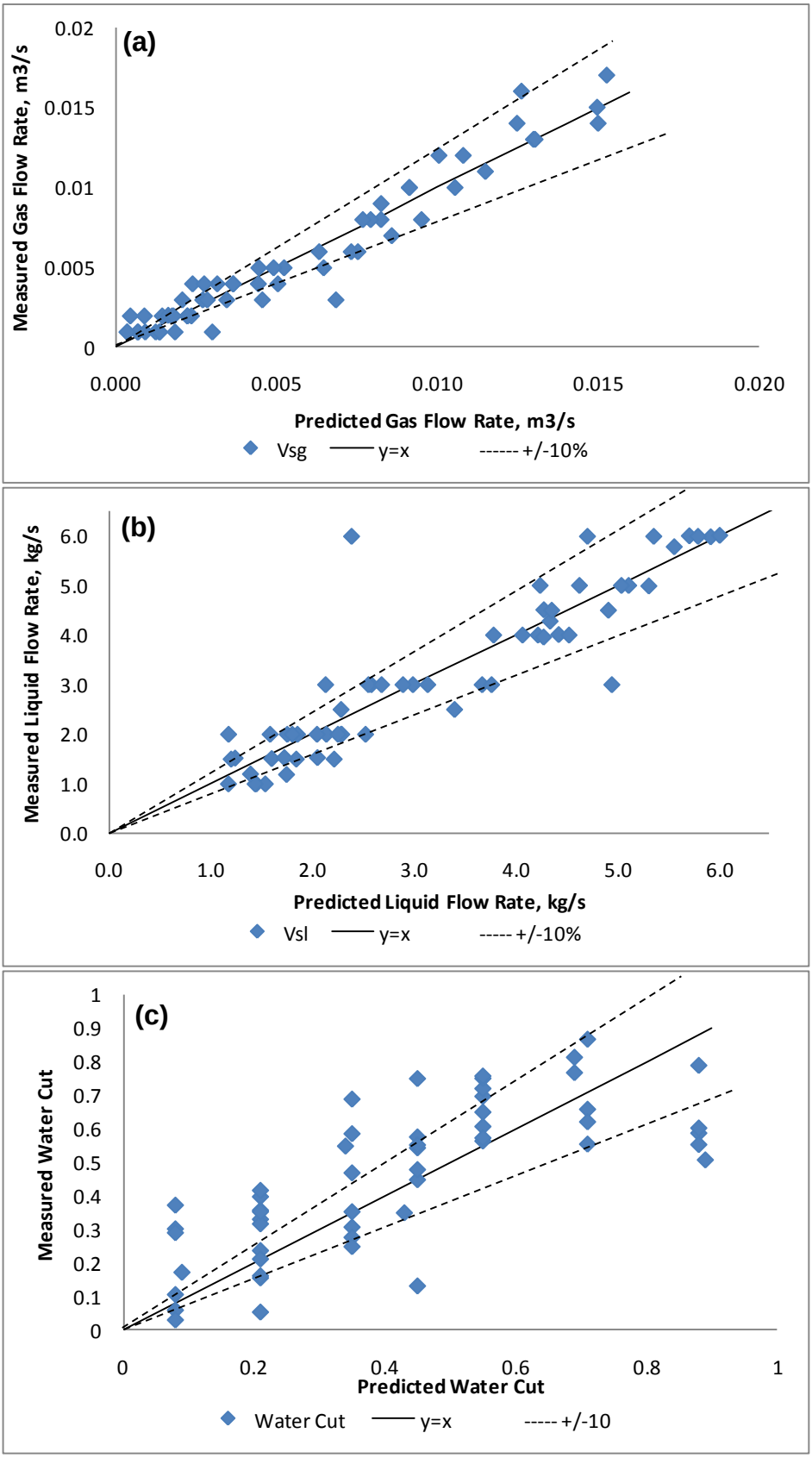

Figure 6-7 (a, b & c) Predicted versus Measured Flow Rates and Water Cut for the Hard Energy Features in Horizontal Three Phase Flows (50.8mm Flow Loop)

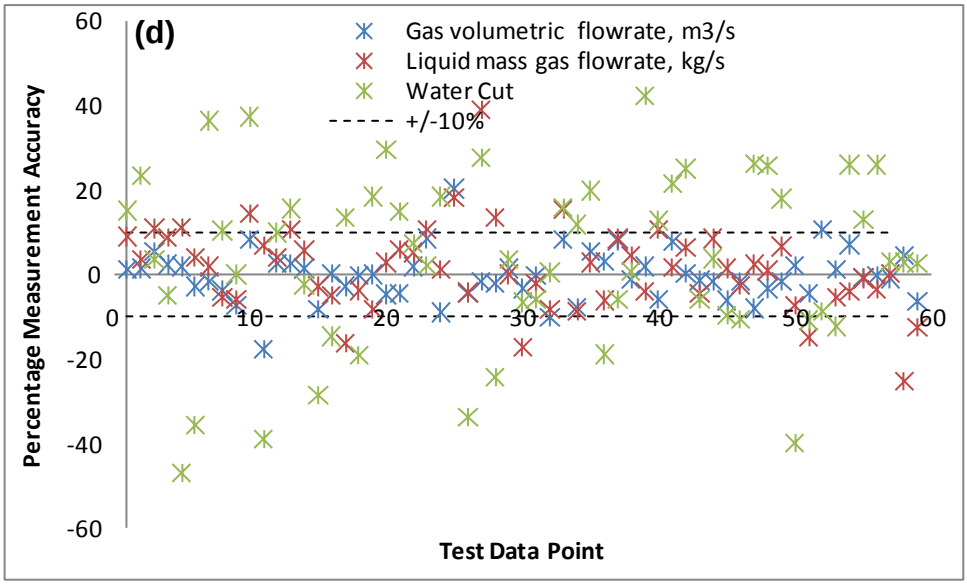

Figure 6-8 (d) Prediction Performance for the Hard Energy Features in Horizontal Three Phase Flows (50.8mm Flow Loop)

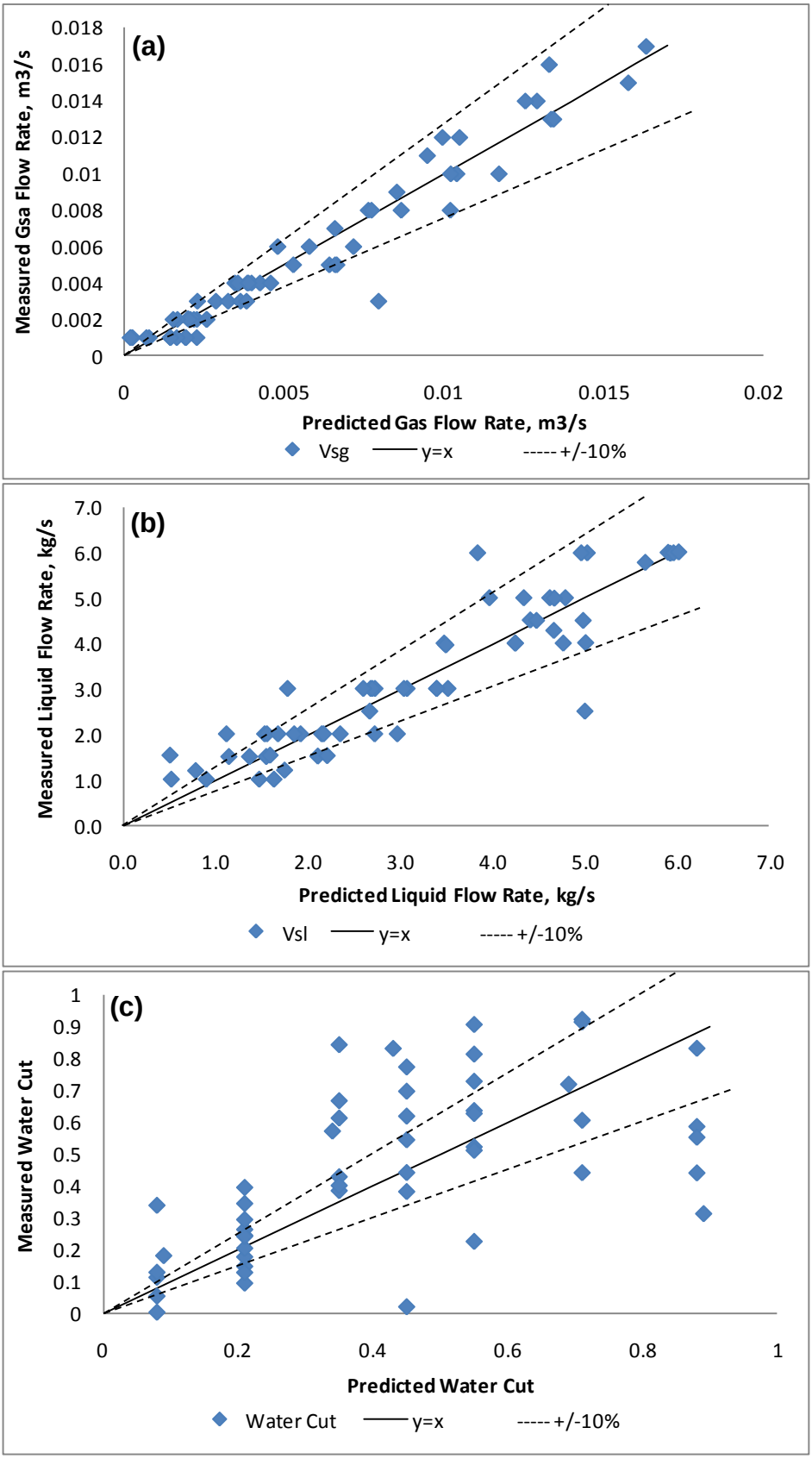

Figure 6-9 (a, b & c) Predicted versus Measured Flow Rates and Water Cut for the Soft Energy Features in Horizontal Three Phase Flows (50.8mm Flow Loop)

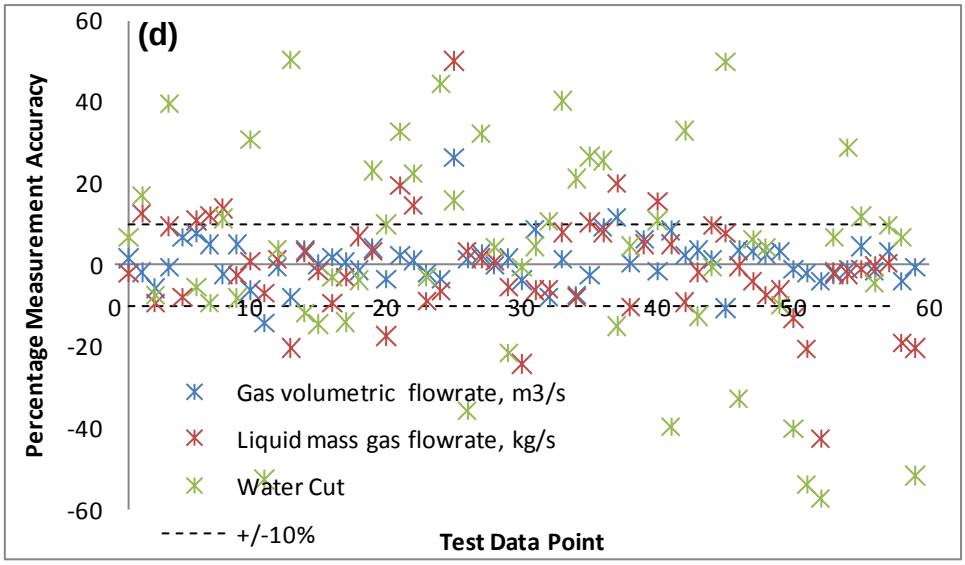

Figure 6-10 (d) Prediction Performance for the Soft Energy Features in Horizontal Three Phase Flows (50.8mm Flow Loop)

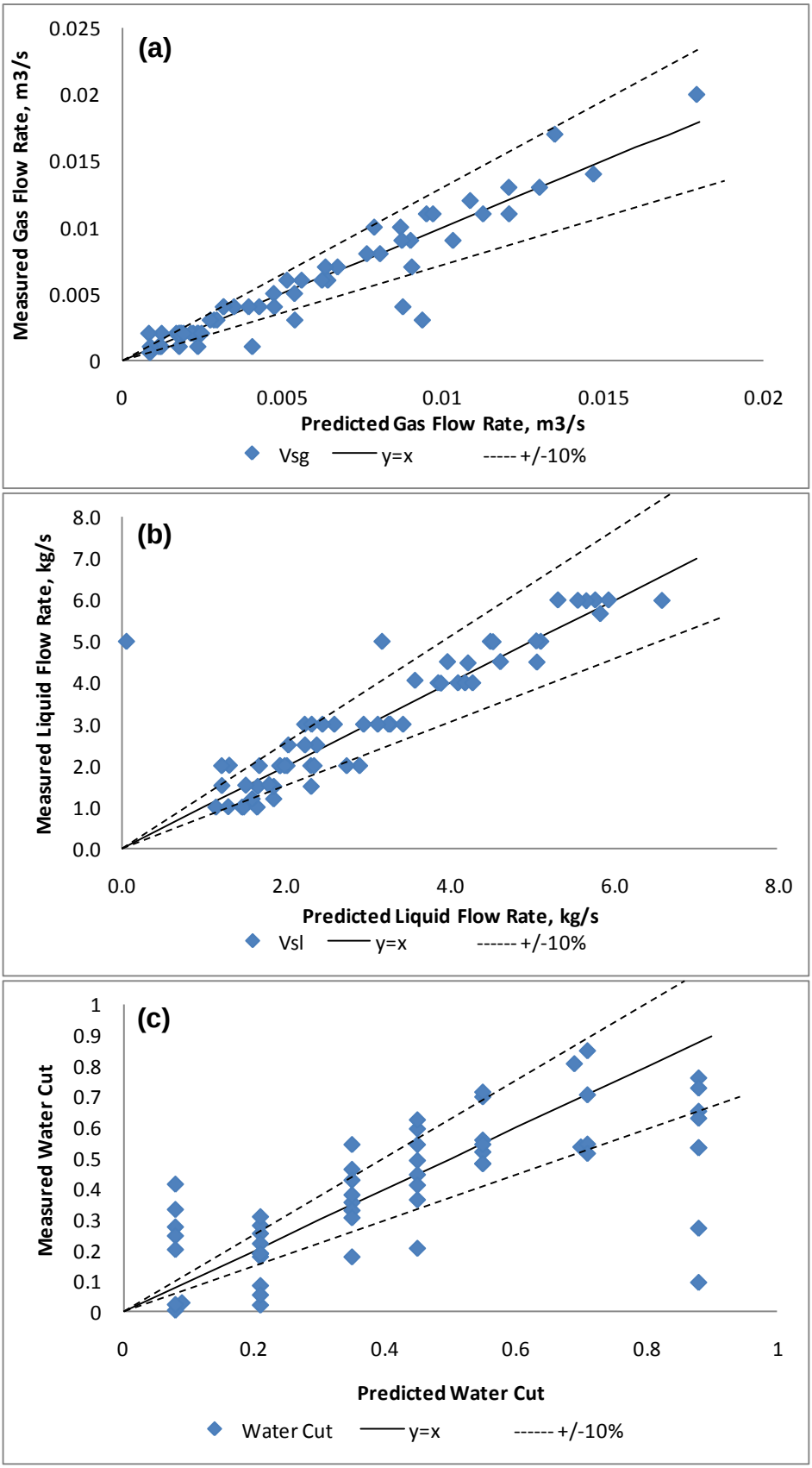

Figure 6-11 (a, b & c) Predicted versus Measured Flow and Water Cut for the Hard-Soft Combined Energy Features in Horizontal Three Phase Flows (50.8mm Flow Loop)

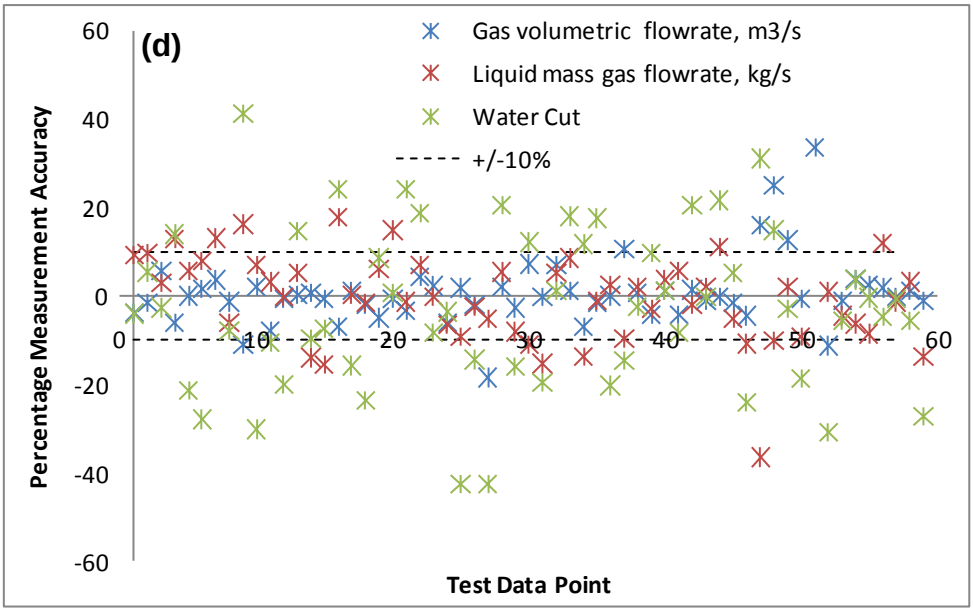

Figure 6-12 (d) Prediction Performance for the Hard-Soft Combined Energy Features in Horizontal Flows (50.8mm Flow Loop)

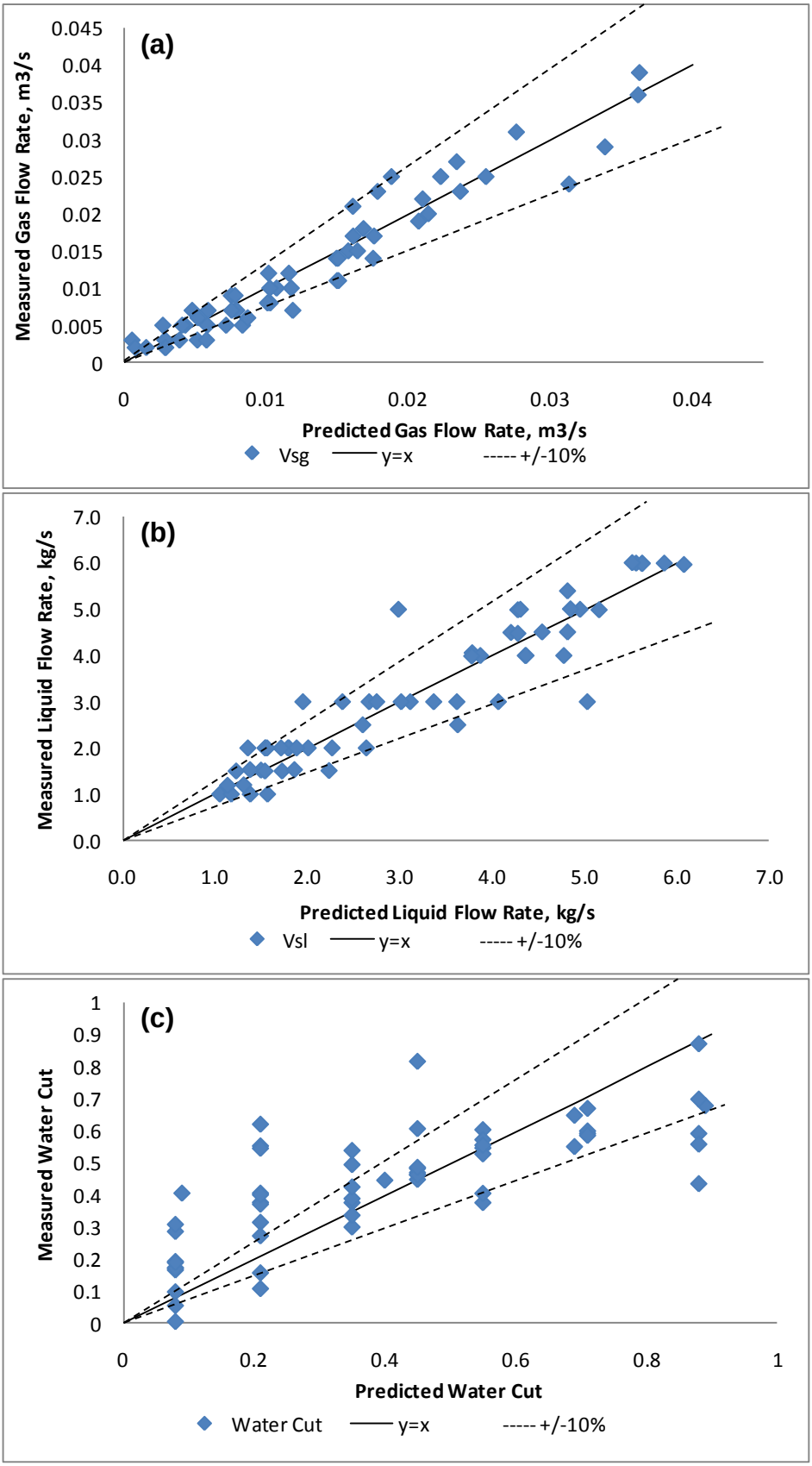

Figure 6-13 (a, b & c) Predicted versus Measured Flow Rates and Water Cut for the Hard Energy Features in Vertical Three Phase Flows (50.8mm Flow Loop)

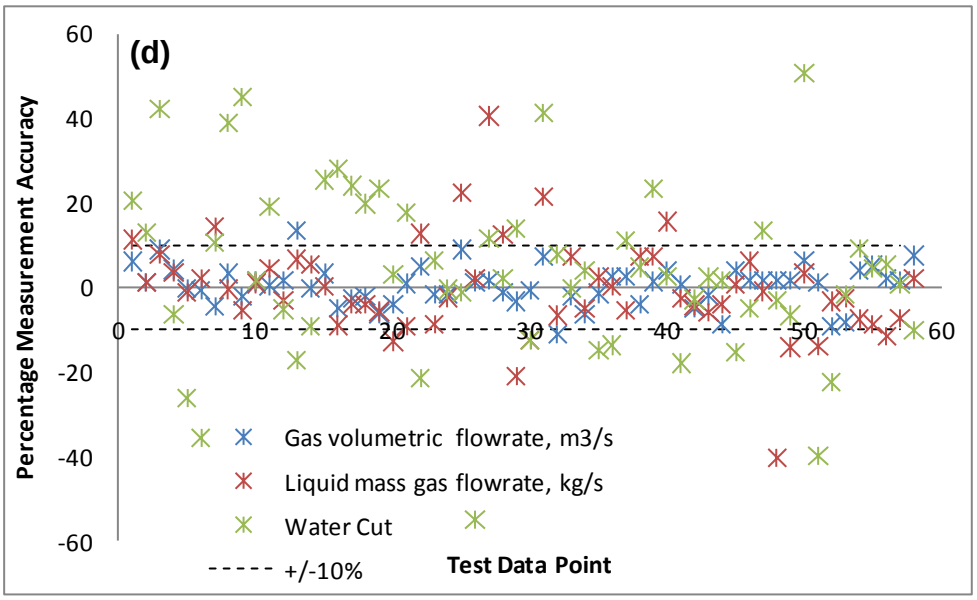

Figure 6-14 (d) Prediction Performance for the Hard Energy Features in Vertical Three Phase Flows (50.8mm Flow Loop)

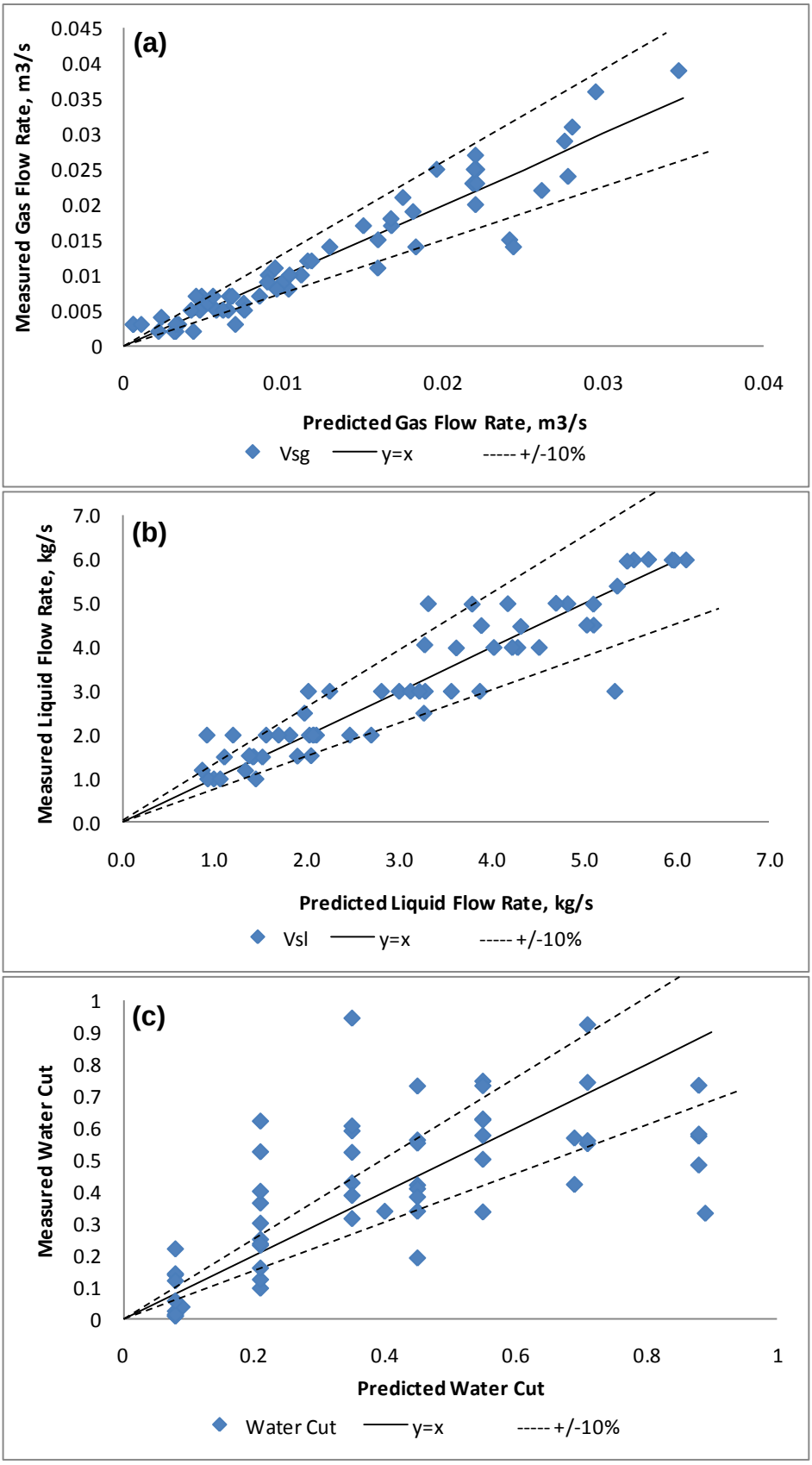

Figure 6-15 (a, b & c) Predicted versus Measured Flow Rates and Water Cut for the Soft Energy Features in Vertical Three Phase Flows (50.8mm Flow Loop)

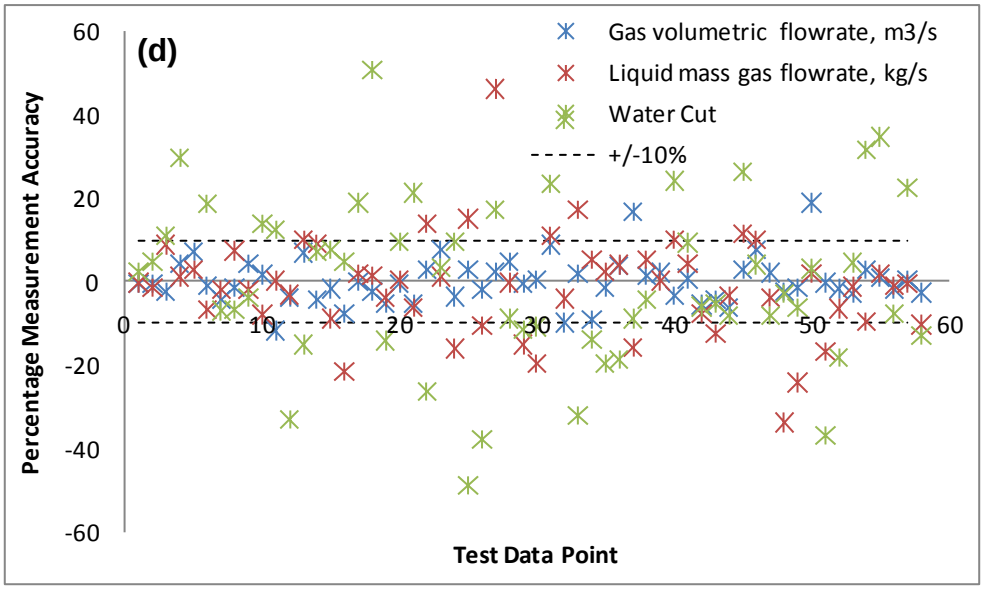

Figure 6-16 (d) Prediction Performance for the Soft Energy Features in Vertical Three Phase Flows (50.8mm Flow Loop)

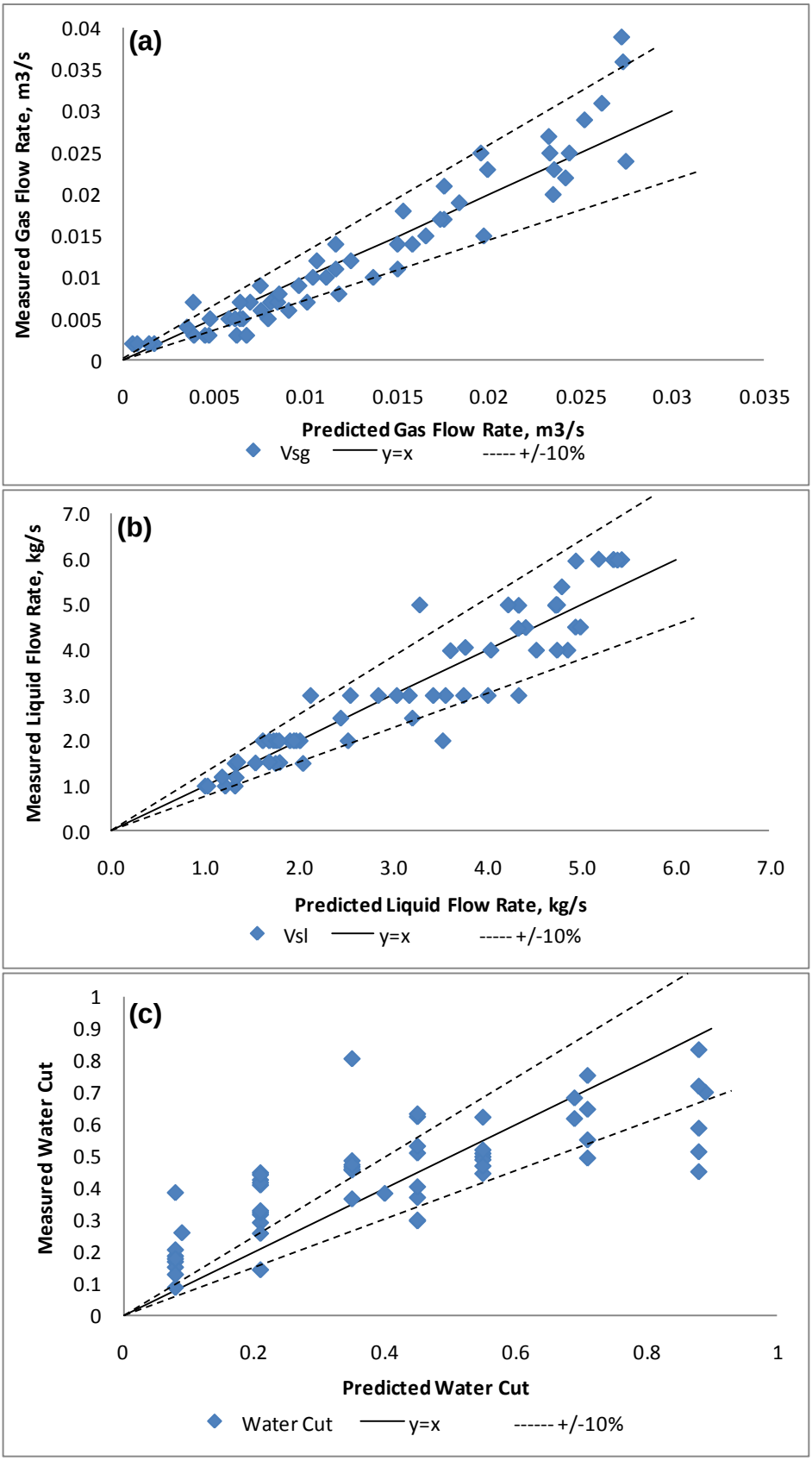

Figure 6-17 (a, b & c) Predicted versus Measured Flow Rates and Water Cut for the Hard-Soft Combined Energy Features in Vertical Flows (50.8mm Flow Loop)

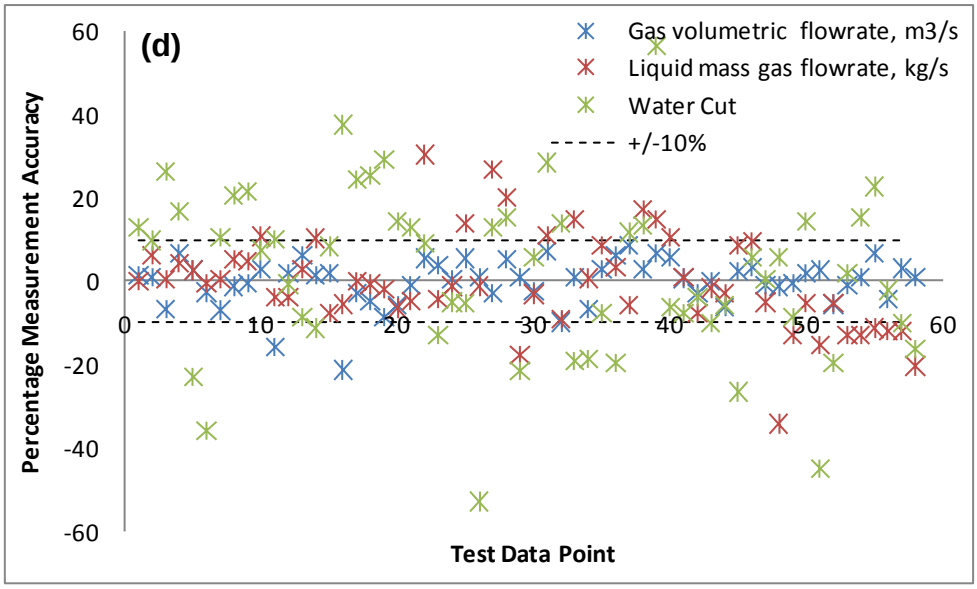

Figure 6-18 (d) Prediction Performance for the Hard-Soft Combined Energy Features in Vertical Flows (50.8mm Flow Loop)

6.5 Neural Network Limitation, Optimisation and Control

In a measurement system that uses artificial neural networks, it is not only important to calculate output data, but it is as well important to obtain correct estimates for the errors of the output data. Flawless output does not exist. Sources of errors are the non-perfect generalization of the network and errors of the input data. This means that the error estimate has to take into account different sources of errors.

Systematic errors of the input data should be avoided during the data collection. If this is not possible, they can be reduced by suitable coding schemes. Statistical errors in the input data are always present. An error-free measurement does not exist. In many cases the statistical errors play a minor role. But since the neural network represents a non-linear function, even a small error in the input data can produce large errors in the output data. Therefore one needs to know how errors propagate in the network.

6.5.1 Optimisation and Control

Neural networks can be (and must be) controlled and optimized even in the operations mode. The aspects that are important to optimize and control in a neural network are:

- **Costs**: Running a neural network may be expensive. There are not only costs for the computational facilities and for the personnel, but also costs for the collection of the input data.
- **Quality**: The output data of a neural network always have an error. One goal of optimization can be to reduce the error.
- **Speed**: In some applications the speed of the network can be a critical quantity and one wants to reduce the calculation time of the network.

6.5.2 Neural Network Refinement

Optimization of the network design, including the optimization of the number of neurons, the properties of the neurons, and the connections between the neurons is usually done during the development stage. During the operations mode one has to check, whether the input data lie in the region where the network was trained. Outliers can be found using statistical methods. Outliers should be removed. If necessary a new training cycle to improve the behaviour of the network should be carried out.

6.1.1 Software Optimisation and Control

Neural networks are a software product. Instabilities may occur after a long time. This may happen if after that time input data occur which have not been taken into account earlier. In many cases neural networks are developed using neural network simulators. These programs have important advantages. Often they offer special tools for analyzing the behaviour of the network. They also provide a graphical user interface which makes it easy to deal with the program. It is recommended that after designing and training network, it should implement using a higher programming language and a fast compiler.

6.1.1 Hardware Optimisation

Neural networks can be developed and programmed on any modern hardware. In optimising the hardware, two aspects play an important role; namely speed and stability. New hardware can improve the speed of the network a lot, but an optimization of the software can increase the speed even more. Stability is important since the network should work on long time scales (several years). It is also

important that the network can easily be ported to newer hardware. The choice and the maintenance of the operating system are important as well.

6.2 Chapter Summary

Features effectiveness was analysed and evaluated with the feature quality index (FQI) saliency criteria, enabling an optimal feature set unique to water cut, gas and liquid flow rates to be obtained.

The feed forward multilayer perceptron gave the following measurement accuracy for the 101.6mm test loop data:

- the hard gamma signal predicted 91% of the gas superficial velocities and 80% of the liquid superficial velocities within the target accuracy of ±5%
- the soft gamma signal outperforms those of the hard signals at the ±5% error band as 95% of the data points were correctly predicted for both the gas and liquid superficial velocities
- the hard-soft combined signal gave results similar to those of the soft gamma signals.

The neural network model developed for the 50.8mm test loop data with the gamma densitometer mounted horizontally outperformed the model developed with the vertical data. In the horizontal flow:

- 95% of the superficial gas, 80% of the superficial liquid and 42% of the water cut samples were identified within the ±10 target accuracy using the hard gamma signal
- 95% of the superficial gas, 73% of the superficial liquid and 41% of the water cut samples were identified within the ±10 target accuracy using the soft gamma signal
- 95% of the superficial gas, 76% of the superficial liquid and 42% of the water cut samples were identified within the ±10 target accuracy using the hard-soft combined gamma signal.

Whereas in the vertical flow:

- 90% of the superficial gas, 67% of the superficial liquid and 43% of the water cut samples were identified within the ±10 target accuracy using the hard gamma signal
- 91% of the superficial gas, 70% of the superficial liquid and 42% of the water cut samples were identified within the ±10 target accuracy using the soft gamma signal
- 92% of the superficial gas, 68% of the superficial liquid and 40% of the water cut samples were identified within the ±10 target accuracy using the hard-soft combined gamma signal.

The MLP neural network model exhibited good gas classification suggesting that the extracted features yielded good correlation with the multiphase flow gas and liquid phase properties across the measurement range studied and discrepancies in the correlations between flow regimes could be sufficiently modelled by a single neural network model.

However, with the current feature set, it is not possible to obtain satisfactory liquid phase water cut parameter predictions using only a single MLP neural network for the three phase flow data. It was anticipated that the liquid phase predictions would be less accurate when compared to those obtained for the gas phase. This is because the densitometer signal is dominated by the passage of gas structures. As such, the underlying features contained in the signals will be more predictive to the gas phase correlations than for those of the liquid phase. To this end, it is suggested that filtering the signals to remove the fluctuations caused by large gas structures, could lead to better prediction performance for the liquid phase parameters.

There is strong tendency for vertical multiphase flow to contain asymmetries and higher phase slip. These asymmetries alter the flow pattern as ‘seen’ by the gamma densitometer and thus the statistical features extracted there from. The implication of this is that the performance of a pattern recognition model based on the features extracted from a horizontally mounted densitometer will differ from that mounted vertically. It was shown that the horizontally mounted gamma densitometer produces better prediction results than those from the vertical.

Previous studies in pattern recognition techniques for horizontal multiphase flows were based on the assumption/assertion that horizontal flows have more features than vertical flows (e.g. in terms of flow regime, there is stratified, wavy stratified, bubbly, plug, slug, annular and mist flow for horizontal compared with bubbly, slug, churn, annular and mist flow for vertical), thus there is a better chance of using feature extractions to determine flow rates using neural network approach, thereby achieving better prediction results in the horizontal than vertical flows. This is the first time this assumption/assertion is been demonstrated.

CHAPTER SEVEN

7. CONCLUSIONS AND FUTURE WORK

This chapter presents a recap of the thesis objective before summarising the main conclusions drawn from the research and concludes with recommendations for future research work.

The need for multiphase flow metering arises when it is necessary or desirable to measure un-separated well streams very close to the well and/or for commingling of such streams. MPFMs also provide continuous monitoring of well performance and thus better reservoir exploitation. This need is ever more justified given the current levels of crude oil prices and the upturn of global economies. The pattern recognition approach for clamp-on multiphase measurement employed in this research study provides one means for meeting this need.

In addition multiphase flow metering is increasingly been seen in the petroleum industry as an important factor in producing oil and gas reserves. This is because of the savings that can be made in CAPEX and OPEX by eliminating test lines, test separator, manifolds, valves and reduced well testing time. Even so, most of these meters are bulky, expensive and require breaking into the flowline. This research work provides a platform for the delivery of non-intrusive, clamp-on, high-speed Multiphase Meters that allow cost effective monitoring and control of oil well assets.

7.1 Conclusions

The objectives of this project are enumerated below:

- Carry out a literature review on multiphase flow, multiphase flow measurement, gamma radiation and pattern recognition techniques in multiphase metering, and measurement uncertainty estimation.
- Undertake experimental data collection of a gamma-densitometer and Coriolis mass flow meter response to a comprehensive multiphase flow conditions typical of operating conditions found in the oil and gas industry.

- Undertake sensors' signal analysis in relation to key multiphase flow parameters and evaluate three phase flows characteristics in horizontal as well as vertical upward flows.
- Apply pattern recognition modelling to predict individual phase flow rates and the liquid phase water cut and validate the claim that gamma densitometer, when mounted horizontally, produces better prediction results in a pattern recognition based multiphase flow measurement system.
- Investigate the effects of upstream conditions on the flow behaviour in the 50.8mm diameter vertical riser.
- Investigate the suitability of predicting the point of phase inversion in the 50.8mm diameter vertical riser using pressure gradient analysis.
- Perform uncertainty evaluation of the gamma densitometer measurement using Monte Carlo Simulation (MCS) methods.

7.1.1 Part – I: General

I. Reviewing commercially available multiphase flow meters reinforces the need for the development of an economical, non-intrusive and robust measurement solution to meet the requirements of the petroleum industry.

II. Several researchers have reported the use of pattern recognition techniques to predict flow rates or to characterise flow and identified flow patterns. Also researchers have used gamma densitometry to resolve the component fractions and to identify the prevalent flow regime in multiphase flow. Employing gamma densitometers in conjunction with neural network modelling in multiphase flow measurement has also been documented wherein the densitometer forms part of a sensor array for horizontal flows or a single gamma densitometer for vertically upward flows. Several commercial multiphase meters use gamma densitometers in these capacities. In some meters, the flow is homogenised by a Venturi constriction or some other means in the measurement section, and involves other intrusive parts.

III. No information has been published in the public domain on the use of a single gamma densitometer in combination with pattern recognition to infer flow rates for horizontal multiphase flows to a measurement uncertainty comparable with several commercially available multiphase flow meters.

IV. The sensors used for this research comprises of two fast sampling gamma densitometer units and Coriolis mass meters. They were installed vertically at the top of the 50.8mm and 101.6mm riser as well as horizontally closed to the riser base in the Cranfield University multiphase flow test facility as discussed in section 3. A comprehensive experimental campaign comprising of air-liquid two, air-liquid three phase and liquid-liquid multiphase flow conditions covering bubbly, slug and churn/annular flow regimes was undertaken.

V. The pattern recognition system developed in this research work relies on features extracted from the gamma densitometer signal. A feedforward multi layer perceptron is then used to relate these features to the superficial gas and liquid velocity, and water cut from which the volumetric flow rates can be calculated for the gas, oil and water.

VI. For the first time a comprehensive evaluation of three phase flows in the horizontal and vertical orientation was simultaneously carried out.

7.1.2 Part – II: Results

I. Signal analysis of the gamma densitometer response to a variety of multiphase flow conditions was undertaken. Time domain plots of the gamma counts gave a good visual indication of the gas and liquid phase distribution in the flow. A range of statistical features, mainly in amplitude, linear prediction coefficients, line spectral frequencies and auto correlation domains, were extracted from these signals and found to exhibit discriminatory trends with variation in flow condition. It was observed that no single feature could be used to conveniently describe all the multiphase flow conditions and that certain correlations were exhibited over a specific range of conditions.

II. Spectral analysis was used to reveal the periodicity in the time-series gamma signals. It was evident from the PSD plots that each hydrodynamic flow regime is distinct, and therefore could be used to identify the prevalent flow regimes; however care should be exercised especially for data points that are close to transition boundaries due to regime duality.

III. Identification of flow patterns was an important aspect of this work. The experimental data was examined to uncover the features of the flow pattern

prevalent in the 50.8mm and 101.6mm pipe sizes in the horizontal as well as vertical orientation.

IV. To ensure that flow patterns are not influenced by developing effects, a waiting time of ten minutes was established in order to allow the flow to stabilise after which the data collection was started. Based on the probability mass function characteristics, the flow in the horizontal 50.8mm flow loop was classify into three basic flow regimes as bubble, slug and wave while for the vertical 50.8mm the flow regimes were bubble, slug and churn. As for the 101.6mm catenary riser, the flow patterns were classified as bubble, slug and churn.

V. Experimental flow pattern maps were developed based on the probability mass function plots for both horizontal and vertical pipe orientation. These flow regime maps were compared with published works and good agreement was found. From the PMFs plots of the full data set, it was found that as the transition from slug to churn/annular flow regime is approached, the distribution becomes more negative skewed due to the presence of large gas bubbles in the liquid core This is a characteristic feature found in small diameter pipes.

VI. The effect of upstream conditions on the 50.8mm vertical riser as a result of two different gas inlet configurations; (a) the upstream horizontal flowline mixing and (b) riser base gas injection, on the flow regimes and void fraction distributions was investigated. It was found that no inlet conditions effect was observed at low gas throughput as similar flow patterns were encountered. However at higher gas and liquid superficial velocities, it was observed that the two inlet configurations exhibited dissimilar flow regimes, for example, agitated bubble for one and fully developed slug for the other at the same experimental conditions. This dissimilarity was attributed to the effect of hydrodynamic slugging from the horizontal flowline carried over to the vertical riser or some unstable processes in the flowline-riser system. This finding shows that, for multiphase phase meters that are flow regime dependent, there will be some measurement implication.

VII. The drift flux modeling approach was employed in predicting void fraction. It was observed that all the data points tend to lie on a straight line regardless of the prevalent flow regime. This behaviour is consistent with the work of Hibiki

and Ishii (2003b) for smaller diameter pipes (D< 100mm) wherein they suggested it is due to the insignificant recirculation and drift velocity among all the flow regimes. It was further found that with increase in gas superficial velocity and enlargement of bubble sizes, the drift velocity also increases, thus the drift velocity for churn flow is large compare to slug flow. The results agree well with those of other researchers for all flow regimes except for vertical bubbly where the drift velocity was over predicted. It was also shown that the drift velocity in horizontal flows is not normally zero.

VIII. A comparative performance assessment study of the density measurement for the Coriolis meter and the gamma densitometer was conducted for both two and three phase flows in horizontal as well as vertical pipe orientation. Density measurements from the Coriolis meter was excellent in liquid-liquid flow and correlates well with those of the gamma densitometer but becomes unreliable when subjected to gas-liquid flow due to the relative motion of gas bubbles in the liquid phase, also known as the 'bubble effect'.

IX. Discrepancies in the density measurement between the hard and soft gamma counts were noted at 70% GVF and above. The mixture densities obtained from Coriolis meter and gamma densitometer correlate quite well in both horizontal and vertical orientation with a percentage difference of ±0.5. In terms of orientation effects, no discernable trend was observed when this percentage difference was plotted against water cut.

X. The phase fraction measurement uncertainty was investigated using Monte Carlo simulation method. MCS was used because the measurement from the detector is a combination of effects e.g. the gamma source, fluid density etc that readily propagates through the entire measurement system. All these effects are highly nonlinear in combination. The phase fraction measurement uncertainty was found to be high.

XI. In this work, efforts were made to identify the phase inversion point and frictional pressure gradient effects for air-oil-water flow in the 10.5m vertical riser in different flow patterns. It was found that phase inversion takes place at a water fraction of about 45% and that the pressure drop peaked at this point. At constant gas flow rate and increasing liquid mixture velocity the pressure gradient increases due to higher friction. Whereas at constant liquid mixture velocity and increasing gas superficial velocity, the pressure gradient is

reduced, due to the lower gravitational pressure drop over the pipe when more gas is present.

XII. Analysis of a real field production data (*Well X*, offshore Brazil) has shown that assumptions made in conventional well testing in the petroleum industry is not always valid because production from a well could be very chaotic and unstable in terms of gas flow rate, oil flow rate and water-in-liquid ratio for a variety of reasons not limited to higher water cuts as the field matures, in-fill drilling, and fluctuation in field production requirements. PMFs plots of the field data revealed that the behaviour of this well is stable (consistent shapes denoting same flow regime) for some period of time and becomes chaotic (different shapes indicating different flow regimes) at other times. This analysis reiterates the need for continuous monitoring of well performance for better reservoir exploitation by utilising low-costs per well monitoring with multiphase flow meters. This will give a considerable economical savings in the long run in addition to wellhead flow measurement information. The analysis also highlights concerns regarding in-situ calibration and performance of multiphase flow meters.

XIII. Feature effectiveness were analysed and evaluated by the feature quality index (FQI) saliency criteria. Optimal feature set unique to water cut, gas and liquid flow rates were obtained by this techniques. Thus reducing dimensionality, enhancing computational efficiency and improving measurement accuracy

XIV. The feed forward multilayer perceptron gave the following measurement accuracy for the 101.6mm test loop data:

a. the hard gamma signal predicted 91% of the gas superficial velocities and 80% of the liquid superficial velocities to within the target accuracy of ±5%
b. the soft gamma signal outperforms those of the hard signals at the ±5% error band as 95% of the data points were correctly predicted for both the gas and liquid superficial velocities
c. the hard-soft combined signal gave results similar to those of the soft gamma signals

XV. The neural network model developed for the 50.8mm test loop data with the gamma densitometer mounted horizontally outperformed the model develop with the vertical data. In the horizontal flow:

a. 95% of the superficial gas, 80% of the superficial liquid and 42% of the water cut samples were identified within the ±10 target accuracy using the hard gamma signal
b. 95% of the superficial gas, 73% of the superficial liquid and 41% of the water cut samples were identified within the ±10 target accuracy using the soft gamma signal
c. 95% of the superficial gas, 76% of the superficial liquid and 42% of the water cut samples were identified within the ±10 target accuracy using the hard-soft combined gamma signal.

In the vertical flow:

d. 90% of the superficial gas, 67% of the superficial liquid and 43% of the water cut samples were identified within the ±10 target accuracy using the hard gamma signal
e. 91% of the superficial gas, 70% of the superficial liquid and 42% of the water cut samples were identified within the ±10 target accuracy using the soft gamma signal
f. 92% of the superficial gas, 68% of the superficial liquid and 40% of the water cut samples were identified within the ±10 target accuracy using the hard-soft combined gamma signal.

XVI. The MLP neural network model exhibited good gas classification suggesting that the extracted features yielded good correlation with the multiphase flow gas and liquid phase properties across the measurement range studied and discrepancies in the correlations between flow regimes could be sufficiently modelled by a single neural network model. However, with the current feature set, it is not possible to obtain satisfactory liquid phase water cut parameter predictions using only a single MLP neural network for the three phase flow data. It was anticipated that the liquid phase predictions would be less accurate when compared to those obtained for the gas phase. This is because the densitometer signal is dominated by the passage of gas structures. As such, the underlying features contained in the signals will be

more predictive to the gas phase correlations than for those of the liquid phase. To this end, it is suggested that filtering the signals to remove the fluctuations caused by large gas structures, could lead to better prediction performance for the liquid phase parameters.

XVII. There is strong tendency for vertical multiphase flow to contain asymmetries and higher phase slip. These asymmetries alter the flow pattern as 'seen' by the gamma densitometer and thus the statistical features extracted there from. The implication of this is that the performance of a pattern recognition model based on the features extracted from a horizontally mounted densitometer will differ from that mounted vertically. It was shown that the horizontally mounted gamma densitometer produces better prediction results than those from the vertical.

XVIII. Previous studies in pattern recognition techniques for horizontal multiphase flows were based on the assumption/assertion that horizontal flows have more features than vertical flows (e.g. in terms of flow regime, there is stratified, wavy stratified, bubbly, plug, slug, annular and mist flow for horizontal compared with bubbly, slug, churn, annular and mist flow for vertical), thus there is a better chance of using feature extractions to determine flow rates using neural network approach thereby achieving better prediction results in horizontal flows than vertical flows. This is the first time this assumption/assertion has been demonstrated.

7.2 Future Work

There are a number of areas that can further enhance the quality of the research work described in this thesis. Given below are some recommendations for further investigation.

I. The PR measurement system developed in this study will only be valid for the same fluids in identical operating conditions in its current form. In order to apply it to other installations, it will require further development work such as 'in-situ calibration'. Development of an enlarged gamma response base should be carried out to cover a much wider range of flow conditions. Attempts should be made to establish the relationship between features

responses and the multiphase fluid properties and other physical parameters such as oil density, oil viscosity, water salinity, operating temperature and pressure, pipe diameter, and orientation. As well as developing the measurement envelope of the device, the data library compiled will be able to act as a look-up reference library for device calibration on new application.

II. The current PR approach requires analysis of the gamma densitometer response over a period of stable flow. In real field conditions, flow stability may not always be available to the meter; such that the changes in flow conditions will affect the gamma count statistics. This will in turn affect measurement accuracy of the system. In order to have a more robust measurement solution, multiple transient multiphase flow experiments, akin to conditions found in oil fields should be simulated and used to develop a real-time measurement system that takes into account historical statistical data from the flow. Also, a novel detection algorithm should be built into the model for cases where the system is expected to experience large and sudden changes in operating conditions.

III. The effectiveness of new input feature groups with strong dependencies on key multiphase flow parameters that could improve the generalisation and accuracy of the measurement model should be examined. Such features should include the interpolation of linear predictive coding parameters in terms of the following representations: reflection coefficient (RC), log-area-ratio (LAR), arc-sine reflection coefficient (ASRC), cepstral coefficient (CC), and impulse response (IR). Though each of these representations provides equivalent information about the LPC spectral envelope, their interpolation performance has been found to be different and as such their inclusion as input feature may add value to the overall system.

IV. Combining new input features with those already examined in this study, will result in a vast number of potential input features. This will lead to a large number of possible combinations of these features to form an input vector group for the neural network model. Consequently, optimisation techniques that will enhance maximal classification accuracy and processing performance of the PR system should be employed. The branch and bound

algorithms could be used to achieve this as they guarantee an optimal solution, if the monotonicity constraint imposed on a criterion function is fulfilled. It also enable efficient identification of an optimal parameter sub-sets from a large pool of potential candidates.

V. Sand production in oil and gas wells have the potential of causing loss of production capacity, pipeline blockage, equipment failure and/or increased pipe corrosion and erosion. The presence of the sand could influence the measurement performance of a clamp-on gamma densitometer system. Experiments should be conducted to investigate the effect of sand at different concentrations on the classification accuracy, and the ability to extract sand concentration, deposition and transportation velocity information from the gamma densitometer signal. On quantifying the effect of sand, a correction algorithm could be developed to account for these effects. This would increase the robustness and marketability of the system while providing valuable information to the petroleum production/reservoir engineer for better reservoir management.

REFERENCES

Abouelwafa, M. S. A. and Kendall, E. J. M. (1979). “Analysis and Design of Helical Capacitance Sensors for Volume Fraction Determination”, *Journal of Phys. E: Rev. Sci. Instrum.*, vol. 50 (7), pp. 872 – 878.

Abouelwafa, M. S. A. and Kendall, E. J. M. (1980). “The Measurement of Component Ratios in Multiphase Systems using γ-ray Attenuation”, *J. Phys. E: Sci. Instrum.*, vol. 13, pp. 341 – 345.

Åbro, E., Khoryakov, V. A., Johansen, G. A. and Kocbach, L. (1999). “Determination of Void Fraction and Flow Regime Using a Neural Network Trained on Simulated Data Based on Gamma-Ray Densitometry”, *Measurement Science and Technology*, vol. 10, pp. 619 – 630.

Åbro, E. and Johansen, G. A. (1999). “Improved Void Fraction Determination by Means of Multibeam Gamma-Ray Attenuation Measurements”, *Flow Measurement and Instrumentation*, vol. 10, pp. 99 – 108.

Açikgöz, M., França, F., and Lahey Jr., R. T. (1992). “An Experimental Study of Three-Phase Flow Regimes", *International Journal of Multiphase Flow*, vol. 18(3), pp. 327 – 336.

Akartuna, S. E. (1994). “Identification of Phase Flow Rates in Oil-Gas-Water Flow from Turbulent Capacitance and Pressure Signals”, *PhD Thesis*, Imperial College of Science, Technology and Medicine, London, United Kingdom.

Ali, S. F. (2009). “Two Phase Flow in Large Diameter Vertical Riser”, *PhD Thesis*, Cranfield University, UK.

Alkaya, B. (2002). “Drift-Flux Models for Multiphase Flow in Wells”, *MSc Thesis*, Stanford University, USA.

Allen C. R. et al. (1995). “Monte Carlo Methods”, *Computational Science Education Project,* Sponsored by United States of America’s Department of Energy (DoE), http://www.phy.ornl.gov/csep/CSEP/MC/MC.html, Accessed: 16/07/2009.

Anklin, M., Drahm, M. and Rieder, A. (2006). “Coriolis Mass Flowmeters: Overview of the Current State of the Art and Latest Research”, *Flow Measurement and Instrumentation, vol.* 17, pp. 317–323.

Arubi I.M.T. and Yeung, H. (2010). “The use of Monte Carlo Simulation for Uncertainty Estimation in Gamma Densitometer Measurements”, *SPE 130910, CPS/SPE International Oil & Gas Conference and Exhibition*, Beijing, China, 8th –10th June.

Barreiri Da Costa E Silva, C., *et al.* (2003). “Multiphase Flow Metering Technology Updated”, *SPE Annual Technical Conference and Exhibition*, New Orleans, Louisiana.

Basil, M. (2008). “Flow Measurement Uncertainty Assessment”, *Production and Upstream Flow Measurement Workshop,* Houston, USA, 12th – 14th February.

Basil, M. and Jamieson, A. W. (1998). “Uncertainty of Complex Systems by Monte Carlo Simulation”, *16th North Sea Flow Measurement Workshop,* Gleneagles, Scotland, 26th – 29th October.

Basil, M., Papadopoulos, C., Sutherland, D., and Yeung, H. (2001). “Application of Probabilistic Uncertainty Methods (Monte Carlo Simulation) in Flow Measurement Uncertaity Estimation”, *Flow Measurement 2001 - International Conference.* (accessed from http://www.mysolv.com/Downloads.htm, on the 20th August, 2009.)

Beg, N. A. (1998). “A Stochastic Method for Multiphase Flow Metering in Pipes”, *PhD Thesis*, Imperial College of Science, Technology and Medicine, London, United Kingdom.

Beg, N. A., McNulty, J. G., Sheppard, C. P. and Frith, A. (1993). “Non-intrusive Multiphase Flow Measurement using Artificial Neural Networks”, *6th Multiphase Production Conference*, Cannes, France.

Bell, S. (1999). “A Beginner's Guide to Uncertainty of Measurement”, *Tech. rep., National Physical Laboratory*, Measurement Good Practice Guide No. 11.

Bernardo, J. and Smith, A. (2000). “Bayesian Theory”, *John Wiley & Sons*, New York, USA.

BIPM, IEC, IFCC, ILAC, ISO, IUPAC, IUPAC and OIML (1995). “Guide to the Expression of Uncertainty in Measurement”, *(Geneva, Switzerland: International Organisation for Standardization) ISBN 92-67-10188-9.*

BIPM, IEC, IFCC, ISO, IUPAC, IUPAC and OIML (2008). “Evaluation of Measurement Data – Supplement 1 to ‘Guide to the Expression of Uncertainty in Measurement’ Propagation of Distribution using Monte Carlo Method”, *(Geneva, Switzerland: International Organisation for Standardization).*

Bishop, C. M. (1995). “Multiphase Flow Monitoring in Oil Pipelines: Application of Neural Networks”, *Kluwer Academic Publishers*, Netherlands, pp. 133 – 155.

Bishop, C. M. (2008). “Neural Network for Pattern Recognition”, *Oxford University Press*, United Kingdom.

Bishop, C.M. and James, G.D. (1993). “Analysis of Multiphase Flows Using Dual-Energy Gamma Densitometry and Neural Networks”, *Nuclear Instruments and Methods in Physics Research*, vol. A327, pp 580 – 593.

Blaney, S. (2008). “Gamma Radiation Methods for Clamp-on Multiphase Flow Metering”, *PhD Thesis*, Cranfield University, UK.

Blaney, S. and Yeung, H. (2007). “Gamma Radiation Methods for Cost-Effective Multiphase Flow Metering” *13th International Conference on Multiphase Production Technology*, Edinburgh, UK.

Blaney, S. and Yeung, H. (2008). “Investigation of the Exploitation of a Fast-Sampling Single Gamma Densitometer and Pattern Recognition to Resolve the Superficial Phase Velocity and Liquid Phase Water Cut of Vertically Upward Multiphase Flows”, *Flow Measurement and Instrumentation*, vol. 19, pp. 57 – 66.

Bonizzi, M. and Issa, R.I. (2003). “On the Simulation of Three-phase Slug Flow in Nearly Horizontal Pipes using the Multi-Fluid Model”, *International Journal of Multiphase Flow,* vol. 29, pp. 1719 – 1747.

Brill, J. P., and Arirachakan, S. J. (1992). “State of the Art in Multiphase Flow”, *Journal of Petroleum Technology*, vol. 44 (5), pp. 538 – 541.

British Petroleum (BP), plc (2010). “Statistical Review of World Energy”, June: *www.bp.com/.../statistical_energy_review.../statistical_review_of_world_energy_full_report_2010.pdf - United States* (Accessed on 30/29/2010).

Brown, G. (2002). “Evaluation of New Technology for High Accuracy Multiphase Flow Measurement: Part 2 – Neural Networks”, *NEL Flow Measurement Guidance Note No. 28*, June.

Brauner, N and Ullmann, A. (2002). “Modeling of Phase Inversion Phenomenon in Two-phase Pipe Flows” *International Journal of Multiphase Flow*, vol. 28, pp. 1177–1204.

Cai, S. (1995). “An Artificial Neural Network Method for Three-Phase Flow Measurement”, *PhD Thesis*, Imperial College of Science, Technology and Medicine, London, United Kingdom.

Cao, Y. and Yeung, H. (2009). “Cranfield University Three-Phase Test Facility Operating Manual” Version 4, Cranfield University, UK.

Chan, A. M. C., and Banarjee, S. (1981). “Design Aspects of Gamma Densitometers for Void Fraction Measurements in Small Scale Two-Phase Flows”, *Nuclear Instruments and Methods in Physics Research*, vol. 190, pp. 135 – 148.

Coughlan, L., Basil, M. and Cox, P. (1999). “How to Optimised Allocation Systems by using Monte Carlo Simulation”, *17th North Sea Flow Measurement Workshop,* Gardemoen, Norway, 25th – 28th October.

Cox, M. G., Dainton M. P., Forbes, A. B., Harris, P. M., Schwenke, P. M., Siebert, B. R. L., and Wöger, W. (2001). “Use of Monte Carlo Simulation for Uncertainty Evaluation in Metrology”, *Advance Mathematical and Computational Tools in Metrologia V,* vol. 57, pp. 93 –105.

Cox, M. G. and Siebert, B. R. L. (2006). “The Use of a Monte Carlo Method for Evaluating Uncertainty and Expanded Uncertainty”, *Metrologia*, vol. 43, pp. S178 – 188.

Darwich, T. (1989). “A Statistical Method for Two-Phase Flow Metering”, *PhD Thesis*, Imperial College of Science, Technology and Medicine, London, United Kingdom.

Darwich, T., Toral, H. and Archer, J. S. (1989). “An Expert System for Multiphase Flow Measurement and Flow Regime Identification”, *SPE Paper 19136, SPE Petroleum Computer Conference*, Texas.

De, R.K., Pal, N.R., and Pal, S.K., (1997). “Feature Analysis: Neural Network and Fuzzy Set Theoretic Approaches”, *Pattern Recognition,* vol. 30 (10), pp. 1579 – 1590.

Department for Business Enterprise and Regulatory Reforms (UK), (2003). “Guidance Notes for Petroleum Measurement”, *DTI – Guidelines Issue 7*, December, pp. 8 – 9.

Descamps, M., *et al.* (2006). “Influence of Gas Injection on Phase Inversion in an Oil-Water Flow through a Vertical Tube”, *International Journal of Multiphase Flow*, vol. 32, pp. 311 – 322.

Descamps, M.N., Oliemans, R.V.A., Ooms, G. and Mudde, R.F. (2007). “Experimental Investigation of Three-phase Flow in a Vertical Pipe: Local Characteristics of the Gas Phase for Gas-lift Conditions”, *International Journal of Multiphase Flow*, vol. 33 pp. 1205 – 1221.

Dickin, F. and Wang, M. (1996). “Electrical Resistance Tomography for Process Applications”, *Measurement Science Technology*, vol. 7, pp.247 – 260.

Doan, C. D. and Liong, S. Y. (2004). “Generalization for Multilayer Neural Network Bayesian Regularization or Early Stopping”, *2nd Asia Pacific Association of Hydrology and Water Resources Conference*, Singapore, 5th – 8th July.

Dyakowski, T. (1996). “Process Tomography Applied to Multiphase Flow Measurement”, *Measurement Science Technology*, vol. 7 pp. 343 – 353.

Dykesteen, E., *et al.* (2005). ‘Handbook of Multiphase Metering’, *Norwegian Society of Oil and Gas Measurement, NFOGM*, *Revision 2*, March.

EMT (Institute of Electrical Measurement and Measurement Signal Processing), Technology Information page http://www.emt.tugraz.at/sensors/aboutect (accessed: 09/02/2011)

ESDU. (2004). “Pressure Gradient in Upward Adiabatic Flows of Gas-Liquid Mixtures in Vertical Pipes”, *Engineering Services Data Unit, The Institution of Mechanical Engineers*. Cited In: Ali, S. F. (2009). “Two Phase Flow in Large Diameter Vertical Riser”, *PhD Thesis*, Cranfield University, UK.

Evans, R. D. (1955). “The Atomic Nucleus, *McGraw-Hill Book Co*., New York, USA.

Fernandes, R.C., Semiat, R. and Duckler, A.E. (1983). “Hydrodynamic Model for Gas-Liquid Slug Flow in Vertical Tubes”, *AIChE J.*, vol. 32, pp. 981 – 989.

Foresee, F. D. and Hagan, M. T. (1997). “Gauss-Newton Approximation to Bayesian Regularisation”, *International Joint Conference on Neural Networks*, pp. 1930 – 1935.

França, F., Açikgöz, M., Lahey, R. T., and Clausse, A. (1991). “The Use of Fractal Techniques for Flow Regime Identification”, *International Journal of Multiphase Flow*, vol. 17, pp. 545 – 552.

França, F., and Lahey Jr., R. T. (1992). “An Experimental Study of Three-Phase Flow Regimes", *International Journal of Multiphase Flow*, vol. 18(3), pp. 327 – 336.

França, F., and Lahey Jr., R. T. (1992). “The Use of Drift-Flux Techniques for the Analysis of Horizontal Two-Phase Flows", *International Journal of Multiphase Flow*, vol. 18(6), pp. 787 – 801.

Frøystein, T., Kvandal, H. and Aakre, H. (2005). “Dual Energy Gamma Tomography System for High Pressure Multiphase Flow”, *Journal of Flow Measurement and Instrumentation*, vol. 16, pp. 99 – 112.

Geman, S., Bienenstock, E. and Doursat, R. (1992). “Neural Networks and the Bias/Variance Dilemma”, *Neural Computation,* vol.4, pp. 1 – 58.

Goda, H., Hibiki, T., Kim, S., Ishii, M. and Uhle, J. (2003). “Drift-Flux Model for Downward Two-Phase Flow”, *International Journal of Heat and Mass Transfer*, vol. 46 (25), pp. 4835 – 4844.

Gong, J., Li, Q., Yao, H. and Yu, D. (2006). “A Model for Predicting Phase Inversion in Oil-Water Two-Phase Flow”, *Journal of Hydrodynamics*, vol. 18(3), pp. 310 – 314.

Goudinakis, G. (2004). “Investigation on the use of Raw Time Series and Artificial Neural Networks for Flow Pattern Identification in Pipelines”, *PhD Thesis*, Cranfield University, United Kingdom.

Griffith, P. and Wallis, G.B. (1961). “Two-Phase Slug Flow”, *J. Heat Transfer*, vol. 83, pp. 307 – 320.

Guet, S., Ooms, G., Oliemans, R.V.A. and Mudde, R.F. (2004). “Bubble Size Effect on Low Liquid Input Drift-Flux Parameters”, *Chemical Engineering Science,* vol. 59, pp. 3315 – 3329.

Haddelland, R., *et al.* (2003). “Online Measurement of Water in Wet Gas Flow”, *South-East Asia Flow Measurement Workshop*.

Hammer, E. A. and Nordtvedt, J. E. (1991). “The Application of a Venturi Meter to Multiphase Flow Meters for Oil Well Production”, *Proc. 5th Conf. Sensors and Applications*, London, UK. Cited In: Thorn, R., Johansen, G. A. and Hammer, E. A. (1997). “Recent Developments in Three-Phase Flow Measurement”, *Measurement Science Technology*, vol. 8, pp. 691–701.

Hardy, J. E., *et al.*, (1999). “Flow Measurement Methods and Applications”, *John Wiley and Sons, Inc.,* New York, USA.

Hassan, A.R. and Kabir, C.S. (1992). “Two-Phase Flow in Vertical and Inclined Annuli”, *Int. J. Multiphase Flow*, vol. 18, pp. 279 – 293.

Henry, M.P. et al (2006). “Two-phase Flow Metering of Heavy Oil using a Coriolis Mass Flowmeter: A case study”, *Flow Measurement and Instrumentation,* vol. 17, pp. 399 – 413.

Hewitt, G. F., Harrison, P. S., Parry, S. J. and Shires, G. L. (1995). “Development and Testing of the “Mixmeter” Multiphase Flow Meter”, *13th North Sea Flow Measurement Workshop*, Lillehammer, Norway.

Hibiki, T. and Ishii, M. (2003a). “One-Dimensional Drift-Flux Model for Two-Phase Flow in Large Diameter Pipe”, *International Journal of Heat and Mass Transfer*, vol. 46(10), pp. 1773 – 1790.

Hibiki, T. and Ishii, M. (2003b). “One-Dimensional Drift–Flux Model and Constitutive Equations for Relative Motion Between Phases in Various Two-Phase Flow Regimes”, *International Journal of Heat and Mass Transfer*, vol. 46, pp. 4935 – 4948.

Ibrahim, A. A. (2009). “Intelligent Multiphase Flow Measurement”, *PhD Thesis,* Cranfield University, United Kingdom.

Ioannou, K., Nydal , O. and Angeli, P. (2005). “Phase Inversion in Dispersed Liquid–Liquid Flows”, *Experimental Thermal and Fluid Science*, vol. 29, pp. 331–339.

Ismail, I., Gamio, J. C., Bukhari, S.F.A. and Yang, W.Q. (2005). “Tomography for Multiphase Flow Measurement in the Oil Industry”, *Flow Measurement and Instrumentation*, vol. 16, pp. 145 – 155.

Industrial Tomography Systems (ITS). (2000). “P2000 Electrical Resistance Tomography System-User’s Manual” *ITS System 2000 Version 6.*

Jama, A. A. (2004). “Wet Gas Flow Metering with Pattern Recognition Techniques”, *PhD Thesis*, Cranfield University.

Jain, A. K., Duin, R. P.W. and Mao, J. (2000). “Statistical Pattern Recognition: A Review”, *IEEE Transactions on Pattern Analysis and Machine Intelligence*, vol. 22, (1).

Jamieson, A. W. (1998). “Multiphase Metering – The Challenge of Implementation”, *16th North Sea Flow Measurement Workshop*, Gleneagles, Scotland.

Jiang, Y. and Rezkallah, K. S. (1993). “An Experimental Study of the Suitability of Using a Gamma Densitometer for Void Fraction Measurements in Gas-Liquid Flow in a Small Diameter Tube”, *Measurement Science Technology*, vol. 4, pp. 496 – 505.

Johansen, G., A. and Jackson, P. (2004). “Radioisotope Gauges for Industrial Process Measurements”, *John Wiley and Sons, Ltd*., England.

Jones, O.C. and Zuber, N. (1975). “The Interrelation between Void Fraction Fluctuations and Flow Patterns in Two Phase Flow”, *Int. J. Multiphase Flow,* vol. 2, pp. 273 – 534.

Joshi, N. B. and Joshi, B. H. (2007). “Multiphase Measurements and Sampling – Operating Experience”, *SPE 108626, SPE Annual Technical Conference and Exhibition*, California, USA.

Kelessidis, V. C. and Dukler, A. E. (1989). “Modelling Flow Pattern Transitions for Upward Gas-Liquid Flow in Vertical Concentric and Eccentric Annuli”, *International Journal for Multiphase Flow*, vol. 15, (2), pp. 173 – 191.

Kelner, E. (2009). “Measurement Matters: Improvements in Multiphase Flow Measurement?”, *Pipeline and Gas Journal*, vol. 236, (11), pp. 18.

Keska, J. K. and Wang, G. (2006). “Pressure Gradient Calculation for Air-Water Heterogeneous Mixture Flow in a Small Square Horizontal Channel based on the in situ Parameters and Flow Pattern Coefficient”, *Experimental Thermal and Fluid Science,* vol. 30, pp. 403 – 413.

Khalifa, K., M. and Sanderson, M., L. (2008). “A Novel Two-Phase Gas/Liquid Slug Flow Measurement System Using a T-Junction Separator and Ultrasonic Measurement”, *IPC2008-64685, 7th International Pipeline Conference*, Calgary, Canada.

Knoll, G. F. (1979). “Radiation Detection and Measurement”, *John Wiley & Sons*, New York.

Kosterin, S. I. (1949). “An Investigation of the Influence of the Diameter and Inclination of a Tube on the Hydraulic Resistance and Flow Structure of Gas Liquid

Mixtures". *Izv. Akad. Nauk SSSR, Otdel Tekh. Nauk,* vol.12, pp. 1824 – 1830. Cited In: Spedding, P. L. and Spence, D. R. (1993). "Flow Regimes in Two Phase Gas-Liquid Flow", *Int. J. Multiphase Flow* Vol. 19, (2), pp. 245 – 280.

Kratirov, V. A., Jamieson, A. W., Blaney, S. and Yeung, H. (2006). "Neftemer – A Versatile and Cost Effective Multiphase Meter", *24th North Sea Flow Measurement Workshop*, St. Andrews, Scotland.

Kumara, W.A.S, Halvorsen, B.M. and Melaaen, M.C. (2010). "Single-beam Gamma Densitometry Measurements of Oil–Water Flow in Horizontal and Slightly Inclined Pipes", *International Journal of Multiphase Flow*, vol. 36, pp. 467 – 480.

Lee, J. Y., Ishii, M. and Kim, N.S. (2008). "Instantaneous and Objective Flow Regime Identification Method for the Vertical Upward and Downward Co-current Two Phase Flow", *International Journal of Heat and Mass Transfer,* vol. 51, pp. 3442 – 3459.

Letton, C., et al. (2010). "Subsea Deepwater Measurement – Technology Gaps and Solutions", 28th International North Sea Measurement Workshop, St. Andrew, Scotland.

Li, D. H., Wu, Y. X., Li, Z. B., and Zhong, X. F. (2005). "Volumetric Fraction Measurement in Oil-Water-Gas Multiphase Flow with Dual Energy Gamma-Ray System", *J. Zhejiang Univ. SCI,* vol. 6A (12), pp. 1405 – 1411.

Lourakis, M. I. A. (2005). "A Brief Description of the Levenberg-Marquardt Algorithm Implemented by levmar", *Institute of Computer Science Report,* Foundation for Research and Technology - Hellas (FORTH), Crete, Greece.

Mandhane, J. M, Gregory, G. A. and Aziz, K. (1974). "A Flow Pattern Map for Gas-Liquid Flow in Horizontal Pipes", *Int. J. Multiphase Flow,* vol. 1, pp. 537 – 553. Cited In: Khalifa, K. M. (2010). "Two-Phase Slug Flow Measurement using Ultrasonic Techniques in Combination with T-Y Junctions", *PhD Thesis*, Cranfield University, UK.

Mareuge, I. C. (2000). "Analysis and Development of Multi-Energy Gamma Densitometry Systems", *Multiphase Fluid Systems Programme*, Imperial College of Science, Technology and Medicine, December. Cited In: Blaney, S. (2008). "Gamma

Radiation Methods for Clamp-on Multiphase Flow Metering", *PhD Thesis*, Cranfield University.

Matsui, G. (1984). "Identification of Flow Regimes in Vertical Gas-Liquid Two-Phase Flow using Differential Pressure Fluctuations", *International Journal of Multiphase Flow*, vol. 10 (6), pp. 711 – 719.

McCulloch, W. and Pitts, W. (1943). "Logical Calculus and the Ideas Immanent in the Nervous Activity", *Bulletin of Mathematical Biophysics*, vol. 5, pp. 115 – 133.

Mehdizadeh, P. and Williamson, J. (2004). "Principles of Multiphase Measurements", *Alaska Oil and Gas Conservation Commission Information Document to accompany 'Guidelines for Qualification of Multiphase Metering Systems for Well Testing'* November.

Mehdizadeh, P., Marrelli, J. and Ting, V.C. (2003). "Meter Designs Provide Wet-Gas Measurement Alternatives", *Oil & Gas Journal*, March.

Mehdizadeh, P., Marrelli, J. and Ting, V.C. (2002). "Wet Gas Metering: Trends in Application and Technical Development", *SPE 77351, SPE Annual Technical Conference and Exhibition*, San Antonio, USA.

Merilo, M., Dechene, R. L. and Cichowlas, W. M. (1977). "Void Fraction Measurement with a Rotating Electric Field Conductance Gauge", *ASME Journal of Heat Transfer*, vol. 99, pp. 330 – 332.

Mi, Y., Ishii, M. and Tsoukalas, L.H. (1998). "Vertical Two Phase Flow Identification using Advanced Instrumentation and Neural Networks", *Nuclear Engineering Design,* vol. 204, pp. 409 – 420.

Mi, Y., Ishii, M and Tsoukala, L. H., (2001). "Flow Regime Identification Methodology with Neural Networks and Two Phase Flow Models", *Journal of Nuclear Engineering and Design,* vol. 204, pp. 87 – 100.

Munson, B.R., Young, D.F., and Okiishi, T.H. (1994). "Fundamentals of Fluid Mechanics", *John Wiley & Sons*, New York, USA.

Nicolis, G. (1995). “Introduction to Non-linear Science”, *Cambridge University Press,* Cambridge, United Kingdom.

Nyfors, E. and Vainikainen, P. (1989). “Industrial Microwave Sensors”, *Artech House*, Massachusetts, USA.

Oddie, G., *et al.* (2003). “Experimental Study of Two and Three Phase Flows in Large Diameter Inclined Pipes”, *International Journal of Multiphase Flow*, vol. 29, pp. 527 – 558.

Oliemans, R. V. A. (1994). “Multiphase Science and Technology for Oil/Gas Production”, *SPE 27958, University of Tulsa Centennial Petroleum Engineering Symposium*, Oklahoma, USA.

Oppenheim, A. V., Willsky, A. S. and Nawab, S. H. (1997). “Signal and Systems”, *2nd Edition Prentice Hall*, New Jersey, USA.

Orr, G. Schraudolph, Ni and Cummins, F. (1999). “Neural Network” *Willamette University Lecture Notes*, Oregon, USA.

Papadopoulos, C. E. (2000). “Uncertainty Analysis in the Management of Gas Metering Systems”, *PhD Thesis*, Cranfield University, UK.

Papadopoulos, C. E. and Yeung, H. (2001). “Uncertainty Estimation and Monte Carlo Simulation Method”, *Flow Measurement and Instrumentation*, vol. 12, pp. 291 – 298.

Polikar, R. (2006). “Pattern Recognition: Wiley Encyclopaedia of Biomedical Engineering”, *John Wiley & Sons, Inc.*, New York, USA.

Piela , K., Delfos, R., Ooms, G., Westerweel, J. and Oliemans, R.V.A. (). “On the Phase Inversion Process in an Oil–Water Pipe Fow”, *International Journal of Multiphase Flow*, vol. 34 pp. 665 – 677

Prepost, R. (2001). “Interaction of Gammas”, *Advanced Physics Laboratory*, University of Wisconsin, USA.

Rodriguez, O.M.H. and Oliemans, R.V.A. (2006). “Experimental Study on Oil–Water Flow in Horizontal and Slightly Inclined Pipes” *International Journal of Multiphase Flow,* vol. 32, pp. 323 – 343.

Rebgetz, M. D., Watt, J. S. and Zastawny, H. W. (1991). “Determination of the Volume Fraction of Oil, Water and Gas by Dual Energy Gamma-ray Transmission”, *Nuclear Geophysics,* vol. 5(4), pp. 193.

Reinecke, N., Petritsch, G., Schmitz, D. and Mewes, D. (1998). “Tomographic Measurement Techniques – Visualization of Multiphase Flow”, *Chemical Engineering Technology*, vol. 21 (1), pp. 7 – 18.

Ruden, L. A. (2010). “Do Multiphase Meters Meet Today’s Offshore Challenges?”, *Offshore Magazine September Edition*, PennWell Publications, Oklahoma, USA.

Sanderson, M. L. (2008). “Process Measurement Systems”, *MSc Module PSE 10*, Cranfield University, Bedfordshire, England.

Scheers, A. M. and Slijkerman, W. F. J. (1996). “Multiphase Flow Measurement Using Multiple Energy Gamma Ray Absorption (MEGRA) Composition”, *SPE Paper 36593-MS*, October, pp. 203 – 211.

Shenitech, LLC Product Technology Information: http://www.shenitech.com/flowmeas.htm (accessed: 10/03/2011).

Sheppard, C. P. and Russell, D. (1993). “The Application of Artificial Neural Networks to Non-Intrusive Multi-Phase Metering”, *Control Engineering Practice*, vol. 1 (2), pp. 299 – 304.

Slijkerman, W.F.J., Jamieson, A.W., Priddy, W.J., Okland, O. and Moestue, H. (1995). “Oil Companies’ Needs in Multiphase Flow Metering”, *13th North Sea Flow Measurement Workshop*, Lillehammer, Norway.

Sommer, K.D. and Siebert, B.R.L. (2006). “Systematic Approach to the Modeling of Measurements for Uncertainty Evaluation”, *Metrologia*, vol. 43, pp. 200 – 210.

Spedding, P. L. and Nguyen, V. T. (1980). “Regime Maps for Air Water Two Phase Flow”, *Chemical Engineering Science*, vol. 35, pp. 799 – 793.

Spedding, P. L. and Spence, D. R. (1993). “Flow Regimes in Two Phase Gas-Liquid Flow”, *Int. J. Multiphase Flow* Vol. 19, (2), pp. 245 – 280.

Spedding, P. L., Donnelly, G. F. and Cole, J. S. (2005). “Three Phase Oil-Water-Gas Horizontal Co-current Flow I: Experimental and Regime Map”, *Chemical Engineering Research and Design*, vol. 83(A4), pp. 401 – 411.

Spedding, P. L., Woods, G. S., Raghunathan, R. S. and Watterson, J. K. (2000). “Flow Pattern, Holdup and Pressure Drop in Vertical and Near Vertical Two- and Three-Phase Upflow”, *Trans IChemE*, vol. 78 (A), pp. 404 – 418.

Stahl, P. and Von Rohr, P. R. (2004). “On the Accuracy of Void Fraction Measurements by Single-Beam Gamma-Densitometry for Gas-Liquid Two-Phase Flows in Pipes”, *Experimental Thermal and Fluid Science*, vol. 28, pp. 533 – 544.

Stapelberg, H. H. and Mewes, D. (1990). “The Flow of Two Immiscible Liquids and Gas in Horizontal Pipes – Pressure Drop and Flow Regime”, *European Two-Phase Flow Group Meetin*g, Varese.

Taitel, Y., Barnea, D. and Dukler, A.E. (1980). “Modelling Flow Pattern Transitions for Steady Upward Gas-Liquid Flow in Vertical Tubes”, *AIChE J*., vol. 26, pp. 345 – 354.

Thiyagarajan, T. K., Dixit, N. S., Satyamurthy, P., Venkatramani, N. and Rohatgi, V. K. (1991). “Gamma-Ray Attenuation Method for Void Fraction Measurement in Fluctuating Two-Phase Liquid Metal Flows”, Measurement Science Technology, vol. 2, pp. 69 – 74.

Toral, H., Beg, N. and Archer, J. S. (1990). “Multiphase Flow Metering by Software”, *International Conference on Basic Principles & Industrial Applications of Multiphase Flow*, London.

Toral, H., Cai, S., Akartuna, E., Stothard, K. and Jamieson, A. W. (1998). “Field Trials of the ESMER Multiphase Flow Meter” *North Sea Flow Measurement Workshop*, Gleneagles, Scotland.

Thorn, R., Johansen, G. A. and Hammer, E. A. (1997). “Recent Developments in Three-Phase Flow Measurement”, *Measurement Science Technology,* vol. 8, pp. 691 – 701.

Tjugum, S. A., Frieling, J. and Johansen, G. A. (2002a). “A Compact Low Energy Multibeam Gamma-Ray Densitometer for Pipe-Flow Measurements”, *Nuclear Instruments and Methods in Physics Research B*, vol. 197, pp. 301 – 309.

Tjugum, S. A., Hjertaker, B. T. and Johansen, G. A., (2002b). “Multiphase Flow Regime Identification by Multibeam Gamma-Ray Densitometry”, *Measurement Science Technol*ogy, vol. 13, pp. 1319 – 1326.

Tuss, B., Perry, D. and Shoup, G. (1996). “Field Tests of the High Gas Volume Fraction Multiphase Flow Meter”, *Proc. SPE Annual Technical Conference*, Denver, USA.

Valle, A. (1998). “Multiphase Pipeline Flows in Hydrocarbon Recovery”, *Multiphase Science Technology*, vol.10 (1), pp. 1 – 139.

Verikas, A. and Bacauskiene, M. (2002). “Feature Selection with Neural Networks” *Pattern Recognition Letters*, vol. 23, pp. 1323 – 1335.

Vince, M. A. and Lahey, R. T. (1982). “On the Development of an Objective Flow Regime Indicator”, *International Journal of Multiphase Flow*, vol. 8, pp. 93 – 124.

Wang, M. (2008). “Introduction to Process Systems Engineering”, *MSc Module 1*, Cranfield University, Bedfordshire, England.

Wang, W. and Gong, J. (2009). “Experiment Research of Phase Inversion in Mineral Oil-Water Two-Phase Flow in Horizontal Pipe”, *Journal of Energy Resources Technology*, vol. 131, pp. 43001 – 43006

Wegmann, A., Melke, J. and Rudolf von Rohr, P. (2007). “Three Phase Liquid-Liquid-Gas Flows in 5.6 mm and 7 mm Inner Diameter Pipes”, *International Journal of Multiphase Flow,* vol. 33, pp. 484 – 497.

Weise, K. and Wöger, W. (1992). “A Bayesian Theory of Measurement Uncertainty”, *Measurement Science Technology*, vol. 3, pp. 1 – 11.

Wood, I. (2002). “Multiphase Measurement”, *20th North Sea Flow Measurement Workshop*, Peebles, Scotland.

Wu, H., Zhou, F., and Wu, Y. (2001). “Intelligent Identification System of Flow Regime of Oil-Gas-Water Multiphase Flows”, *International Journal of Multiphase Flow*, vol. 27, pp. 459 – 475.

Wübbeler, G., Krystek, M. and Elster, C. (2008). “Evaluation of Measurement Uncertainty and its Numerical Calculation by a Monte Carlo Method”, *Measurement Science and Technology*, vol. 19, pp. 4 – 8.

Wylie, S. R., Shaw, A. and Al-Shamma’a, A. I. (2006). “RF Sensor for Multiphase Flow Measurement through an Oil Pipeline”, *Measurement Science and Technology*, vol. 17, pp. 2141 – 2149.

Xu, X. (2007). “Study on Oil-Water Two-Phase Flow in Horizontal Pipelines”. *Journal of Petroleum Science and Engineering*, vol. 59, pp 43 – 58.

Xie, T., Ghiaasiaan, S.M. and Karrila, S. (2004). “Artificial Neural Network Approach for Flow Regime Classification in Gas–liquid–fibre Flows Based on Frequency Domain Analysis of Pressure Signals”, *Chemical Engineering Science,* vol. 59, pp. 2241 – 2251.

Xu, J., Li, D., Guo, J., and Wu, Y. (2010). “Investigations of Phase Inversion and Frictional Pressure Gradients in Upward and Downward Oil–Water Flow in Vertical Pipes”, *International Journal of Multiphase Flow*, vol. 36, pp. 930 – 939.

Yang, Y.S., Scott, B.N. and Cregger, B.B. (1990). “The Design, Development, and Field Testing of a Water-Cut Meter Based on a Microwave Technique”, *SPE Paper 20697-MS, SPE Annual Technical Conference and Exhibition*, New Orleans, USA, 23-26 September.

Zuber, N. and Findlay, J. A. (1965). “Average Volumetric Concentration in Two-Phase Flow Systems”, *Journal of Heat Transfer Transactions of the ASME*, vol. 87, pp. 453–468. Cited In: Guet, S., Ooms, G., Oliemans, R.V.A. and Mudde, R.F. (2004). “Bubble Size Effect on Low Liquid Input Drift-Flux Parameters”, *Chemical Engineering Science,* vol. 59, pp. 3315 – 3329.

APPENDICES:

Abbon AS, AFM Product Technology Information: http://www.abbon.com/abbon/measurement-technology (accessed on 31/01/2011).

Accuflow AMMS Product Technology Information: http://www.accuflow.com/default2.asp?active_page_id=197 (accessed on 31/01/2011)

Agar Corporation Product Technology Information: http://www.agarcorp.com/Technology/MPFM50.html and http://www.zirco.com/product_mpfm.php (accessed on 31/01/2011)

Al-Bourni, H. A., Samizo, N., Bakhteyar, Z. and Alvi, A. (2005) "Application of New Multiphase Flow Measurement Systems with Satellite-Based Monitoring in Offshore Khafji Field", *IPTC 10312 International Petroleum Technology Conference*, Doha, Qatar, 21st – 23rd November.

Al-Taweel, A. B. and Barlow, S. G. (1999). "Field Testing of Multiphase Meters", *SPE Paper 56583, SPE Annual Technical Conference and Exhibition*, Houston, USA.

Basaidi, K and Bhaskaran, H. (2003). "Multiphase Flow Meters: Experience and Assessment in PDO", *SPE Paper 84505, SPE Annual Technical Conference and Exhibition*, Denver, USA, 5th – 8th October.

Bastardo, R., Imam, A. and Scoglio, J. (2008). "Field Testing of an Automated Well tester in Extra and Diluted Oil Application", *SPE Paper 116460, SPE Annual Technical Conference and Exhibition*, New Orleans, USA.

Cai, S., Toral, H., Sinta, D. and Tajak, M. (2004). "Experience In Field Tuning And Operation Of A Multiphase Meter Based On Neural Net Characterization Of Flow Conditions", *FLOMEKO*, September.

Cameron/Jiskoot Product Technology Information: http://www.benchmarkinc.ca/Brochures/ProductBrochurePDF/Jiskoot/Mixmeter%20Multiphase.pdf (accessed: 02/02/2011).

Deller, J. R., Proakis, J. G. and Hansen, J. H. L. (1993). “Discrete-Time Processing of Speech Signals”, *MacMillan Publishers*.

Emerson Process Management. Product Technology Information: http://www2.emersonprocess.com/en-US/brands/roxar/FlowMetering/meteringsystems/Pages/RoxarMultiphasemeter2600.aspx (accessed: 04/02/2011).

EESIFLO International Pte Ltd. Product Technology Information: http://www.eesiflo.com/products/easz1_bsw_01.html (accessed: 02/03/2011).

FMC Measurement Solution Product Technology Information: http://info.smithmeter.com/literature/docs/ssmp001.pdf (accessed: 01/02/2011).

Framo Engineering Product Technology Information: http://www.framoeng.no/?page=136&show=257 (accessed: 01/02/2011).

Golub, G. H. and Loan, C. F. V. (1989) “Matrix Computation”, *The John Hopkins University Press,* 2nd Ed.

Haimo MFM Technologies Product Information: http://www.haimo.com.cn/en/detail.jsp?articleId=697&classid=92&preid=91 (accessed: 01/02/2011).

Hall, A. R. W. (2000) “Evaluation of the FlowSys TopFlow Multiphase Flowmeter”, *National Engineering Laboratory,* Project No FSY001, Report No 200/2000, October.

Haldipur, P. and Metcalf, G. (2008) “Virtual Metering Technology Field Experience Examples”, *Offshore Technology Conference*, Texas, USA. 5th – 8th May.

Jackson, J. E. (1991). “A User’s Guide to Principal Components”, *John Wiley and Sons Inc*.

Kabal, P. and Ramachandran, R. P. (1986). “The Computation of Line Spectral Frequencies using Chebyshev Polynomials”, *IEEE Trans. Acoustics, Speech Signal Processing*, vol. 34, pp. 1419 – 1426.

Klepsvik, I., Dahl, E., O. and Baker, A. C. (2000) “Multiphase Flow Test Report – TopFlow”, *Christian Michelsen Research*, Report CMR-00-F10021, September.

Leggett, R. B., Borling, D. C., Powers, B. S. and Shehata, K. (1996). “Multiphase Meter Successfully Measures Three-Phase Flow at Extremely High Gas Volume Fraction”, *SPE Paper 36837, European Petroleum Conference*, Milan, Italy.

Letton, W., Svaeren, J. A. and Conort, G. (1997). “Topside and Subsea Experience with the Multiphase Flow Meter”, *SPE Paper 38783*, *SPE Annual Technical Conference and Exhibition*, San Antonio, USA. 5th – 8th October.

Makhoul, J. (1975). “Linear Prediction: A Tutorial Review”, *Proc. IEEE*, vol. 63, pp. 561 – 580.

Mazzoni, A., Halvorsen, M. and Aspelund, A. (2001). “Field Qualification – FlowSys TopFlow Meter”, *Agip Test Facility*, Trecrate, Italy, April.

McNulty, J. G. and Beg, N. A. (1997) “Survey of Multi-Phase Flow Metering Systems”, *Caltec Report CR 6660*, BHR Group, UK.

Mohamed, P. G. and Al Saif, K. H. (1998). “Field Trial of a Multiphase Flow Meter”, *SPE Paper 49161, SPE Annual Technical Conference and Exhibition*, Denver, USA.

MSi Kenny Product Technology Information: http://www.multiphase.com/Software%20Solutions.html# (accessed: 02/02/2011).

Multi Phase Meters Product Technology Information: http://www.mpm-no.com/products/ (accessed: 02/02/2011).

Neftermer Ltd Corporate Website: http://www.neftemer.com/multiphase-meters.html (accessed: 07/02/2011).

Petroleum Software Ltd. Product Technology Information: http://www.petroleumsoftware.co.uk/esmermpm.pdf (accessed: 04/02/2011).

Phase Dynamics Inc. Product Technology Information: http://www.phasedynamics.com/ccmfeat.html (accessed: 04/02/2011).

Schlumberger Product Technology Information: https://www.slb.com/~/media/Files/testing/product_sheets/multiphase/phasewatcher.ashx (accessed: 01/02/2011).

Scheers, L. and Wee, A. (2007). "Challenges at High Accuracy Multi-Phase and Wet-Gas Measurements", *Multiphase Measurement Roundtable*, April.

Scott, B.N. and Kvamsdal, D. (2000). "A New Concept in Well Testing: The Compact Cyclone Multiphase System", *SPE Paper 59711, SPE Permian Basin Oil and Gas Recovery Conference*, Texas, USA, 21st – 23rd March.

Sentech AS Product Technology Information: http://www.sentech.no/Products/waterfract.htm (accessed: 01/03/2011).

Shen, J. J. S. and Riley, R. C. (1998) "Field Evaluation of a Multiphase Meter in Well-Testing Operation", *SPE Production & Facilities Journal*, pp. 109 – 117.

Stobie, G. and Saettenes, B. (2007). "Closing the Gaps in Subsea Multiphase and Wetgas Metering", *Multiphase Measurement Roundtable*, 1st – 2nd May.

Subsea Oil and Gas Directory: http://www.subsea.org/products/specification.asp?prod=3610 (accessed: 02/02/2011).

TEA Sistemi S.p.a. Product Technology Information: http://www.tea-group.com/pdf_03/metering.pdf (accessed: 07/02/2011).

Toral, H., Cai, S., Akartuna, E., Stothard, K. and Jamieson, A. (1998). "Field Tests of the ESMER Multiphase Flowmeter", 16th *North Sea Flow Measurement Workshop*, Gleneagles, Scotland, October.

Weatherford International Product Technology Information: http://weatherford.com/weatherford/groups/web/documents/weatherfordcorp/WFT118301.pdf (accessed: 01/02/2011).

PUBLICATIONS

1. Arubi, I.M.T. and Yeung, H. (2011). "Pattern Recognition Techniques in Simultaneous Horizontal and Vertically Upward Multiphase Flow Measurement", to be presented at *The 7th International Symposium on Measurement Techniques for Multiphase Flows*, Tianjin, China, 17th –19th September

2. Arubi, I.M.T. and Yeung, H. (2010). "The Use of Monte Carlo Simulation for Uncertainty Estimation in Gamma Densitometry Measurements", *CPS/SPE International Oil & Gas Conference and Exhibition*, Beijing, China, 8th –10th June.

3. Duru, U.I., Ossai, C.I., and Arubi, I.M.T. (2010). "An Appraisal of Soil Pollution in Oil and Gas Production Environment: A Case Study of Heavy Metals Concentration in Ebocha and Akri Oil Fields", *International Oil & Gas Conference and Exhibition in China (IOGCEC)*, Beijing, China, 8th – 10th June.

4. Duru, U.I., Ossai, I.A., Ossai, C.I., and Arubi, I.M.T. (2009). "The After Effect of Crude Oil Spillage on Some Associated Heavy Metals in the Soil", *4th International Petroleum Technology Conference*, Doha, Qatar, 7th – 9th December.

5. Arubi, I.M.T. and Duru, U.I. (2008). "Optimizing Glycol Dehydration System for Maximum Efficiency: A Case Study of a Gas Plant in Nigeria", *CIPC/SPE Gas Technology Symposium Joint Conference*, Calgary, Canada, 16th –19th June.

6. Ossai, C.I., Duru, U.I., Ossai, I.A. and Arubi, I.M.T. (2008). "Industrial Operations and Water Quality: A Case Study of UTU River Pollution by Oil Production Activities", *SPE Latin American and Caribbean Petroleum Engineering Conference*, Cartagena, Colombia, 31st May – 3rd June.

APPENDICES

Appendix A Review of Commercial Multiphase Meters

A.1 Abbon 3PM

The Abbon 3PM multiphase meter is entering its final stage of development. The 3PM combines electrical impedance measurement with velocity determination and pressure drop measurement over a restriction designed within the meter unit, Figure A.1 (Abbon, 2011). The differential pressure generating restriction is a centrally placed body serving several purposes. It gives the well-known pressure drop proportional to the product of the volume and mass flow rate, also known as the Venturi effect. In addition it contains electrodes used for measuring the impedance resulting from the composition of the fluid passing it. In the opening between the body and the inner pipe wall of the pipe, there is a zone where a high degree of turbulence is created. The effects of this turbulence are twofold; first that the three phases are well mixed, thereby enhancing fraction measurement; secondly that any velocity difference between gas and liquid is reduced to a minimum.

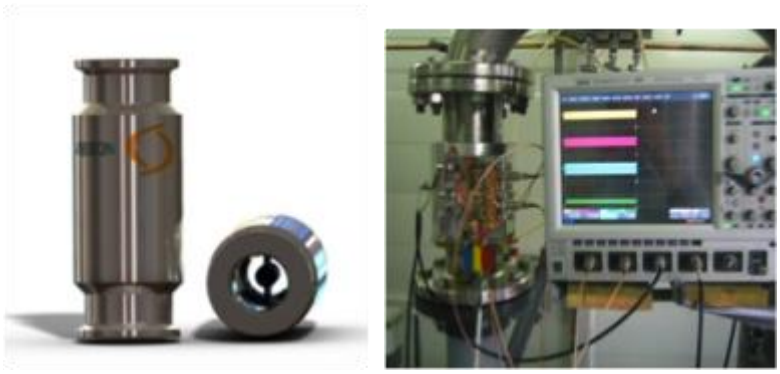

Figure A.1 –Abbon 3PM (Abbon, 2011)

The electrodes placed on the central body have counter electrodes implemented into the inner wall of the meter housing so that the impedance between them can be measured. The Abbon 3PM patented design ensures that the distance between these electrode pairs is very short, which is beneficial for the sensitivity and the accuracy of the impedance measurements. There are two pairs of electrodes though one pair of electrodes would be sufficient for fraction measurements. However, the velocity measurement requires two signals, here the time varying signals from ideally

identical impedance sensors are subject to cross-correlation in order to determine the velocity of the fluid. All these measurement principles are then combined into one system in order to determine the individual flow rates of the three phases.

A.2 Accuflow Multiphase Metering System

The Accuflow Multiphase Metering System (AMMS) comes in the SR series and the LT series. The SR series covers low to high production rates as well as light to heavy crude whereas the LT series is a compact version of the SR and it is suitable for applications with relatively light crude oil and low to medium liquid production rate.

Figure A.2 shows the process flow scheme and major components of the Accuflow Multiphase Metering System. It consists of a vertical pipe section and a horizontal pipe section connected together as shown, (Accuflow, 2011). Multiphase fluid from the production flowline enters the vertical pipe tangentially, creating a cyclonic action in the vertical pipe where majority of the gas is separated and flows upward. The slightly downward inclination of the inlet pipe promotes liquid/gas stratification in the inlet pipe that enhances gas/liquid separation in the vertical separator pipe. The remaining gas, mostly in the form of small bubbles, is carried downward with the liquid stream and enters the horizontal pipe section.

Liquid level in the horizontal separator pipe section is controlled in the middle of the pipe using a control valve located in the gas flowline. As the liquid level in the horizontal pipe rises, a liquid level signal is transmitted to the gas control valve. This causes the control valve to “pinch” or close slightly and creates a slightly higher back pressure in the gas phase. The back pressure then “pushes” the liquid to flow at a higher-than-average flow rate which in turn causes the liquid level in the horizontal pipe to fall and stabilize to the set point. Conversely, when the liquid level falls, the control valve opens slightly to reduce the back pressure in the gas phase. This reduction of back pressure causes the liquid to flow out of the system at a lower-than-average flow rate. Consequently, liquid level rises and stabilizes to the set point.

As the liquid stream flows through the horizontal pipe, gas bubbles rise to the gas/liquid interface and are completely separated as the liquid stream flows toward the outlet end of the horizontal pipe. Large gas/liquid interface area, thin gas-bearing

liquid layer, and quiescent flow in the horizontal pipe, all contribute to efficient removal of entrained gas bubbles from the liquid stream.

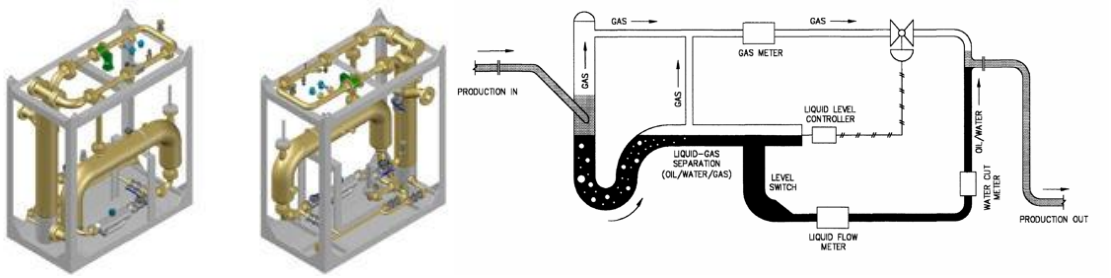

Figure A.2 – Main Components and Operating Theory of the AMMS

Coriolis flow meter is used to measure liquid flow rate. Water cut in the liquid stream is measured by one of two methods, density differential or conventional water cut meter. The conventional water cut meter is based on microwave frequency shift principle. A net oil transmitter or PLC receives liquid flow rate signal from the Coriolis flow meter to perform net oil calculations and display net oil and water rates and volumes. For gas measurement, several different technologies can be used depending on application and process conditions, typically ultrasonic, vortex or Coriolis. Temperature and pressure sensors are also installed in the gas flowline. A gas flow computer or PLC performs temperature and pressure compensation calculations and displays gas flow rate and volume at standard condition. After measurement, gas and liquid streams are then recombined and returned to the multiphase flowline.

The Accuflow meters have been deployed in the Lost Hills and Cymric Fields in California, USA, since 1996 by Chevron Texaco, (Shen and Riley, 1998) Chevron Texaco reported AMMS volumetric liquid measurements to within 2% of those of the test separator and agreement to within 3% was obtained for the liquid phase water cut. No gas phase measurements were performed.

A.3 Agar MPFM

The AGAR MPFM currently comes in three models, namely; models 50, 300 and 400. Agar's MPFM-400 is shown in Figure A.3. It is a phase separation type meter comprising a patented Fluidic Flow Diverter (FFD) device and a gas bypass loop.

The FFD device employs the difference in flow momentum in the gas and liquid phases to divert most of the free gas in the multiphase stream into a secondary measurement loop around the core of the MPFM.

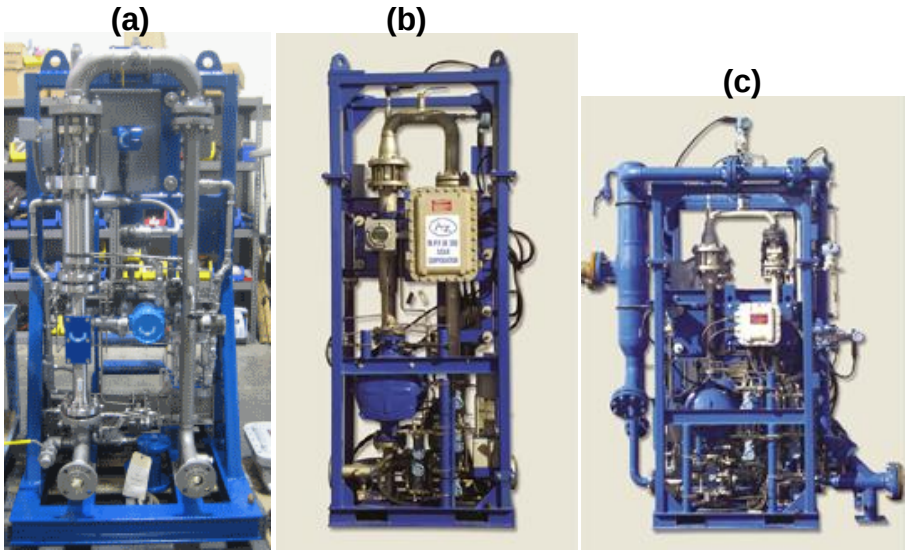

Figure A.3 – Agar MPFMs: (a) Model 50, (b) Model 300 and (c) Model 400 (Agar, 2011)

This secondary measurement loop is essentially a wet gas metering system and consists of a Venturi and a vortex shedding flow meter in series. The primary metering loop comprises three components: a positive displacement meter to determine the total volumetric flow of the mainly liquid stream; a momentum meter (dual Venturi) which measures the gas fraction of the flow; and a microwave water-cut meter. After metering, the gas in the secondary bypass loop is recombined with the oil, water and gas measured by the core meter.

Their latest generation model 50 uses three sub-systems to achieve accuracy:

- It uses a Coriolis meter to measures the total mass flow and the total density (gas and liquid). This is then fed into the Data Analysis System (DAS) which performs calculations for the multiphase measurement.
- It uses as a microwave-based water cut meter for water cut measurement. This water cut meter uses a microwave transmitter operating at over 2GHz to measure bulk electrical properties of the flow stream. Water cut data is fed into the DAS.

- The Data Analysis System performs on-line analysis of data acquired from the above subsystems to determine the oil, water, gas, and total fluid flow rates. It also supports a variety of PVT calculations that convert the process conditions to standard conditions.

The Agar MPFM is reported to have performed to its performance accuracy of ±10% for gas, oil and water flow rate for gas volume fractions ranging up to 99.9% relative to test separator references for a number of fields that it has been tests on as documented in (McNulty and Beg, 1997; Mohamed and Al Saif, 1998; and Al-Taweel and Barlow, 1999).

A.4 Emerson/Roxar MPFM 1900VI

Launched In February 2009, the Roxar MPFM 2600 with the Zector® technology is the third generation of Roxar multiphase meters. The Zector® technology is the 'engine' of the MPFM 2600 and consists of (Emerson, 2011):

- 2-6 electrode geometry sensors which allows for measurements in separate sections of the pipe, in addition to the full cross sectional area. This enables the system to perform both rotational near wall measurements and cross-volume measurements, thereby providing a comprehensive mapping of the flow regimes.

- High speed field electronics system that combines capacitance and conductance measurements in one.

- Advanced signal processing techniques are used to handle asymmetrical flow of mixtures of the gas and dispersed phase.

In some applications, oil, gas and water fractions are determined by gamma ray density measurements. A cross-correlation algorithm is used to measure individual phase flow rates. The range of the MPFM is extended to cover single-phase liquid flow rate by employing a Venturi meter, (Leggett *et al*, 1996).

The manufacturer stated that the Roxar Multiphase meter 2600 has been extensively tested, in partnership with Christian Michelsen Research AS, Norway and benchmarked against Roxar's second generation multiphase meter claiming that all

tests have demonstrated superior measurement but no data was published. According to Leggett *et al*, (1996) field tests carried out by Gulf of Suez Petroleum Company (GUPCO) in Egypt on seven wells covered a flow regime range from severe slugging through to annular due to the dynamics of the artificial lift (gas-lift) production system employed. With average GVF ranging between 93 - 96%, the gas and liquid phase flow rates were measured to within ±10%, relative to the test separator. Liquid flow rate measurements deteriorated for tests where the GVF was in excess of 96%.

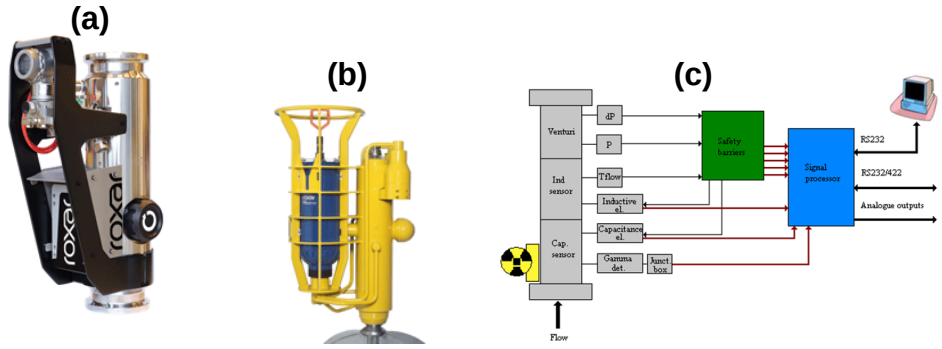

Figure A.4 – Roxar MPFM: (a) Topside, and (b) Subsea Versions (c) Schematic Diagram (Emerson, 2011)

A.5 FMC FlowSys TopFlow

The FMC Measurement Solutions FlowSys TopFlow is an in-line multiphase meter with a Venturi insert and impedance electrodes incorporated inside the throat of the Venturi insert. The differential pressure is measured across the inlet of the Venturi insert while the capacitance or conductance of the mixture flowing through the Venturi insert is measured by the electrodes inside the Venturi throat. Fluid velocity is found from cross-correlation of the high-resolution time signals from pairs of electrodes within the Venturi insert.

Figure A.5 shows the 2” and 6” meter and a schematic diagram depicting how the flow rates of the oil, water and gas are then calculated based on the measurements obtained by the electrodes and the differential pressure across the Venturi insert (FMC, 2011).

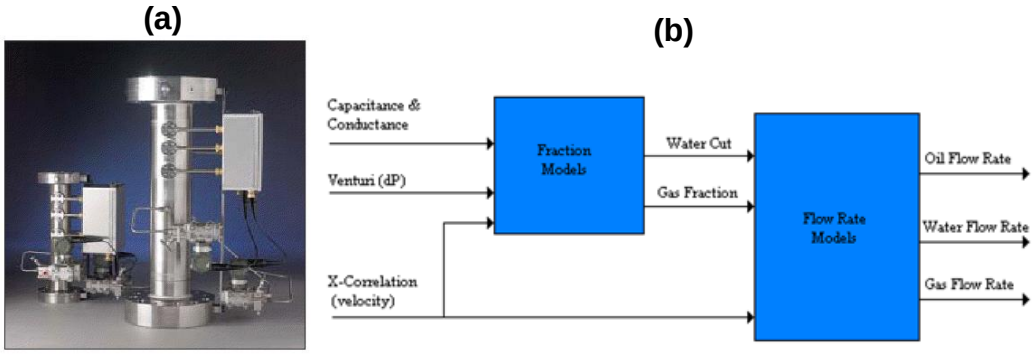

Figure A.5 – (a) 2" and 6" FlowSys TopFlow Meter (b) Schematic Diagram (FMC, 2011

FlowSys TopFlow meter was tested at the National Engineering Laboratory (NEL). The experimental range was 0-60 m^3/h for liquid and 0-340 m^3/h for gas flow rates. The test results show liquid phase and oil flow rate measurements obtained were within a relative uncertainty band of ±5%, while the gas flow rate measurements were found to be within ±20% across a large proportion of the operating envelope. However, for tests points with a GVF greater than 70%, or water cuts in excess of 75%, large deviations from the test separator reference values were reported (Hall, 2000).

Another laboratory testing of the FlowSys TopFlow meter was carried out at the Christian Michelsen Research (CMR). The experimental range was 15-40 m^3/h for liquid and 20-90 m^3/h for gas flow rates. Klepsvik *et al*, (2000) reported that 99% of the liquid flow rate measurements were within a relative deviation of ±10% from reference values; 78% of oil flow rate measurements were within ±10%; and 84% of the gas flow rate measurements were within ±15%.

In 2001, the FlowSys TopFlow meter was field tested by Eni in Trecate, Italy. Mazzoni et al, (2001) reported phase flow rate measurements of within ±10% for GVFs up to 92-93% for the gas flow rate and GVFs of up to 86-87% for the liquid flow rates in a text matrix that ranged between 6-35 m^3/h and 35-145 m^3/h for liquid and gas flow rates respectively. The liquid flow rate measurement accuracy deteriorated to approximately ±20% at GVFs above 93%. Due to test wells constraints, the meter was tested for water cut between 41-51% for which majority of the test points where classify within ±5% accuracy.

A.6 Framo/Schlumberger PhaseWatcher Vx

The Framo/Schlumberger PhaseWatcher Vx multiphase meter combines two measurement techniques, namely; a Venturi with pressure, temperature and differential pressure sensors for mass flow measurement and dual-gamma densitometry for phase fraction determination. This combination in turn determines the oil, water, and gas flow rates (Schlumberger, 2011).

Following a blind tee, the multiphase stream flows vertically upwards through the metering area. All the measurements are made in the Venturi throat, i.e. absolute pressure, temperature, differential pressure relative to upstream conditions and phase fractions and the meter come in both topside and subsea versions as shown Figure A.6.

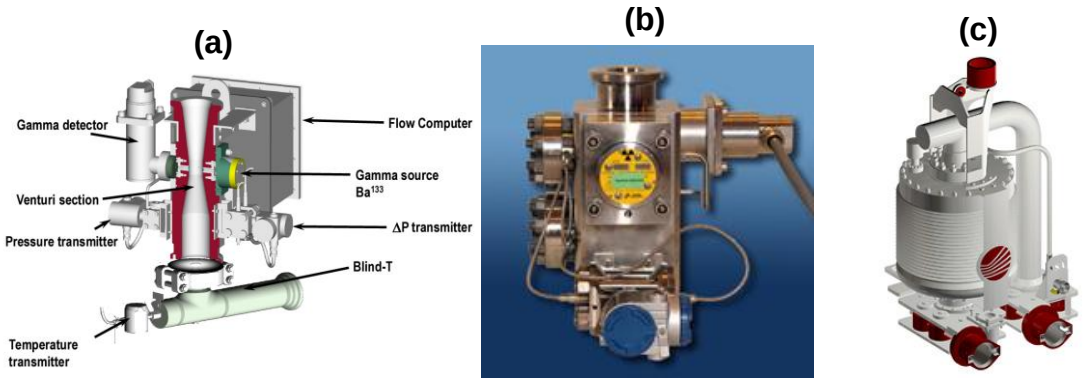

Figure A.6 – PhaseWatcher Vx MPFM: (a) Schematic (b) Topside, (c) Subsea Versions (Schlumberger, 2011)

The dual-energy gamma densitometer employs a barium-133 radionuclide source to measure phase fractions. The gamma densitometer is located at the narrowest part of the flow conduit, having a source with energy levels appropriate for measurement of gas fraction and water cut (29 keV and 80 keV), allows these energy levels to be feasibly used with a low strength source.

The PhaseWatcher Vx has been evaluated on many occasions by several operators in flow loops and field trials. These include the National Engineering Laboratory (NEL), Joint Industry Projects (JIP), the Multiphase II JIP for oil applications and Wet Gas JIP at CEESI (Framo, 2011). For the NEL flow loop test, the experimental test points ranges between 0 to 95% GVF. A ±10% relative uncertainty band was reported for the liquid phase and oil flow rate measurements while water cut

readings had an associated absolute error of ±6% (Letton *et al*, 1997). No quantification of the gas phase measurement performance was reported.

The Al-Khafji Joint Operations installed five PhaseWatcher Vx MPFMs in the offshore Al-Khafji field for satellite-based well monitoring in 2005. (Al-Bourni *et al*, 2005). The well tests results were referenced against a conventional three-phase separator housed in a test barge with the oil and water flow rates achieving a 5-10% relative and over 15% for the gas phase flow rate.

A.7 Haimo MPFM

The Haimo multiphase flow meter is a combination of gas-liquid two phase flow meter and three phase water cut meter. It combines the features of inline and partial separation type MPFMs as shown in Figure A.7 (Haimo, 2011). Measurement of the gas and liquid flow rates are carried out in the gas-liquid two phase meter that consist of a Venturi and single gamma meter. The Water Liquid Ratio (WLR) is measured in the dual gamma meter located downstream of the flow conditioner. The phase fractions are derived from these two independent measurements and net oil flow rate is finally calculated using the gross liquid flow rate and water cut measurement. The flow conditioner upstream of the dual energy gamma water cut meter homogenises the multiphase flow by mitigating slugs and reducing the GVF level. This helps achieve the water cut measurement error within ±2% absolute for the full range of stated GVF in the meter's operating envelope.

The Haimo meter gave a +/-10% relative on net oil, gas and water flow rates and +/-2% absolute on water cut measurement over the full range of 0 – 99% GVF when tested in the Daqing Oil Field Multiphase Flow Facility, Daqing City, China.(Basaidi and Bhaskaran, 2003).

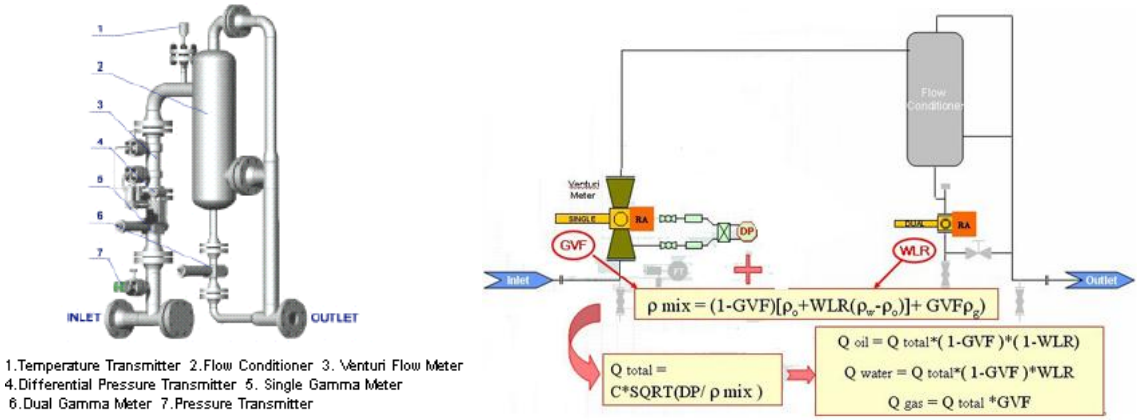

Figure A.7 – Haimo MPFM, (Haimo, 2011)

A.8 Jiskoot Mixmeter

The Cameron/Jiskoot Mixmeter is a simple, compact, in-line multiphase meter that utilises a patented upstream mixer to homogenise the flow stream in the measurement section of the meter (Jiskoot/Cameron, 2011). The mixer attempts to equalise the velocity of the three phases and removes the need for complex slip correction calculations, see Figure A.8. Phase fractions are measured by a dual-energy gamma densitometry system which has a single Caesium137 source. The homogeniser in the Mixmeter generates a characteristic differential pressure (DP) for bulk velocity measurement from which the phase velocities are determined. No field or laboratory performance of this meter was found in the public domain.

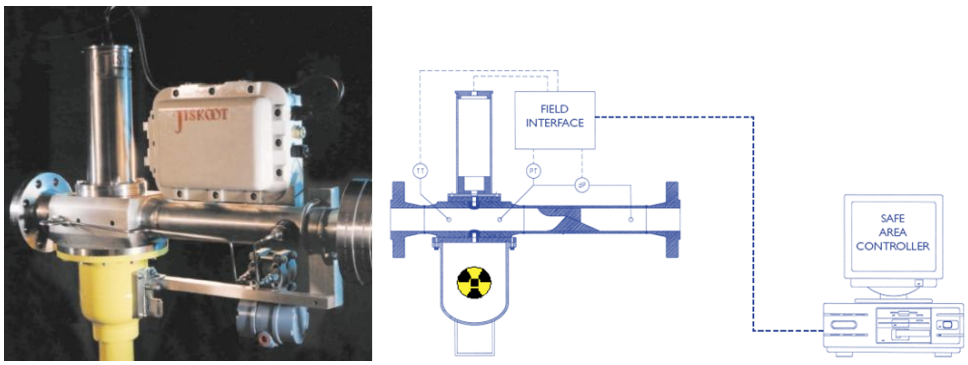

Figure A.8 – Mixmeter MPFM (Jiskoot/Cameron, 2011)

A.9 MSi Kenny VMS.

The Virtual Metering System (VMS) is now part of the MSi Kenny's Virtuoso™ suite of software products. The Virtuoso/*VMS* package uses pressure and temperature

instrumentation data from existing sensors in and around the well to provide continuous estimates of multiphase well flow rates (MSi Kenny, 2011). VMS can use several predictive models to determine flow rate. It approximates the uncertainty of each estimate and then combines these values to achieve the lowest overall uncertainty (Subsea, 2011). Haldipur and Metcalf (2008) reported field testing of the VMS in the Gulf of Mexico and other location globally. They claimed “that this technology has provided very reliable and accurate flow rate predictions over a variety of well configurations and reservoir characteristics”, however no data were presented regarding the measurement uncertainties.

A.10 Multi Phase Meters AS mpm

Multi Phase Meters AS’s mpm is marketed as a high-performance meter and was developed through a JIP involving Eni, Hydro, Shell, Total, Statoil and ConocoPhillips (Stobie and Saettenes, 2007). The MPM meter, which has topside and subsea versions, combines input from a Venturi, a gamma densitometer, pressure and temperature transmitters and a EM (electromagnetic waves) based system for dielectric measurements to form a multi-modal tomographic system (Multi Phase Meters, 2011). A patented 3D Broadband technology uses high frequency electromagnetic waves on multiple planes to measures the dielectric constant use for calculating the water cut, salinity, composition, and the liquid/gas distribution within the pipe cross section. Figure A.10 shows the topside and subsea versions and the main components of the meter. A Venturi section conditions the flow and measures its velocity while the gamma densitometer measures phase composition of the stream. By combining the EM and gamma measurements with advanced Venturi models, the flow rates of oil, gas, water and salt content are calculated. FMC Technologies acquired Multi Phase Meters AS (MPM), based in Stavanger, Norway in 2009.

Scheers and Wee (2007) reported gas and oil flow rate measurement accuracies to within ±8% and ±3% respectively across the full range of gas volume fractions and water in liquid ratios for a field validation tests carried out in January 2007 in the Gullfaks field operated by Statoil. Another test conducted at the Southwest Research Institute (SwRI) multiphase flow loop in November 2007 only report the results of two phase tests at high GVFs (95 – 100%), when the MPM meter was operated in the

wet gas mode. Measurement accuracies referenced to test separator are; gas and liquid volumetric flow rate to within ±3%, water fraction to within ±0.04% and water salinity to within ±1%. However measurement results were not reported when the meter was operated in multiphase mode (Stobie and Saettenes, 2007).

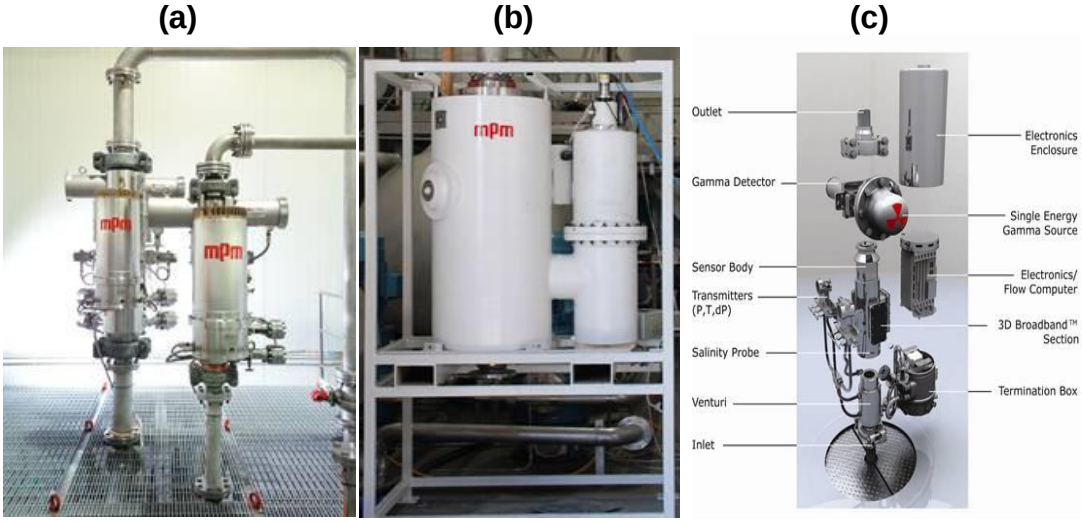

Figure A.10 – MPM Meter: (a) Topside, and (b) Subsea Versions (c) Main Component (Multi Phase Meters, 2011)

A.11 Neftemer MPFM

The Neftemer Multiphase Meter is a non-intrusive unit that is based on a nucleonic two-phase meter that had been developed for the Russian nuclear industry by the Space Institute in Leningrad (now St. Petersburg) far back in the late 1970s (Neftemer, 2011). Neftemer comprises two elements: a gamma source housed in a holder unit and a gamma detection unit. As shown in Figure A.11, these units are mounted diametrically opposite each other on a vertical pipe section containing a vertically upward multiphase flow.

The detection unit uses a sodium iodide crystal with a photomultiplier for the gamma ray detection. The gamma source is the radioisotope caesium-137. This source emits a narrow gamma-ray beam directed along the pipe's cross-sectional diameter towards the sodium iodide crystal in the detector unit (Kratirov et al, 2006).

Figure A.11 – Neftemer MPFM (Neftemer, 2011)

Neftemer is a multi-energy multiphase meter that depends on fluctuations in the density of the mixture. The density of multiphase fluid is inferred from the raw gamma count induced by density fluctuations in the pipe during the passage of free gas bubbles in liquid through the measurement section. The passage of an individual bubble of free gas through the pipe section gives an increase in the gamma count as a result of the decrease in absorbing matter along the path of the gamma beam. The count fluctuation pulse amplitude is dictated by the physical size of the bubble while its width is a function of both the bubble size and the fluid velocity. By analysing the multiphase mixture density fluctuations, the velocities for bubbles of different sizes are determined. It is well known that gas bubbles below a critical size will not exhibit phase slip and are effectively entrained in the liquid phase. Thus, the analysis of the motion of liquid entrained bubbles facilitates liquid phase velocity determination. Determination of the average velocity of all gas bubbles yields the gas phase velocity. The high scan rate, 250 Hz, allows velocities to be determined over a wide range.

The phase fractions of oil, water and gas across the pipe section for each scan are determined using

- First, the overall gamma density
- Second, the standard dual energy equations, taking the absorptions at two pre-defined energy levels in the detected spectra
- Third, the overall shape of the detected spectrum, which is related to the oil, water and gas fractions.

From the liquid and gas velocities and the oil, water and gas fractions, the oil, water and gas flow rates are then determined. This method required a detailed mathematical analysis and sophisticated statistical processing techniques to generate accurate measurements, however in practice, simplifications are made to allow Neftemer to operate in real time and tuning is required for a new application.

A.12 Phase Dynamics Inc. CCM

The Phase Dynamics Inc Compact Cyclone Multiphase meter (CCM meter), shown in Figure A.12, utilises a compact gas-liquid cyclone, to separate the liquid and gas phases prior to measurement. The system is actually a modern version of a traditional two phase separator. The first stage of gas liquid separation uses a swirl element that provides very high centrifugal forces to the multiphase stream. This result in increased gas separation capabilities and better control of the separator dynamics. Additional swirl elements are then used in the second stage to complete the separation of liquids from the gas. The separated liquid is routed through a full-range microwave water cut meter forming an integral part of the CCM. Coriolis meters are used to measure the separated gas and liquid flow rates. The gas is then recombined with the liquid after the control valves (Phase Dynamics, 2011).

Figure A.12 – Compact Cyclone Multiphase meter (Phase Dynamics, 2011)

Measurement accuracies of ±5% were claimed for the gas flow rate, liquid flow rate and liquid phase water cut from a test that was carried out at the Norsk Hydro Test Facility, Porsgrunn in January 1998 (Scott and Kvamsdal, 2000).

A.13 PSL ESMER Multiphase Meter

Expert System for Multiphase Flow Metering (ESMER) is the flagship product of Petroleum Software Limited (PSL). This meter exploits a combination of traditional fluid flow theory and modern signal processing and neural network techniques to determine the individual phase flow rates of a multiphase flow mixture (PSL, 2011). The system comprises two modular sub-spools, namely; the Cone spool and the Coriolis spool. The Cone spool contains two differential pressure transmitters (one across the cone, the other measuring recovery pressure downstream), one absolute pressure transmitter and a resistance temperature device. The Cone also acts as a capacitance sensor for oil-continuous flow and as a conductance sensor for water-continuous flow. The spool is normally installed horizontally and the flow passes through the spool in a straight line with very low pressure drop. The Coriolis spool carries out mass flow rate and fluid density measurements independently. This is then corrected by feed-back from the Cone spool for multiphase effects.

According to Toral *et al* (1998), ESMER is a pattern recognition based meter that establishes the non-linear relationships between an array of sensor measurements and the individual phase flow rates by a combination of pattern recognition and neural network training.

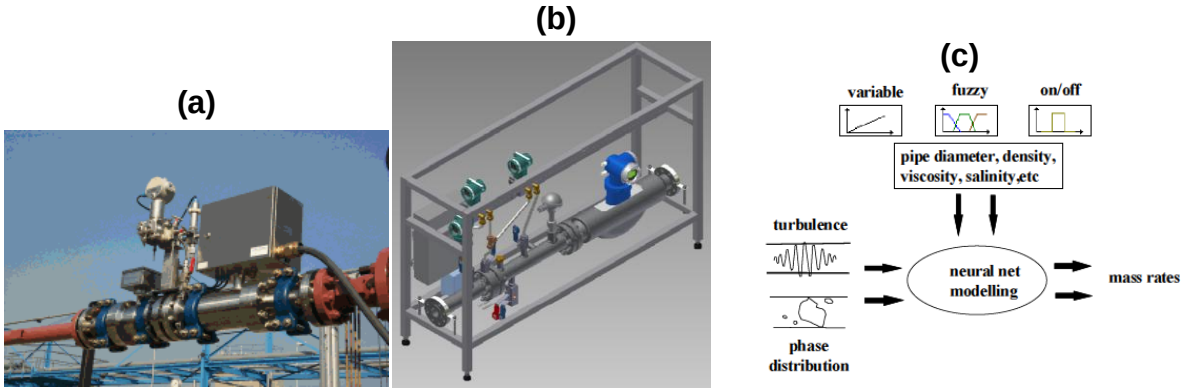

Figure A.13 – ESMER Multiphase Meter: (a) Cone Spool, (b) Coriolis Spool and (c) Concept Model (PSL, 2011)

A series of tests conducted in one of the offshore platform of Sarawak Shell Berhad, Malaysia in 2002 over a 20-month period, the ESMER measurements were compared against those obtained from a conventional test separator. Good repeatability and trending of the meter against different production rates and flow patterns were reported and it was claimed that ESMER measurements matched the separator measurements to within ±10% for wells which were inside the operating envelope (Cai, 2004), with the accuracy of the meter deteriorating for well test data located at the boundary of the operating envelope of the meter with time.

A.14 TEA Sistemi S.p.a. LYRA

The TEA LYRA multiphase meter measures total mass flow rate with a differential pressure producer such as Venturi meter, nozzle or orifice, (according to the fluids and process specifications) in conjunction with a with a density meter as shown in Figure A.14.

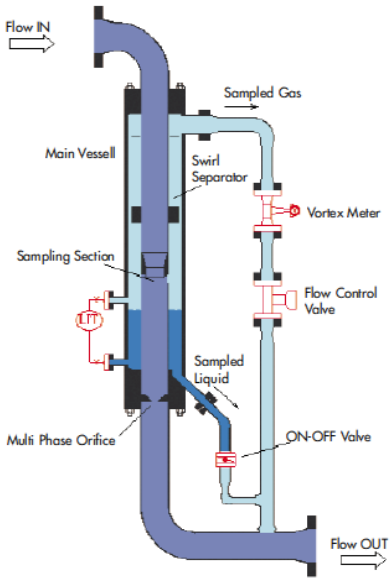

Figure A.14 – LYRA MPFM (TEA Sistemi S.p.a., 2011)

Water-cut is measured with an impedance meter (patented), which also requires as input the value of the mean density of the gas-liquid mixture. The mean density is measured with a gamma-densitometer. For application where the liquid fraction is about 30%, the total mass flow rate and the mixture density are derived from the pressure drops through a vertical section of the meter coupled with the reading of the differential pressure producer, using a proprietary procedure. For such applications,

the gamma densitometer is not used. In LYRA signal processing is based on mechanistic models of the flow structure and, when possible, on an artificial neural network trained with well test data.

From the manufacturer's website (TEA Sistemi S.p.a., 2011), LYRA has been marketed in Italy since 1995 and has been installed in Prezioso, Dirillo and Trecate oil fields operated by Agip, claiming excellent performance results but the meter's accuracies were not quantified.

A.15 Weatherford. REMMS

The *Red Eye* multiphase metering system (REMMS), combines partial separation technology with conventional liquid and gas metering to provide a complete multiphase measurement solution as shown in Figure A.15 (Weatherford, 2011). An advanced controller governs the operation of the system as well as interpreting and recording data and providing communications with external host systems.

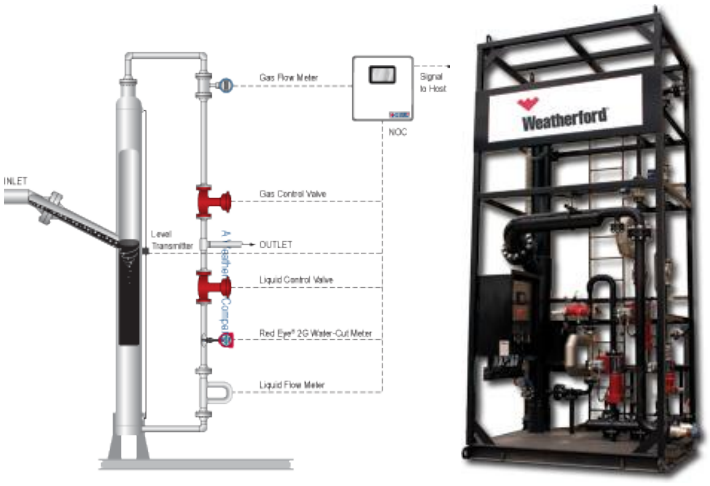

Figure A.15 – Weatherford REMMS (Weatherford, 2011)

The main components of these REMMS are a gas-liquid cylindrical cyclone (GLCC) separator, flow metering instruments, and level control valves. The principle of operation is based on inducing bulk separation of the liquid and gas phases by creating a cyclonic flow pattern. The three-phase fluid enters the GLCC through a narrow tangential inlet. This forces the liquid and gas to accelerate through the inlet and around the vertical axis of the GLCC, creating a vortex. This vortex causes the gas to separate from the liquid and due to the large density difference between the

gas and liquid phases, the gas migrates quickly to the top of the GLCC and the liquid travels to the bottom. Once separated, the individual streams are measured with conventional liquid and gas meters.

Oil and water flow rates are measured using a liquid flow meter and the *Red Eye* 2G water-cut meter. A gas flow meter is used to measure the gas rate and then the two phases can be recombined or transported in separate flow lines. Level inside the GLCC is monitored by using a differential pressure transmitter. Gauge pressure and temperature transmitters are also installed on the separator to measure the process temperature and pressure conditions. Liquid and gas control valves are used to maintain an optimum separation level inside the GLCC. The signals from all these instruments are sent to the REMMS remote terminal unit (RTU) which controls the separation and metering processes and displays the well test results.

Recent field testing has reported an accuracy of ±5% for water cut measurement and ±10% total liquid volume measurement with a confidence interval of 90%. (Bastardo *et al*, 2008).

Appendix B Review of Commercial Watercut Meters

Water cut is the water volume flow rate, relative to the total liquid volume flow rate (oil and water) both converted to volumes at standard pressure and temperature, expressed as a percentage. In other words, it is the ratio of water produced compared to the volume of total liquids produced. A typical watercut meter measures the water content (cut) of a specific product as it flows through a pipe.

Watercut meters measure the differential characteristics of water and other components of the liquid to determine the percentage of water in them. This is done by various methods including dielectric measurements (capacitance) microwave, infra red and other inferential techniques. These meters are typically used in the oil production and distribution, refineries, chemical and petrochemical plants and in the aviation and pharmaceutical industries.

This section presents a review of commercially available watercut meters that are used the oil and gas industry. The measurement of water content in crude oil is an important and widely encountered practice in all aspects of oil industry operations - crude oil production, processing, transportation, and refining, (Yang et al, 1990). Water cut measurement is used to help determine oil production rates, custody transfer, and pipeline oil quality control. Also, the separation efficiency of production operations may be optimized by monitoring the water content of the process fluid at various points throughout the processing facility.

B.1 Agar OW-200/300 Watercut Meter

The Agar's oil/water meter comes in two series; OW-200 and OW-300. The OW-200 Series oil/water meters, consisting of the OW-201 and the OW-202 meters, utilize a microwave transmitter (2.45GHz) to measure bulk dielectric properties of the flow stream (Agar, 2011). They measure hydrocarbon/water mixtures over the full range of 0-100%, regardless of the continuous phase and the accuracy of the measurement is not affected by changes in salinity, density, viscosity, temperature or velocity of the components being analyzed.

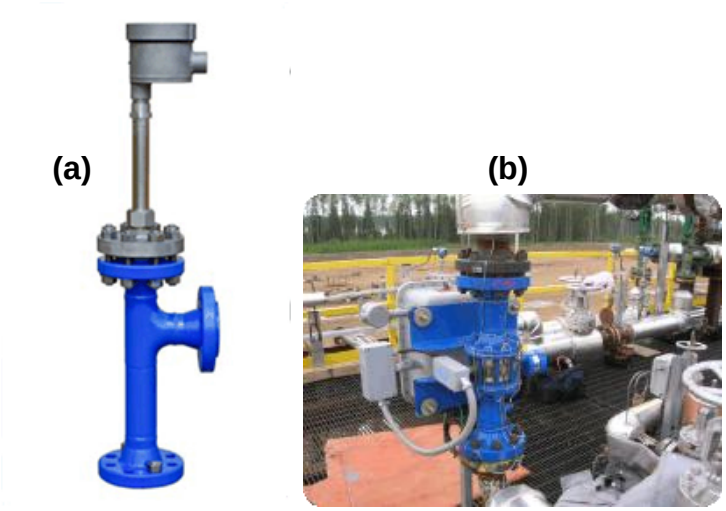

Figure B.1 – Agar Watercut Meter, (a) OW-300 and (b) 200 Series (Agar, 2011)

The AGAR OW-300 Series oil/water meters measure liquid-in-liquid concentrations over the full range of 0-100% water cut, by measuring the complex permittivity properties of the flow stream using a multiple high frequency method and is available in line sizes up to 4".

B.2 EASZ-1

The EASZ1 loop-powered watercut monitor is a solid state electronic instrument that that employs a capacitance probe technique to determine the percent water cut in an oil emulsion without requiring the physical separation of the fluids. The frequency generated by the capacitance probe is determined by the water cut of the emulsion stream in the probe (EESIFLO, 2011). It calculates capacitance measurement by digital techniques and produces a 4-20mA output signal which varies linearly with water cut.

Figure B.2 – EASZ1 Watercut Meter (EESIFLO, 2011)

B.3 ESMER Water-in-Oil Meter

The ESMER Water-in-oil (WIO) meter is based on a cone differential meter which also acts as a capacitance sensor and it measures oil-water mass flow rate as well as water composition based on the characterisation of the dielectric property of the fluid. The dielectric constant of a material is a measure of its ability to transmit electrical potential energy. A dielectric material has poor conductivity, but it can hold a charge with an applied electric field. The value of the dielectric constant varies with the frequency of the applied electric field, but below 106Hz the dielectric constant is virtually independent of frequency.

ESMER WIO works in the range 0-50% water cut and can tolerate up to 5 % GVF within its accuracy specification (PSL, 2011). Effects of changing oil density and temperature are taken into account in the factory calibration of the meter and are automatically compensated for in field measurements. This meter makes two primary measurements which are combined in the flow computer to provide the oil flow rate in mass or volumetric units. The primary measurements are those of dielectric constant (water composition) and differential pressure across the cone (mass flow rate).

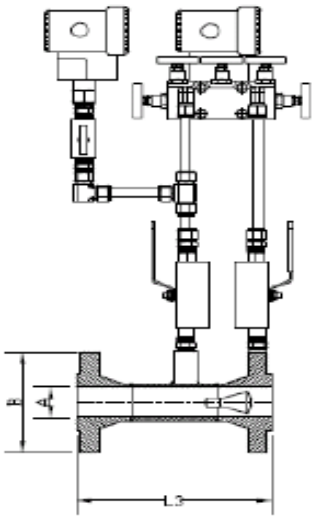

Figure B.3 –Schematics of the ESMER Watercut Meter (PSL, 2011)

Flow rate and watercut measurement accuracy are given by the manufacturer as: Best case: liquid flow rate; 1 % (relative) and watercut; 0.5% (absolute). Worst case: liquid flow rate; 2 % (relative) and watercut; 1% (absolute).

B.4 NUFLO Series 1000 Watercut Monitor

The Cameron NUFLO™ Series 1000 Watercut meter determines the percent watercut in an oil emulsion using capacitance probe technique. The frequency generated by the capacitance probe oscillator is determined by the water cut of the emulsion stream in the probe (Cameron, 2011). It uses digital techniques to compensate for the non-linear relationship between frequency and water cut and produces a 4-20mA output signal which varies linearly with water cut (0-100%).

The manufacturer claims an accuracy of 1% over 0-100% range with homogeneous emulsion.

Figure B.4 – Cameron NUFLO Watercut Meter (Cameron, 2011)

B.5 Phase Dynamics Watercut Analyser

Phase Dynamics offers a range of watercut meters that utilizes a unique, patented, "Oscillator Load Pull" microwave technology to determine water in liquid ratios. The technology was developed in conjunction with ARCO (now BP) in the late eighties and has installed over 2500 worldwide (Phase Dynamics, 2011).

In the operational mode, an electrical signal is sent from the electronics on the end of the measurement section down through the fluids. This generates a standing wave similar to the vibrations of a rubber band held at both ends and plucked as shown in Figure B.5. This standing wave changes position within the section as the water content changes. The change in position is automatically detected by the microwave oscillator that originally sent out the signal and it changes its basic frequency depending upon how much water is in the section.

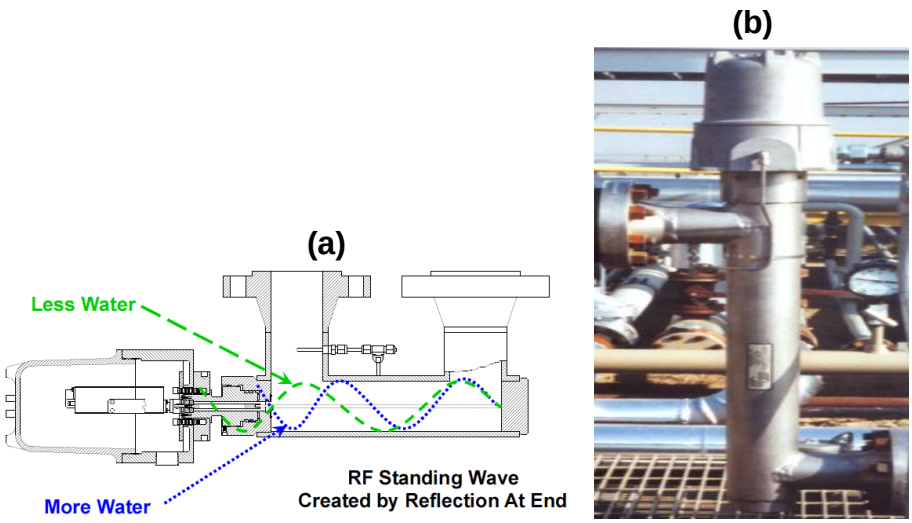

Figure B.5 – Phase Dynamics Watercut Meter (a) Schematics (b) Field Installation (Phase Dynamics, 2011)

The following measurement uncertainty is claimed by the manufacturer for her Full Range series: ±0.5% for oil phase and ±1% for water phase.

B.6 Red Eye 2G Watercut Meter

The Red Eye 2G watercut meter from Weatherford International Ltd uses patented optical sensor technology to measure the full range of water cut (0 to 100%) in a commingled oil and water stream, pictured in Figure B.6 (Weatherford, 2011) The measurement is based on near-infrared absorption spectroscopy where oil and water are easily differentiated. The Red Eye 2G watercut meter can function at high water-cut levels as well as lower water-cut measurements by simultaneously measuring multiple wavelengths that include both water and oil absorbent peaks.

Figure B.6 – Red Eye 2G (Weatherford, 2011)

Manufacturer's claimed measurement uncertainties are less than 2% even with situations of varying salinity and when entrained gas is present. It was further claimed that GVFs of up to 5% have no effect on the unit's accuracy and up to 20% have only minimal effect and that the Red Eye 2G watercut meter works with emulsions as well as fluids that separate easily.

B.7 Roxar Watercut Meter

The Roxar Watercut meter has a Fullcut, Highcut and Lowcut models. It uses a unique and patented microwave resonance technology, which use a close correlation between the density and the permittivity of a dry hydrocarbon liquid to measure the permittivity of an oil/water mixture. This patented relationship enables the Meter to continuously compensate for changes such as salinity and density in the hydrocarbon liquid composition (Emerson, 2011). The Roxar Watercut meter is a full-bore, in-line field mounted instrument for continuous and real time measurements.

Figure B.7 – Roxar Watercut Meter (Emerson, 2011)

B.8 Sentech Watercut Meter

The Sentech watercut meter, made by Sentech As (now own by Cameron's Measurement Systems division (formerly NuFlo Measurement Systems)), is a non-intrusive water monitoring device. It uses the NuFlo Single Electrode Capacitance (SeCap) solution that is based on the measurement of capacitance by a single electrode utilizing the effect dielectric constant has on the frequency of an oscillator.

Figure B.8 – Sentech Watercut Meter (Sentech, 2011)

The measurement system is called SeCaP™ because only one electrode is active and not exposed to the measured fluid such that short circuiting does not occur. The basic oscillator circuit operates at a frequency of approximately 20MHz. The fluid in the vicinity of the capacitor plate affects the oscillating frequency of the circuit. This change in frequency is related to an equivalent change in the dielectric permittivity of the mixture. If a gas is present adjacent to the capacitor plate, no reduction in frequency is observed, but if pure water is present adjacent to the capacitor plate, a much larger reduction in frequency is observed (Sentech, 2011).

This watercut meter is calibrated for each application and has a dedicated software package that takes all necessary adjustments and compensations into consideration. The output signal is then transformed into a client preferred signal. Accuracy and sensitivity levels ranges from 0.01% to 0.1% depending on application, are claimed by the manufacturer. The instrument is preferably installed vertically in the piping system and fitted between two standard flanges see Figure B.8.

Appendix C Feature Extraction

C.1 Probability Density Function

The probability density function (PDF) defines the probability that a sampled signal will assume a particular value within a definite range at any instant in time. The probability density function, *P(x)*, can be defined as follows:

Eqn.C1.1

Eqn.C1.2

where *P(x)* is the PDF of sample time history record *x (t)*, T_x is the total time, during which the signal will assume a value between *x* and *Δx*. The probability density function is mainly used to describe the probabilistic distribution of instantaneous values of continuous random data.

C.2 Mean

The mean $\bar{x}$ is defined as the arithmetic average value of the data, and it estimates the value around which a central clustering occurs. It is expressed mathematically as:

Eqn.C1.3

where *x* is the amplitude value of the i^{th} data and *N* represents the total number of data in the sampled record.

C.3 Standard Deviation

The standard deviation (SD) of a data set is the root mean square of the amplitude deviations from the arithmetic mean and is a measure of the dispersion of the data. The *SD* is defined as:

Eqn.C1.4

C.4 Coefficient of Variance

The coefficient of variance (CV) is another non-dimensional quantity. It measures the scatter in the data distribution in relative terms by dividing the standard deviation by the mean of the data. It is defined in mathematical terms as:

— Eqn.C1.5

C.5 Coefficient of Skewness

The coefficient of skewness (CS) characterises the degree of asymmetry of the distribution around its mean. A positive coefficient implies a distribution with a higher number of large values of the parameter than would expect for normal distribution. On the other hand, a negative coefficient implies a higher occurrence of smaller values. For distributions exhibiting normality, the coefficient of skewness is zero. The *CS* is defined by the equation shown below:

——— Eqn.C1.6

C.6 Coefficient of Kurtosis

The coefficient of kurtosis measures the degree of peakedness or flatness in a distribution compared to a normal distribution of the same mean and standard deviation. A positive coefficient corresponds to a distribution with a greater extent of peakedness than a normal distribution. On the other hand, a negative value for the coefficient implies a lesser degree of peakedness. For a normal distribution, the coefficient of kurtosis is zero. Mathematically, *CK* can be expressed as:

——— Eqn.C1.7

The skewness and kurtosis of a distribution are non-dimensional moments in contrast to the mean and the standard deviation which have the same dimensions as the measured quantity.

C.7 Signal Energy

Energy in this context is not, strictly speaking, the same as the conventional notion of energy in physics and the other sciences. The two concepts are, however, closely

related, and it is possible to convert from one to the other. The energy of a signal is another useful amplitude feature that can be extracted from its time domain. The total energy in a discrete-time signal *x(n)* over a time interval $n_1 \leq n \leq N$ is defined as:

Eqn.C1.8

C.8 Linear Prediction Coefficients

Linear prediction is a common technique used in speech coding. It exploits the redundancies of a speech signal by modelling the speech signal as a linear filter, excited by a signal called the excitation or residual signal. Linear prediction coefficients (LPCs) contain unique information on the spectral content of a waveform that is generated by a physical process (multiphase flow in our case). They provide an effective method of representing different signals using a small number of parameters and can be used as data compression and source different statistical features (Makhoul, 1975).

The linear prediction can be modelled in the time domain by minimising the sum of the squared differences between the actual signal and the predicted one resulting in a residual error. By so doing, a distinct set of predictor coefficients, which were used as the weighting coefficients in the linear combinations are found. The present signal sample *x(n)* is modelled as a linear combination of the past outputs and the present and past inputs. This is shown in the following mathematical relationship:

Eqn.C1.9

Where G is a gain factor, a_k and b_l are the filter coefficients of an unknown input u_n. p represents the number of past output samples being considered which is also the order of the linear prediction. Applying a z-transform on Equation C1.9, the transfer function of the system can be obtained as:

Eqn.C1.10

where *X(z)* denotes the z-transform of *x(n)*, *U(z)* is the z-transform of *u(n)* and *H(z)* is the transfer function of the system, which is the general pole-zero model. There are two special cases for the general pole-zero model, these are: 1) when a_k=0, for $1 \leq l \leq$

p, $H(z)$ reduces to an all-pole model also referred to as the autoregressive model; 2) when a_k=0, for 1 ≤ k ≤ p, $H(z)$ transforms to an all-zero or moving average model.

The all-pole model is widely used owing to its simplicity and computational efficiency. To use the moving average model, it is necessary to solve a set of non-linear equations; whereas the autoregressive model only requires a set of linear equations to be solved. The residual error, $e(n)$, is a by-product of the linear prediction techniques and is the difference between the actual input signal and the predicted signal. Hence, the following relationship holds:

Eqn.C1.11

The above relationship is used in obtaining the optimal linear prediction order p_o by checking the variation of the residual error with predictor error, which is almost flat for $p > p_o$.

The two widely used methods for estimating LPCs are the autocorrelation and covariance (Jama, 2004). Both methods choose the short-term filter coefficients in such a way as to minimise the residual error using the least-squares technique. For the autocorrelation method, Toeplitz matrix is used. This is a matrix in which all the elements along a given diagonal are equal, which guarantees the stability of the filter. This allows the application of the Levinson-Durbin recursion algorithm to solve the set of linear equations produced by the least-squares procedure.

Correlation is the relationship between two random signals that measures the average dependency between them. The correlation between pairs of a signal sample is known as autocorrelation (AC). The autocorrelation function of a signal is an average measure of its time domain properties and is given by the equation below:

— Eqn.C1.12

where, r_{xx}, is the autocorrelation function and τ is the time shift or lag.

C.9 Line Spectral Frequencies (LSFs)

Linear prediction coefficients have other forms of representations such as line spectral frequencies (LSF), reflection coefficients (RC), log area ratio (LAR), arcsine of reflection coefficients (ASRC), impulse response of LP synthesis filter (IR) etc. These parameters all have a direct relationship with the LPCs and will preserve all information contained within the LPCs.

From the published literature domain, LSFs have been reported to be the most computationally efficient and have a good quantisation and interpolation property that leads to an improved system approximation. Compared to other transmission parameters, the line spectral frequencies have been found to encode speech spectral data much more efficiently (Deller et al, 1993). This is attributed to the intimate relationship between the LSFs and the formant frequencies. Additionally, LSFs lend themselves to frame-to-frame interpolation with smooth spectral changes due to their frequency domain interpolation (Kabal *et al,* 1986).

The prediction error filter or linear prediction analysis filter can be expressed in terms of LPCs, a_k, as shown in the following equation:

Eqn.C1.13

Where p is the order of the function $A(z)$. The $(p+1)^{th}$ order symmetric and anti-symmetric polynomials $P(z)$ and $Q(z)$ can be obtained from $A(z)$:

Eqn.C1.14

Eqn.C1.15

The roots of the two polynomials lie on a unit circle and they form the LSFs. According to Kabal *et al* (1986), their algorithm can computes the LSFs directly from the LPCs using the Chebyshev polynomial root finding method.

Appendix D Probability Mass Functions

D.1 Table E.1 PMFs plots for the air-oil-water flow generated from the horizontal gamma densitometer data of the 50.8mm test rig

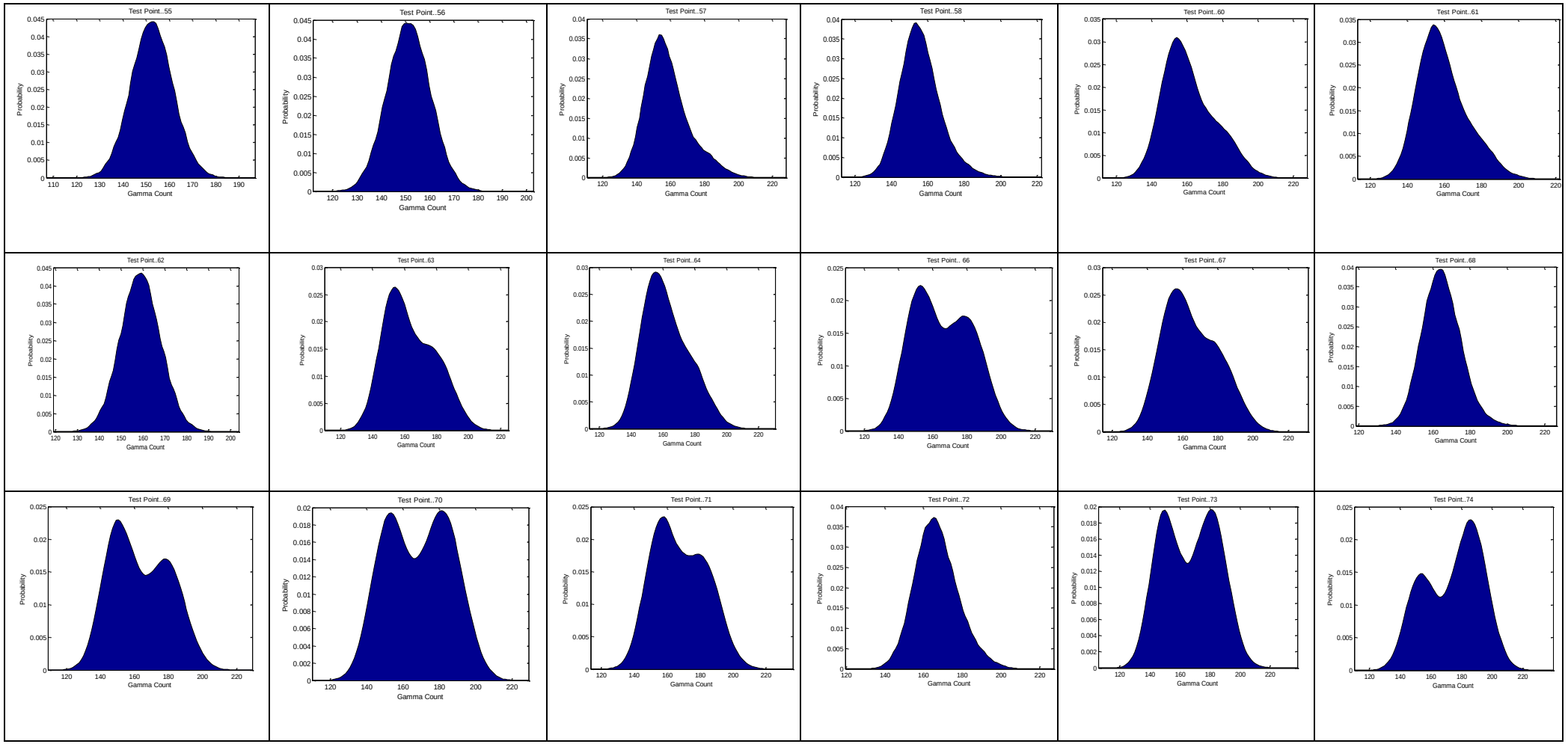

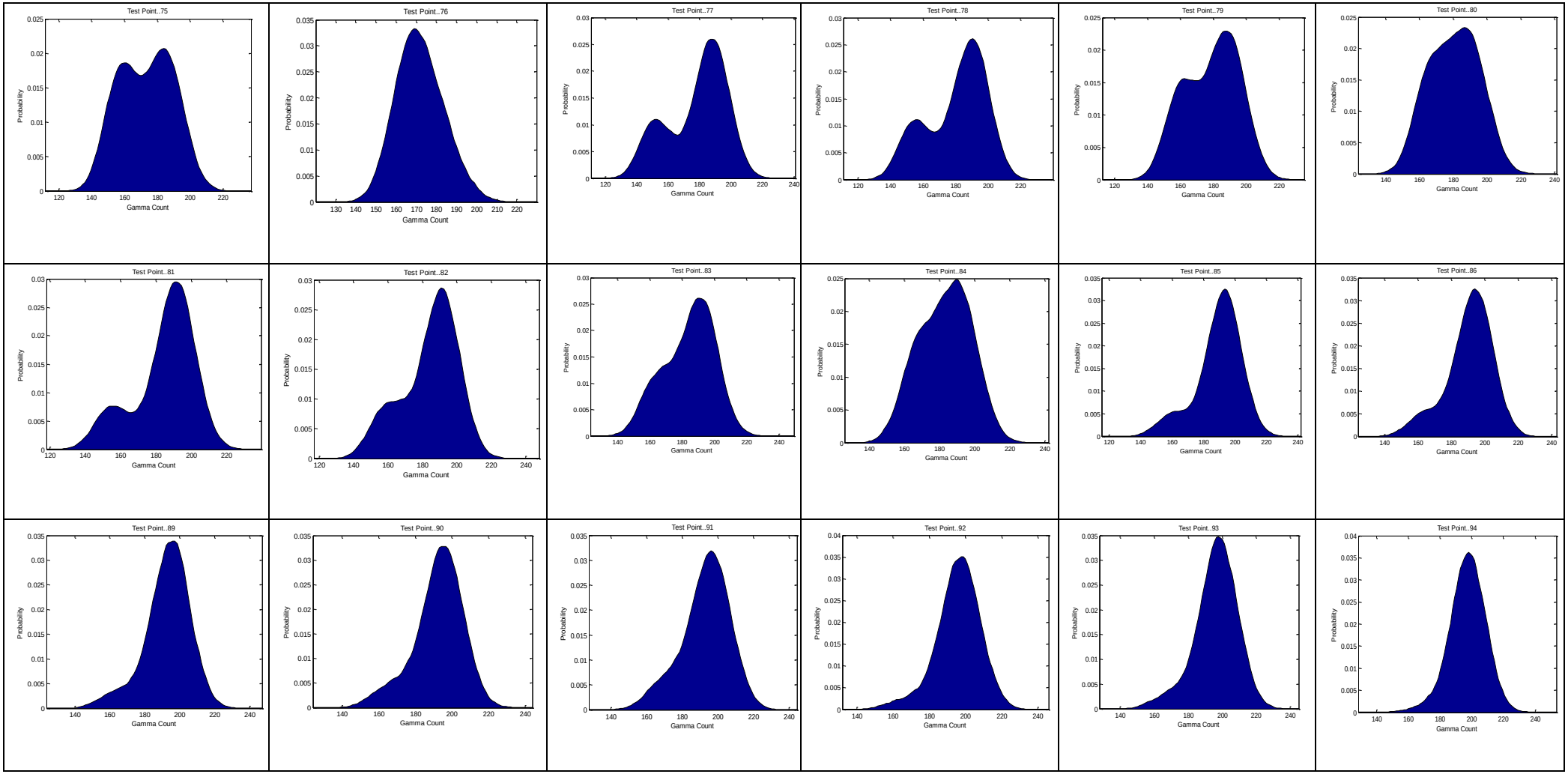
Test Point..75
Test Point..76
Test Point..77
Test Point..78
Test Point..79
Test Point..80
Test Point..81
Test Point..82
Test Point..83
Test Point..84
Test Point..85
Test Point..86
Test Point..89
Test Point..90
Test Point..91
Test Point..92
Test Point..93
Test Point..94
Probability
Gamma Count

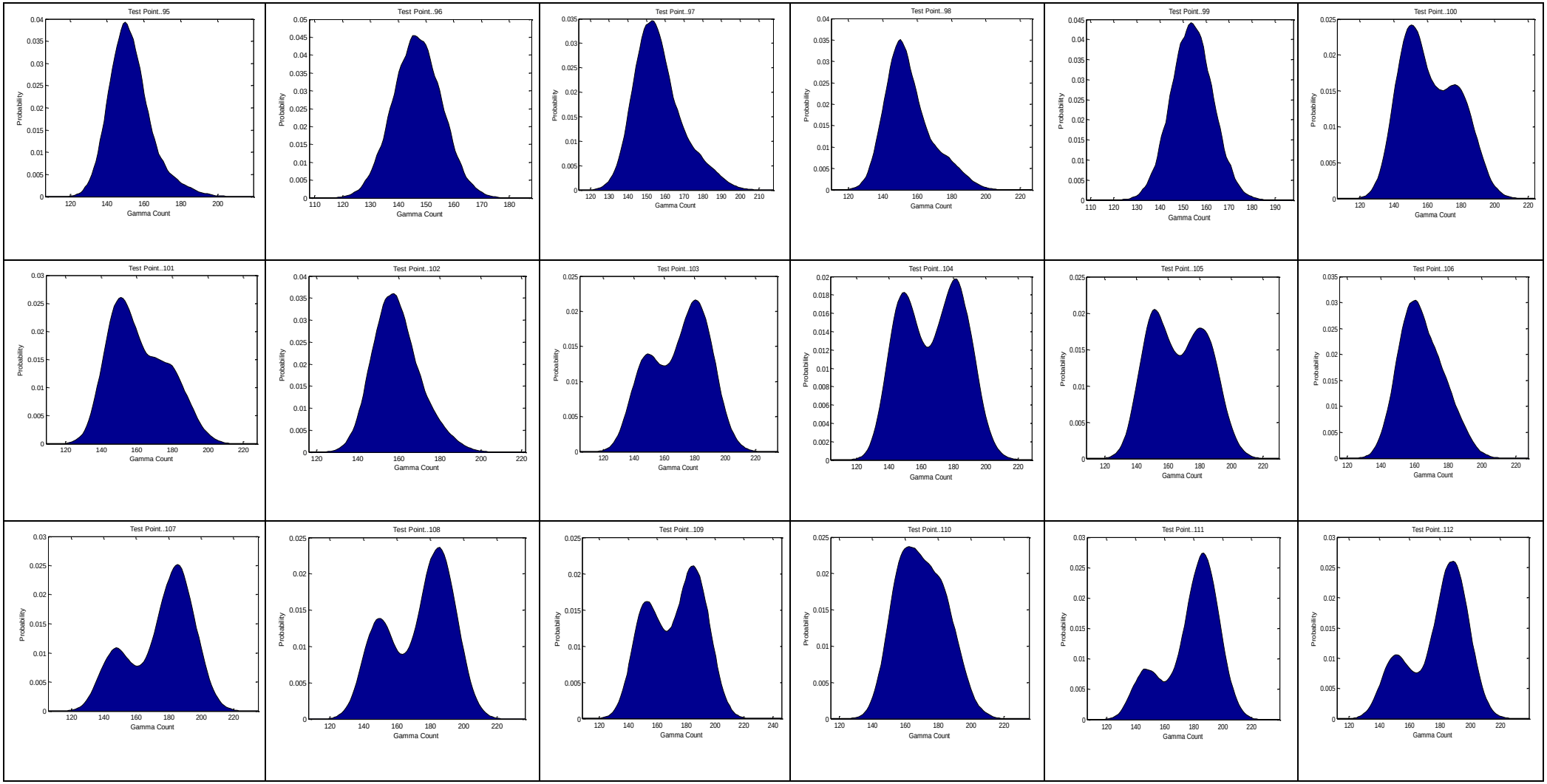
Test Point..95
Test Point..96
Test Point..97
Test Point..98
Test Point..99
Test Point..100
Test Point..101
Test Point..102
Test Point..103
Test Point..104
Test Point..105
Test Point..106
Test Point..107
Test Point..108
Test Point..109
Test Point..110
Test Point..111
Test Point..112
Probability
Gamma Count

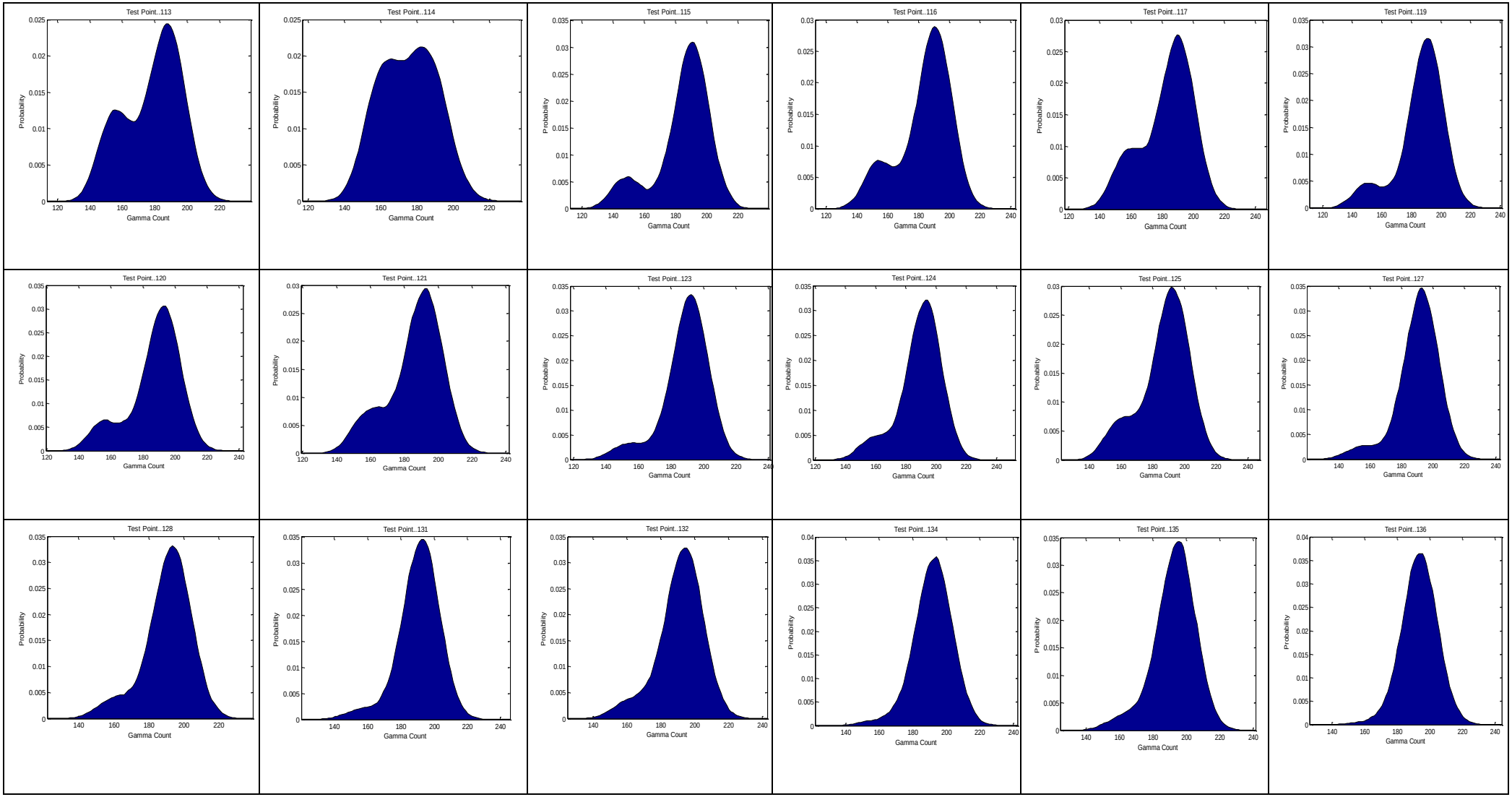
Test Point..113
Test Point..114
Test Point..115
Test Point..116
Test Point..117
Test Point..119
Test Point..120
Test Point..121
Test Point..123
Test Point..124
Test Point..125
Test Point..127
Test Point..128
Test Point..131
Test Point..132
Test Point..134
Test Point..135
Test Point..136
Probability
Gamma Count

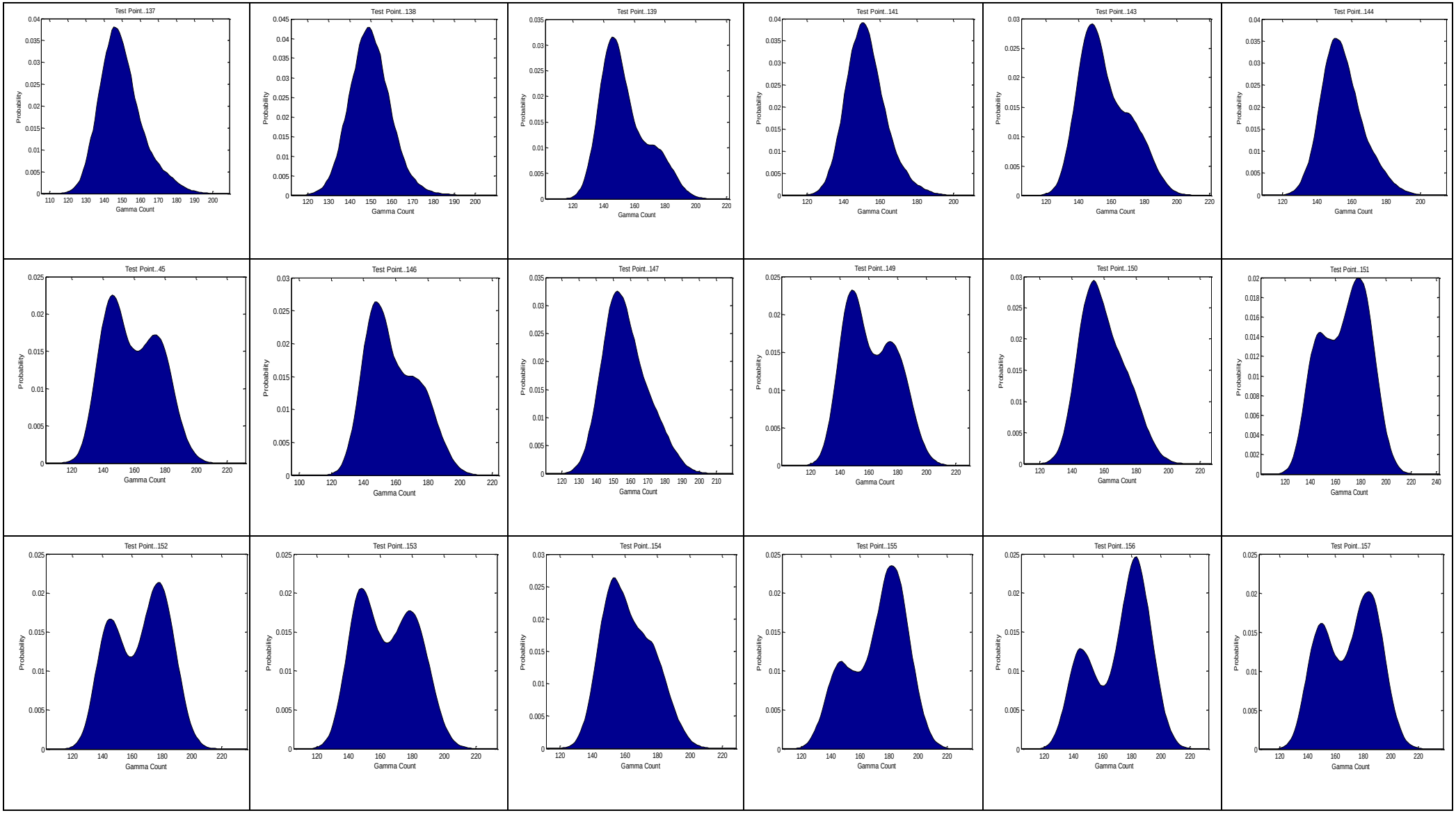
Test Point..137
Test Point..138
Test Point..139
Test Point..141
Test Point..143
Test Point..144
Test Point..45
Test Point..146
Test Point..147
Test Point..149
Test Point..150
Test Point..151
Test Point..152
Test Point..153
Test Point..154
Test Point..155
Test Point..156
Test Point..157
Probability
Gamma Count

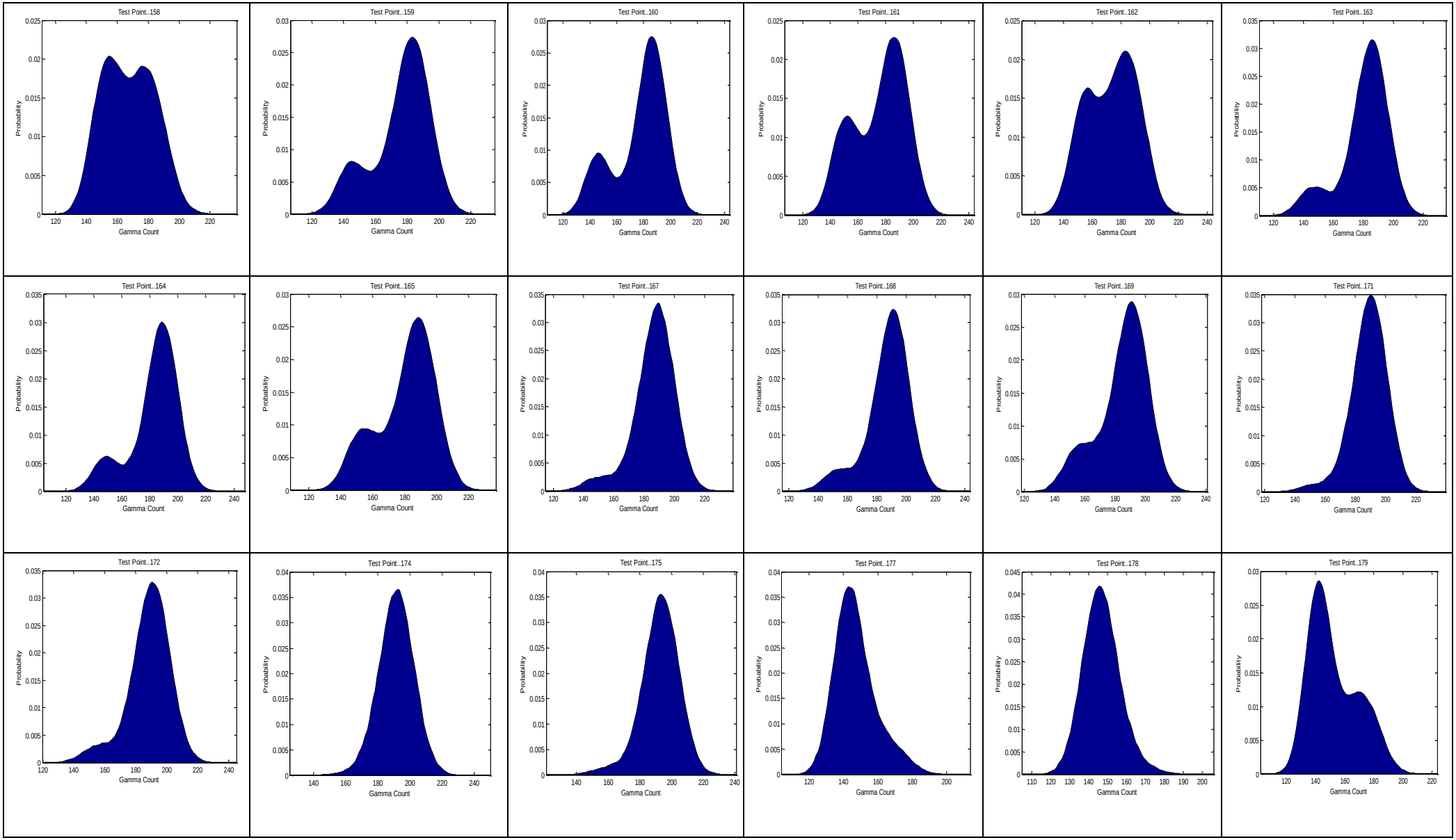
Test Point..158
Test Point..159
Test Point..160
Test Point..161
Test Point..162
Test Point..163
Test Point..164
Test Point..165
Test Point..167
Test Point..168
Test Point..169
Test Point..171
Test Point..172
Test Point..174
Test Point..175
Test Point..177
Test Point..178
Test Point..179
Probability
Gamma Count

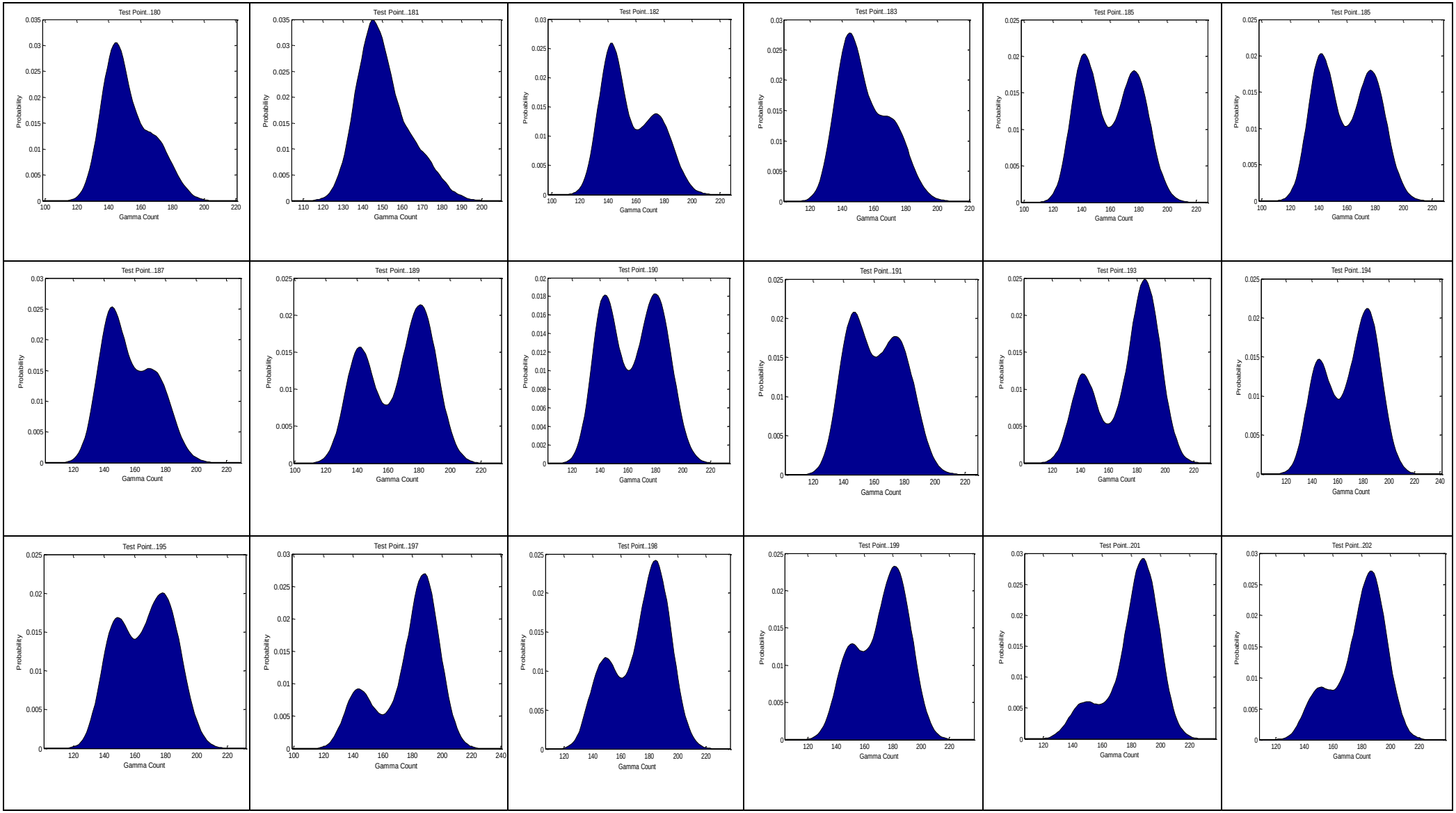
Test Point..180
Test Point..181
Test Point..182
Test Point..183
Test Point..185
Test Point..185
Test Point..187
Test Point..189
Test Point..190
Test Point..191
Test Point..193
Test Point..194
Test Point..195
Test Point..197
Test Point..198
Test Point..199
Test Point..201
Test Point..202
Probability
Gamma Count

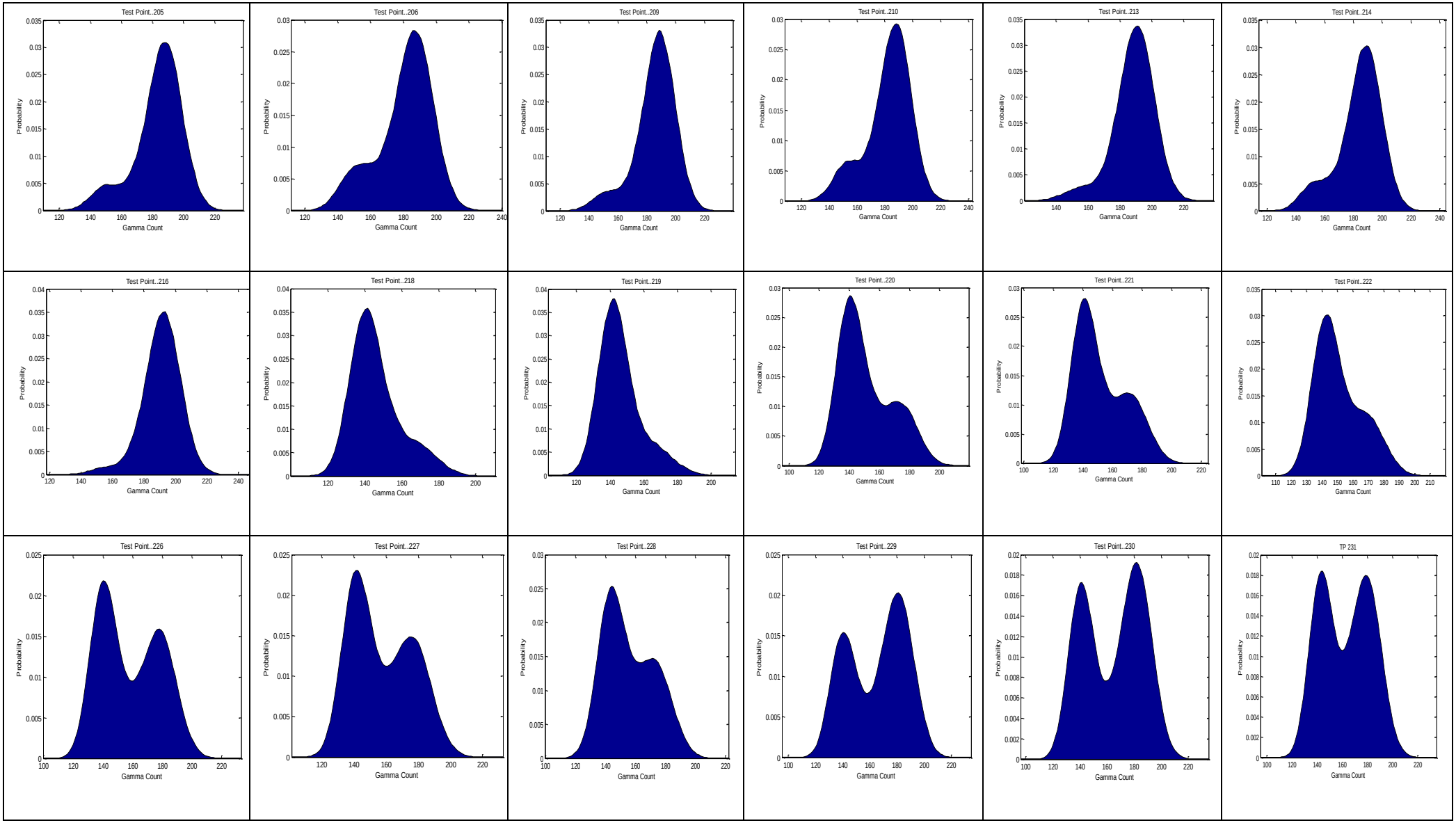
Test Point..205
Test Point..206
Test Point..209
Test Point..210
Test Point..213
Test Point..214
Test Point..216
Test Point..218
Test Point..219
Test Point..220
Test Point..221
Test Point..222
Test Point..226
Test Point..227
Test Point..228
Test Point..229
Test Point..230
TP 231
Probability
Gamma Count

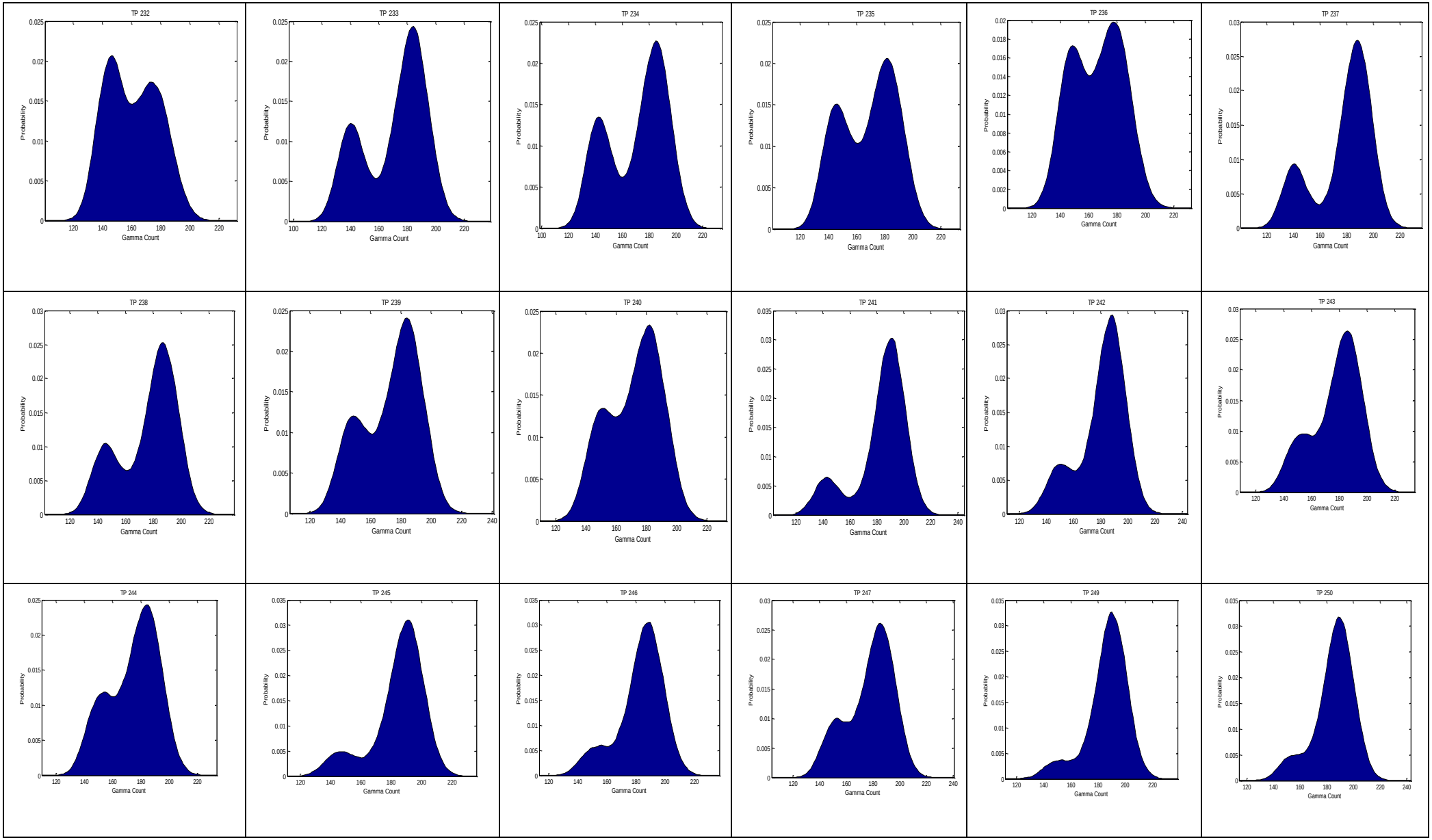
TP 232
TP 233
TP 234
TP 235
TP 236
TP 237
TP 238
TP 239
TP 240
TP 241
TP 242
TP 243
TP 244
TP 245
TP 246
TP 247
TP 249
TP 250
Probability
Gamma Count

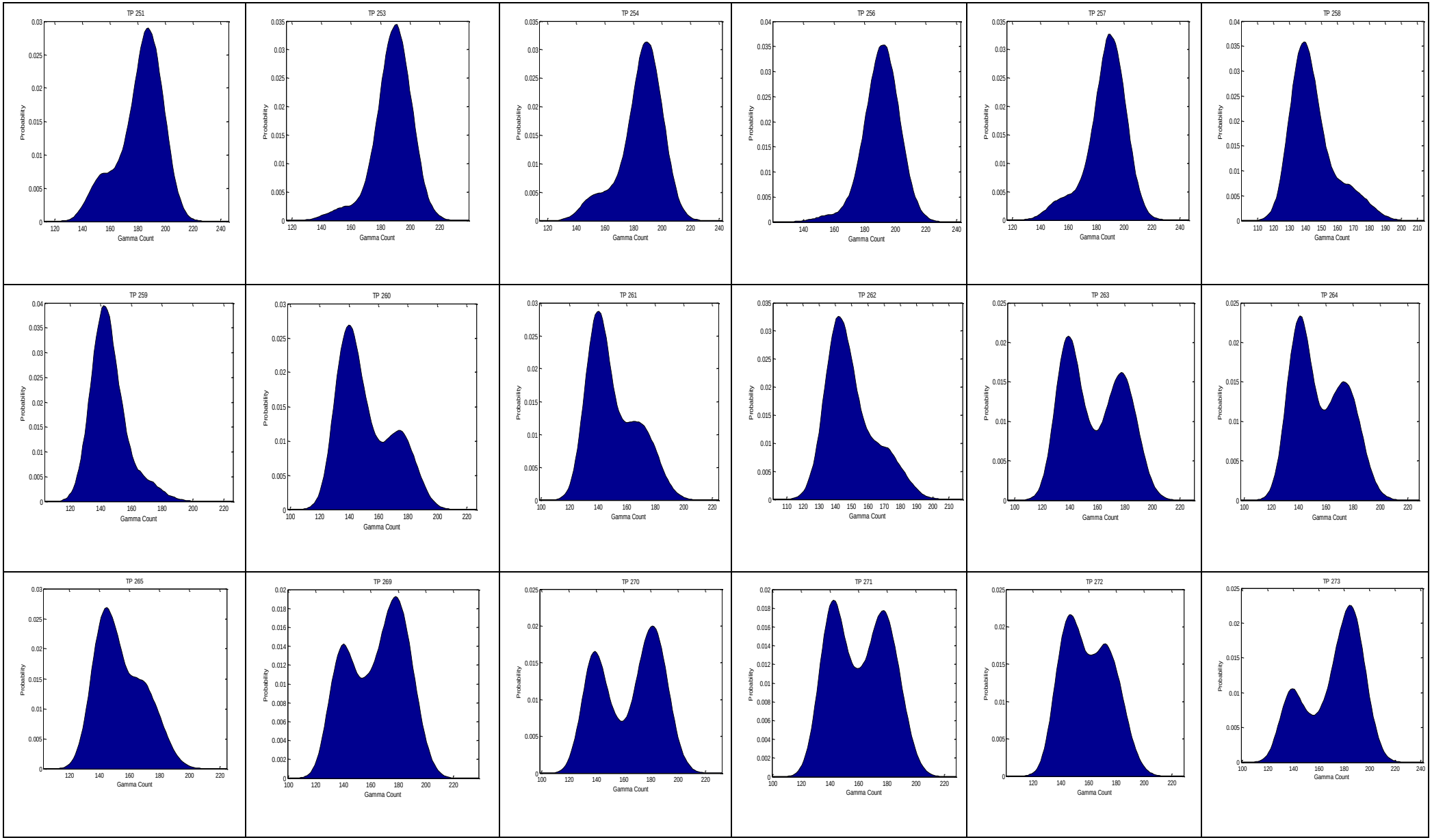
TP 251
TP 253
TP 254
TP 256
TP 257
TP 258
TP 259
TP 260
TP 261
TP 262
TP 263
TP 264
TP 265
TP 269
TP 270
TP 271
TP 272
TP 273
Probability
Gamma Count

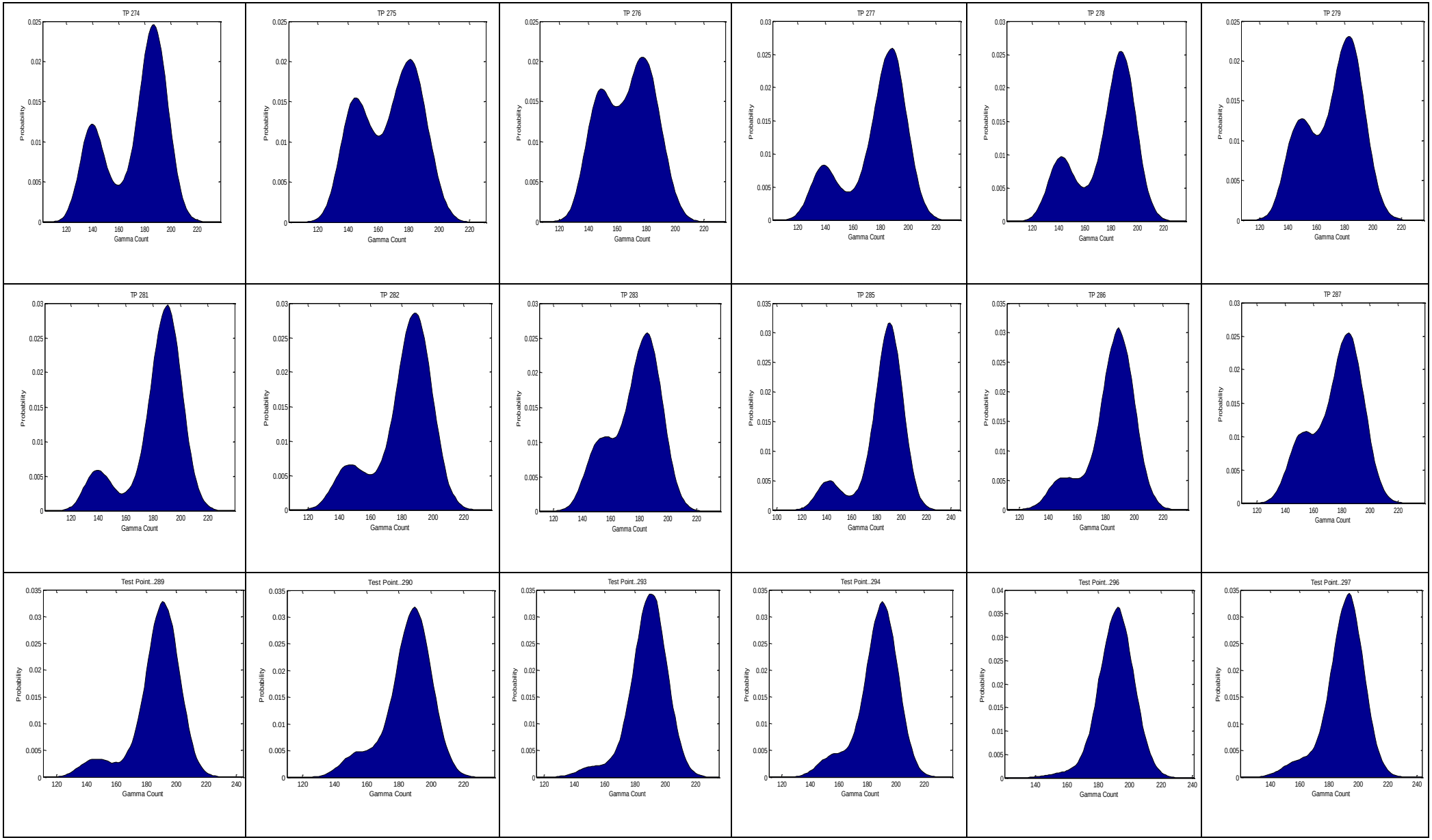
TP 274
TP 275
TP 276
TP 277
TP 278
TP 279
TP 281
TP 282
TP 283
TP 285
TP 286
TP 287
Test Point..289
Test Point..290
Test Point..293
Test Point..294
Test Point..296
Test Point..297
Probability
Gamma Count

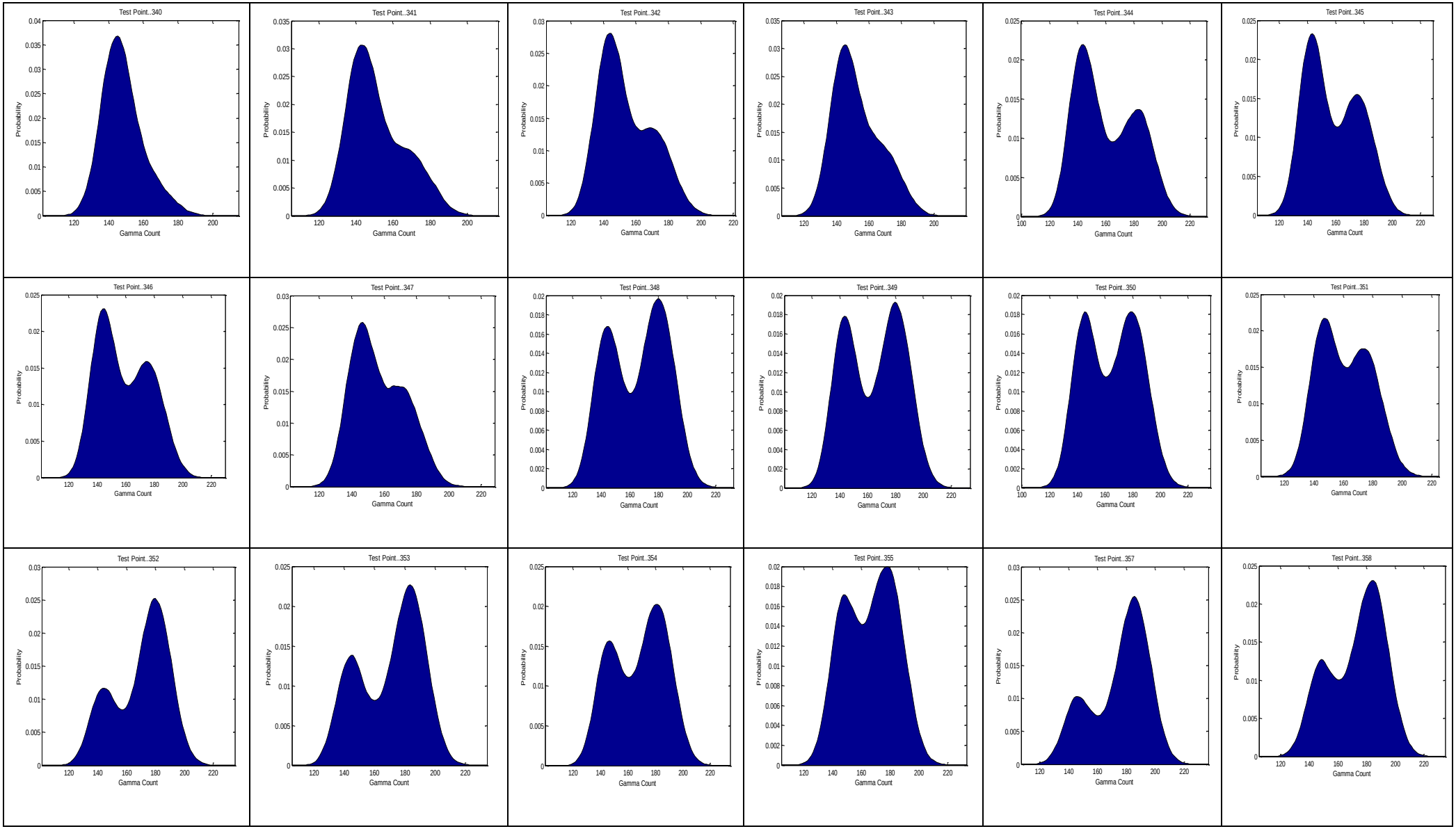
Test Point..340
Test Point..341
Test Point..342
Test Point..343
Test Point..344
Test Point..345
Test Point..346
Test Point..347
Test Point..348
Test Point..349
Test Point..350
Test Point..351
Test Point..352
Test Point..353
Test Point..354
Test Point..355
Test Point..357
Test Point..358
Probability
Gamma Count

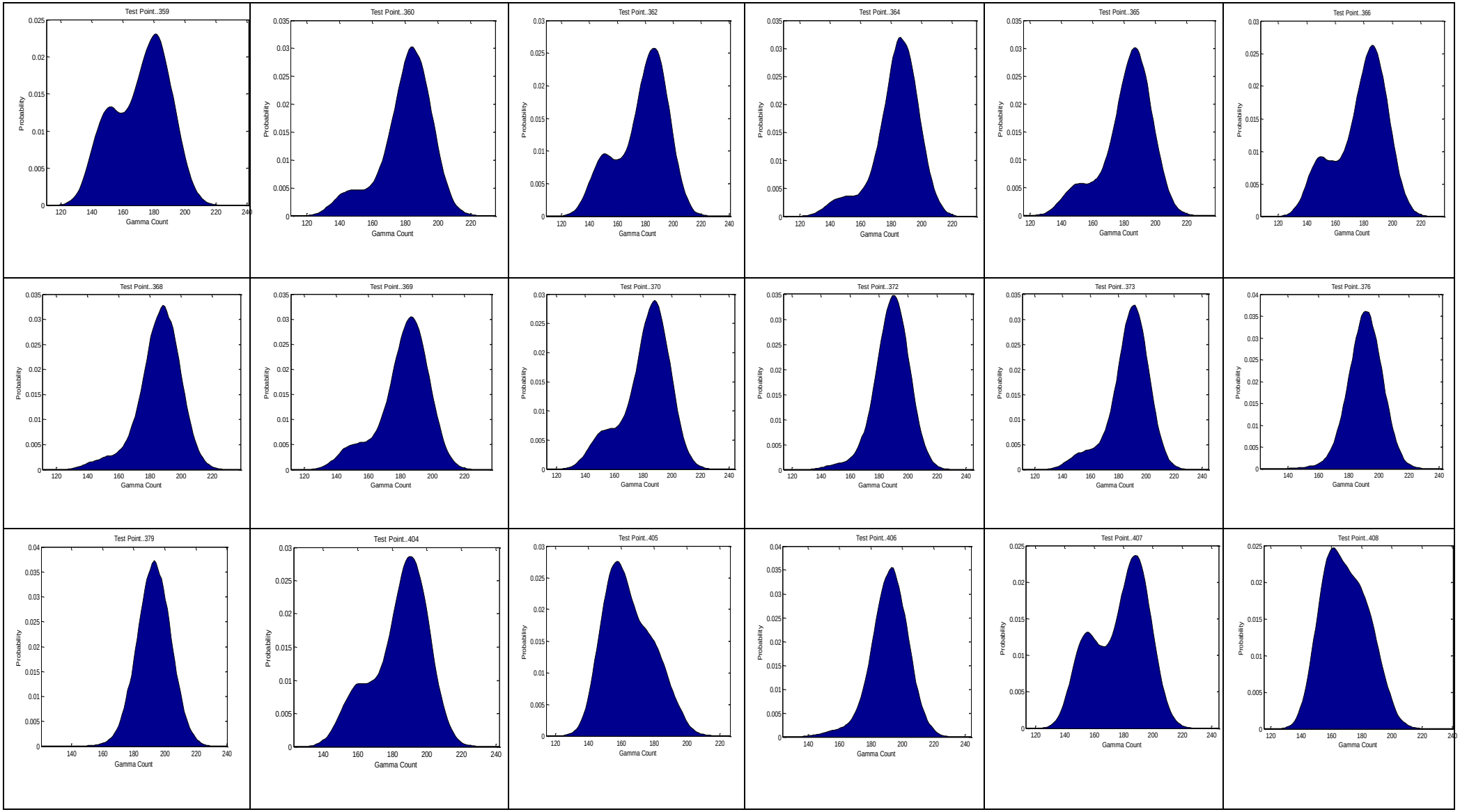
Test Point...359
Test Point...360
Test Point...362
Test Point...364
Test Point...365
Test Point...366
Test Point...368
Test Point...369
Test Point...370
Test Point...372
Test Point...373
Test Point...376
Test Point...379
Test Point...404
Test Point...405
Test Point...406
Test Point...407
Test Point...408
Probability
Gamma Count

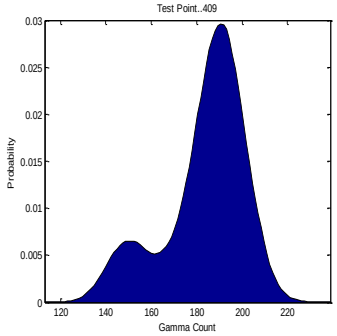

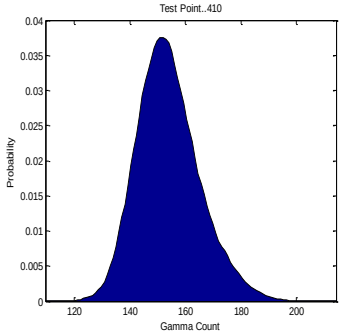

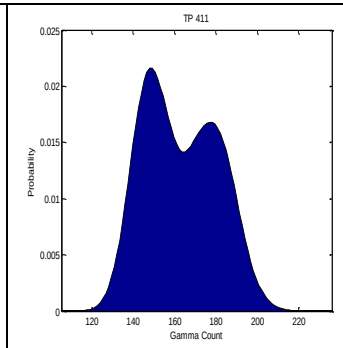

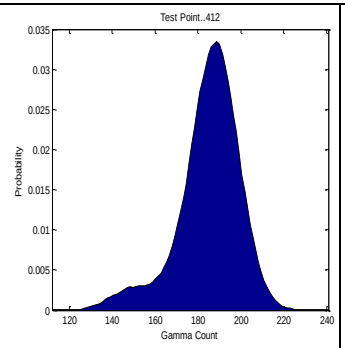

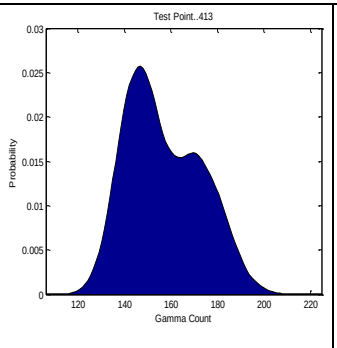

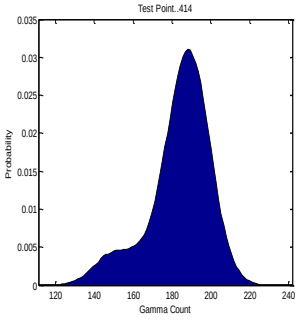

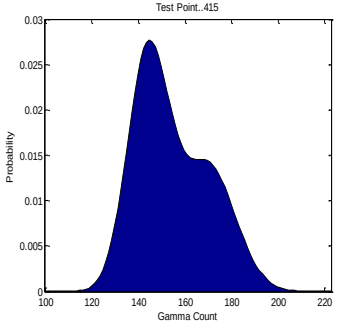

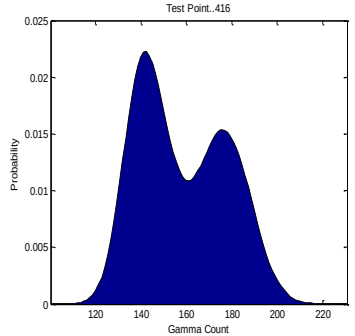

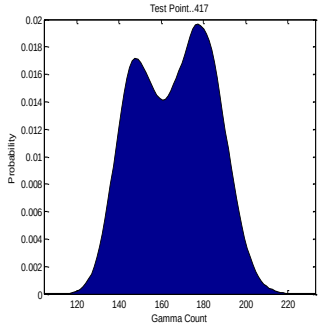

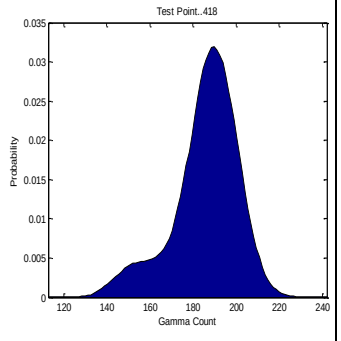

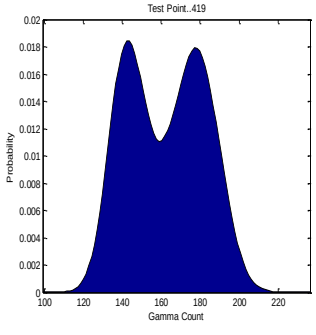

THIS SPACE IS INTENTIONAL LEFT BLANK

D.2 Table E.2 PMFs plots for the air-oil-water flow generated from the vertical gamma densitometer data of the 50.8mm test rig

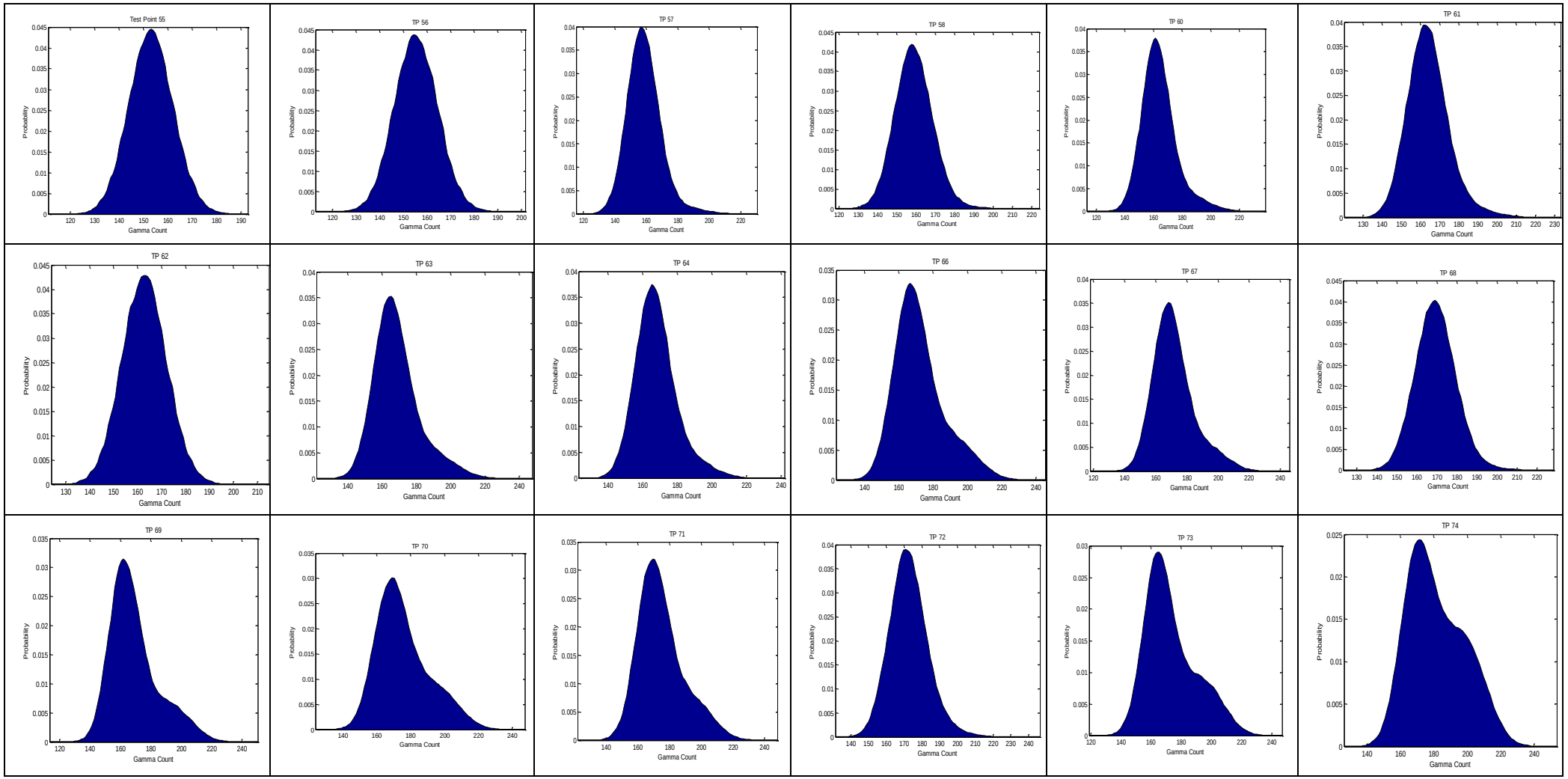

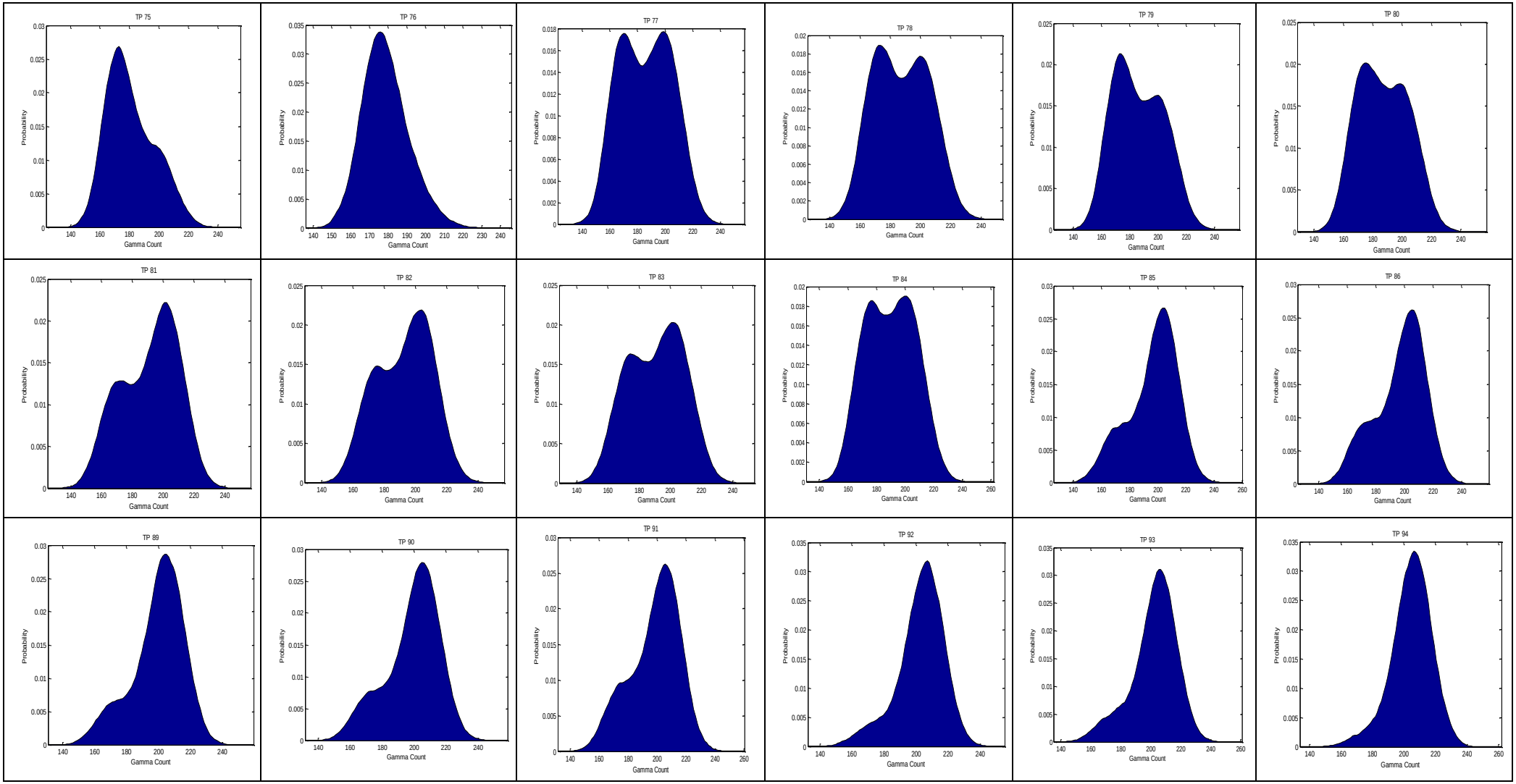
TP 75
TP 76
TP 77
TP 78
TP 79
TP 80
TP 81
TP 82
TP 83
TP 84
TP 85
TP 86
TP 89
TP 90
TP 91
TP 92
TP 93
TP 94
Probability
Gamma Count

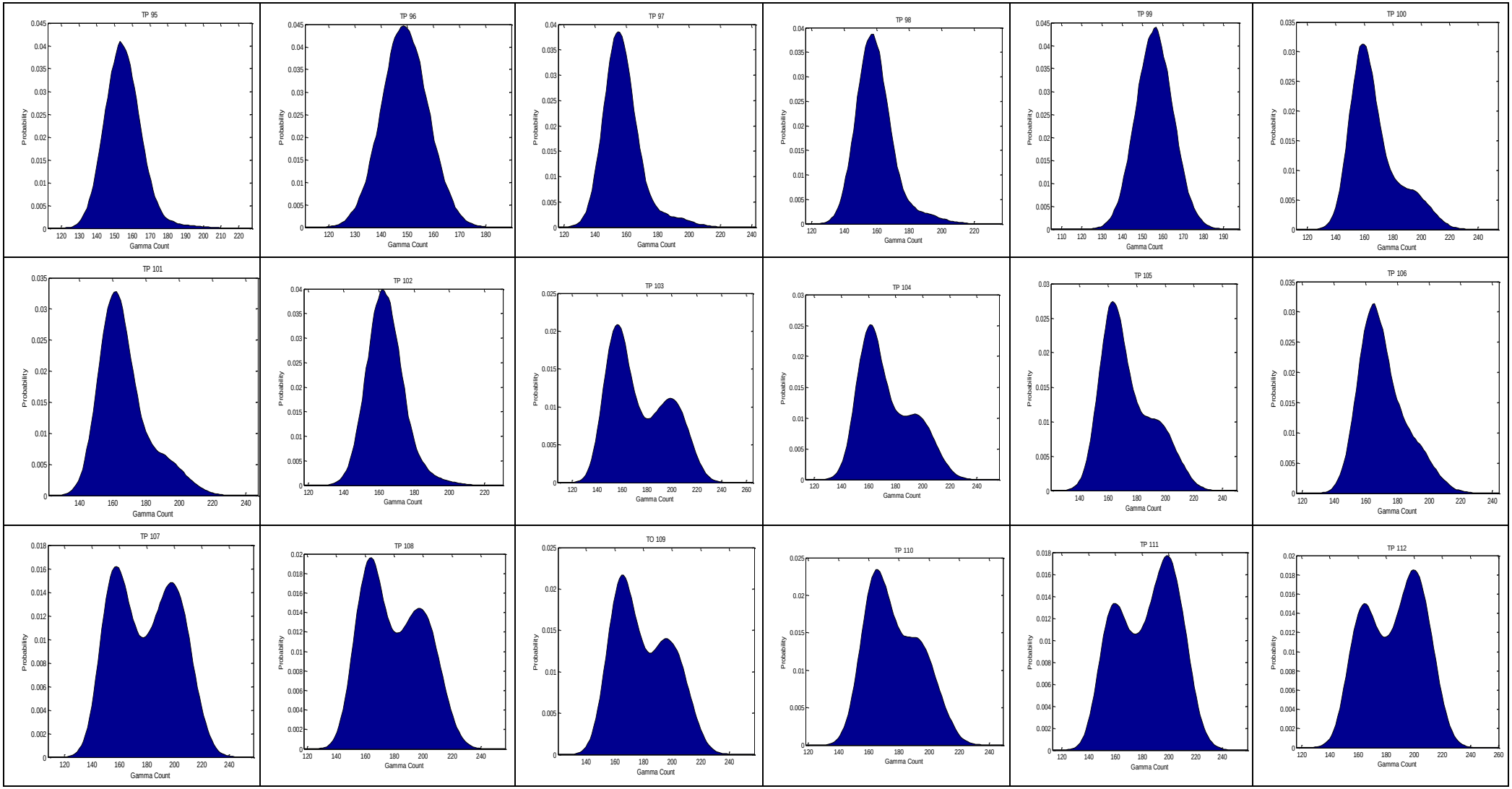
TP 95
TP 96
TP 97
TP 98
TP 99
TP 100
TP 101
TP 102
TP 103
TP 104
TP 105
TP 106
TP 107
TP 108
TO 109
TP 110
TP 111
TP 112
Probability
Gamma Count

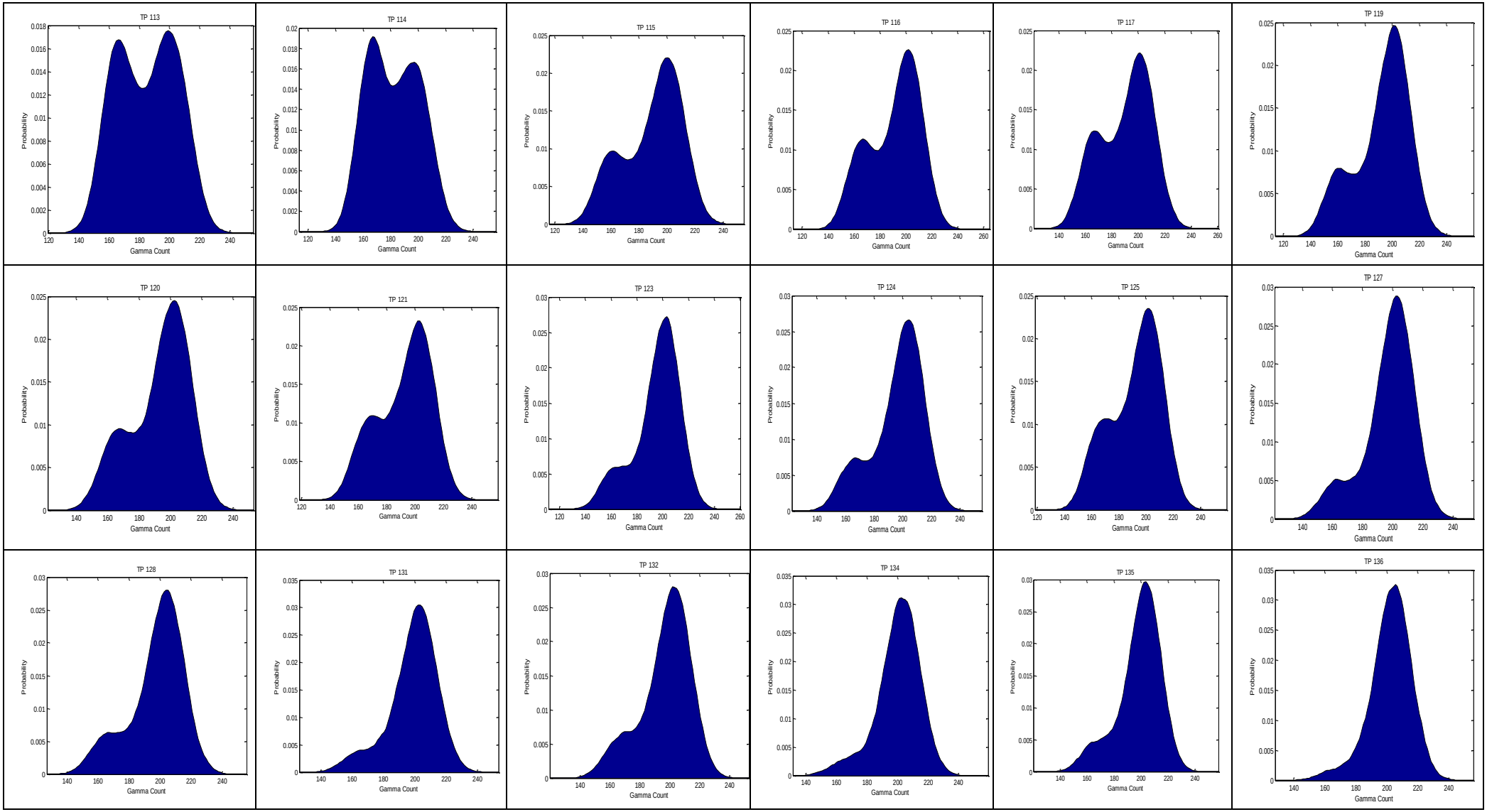
TP 113
TP 114
TP 115
TP 116
TP 117
TP 119
TP 120
TP 121
TP 123
TP 124
TP 125
TP 127
TP 128
TP 131
TP 132
TP 134
TP 135
TP 136
Probability
Gamma Count

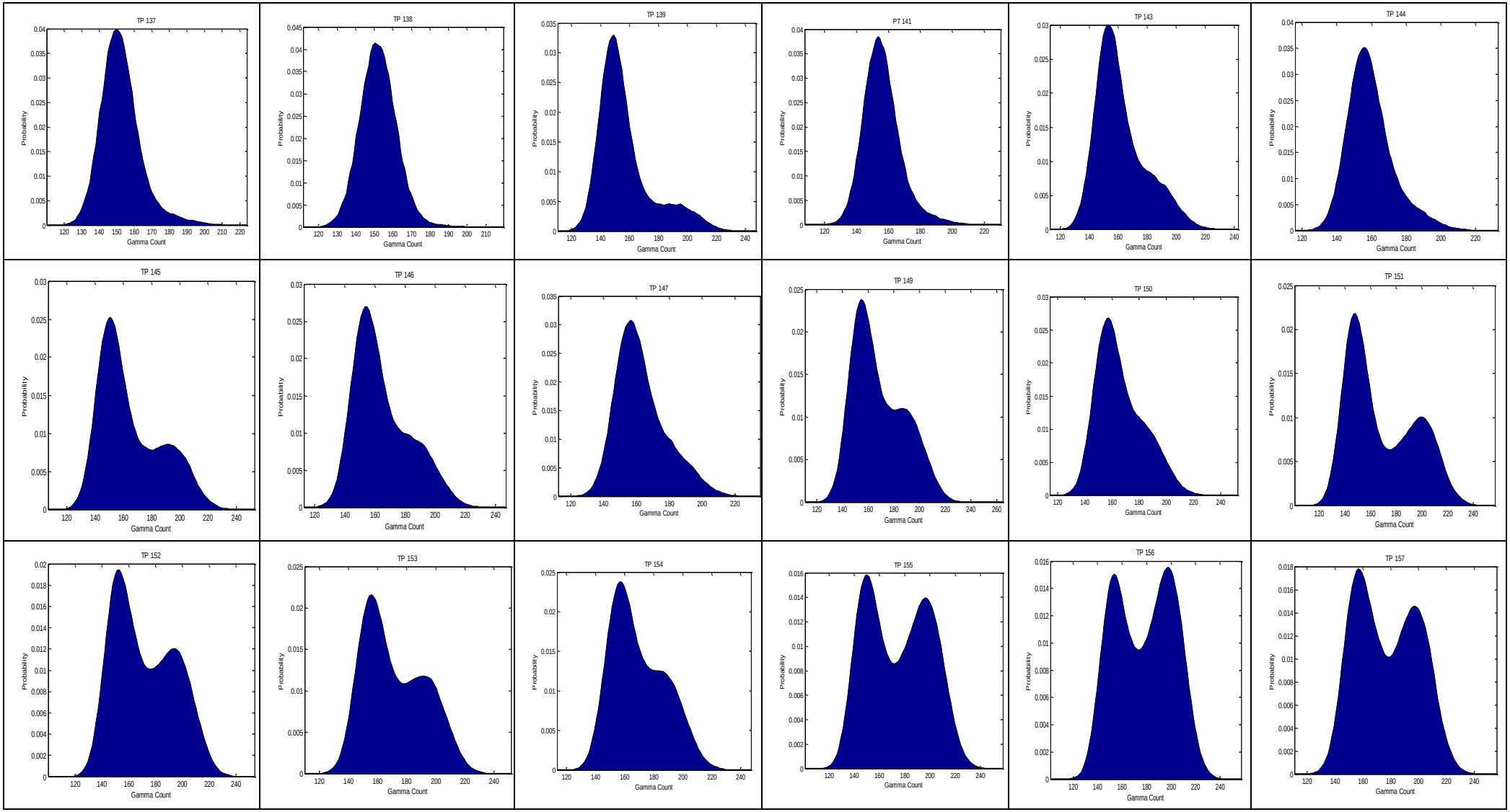
TP 137
TP 138
TP 139
PT 141
TP 143
TP 144
TP 145
TP 146
TP 147
TP 149
TP 150
TP 151
TP 152
TP 153
TP 154
TP 155
TP 156
TP 157
Probability
Gamma Count

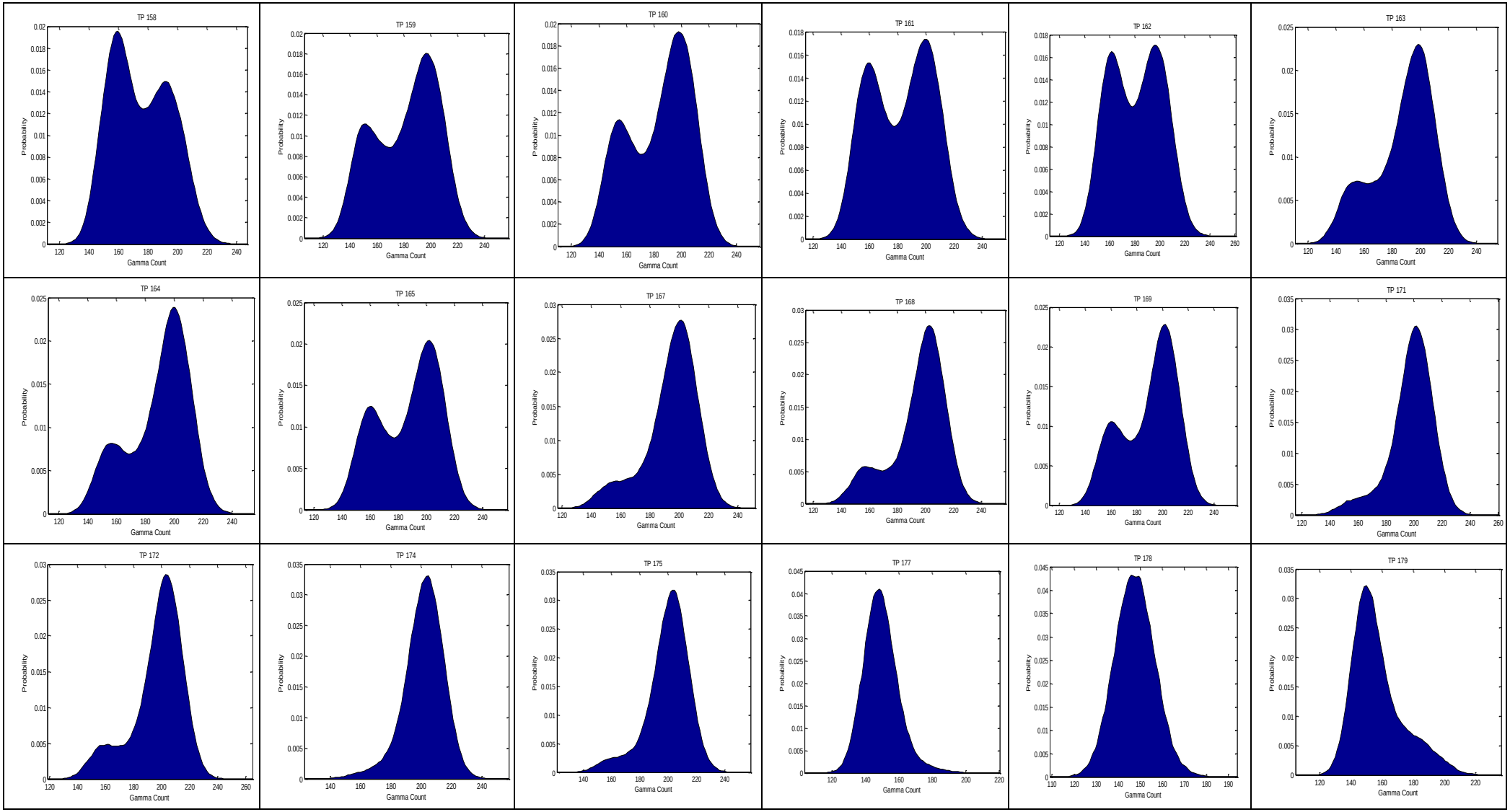
TP 158
TP 159
TP 160
TP 161
TP 162
TP 163
TP 164
TP 165
TP 167
TP 168
TP 169
TP 171
TP 172
TP 174
TP 175
TP 177
TP 178
TP 179
Probability
Gamma Count

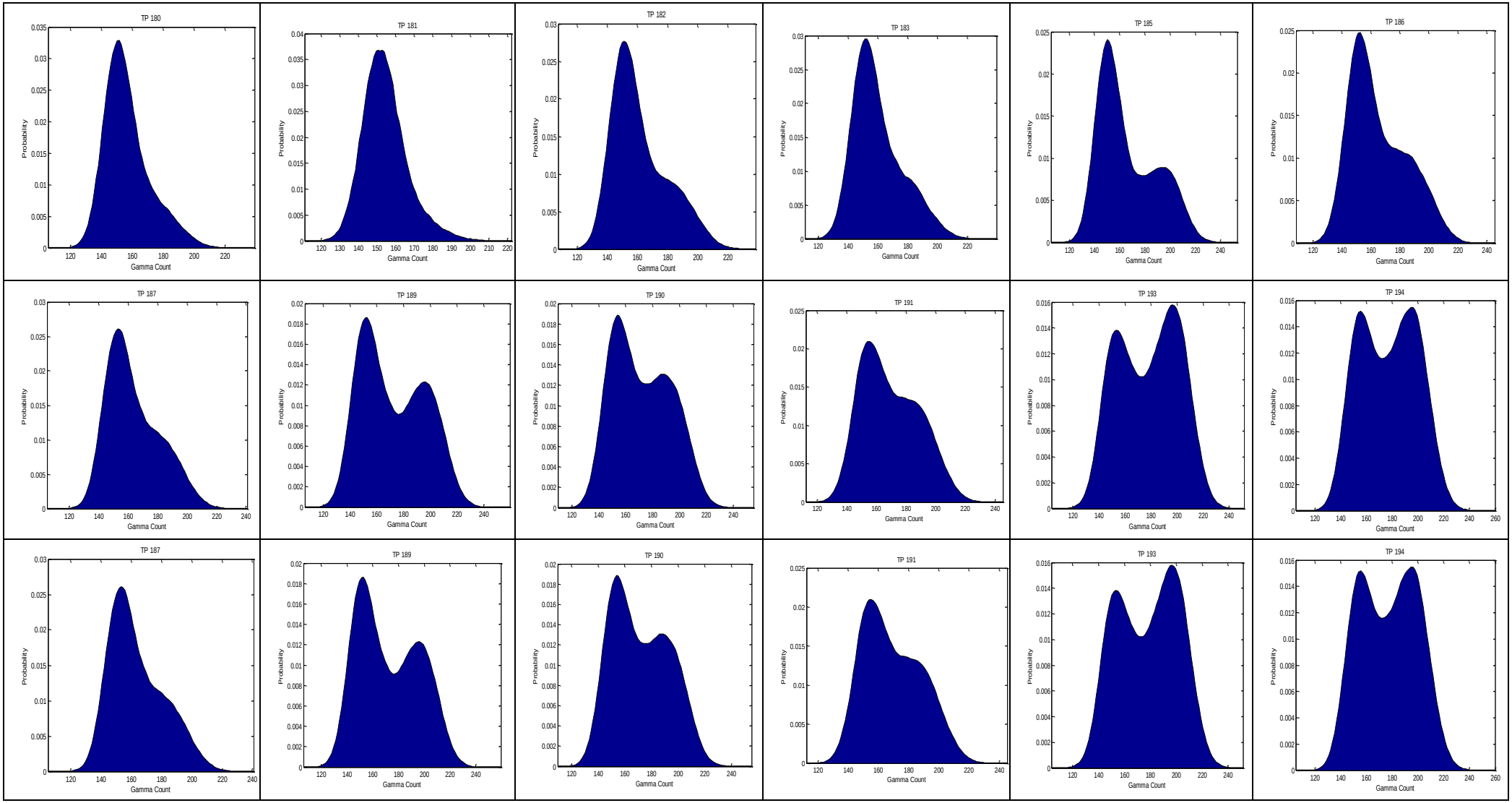
TP 180
TP 181
TP 182
TP 183
TP 185
TP 186
TP 187
TP 189
TP 190
TP 191
TP 193
TP 194
TP 187
TP 189
TP 190
TP 191
TP 193
TP 194
Probability
Gamma Count

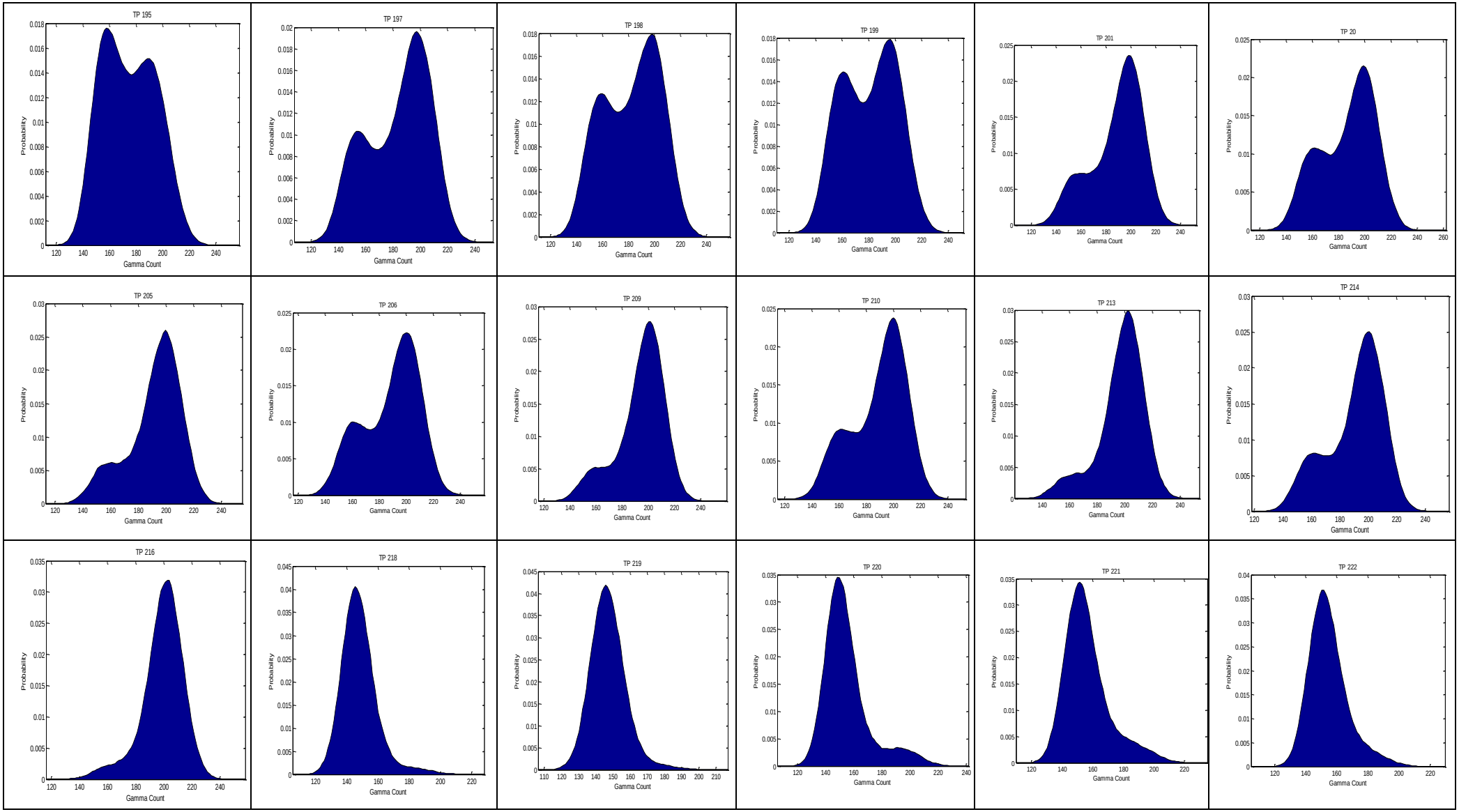
TP 195
TP 197
TP 198
TP 199
TP 201
TP 20
TP 205
TP 206
TP 209
TP 210
TP 213
TP 214
TP 216
TP 218
TP 219
TP 220
TP 221
TP 222
Probability
Gamma Count

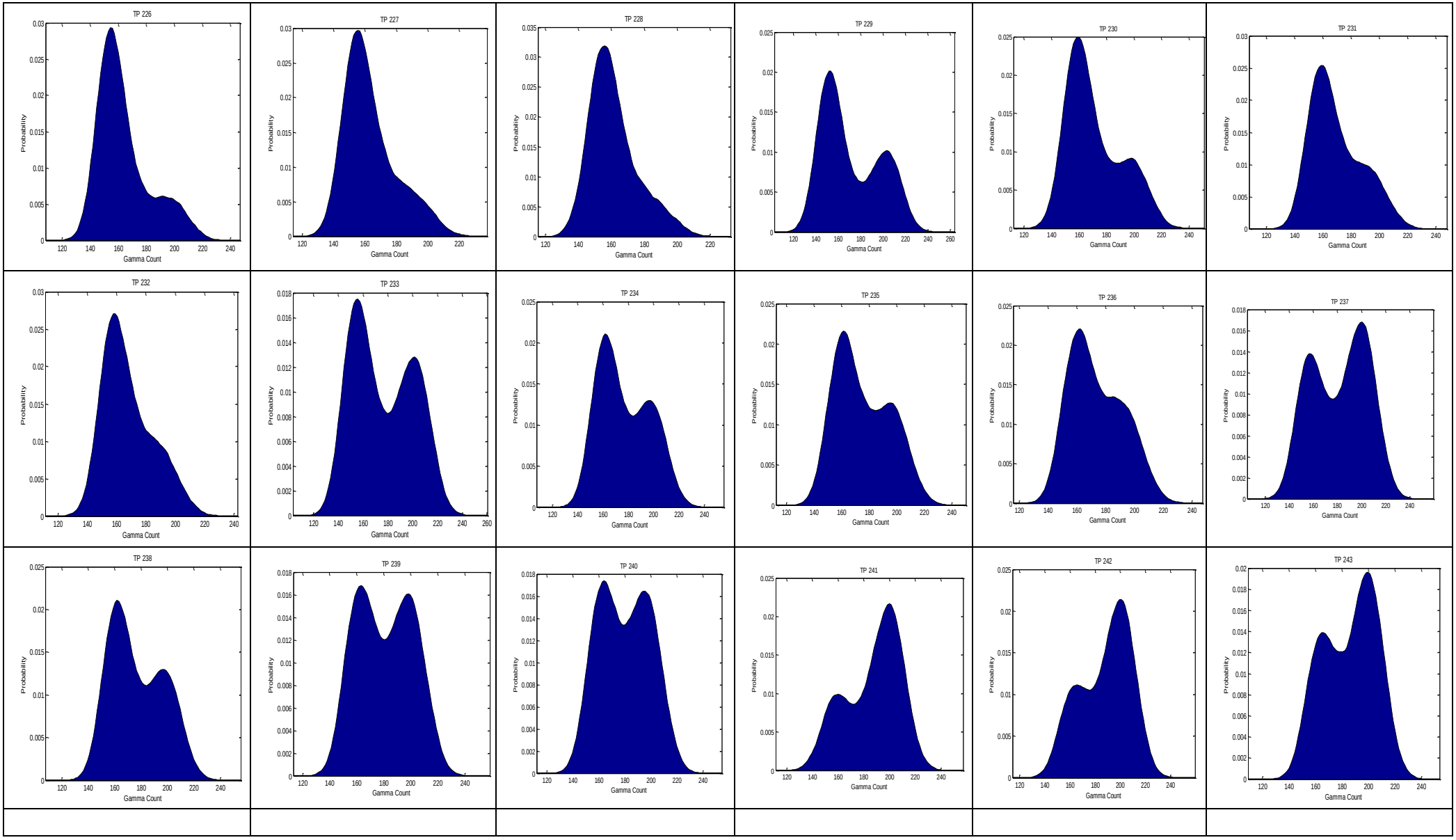
TP 226
TP 227
TP 228
TP 229
TP 230
TP 231
TP 232
TP 233
TP 234
TP 235
TP 236
TP 237
TP 238
TP 239
TP 240
TP 241
TP 242
TP 243
Probability
Gamma Count

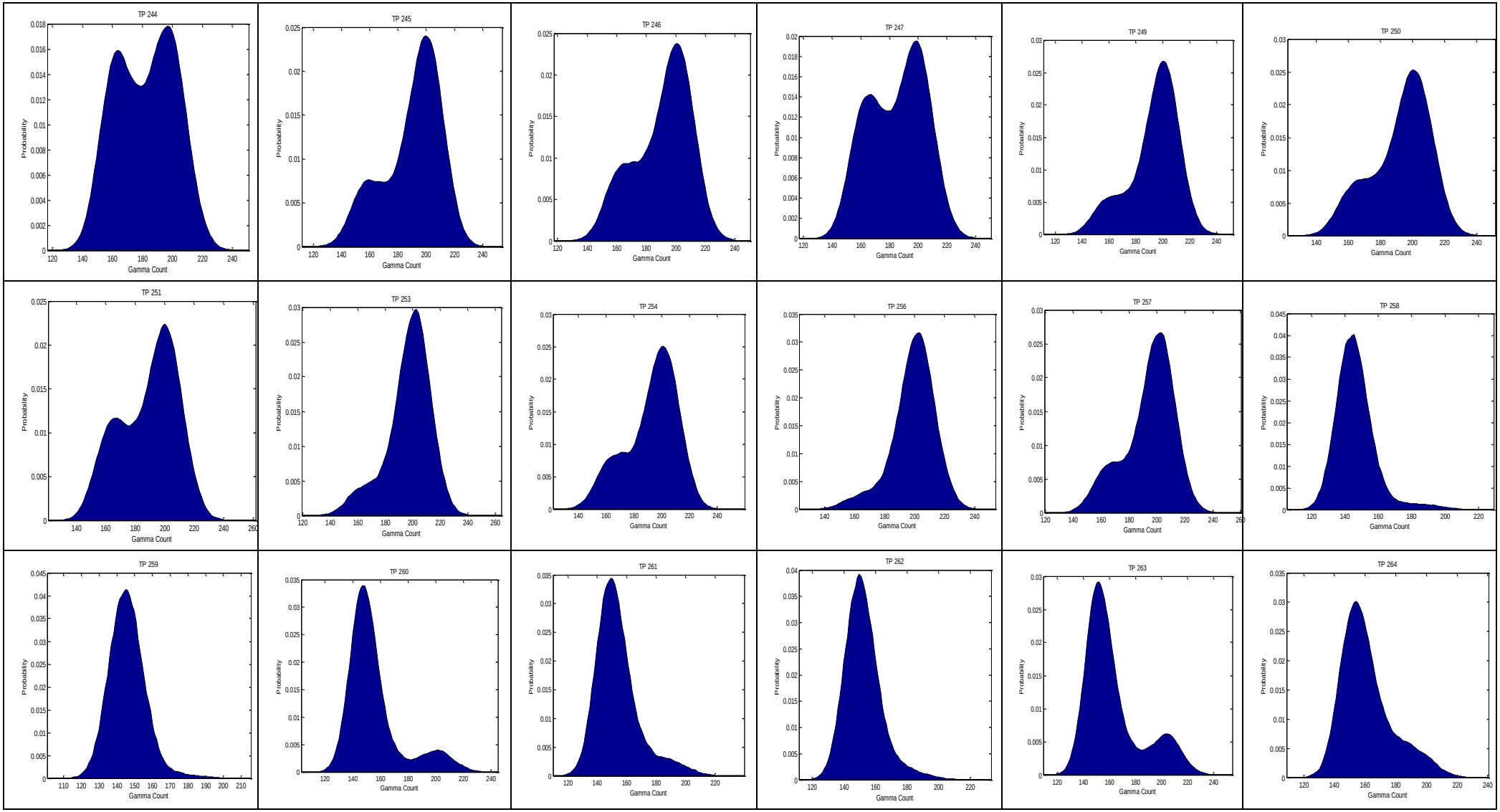
TP 244
TP 245
TP 246
TP 247
TP 249
TP 250
TP 251
TP 253
TP 254
TP 256
TP 257
TP 258
TP 259
TP 260
TP 261
TP 262
TP 263
TP 264
Probability
Gamma Count

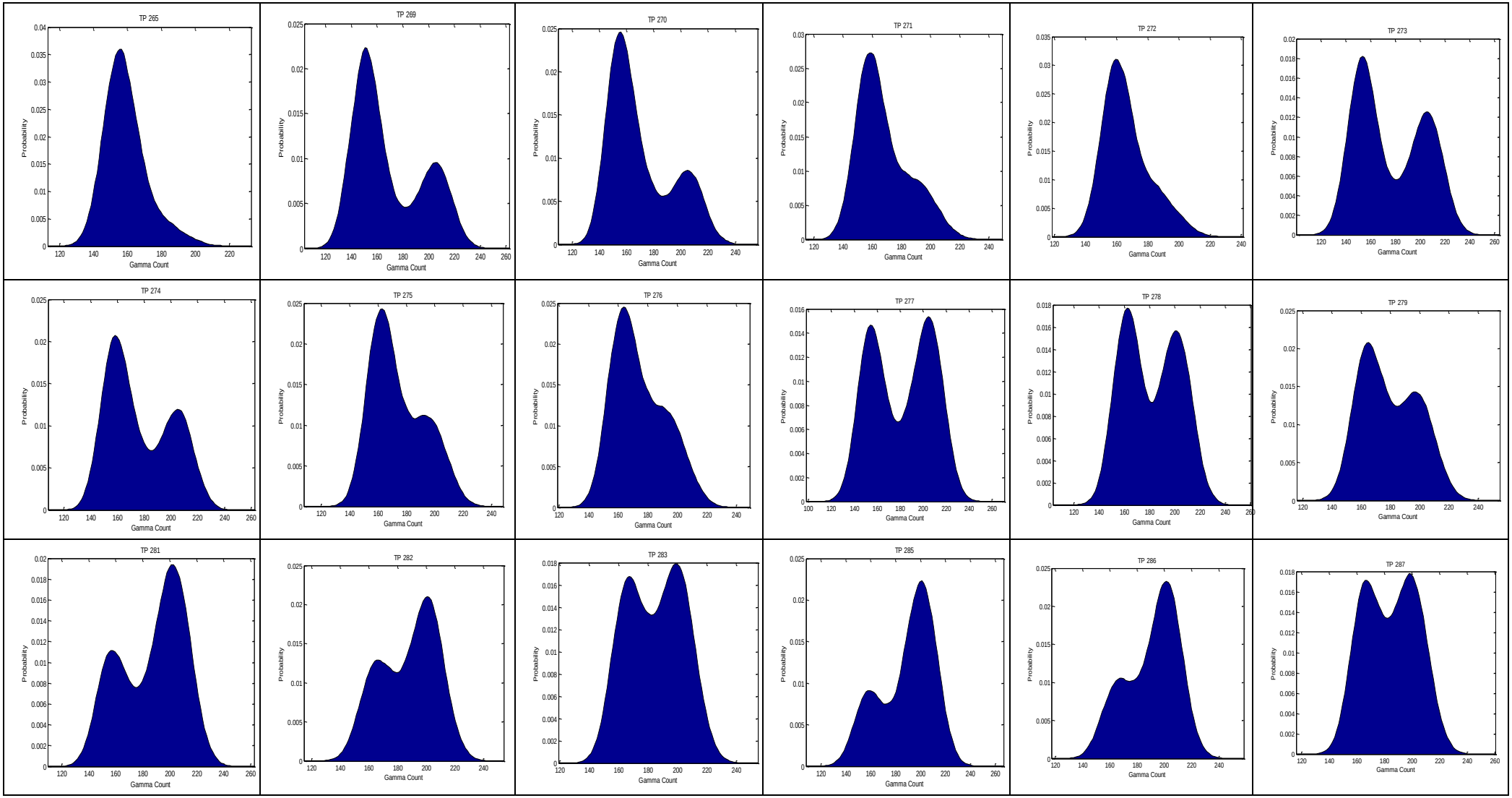
TP 265
TP 269
TP 270
TP 271
TP 272
TP 273
TP 274
TP 275
TP 276
TP 277
TP 278
TP 279
TP 281
TP 282
TP 283
TP 285
TP 286
TP 287
Probability
Gamma Count

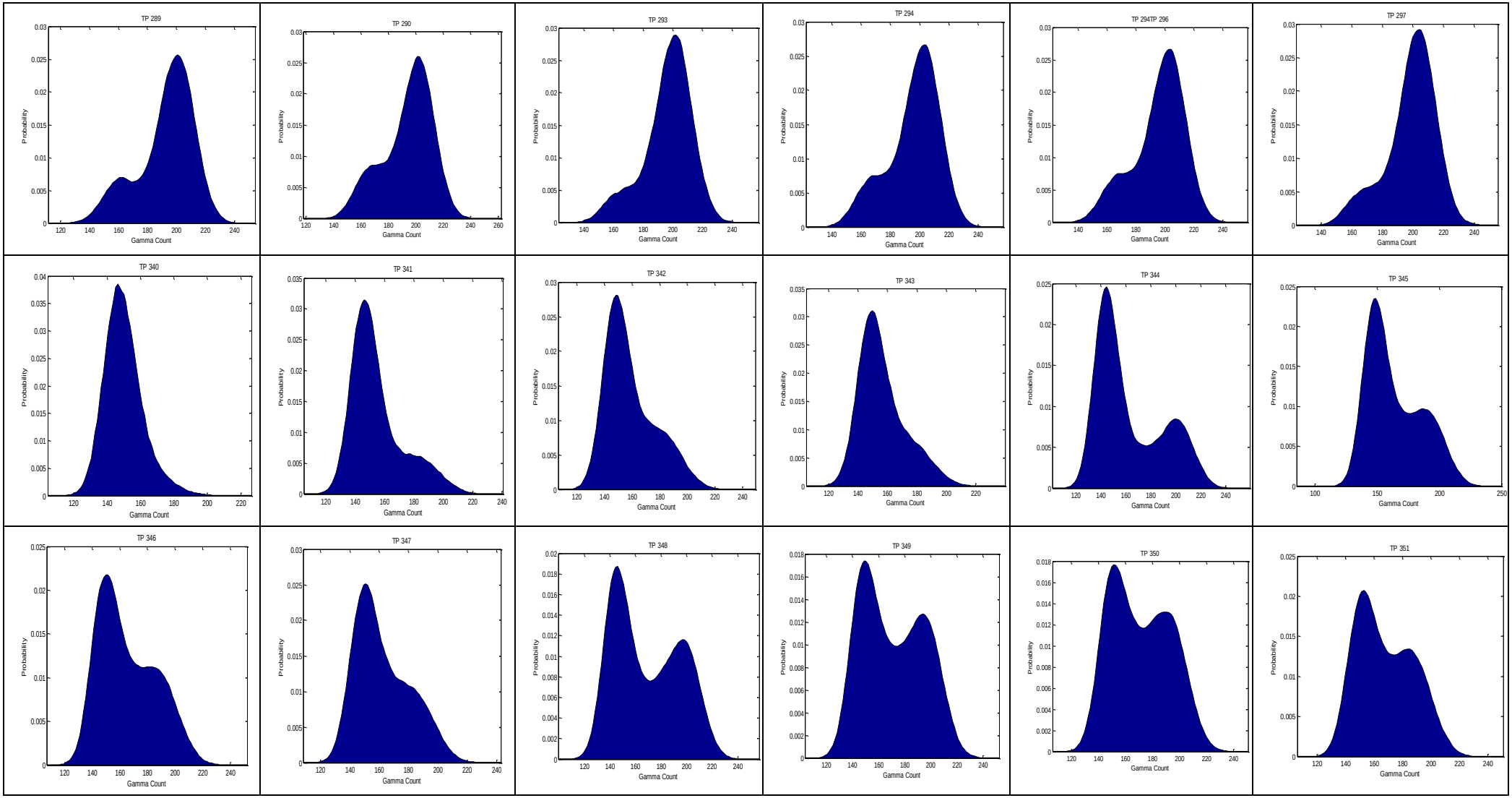
TP 289
TP 290
TP 293
TP 294
TP 294TP 296
TP 297
TP 340
TP 341
TP 342
TP 343
TP 344
TP 345
TP 346
TP 347
TP 348
TP 349
TP 350
TP 351
Probability
Gamma Count

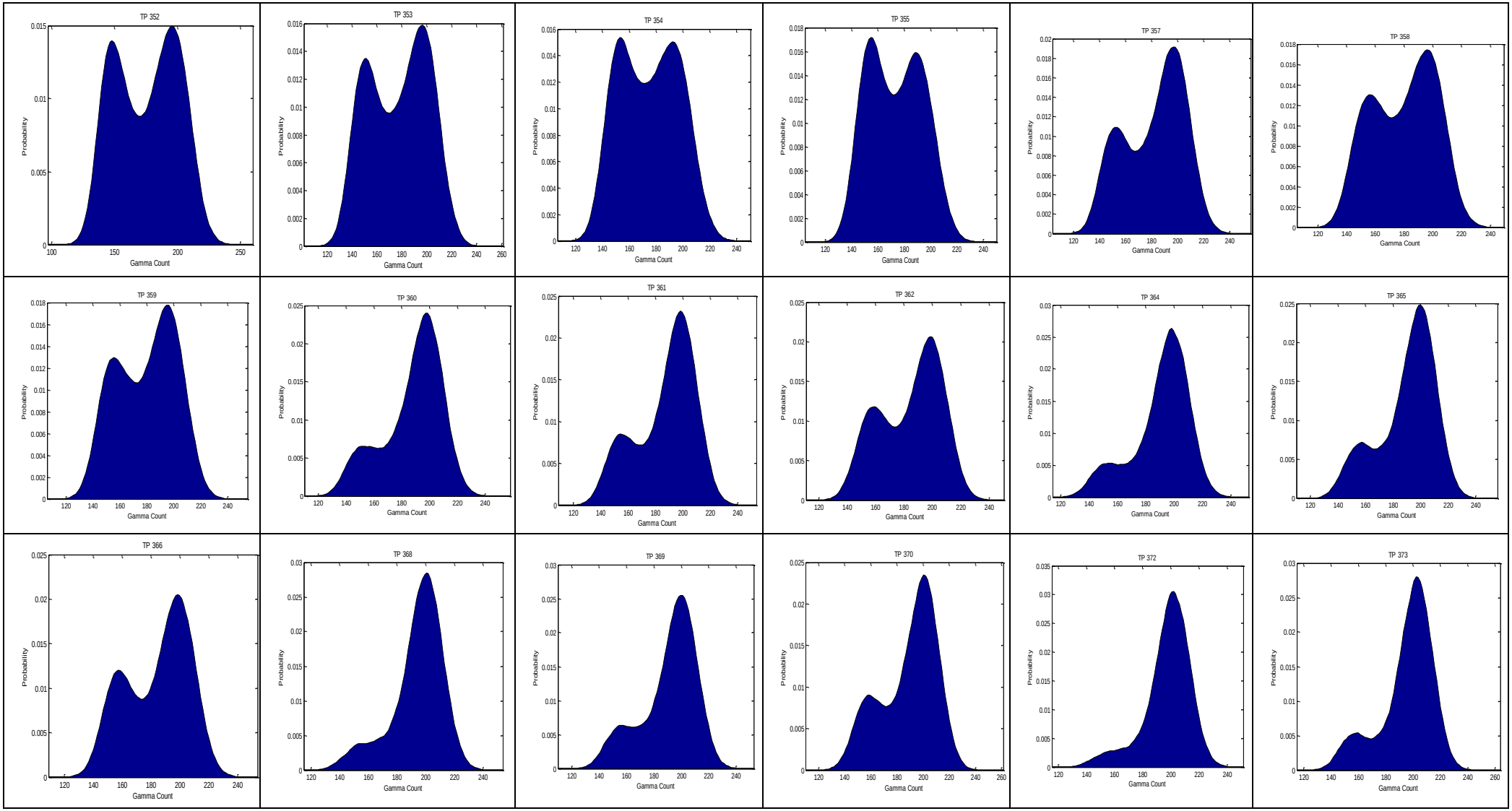
TP 352
TP 353
TP 354
TP 355
TP 357
TP 358
TP 359
TP 360
TP 361
TP 362
TP 364
TP 365
TP 366
TP 368
TP 369
TP 370
TP 372
TP 373
Probability
Gamma Count

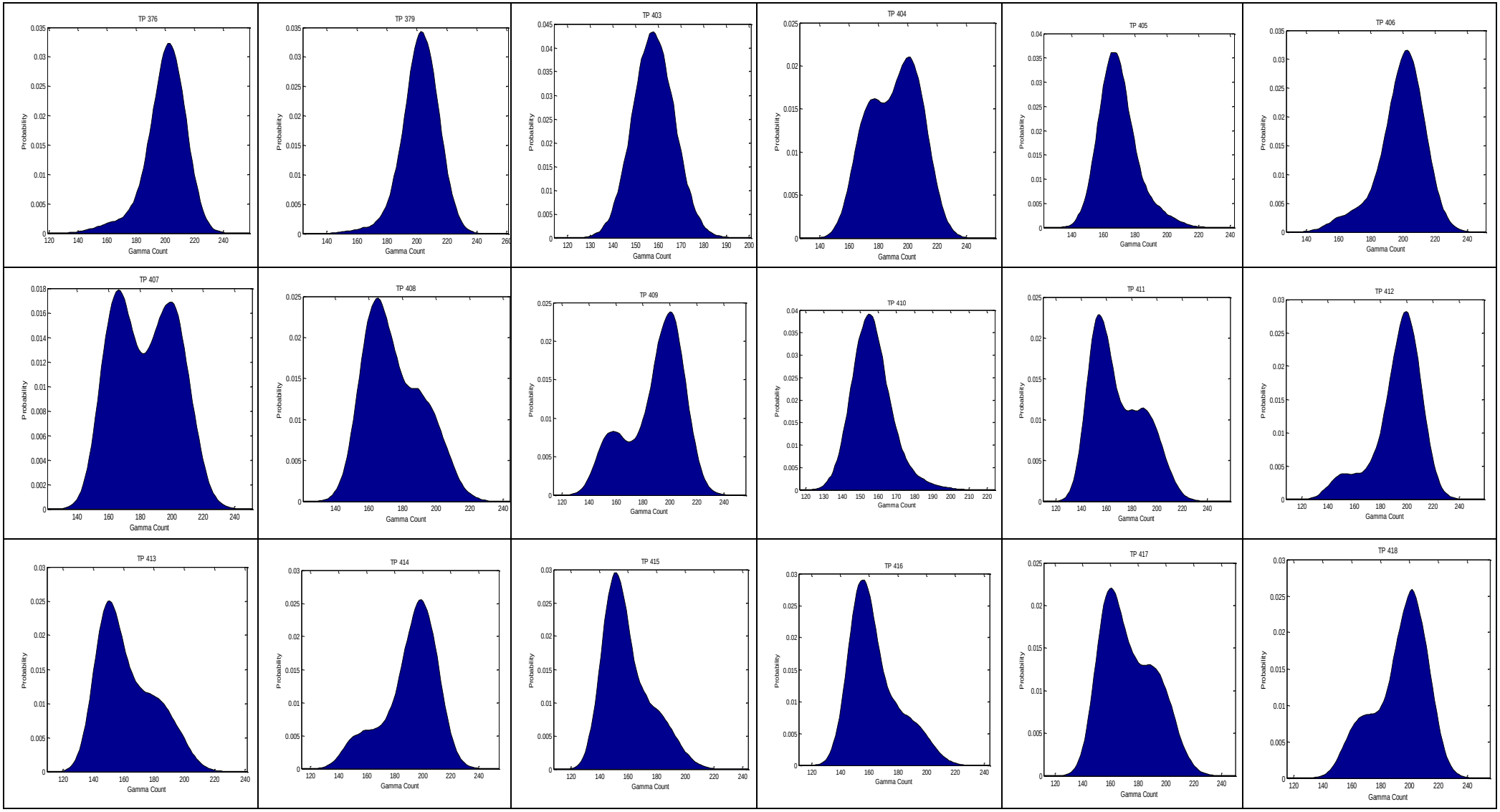
TP 376
TP 379
TP 403
TP 404
TP 405
TP 406
TP 407
TP 408
TP 409
TP 410
TP 411
TP 412
TP 413
TP 414
TP 415
TP 416
TP 417
TP 418
Probability
Gamma Count

Appendix E Test Data Points

E.1 Table F.1 documents the experimental conditions for the air-oil-water three phase tests from the 50.8mm test rig

Test Point	T_{base}	Q_{MA}	Q_{MW}	Q_{MO}	Q_{total}	GVF	Watercut	U_{sl} (Oil)	U_{sg}	U_{sl} (water)	P_{top}	P_{base}
	˚C	Sm3/hr	kg/s	kg/s	kg/s	%	%	m/s	m/s	m/s	barg	barg
1a	17.812	300.362	0.000	0.000	0.000	100.000	0.000	0.000	37.613	0.000		
2a	17.691	100.150	0.000	0.000	0.000	100.000	0.000	0.000	12.996	0.000		
3 a	18.406	199.798	0.000	0.000	0.000	100.000	0.000	0.000	25.281	0.000		
4a	18.716	0.000	0.000	1.002	1.002	0.000	0.000	0.609	0.000	0.000		
4b	23.838	5.993	0.000	3.998	3.998	14.134	0.000	2.438	0.401	0.000		
5a	18.443	0.000	0.000	2.002	2.002	0.000	0.000	1.217	0.000	0.000		
6a	21.017	0.000	0.000	4.005	4.005	0.000	0.000	2.436	0.000	0.000		
8a	22.910	0.000	2.000	0.000	2.000	0.000	100.000	0.000	0.000	0.989		
9a	22.686	0.000	3.999	0.000	3.999	0.000	100.000	0.000	0.000	1.977		
10a	22.796	0.000	0.201	3.797	3.998	0.000	4.135	2.312	0.000	0.100		
10b	25.118	7.489	0.000	1.996	1.996	34.363	0.000	1.219	0.638	0.000		
11a	23.759	0.000	0.404	3.599	4.004	0.000	8.363	2.193	0.000	0.200		
12a	23.719	0.000	0.606	3.401	4.007	0.000	12.628	2.073	0.000	0.300		
13a	23.760	0.000	0.799	3.202	4.002	0.000	16.847	1.952	0.000	0.395		
14a	23.844	0.000	1.201	2.803	4.005	0.000	25.813	1.709	0.000	0.595		
14b	25.173	9.999	0.000	1.999	1.999	40.492	0.000	1.221	0.831	0.000		
15a	23.735	0.000	1.403	2.600	4.003	0.000	30.445	1.586	0.000	0.694		
16a	21.090	0.000	1.608	2.419	4.027	0.000	35.117	1.470	0.000	0.796		
17a	21.978	0.000	1.797	2.196	3.992	0.000	39.974	1.335	0.000	0.889		
18a	22.187	0.000	0.498	1.502	2.000	0.000	21.254	0.914	0.000	0.247		

19a	23.010	0.000	0.748	2.252	2.999	0.000	21.258	1.371	0.000	0.370		
20a	22.554	0.000	1.498	4.464	5.962	0.000	21.418	2.719	0.000	0.741		
21a	24.005	0.000	1.001	1.000	2.001	0.000	44.837	0.610	0.000	0.496		
22a	23.205	0.000	2.502	2.497	4.999	0.000	44.835	1.523	0.000	1.238		
22b	25.361	16.146	0.000	2.001	2.001	52.977	0.000	1.222	1.377	0.000		
23a	22.941	0.000	3.501	3.517	7.018	0.000	44.685	2.144	0.000	1.732		
24a	23.484	0.000	2.398	1.598	3.996	0.000	54.899	0.975	0.000	1.187		
25a	23.425	0.000	2.800	1.199	3.999	0.000	65.450	0.731	0.000	1.386		
25a	25.065	10.012	0.000	0.999	0.999	60.141	0.000	0.610	0.920	0.000		
26a	25.471	19.967	0.000	1.998	1.998	58.431	0.000	1.221	1.716	0.000		
27a	23.552	0.000	3.003	1.001	4.004	0.000	70.873	0.611	0.000	1.486		
28a	23.496	0.000	4.801	1.200	6.001	0.000	76.448	0.732	0.000	2.377		
29a	23.721	0.000	5.950	1.049	6.999	0.000	82.141	0.640	0.000	2.946		
29b	25.287	15.025	0.000	0.999	0.999	70.339	0.000	0.610	1.447	0.000		
30a	23.803	0.000	7.483	0.995	8.478	0.000	85.907	0.608	0.000	3.703		
30b	25.586	29.976	0.000	1.999	1.999	67.995	0.000	1.221	2.593	0.000		
33a	25.336	22.621	0.000	1.000	1.000	78.540	0.000	0.611	2.235	0.000		
34a	25.621	44.926	0.000	2.002	2.002	75.926	0.000	1.223	3.856	0.000		
37a	25.321	35.094	0.000	1.000	1.000	85.269	0.000	0.611	3.535	0.000		
38a	25.699	69.814	0.000	1.999	1.999	82.563	0.000	1.221	5.782	0.000		
41a	25.400	60.313	0.000	0.999	0.999	90.925	0.000	0.610	6.114	0.000		
42a	25.763	119.595	0.000	1.976	1.976	88.253	0.000	1.207	9.069	0.000		
45a	25.550	84.936	0.000	0.998	0.998	93.411	0.000	0.610	8.643	0.000		
48a	25.637	134.988	0.000	0.999	0.999	95.556	0.000	0.610	13.124	0.000		
52a	25.589	285.879	0.000	1.000	1.000	97.342	0.000	0.611	22.367	0.000		

1	20.380	100.003	0.000	0.000	0.000	100.000	#DIV/0!	0.000	13.345	0.000		
2	20.851	300.127	0.000	0.000	0.000	100.000	#DIV/0!	0.000	38.149	0.000		
3	20.673	200.290	0.000	0.000	0.000	100.000	#DIV/0!	0.000	25.932	0.000		
7	24.880	8.008	0.000	3.003	3.003	16.208	0.000	1.834	0.355	0.000	1.274	3.242
8	24.918	10.592	0.000	3.996	3.996	14.770	0.000	2.441	0.423	0.000	1.377	3.597
10	22.657	7.491	0.000	1.998	1.998	22.946	0.000	1.218	0.363	0.000	1.196	2.944
11	24.774	11.284	0.000	3.000	3.000	21.367	0.000	1.832	0.498	0.000	1.292	3.254
12	24.918	15.028	0.000	4.001	4.001	19.430	0.000	2.444	0.589	0.000	1.419	3.663
14	22.618	9.991	0.000	2.001	2.001	28.520	0.000	1.220	0.487	0.000	1.200	2.926
15	24.691	14.981	0.000	3.000	3.000	26.395	0.000	1.832	0.657	0.000	1.314	3.274
16	25.133	20.006	0.000	3.998	3.998	23.972	0.000	2.442	0.770	0.000	1.465	3.735
18	22.620	12.900	0.000	2.001	2.001	34.144	0.000	1.219	0.632	0.000	1.203	2.908
19	24.537	19.276	0.000	3.001	3.001	31.367	0.000	1.832	0.837	0.000	1.336	3.302
20	25.281	25.737	0.000	3.999	3.999	28.445	0.000	2.443	0.971	0.000	1.509	3.811
22	22.127	16.236	0.000	2.001	2.001	39.591	0.000	1.219	0.799	0.000	1.210	2.892
23	24.430	24.049	0.000	3.001	3.001	36.062	0.000	1.832	1.033	0.000	1.360	3.337
24	25.386	32.381	0.000	4.000	4.000	32.786	0.000	2.444	1.192	0.000	1.562	3.908
25	23.295	9.988	0.000	1.000	1.000	47.421	0.000	0.609	0.550	0.000	1.121	2.596
26	21.116	20.042	0.000	1.999	1.999	44.623	0.000	1.217	0.980	0.000	1.219	2.899
27	24.278	30.059	0.000	2.999	2.999	40.984	0.000	1.831	1.271	0.000	1.393	3.388
28	25.510	40.112	0.000	3.999	3.999	37.059	0.000	2.443	1.439	0.000	1.620	4.013
29	23.742	14.988	0.000	0.999	0.999	57.929	0.000	0.609	0.839	0.000	1.119	2.556
30	19.761	30.035	0.000	1.999	1.999	54.479	0.000	1.216	1.455	0.000	1.239	2.914
31	24.139	45.018	0.000	3.001	3.001	49.946	0.000	1.832	1.828	0.000	1.465	3.528
32	25.585	60.066	0.000	3.989	3.989	45.288	0.000	2.437	2.018	0.000	1.759	4.286
33	23.732	22.540	0.000	0.998	0.998	68.783	0.000	0.608	1.340	0.000	1.121	2.406
34	26.058	45.027	0.000	2.000	2.000	64.574	0.000	1.222	2.228	0.000	1.203	2.914
35	23.989	68.118	0.000	3.001	3.001	58.498	0.000	1.831	2.581	0.000	1.575	3.779

36	25.727	89.833	0.000	3.932	3.932	53.716	0.000	2.403	2.789	0.000	1.940	4.639
37	23.759	34.996	0.000	0.997	0.997	76.550	0.000	0.608	1.985	0.000	1.134	2.523
38	25.946	70.104	0.000	1.998	1.998	72.846	0.000	1.220	3.274	0.000	1.284	3.086
39	23.810	104.910	0.000	3.000	3.000	66.321	0.000	1.831	3.605	0.000	1.765	4.164
40	25.915	140.058	0.000	3.515	3.515	65.557	0.000	2.148	4.089	0.000	2.114	4.937
41	23.773	60.079	0.000	0.998	0.998	84.543	0.000	0.609	3.330	0.000	1.167	2.582
42	25.763	119.773	0.000	2.002	2.002	80.141	0.000	1.223	4.935	0.000	1.465	3.496
43	23.621	179.692	0.000	3.033	3.033	74.963	0.000	1.851	5.542	0.000	1.992	4.637
44	26.036	239.587	0.000	2.884	2.884	79.509	0.000	1.763	6.841	0.000	2.238	5.049
45	23.812	85.174	0.000	1.002	1.002	89.224	0.000	0.612	5.063	0.000	1.205	2.407
46	23.520	169.807	0.000	1.999	1.999	84.161	0.000	1.219	6.478	0.000	1.633	3.747
48	23.843	135.433	0.000	1.001	1.001	91.667	0.000	0.611	6.719	0.000	1.298	2.885
49	23.377	271.064	0.000	1.999	1.999	87.696	0.000	1.220	8.692	0.000	2.003	4.456
52	23.846	286.070	0.000	1.001	1.001	94.940	0.000	0.610	11.454	0.000	1.639	3.574
55	20.728	7.796	0.300	2.703	3.003	32.698	8.297	1.644	0.871	0.149	1.268	3.263
56	24.953	12.985	0.501	4.500	5.001	28.629	8.268	2.749	1.202	0.248	1.552	4.124
57	24.071	7.290	0.198	1.803	2.001	43.087	8.170	1.101	0.908	0.098	1.150	2.931
58	21.871	11.020	0.297	2.692	2.989	39.984	8.250	1.638	1.189	0.147	1.318	3.217
60	23.709	9.793	0.201	1.804	2.005	49.104	8.283	1.101	1.158	0.099	1.210	2.945
61	22.433	14.727	0.300	2.701	3.002	46.957	8.288	1.644	1.587	0.149	1.322	3.249
62	24.793	24.543	0.498	4.500	4.998	41.160	8.234	2.746	2.093	0.246	1.683	4.317
63	24.164	12.640	0.199	1.802	2.000	55.677	8.213	1.099	1.504	0.098	1.204	2.895
64	22.863	18.925	0.299	2.700	2.999	59.618	8.273	1.643	2.645	0.148	1.020	3.275
66	24.539	15.848	0.200	1.800	2.000	61.073	8.266	1.098	1.878	0.099	1.210	2.889
67	23.135	23.822	0.302	2.701	3.003	58.163	8.322	1.645	2.495	0.149	1.363	3.318
68	24.729	39.612	0.503	4.500	5.003	50.892	8.310	2.746	3.104	0.249	1.832	4.579
69	17.304	9.995	0.150	1.355	1.505	59.374	8.303	0.821	1.309	0.074	1.068	2.736
70	24.693	19.637	0.200	1.799	1.999	65.906	8.259	1.098	2.313	0.099	1.218	2.875

71	23.349	29.312	0.299	2.700	2.999	62.675	8.265	1.645	3.011	0.148	1.391	3.352
72	24.577	48.989	0.502	4.503	5.005	54.976	8.290	2.748	3.659	0.248	1.921	4.748
73	18.405	14.675	0.148	1.351	1.499	65.780	8.215	0.820	1.717	0.073	1.201	2.820
74	24.822	29.311	0.201	1.801	2.002	73.902	8.289	1.099	3.394	0.099	1.240	2.894
75	23.538	44.070	0.299	2.700	2.999	70.649	8.252	1.646	4.318	0.148	1.459	3.481
76	24.535	73.561	0.502	4.501	5.003	62.311	8.293	2.748	4.954	0.248	2.130	5.160
77	19.601	32.994	0.167	1.350	1.517	81.199	9.171	0.820	3.898	0.083	1.194	2.727
78	24.956	44.172	0.200	1.797	1.997	80.518	8.264	1.097	4.942	0.099	1.284	2.954
79	23.726	66.107	0.301	2.701	3.002	77.158	8.305	1.647	6.067	0.149	1.559	3.680
80	23.984	109.738	0.402	3.661	4.062	75.538	8.174	2.233	7.509	0.199	2.092	4.953
81	20.621	51.580	0.174	1.348	1.521	85.632	9.491	0.819	5.392	0.086	1.354	2.784
82	24.954	68.747	0.202	1.798	2.000	85.896	8.362	1.097	7.293	0.100	1.354	3.096
83	23.856	102.864	0.302	2.699	3.001	82.429	8.318	1.647	8.425	0.149	1.747	4.086
84	24.403	136.987	0.401	3.604	4.006	78.441	8.278	2.201	8.730	0.199	2.250	5.246
85	21.114	88.205	0.170	1.350	1.520	91.283	9.303	0.820	9.472	0.084	1.320	2.965
86	25.063	117.590	0.198	1.802	2.000	90.283	8.192	1.100	11.127	0.098	1.519	3.462
89	21.421	124.785	0.161	1.350	1.511	93.310	8.837	0.821	12.558	0.080	1.410	3.178
90	25.140	167.099	0.200	1.799	2.000	92.520	8.279	1.098	14.812	0.099	1.622	3.680
91	25.168	249.448	0.297	2.517	2.814	90.497	8.745	1.536	16.032	0.147	2.237	5.002
92	21.585	198.580	0.150	1.349	1.499	95.224	8.308	0.820	17.839	0.074	1.581	3.534
93	25.143	264.426	0.199	1.800	1.999	94.113	8.237	1.099	19.143	0.099	1.985	4.402
94	21.704	272.410	0.146	1.349	1.495	95.989	8.112	0.820	21.370	0.072	1.811	3.977
95	26.955	7.503	0.752	2.247	2.999	32.506	21.311	1.375	0.842	0.373	1.289	3.229
96	26.894	7.898	1.248	3.748	4.996	20.582	21.222	2.294	0.755	0.618	1.513	4.035
97	27.533	7.110	0.501	1.498	1.999	42.504	21.293	0.917	0.861	0.248	1.196	2.941
98	26.776	10.730	0.752	2.250	3.003	39.939	21.290	1.378	1.164	0.373	1.332	3.302
99	24.089	17.796	1.251	3.752	5.003	35.792	21.292	2.289	1.621	0.619	1.572	4.149
100	26.559	12.227	0.501	1.500	2.001	55.638	21.274	0.918	1.463	0.248	1.207	2.884

101	26.801	18.288	0.753	2.254	3.007	53.017	21.268	1.380	1.978	0.373	1.336	3.274
102	24.775	30.456	1.248	3.747	4.995	46.768	21.259	2.287	2.552	0.618	1.713	4.339
103	25.712	9.498	0.249	0.749	0.998	72.784	21.196	0.458	1.554	0.123	0.880	2.405
104	26.646	19.004	0.496	1.501	1.997	65.865	21.106	0.919	2.247	0.246	1.222	2.867
105	26.917	28.505	0.751	2.248	2.998	63.090	21.273	1.376	2.987	0.372	1.380	3.301
106	25.070	47.603	1.251	3.750	5.001	63.017	21.285	2.290	4.958	0.619	1.380	4.640
107	27.441	14.231	0.251	0.752	1.003	79.989	21.239	0.460	2.336	0.124	0.883	2.321
108	26.818	28.508	0.501	1.503	2.004	79.987	21.243	0.920	4.669	0.248	0.883	2.863
109	26.971	42.650	0.750	2.249	2.998	71.162	21.238	1.377	4.313	0.371	1.430	3.405
110	25.315	71.090	1.249	3.751	5.000	63.072	21.232	2.293	4.972	0.618	2.056	5.018
111	27.802	21.427	0.249	0.750	0.999	82.055	21.174	0.459	2.664	0.123	1.167	2.573
112	27.066	42.660	0.502	1.502	2.003	80.538	21.279	0.919	4.831	0.248	1.277	2.923
113	27.052	64.005	0.753	2.251	3.003	80.546	21.296	1.378	7.248	0.373	1.277	3.588
114	25.569	106.502	1.247	3.746	4.993	69.461	21.227	2.291	6.615	0.617	2.317	5.525
115	27.914	33.149	0.250	0.750	1.000	87.852	21.223	0.459	4.216	0.124	1.141	2.530
116	27.136	66.528	0.502	1.498	2.000	85.995	21.333	0.917	7.159	0.249	1.345	3.068
117	27.098	99.835	0.750	2.248	2.998	82.861	21.249	1.376	8.449	0.371	1.710	3.946
119	27.923	42.676	0.250	0.750	1.000	91.180	21.195	0.459	6.027	0.124	1.027	2.518
120	27.207	85.446	0.503	1.498	2.001	88.313	21.359	0.917	8.813	0.249	1.403	3.174
121	27.174	128.403	0.750	2.247	2.997	85.087	21.248	1.376	9.969	0.371	1.864	4.234
123	27.896	57.012	0.250	0.751	1.001	92.401	21.189	0.460	7.092	0.124	1.166	2.549
124	27.254	113.873	0.498	1.500	1.998	90.443	21.191	0.918	11.025	0.247	1.495	3.396
125	29.306	171.878	0.750	2.249	2.999	87.504	21.269	1.379	12.263	0.372	2.043	4.462
127	27.914	67.154	0.253	0.749	1.001	93.403	21.421	0.458	8.259	0.125	1.180	2.578
128	27.275	134.451	0.499	1.500	1.999	91.398	21.214	0.918	12.382	0.247	1.572	3.541
131	27.369	80.707	0.250	0.750	1.001	94.349	21.279	0.460	9.749	0.124	1.199	2.605
132	30.832	160.715	0.500	1.501	2.000	91.932	21.295	0.922	13.349	0.249	1.764	3.759
134	27.977	99.591	0.252	0.753	1.004	95.244	21.282	0.461	11.726	0.125	1.232	2.684

135	29.915	198.657	0.503	1.499	2.002	92.956	21.378	0.920	15.438	0.250	1.879	4.023
136	27.908	128.293	0.251	0.753	1.005	96.113	21.266	0.461	14.480	0.125	1.285	2.792
137	27.021	9.692	1.600	2.399	3.999	30.211	35.026	1.469	0.979	0.792	1.432	3.622
138	27.874	14.639	2.396	3.592	5.989	26.693	35.013	2.203	1.234	1.187	1.721	4.572
139	27.733	6.916	0.798	1.201	1.999	42.405	34.953	0.735	0.832	0.395	1.204	2.962
141	27.917	20.724	2.401	3.595	5.996	33.117	35.043	2.204	1.680	1.189	1.789	4.707
143	27.182	18.473	1.603	2.402	4.005	44.868	35.041	1.471	1.843	0.794	1.450	3.721
144	28.056	27.636	2.401	3.603	6.003	38.791	34.985	2.210	2.154	1.189	1.862	4.820
145	27.094	11.808	0.801	1.204	2.006	55.241	34.973	0.738	1.400	0.397	1.220	2.889
146	27.066	23.521	1.600	2.398	3.998	50.170	35.045	1.468	2.276	0.792	1.495	3.727
147	28.093	35.462	2.400	3.601	6.001	43.945	34.992	2.209	2.664	1.189	1.932	4.950
149	27.353	29.735	1.602	2.401	4.003	55.426	35.039	1.471	2.816	0.793	1.529	3.784
150	28.203	44.569	2.401	3.602	6.002	48.558	34.987	2.210	3.208	1.189	2.017	5.129
151	27.107	9.190	0.400	0.602	1.002	53.786	34.944	0.368	0.659	0.198	2.017	2.796
152	27.133	18.396	0.799	1.204	2.003	65.803	34.931	0.737	2.180	0.396	1.221	2.862
153	27.543	36.781	1.599	2.402	4.001	60.015	34.979	1.472	3.397	0.792	1.569	3.920
154	28.319	55.348	2.400	3.599	6.000	52.805	34.994	2.209	3.801	1.189	2.115	5.290
155	28.729	13.791	0.398	0.600	0.998	75.702	34.908	0.367	1.759	0.197	1.141	2.601
156	27.155	27.539	0.799	1.201	2.000	73.948	34.971	0.736	3.211	0.396	1.241	2.889
157	27.717	55.119	1.600	2.401	4.001	68.072	34.995	1.472	4.827	0.792	1.656	4.005
158	28.400	82.604	2.390	3.592	5.982	60.153	34.941	2.204	5.115	1.184	2.347	5.697
159	28.810	20.661	0.401	0.601	1.002	82.314	35.012	0.369	2.640	0.199	1.139	2.577
160	27.279	41.367	0.798	1.201	1.999	80.607	34.949	0.735	4.699	0.395	1.275	2.927
161	27.833	82.866	1.601	2.400	4.000	74.495	35.019	1.471	6.611	0.793	1.818	4.339
162	28.509	124.348	2.222	3.553	5.776	67.577	33.546	2.181	6.840	1.101	2.643	6.217
163	28.809	32.196	0.402	0.594	0.995	87.929	35.322	0.364	4.099	0.199	1.143	2.557
164	27.372	64.429	0.801	1.201	2.003	86.072	35.037	0.736	6.998	0.397	1.333	3.045
165	27.909	128.762	1.600	2.399	3.998	79.689	35.010	1.471	8.878	0.792	2.104	4.871

167	28.760	55.144	0.401	0.600	1.001	92.379	35.087	0.368	6.863	0.199	1.169	2.585
168	27.547	110.316	0.797	1.200	1.997	90.556	34.944	0.735	10.832	0.395	1.476	3.319
169	30.062	220.845	1.587	2.387	3.974	85.003	34.981	1.466	12.777	0.789	2.525	5.515
171	28.729	78.204	0.399	0.603	1.002	94.358	34.837	0.369	9.478	0.197	1.200	2.626
172	27.545	129.727	0.799	1.200	1.999	91.540	34.993	0.735	12.229	0.396	1.537	3.485
174	28.542	124.353	0.404	0.602	1.006	96.135	35.185	0.369	14.150	0.200	1.278	2.786
175	28.731	248.093	0.799	1.201	2.000	93.991	35.022	0.736	17.722	0.397	2.036	4.322
177	28.066	8.815	3.594	2.394	5.988	20.138	54.867	1.465	0.818	1.781	1.564	4.246
178	28.357	11.811	5.105	3.218	8.323	16.228	56.207	1.972	0.872	2.531	1.967	5.643
179	29.321	12.987	2.396	1.601	3.997	38.237	54.709	0.983	1.344	1.187	1.409	3.522
180	28.058	19.834	3.593	2.397	5.990	34.384	54.832	1.467	1.702	1.780	1.692	4.516
181	28.575	26.220	4.589	3.159	7.748	30.656	54.032	1.935	1.861	2.275	2.048	5.683
182	29.355	17.656	2.398	1.600	3.998	45.623	54.753	0.982	1.821	1.189	1.413	3.515
183	28.094	26.454	3.604	2.402	6.006	40.449	54.849	1.470	2.212	1.786	1.736	4.736
185	29.304	11.383	1.203	0.799	2.002	59.282	54.865	0.490	1.582	0.596	1.049	3.015
186	29.541	22.656	2.400	1.599	3.998	51.508	54.791	0.981	2.305	1.189	1.433	3.573
187	28.170	34.121	3.604	2.404	6.008	45.560	54.832	1.471	2.726	1.786	1.817	4.844
189	29.696	17.663	1.198	0.799	1.997	66.176	54.744	0.491	2.121	0.594	1.215	2.842
190	29.694	39.003	2.394	1.593	3.987	63.536	54.837	0.978	3.772	1.187	1.509	3.722
191	28.255	52.869	3.599	2.401	6.000	60.994	54.819	1.470	5.088	1.784	1.509	5.196
193	29.696	26.475	1.201	0.799	2.000	74.470	54.812	0.491	3.166	0.595	1.220	2.855
194	29.871	52.903	2.400	1.596	3.995	68.959	54.842	0.979	4.819	1.190	1.603	3.952
195	28.323	79.206	3.572	2.396	5.968	61.361	54.682	1.467	5.142	1.770	2.238	5.596
197	29.741	39.788	1.200	0.806	2.006	80.886	54.593	0.495	4.610	0.595	1.260	2.960
198	26.776	79.475	2.400	1.599	4.000	75.274	54.936	0.975	6.589	1.189	1.743	4.323
199	28.403	118.937	3.285	2.390	5.674	69.083	52.657	1.464	6.909	1.628	2.501	6.090
201	29.732	61.918	1.198	0.801	1.999	86.355	54.702	0.492	6.869	0.594	1.316	3.041
202	27.686	129.701	2.382	1.590	3.972	81.124	54.842	0.972	9.247	1.180	2.033	4.840

205	29.770	79.479	1.200	0.804	2.004	88.616	54.620	0.494	8.472	0.594	1.369	3.168
206	27.724	149.726	2.399	1.602	4.001	82.040	54.832	0.979	9.901	1.189	2.193	5.176
209	29.770	106.613	1.199	0.800	2.000	90.780	54.742	0.491	10.688	0.594	1.456	3.374
210	28.552	211.303	2.387	1.599	3.986	85.074	54.687	0.982	12.352	1.185	2.487	5.592
213	29.770	149.910	1.199	0.800	1.998	92.677	54.751	0.491	13.732	0.594	1.594	3.678
214	28.475	249.501	2.370	1.594	3.964	86.280	54.606	0.978	13.551	1.177	2.676	5.948
216	29.497	238.712	1.198	0.801	1.999	94.124	54.704	0.492	17.414	0.595	1.999	4.323
218	30.502	6.452	3.378	1.131	4.509	23.708	70.698	0.695	0.737	1.677	1.281	3.537
219	31.062	8.585	4.496	1.494	5.989	20.614	70.834	0.919	0.818	2.232	1.538	4.134
220	29.914	9.715	2.248	0.753	3.001	41.398	70.641	0.463	1.115	1.115	1.272	3.110
221	30.600	14.521	3.384	1.135	4.519	38.884	70.657	0.698	1.512	1.680	1.405	3.709
222	31.135	19.243	4.505	1.501	6.006	34.550	70.769	0.924	1.668	2.236	1.691	4.485
226	29.694	16.636	2.253	0.748	3.001	54.049	70.829	0.460	1.856	1.118	1.308	3.135
227	30.694	24.822	3.378	1.128	4.505	50.705	70.746	0.693	2.438	1.677	1.491	3.761
228	31.224	33.060	4.504	1.504	6.008	46.022	70.728	0.926	2.696	2.236	1.799	4.628
229	31.454	12.896	1.128	0.406	1.534	66.746	68.938	0.252	1.629	0.559	1.162	2.685
230	29.880	25.625	2.250	0.750	3.000	64.237	70.755	0.461	2.834	1.116	1.321	3.153
231	30.806	38.594	3.379	1.129	4.508	59.820	70.726	0.694	3.531	1.677	1.601	3.923
232	31.289	51.481	4.500	1.503	6.003	54.613	70.725	0.925	3.801	2.234	1.987	5.006
233	30.692	19.290	1.131	0.397	1.528	75.253	69.562	0.245	2.451	0.561	1.152	2.675
234	30.104	38.578	2.247	0.751	2.998	72.379	70.713	0.462	4.132	1.115	1.364	3.206
235	30.874	57.711	3.381	1.131	4.512	67.378	70.714	0.695	4.903	1.679	1.725	4.210
236	31.381	77.062	4.486	1.501	5.987	61.799	70.681	0.924	5.098	2.227	2.218	5.539
237	30.479	28.924	1.129	0.400	1.530	81.680	69.380	0.247	3.598	0.560	1.176	2.734
238	30.322	57.720	2.251	0.754	3.005	78.769	70.671	0.464	5.864	1.117	1.439	3.445
239	30.951	86.818	3.379	1.130	4.509	73.712	70.717	0.695	6.652	1.678	1.912	4.593
240	31.445	115.281	4.248	1.494	5.741	69.206	69.644	0.919	6.807	2.109	2.486	5.918
241	30.401	45.070	1.131	0.402	1.533	87.158	69.380	0.248	5.486	0.561	1.202	2.713

242	30.437	90.002	2.250	0.749	2.999	83.916	70.798	0.461	8.229	1.117	1.600	3.773
243	31.038	134.835	3.379	1.126	4.504	78.742	70.782	0.692	8.777	1.677	2.252	5.264
244	28.250	179.971	3.869	1.497	5.366	77.631	67.615	0.920	9.857	1.920	2.652	6.022
245	30.327	57.973	1.130	0.400	1.530	89.594	69.446	0.247	6.948	0.560	1.220	2.780
246	30.508	115.970	2.250	0.750	3.000	86.162	70.792	0.461	9.823	1.117	1.728	3.998
247	27.805	174.054	3.382	1.131	4.512	81.706	70.714	0.695	10.599	1.678	2.382	5.325
249	30.322	76.992	1.131	0.406	1.537	91.660	69.177	0.250	8.911	0.561	1.264	2.871
250	30.544	150.053	2.251	0.748	2.999	87.297	70.837	0.460	10.838	1.117	2.026	4.445
251	28.097	231.548	3.256	1.120	4.375	84.351	70.133	0.688	12.419	1.616	2.707	5.971
253	30.323	109.304	1.130	0.400	1.530	93.614	69.458	0.246	11.828	0.560	1.351	3.066
254	27.862	182.276	2.248	0.750	2.998	89.103	70.762	0.461	12.895	1.116	2.050	4.519
256	28.495	173.943	1.129	0.378	1.507	95.124	70.668	0.233	15.468	0.560	1.635	3.470
257	27.878	218.061	2.253	0.752	3.005	90.063	70.758	0.462	14.323	1.118	2.208	4.855
258	27.577	7.038	4.495	0.498	4.994	23.155	87.925	0.306	0.765	2.231	1.334	3.589
259	28.055	9.683	6.285	0.699	6.984	30.605	87.914	0.429	1.565	3.119	0.898	4.505
260	26.716	7.798	2.248	0.254	2.502	41.714	87.746	0.156	0.910	1.115	1.239	3.106
261	27.468	15.584	4.504	0.501	5.005	32.423	87.905	0.308	1.220	2.235	1.850	4.000
262	28.092	21.861	6.282	0.703	6.985	37.598	87.841	0.432	2.138	3.117	1.484	4.869
263	27.133	13.427	2.250	0.246	2.496	45.316	88.084	0.151	1.050	1.116	1.850	2.994
264	27.577	26.782	4.500	0.502	5.002	49.636	87.876	0.308	2.505	2.233	1.549	4.061
265	28.193	37.445	6.256	0.696	6.952	43.120	87.899	0.427	2.677	3.104	2.031	5.500
269	31.901	10.014	1.077	0.110	1.187	68.714	88.664	0.068	1.324	0.535	1.111	2.654
270	27.168	20.921	2.250	0.252	2.502	65.708	87.809	0.155	2.435	1.116	1.243	2.875
271	27.719	41.652	4.498	0.502	5.000	58.351	87.881	0.308	3.559	2.232	1.697	4.216
272	28.286	58.403	6.065	0.700	6.765	52.649	87.505	0.430	3.824	3.009	2.218	5.518
273	32.219	15.037	1.081	0.123	1.204	75.957	87.500	0.077	1.938	0.537	1.142	2.698
274	27.125	31.300	2.250	0.250	2.500	73.912	87.894	0.154	3.598	1.116	1.259	2.906
275	27.767	62.641	4.499	0.501	5.000	65.825	87.898	0.307	4.893	2.233	1.856	4.491

276	28.389	87.612	5.469	0.700	6.169	63.158	86.310	0.430	5.388	2.713	2.363	5.701
277	32.699	22.509	1.080	0.119	1.198	82.577	87.855	0.074	2.892	0.536	1.147	2.620
278	27.128	46.874	2.250	0.251	2.501	80.293	87.837	0.155	5.177	1.116	1.310	3.041
279	27.868	93.767	4.497	0.499	4.996	71.960	87.938	0.306	6.513	2.232	2.088	4.949
281	32.882	35.003	1.078	0.117	1.196	88.087	87.969	0.073	4.501	0.535	1.147	2.568
282	27.241	72.916	2.250	0.252	2.502	85.488	87.804	0.155	7.488	1.116	1.409	3.319
283	28.129	145.981	4.462	0.500	4.962	85.637	87.836	0.307	15.036	2.215	1.409	4.907
285	32.954	44.965	1.082	0.121	1.203	90.345	87.670	0.076	5.733	0.537	1.157	2.585
286	27.315	93.825	2.249	0.246	2.495	87.818	88.042	0.152	9.138	1.116	1.487	3.428
287	28.018	187.912	4.505	0.501	5.006	81.305	87.912	0.307	11.061	2.236	2.465	5.742
289	33.067	60.183	1.079	0.119	1.198	92.482	87.791	0.074	7.505	0.536	1.183	2.663
290	27.451	124.861	2.250	0.251	2.501	89.821	87.854	0.154	11.216	1.117	1.612	3.685
293	33.077	85.079	1.078	0.124	1.203	94.351	87.315	0.078	10.238	0.535	1.226	2.735
294	27.523	177.523	2.253	0.253	2.506	92.180	87.760	0.156	15.017	1.118	1.713	3.938
296	32.959	135.134	1.078	0.118	1.196	96.099	87.874	0.074	15.001	0.535	1.329	2.957
297	27.541	252.836	2.247	0.250	2.497	95.599	87.866	0.154	27.571	1.115	1.329	4.518
299	28.043	9.493	6.998	0.000	6.998	7.953	100.000	0.000	0.300	3.469	1.693	4.597
300	28.903	9.189	2.997	0.000	2.997	23.373	100.000	0.000	0.453	1.486	1.134	2.950
301	27.906	15.354	4.992	0.000	4.992	19.430	100.000	0.000	0.597	2.475	1.440	3.731
302	28.063	21.569	6.987	0.000	6.987	15.656	100.000	0.000	0.643	3.463	1.832	4.870
303	28.977	15.864	3.000	0.000	3.000	32.804	100.000	0.000	0.726	1.488	1.248	3.180
304	27.886	26.245	5.001	0.000	5.001	27.034	100.000	0.000	0.919	2.480	1.567	4.144
305	28.096	36.855	6.935	0.000	6.935	23.215	100.000	0.000	1.039	3.437	2.000	5.148
306	28.956	12.279	1.496	0.000	1.496	47.442	100.000	0.000	0.669	0.742	1.174	2.670
307	29.063	24.623	2.998	0.000	2.998	43.595	100.000	0.000	1.149	1.487	1.279	3.120
308	27.908	41.124	4.997	0.000	4.997	36.160	100.000	0.000	1.403	2.478	1.671	4.251
309	28.129	57.495	6.626	0.000	6.626	31.957	100.000	0.000	1.542	3.283	2.184	5.413
310	29.053	18.424	1.500	0.000	1.500	56.963	100.000	0.000	0.984	0.744	1.150	2.726

311	29.107	36.897	3.000	0.000	3.000	52.201	100.000	0.000	1.625	1.488	1.334	3.308
312	27.906	61.483	4.999	0.000	4.999	44.712	100.000	0.000	2.005	2.479	1.833	4.449
313	28.175	85.952	6.036	0.000	6.036	42.739	100.000	0.000	2.233	2.991	2.318	5.590
314	29.036	27.624	1.501	0.000	1.501	67.000	100.000	0.000	1.511	0.744	1.100	2.663
315	27.562	55.332	2.998	0.000	2.998	61.527	100.000	0.000	2.378	1.487	1.409	3.372
316	27.949	91.997	4.996	0.000	4.996	52.034	100.000	0.000	2.687	2.477	2.079	4.967
317	28.241	129.322	5.303	0.000	5.303	55.507	100.000	0.000	3.278	2.628	2.464	5.729
318	29.062	42.980	1.500	0.000	1.500	75.971	100.000	0.000	2.352	0.744	1.180	2.661
319	27.913	85.874	3.001	0.000	3.001	69.851	100.000	0.000	3.448	1.488	1.549	3.613
320	27.975	142.977	4.922	0.000	4.922	60.215	100.000	0.000	3.694	2.441	2.435	5.616
321	28.272	200.419	4.922	0.000	4.922	67.290	100.000	0.000	5.016	2.438	2.550	5.803
322	29.062	55.180	1.499	0.000	1.499	79.865	100.000	0.000	2.949	0.744	1.201	2.725
323	27.835	110.381	3.000	0.000	3.000	73.584	100.000	0.000	4.143	1.488	1.616	3.864
324	27.984	184.077	4.909	0.000	4.909	65.638	100.000	0.000	4.650	2.434	2.522	5.744
326	29.062	73.738	1.500	0.000	1.500	83.703	100.000	0.000	3.821	0.744	1.241	2.810
327	27.845	147.306	3.000	0.000	3.000	77.303	100.000	0.000	5.066	1.487	1.832	4.217
330	29.061	104.178	1.499	0.000	1.499	87.278	100.000	0.000	5.101	0.743	1.314	2.974
331	27.877	208.723	2.998	0.000	2.998	81.878	100.000	0.000	6.716	1.487	1.995	4.508
334	29.014	165.625	1.497	0.000	1.497	91.043	100.000	0.000	7.548	0.743	1.421	3.195
335	27.873	258.406	2.999	0.000	2.999	83.471	100.000	0.000	7.509	1.487	2.229	4.992
337	29.019	227.943	1.498	0.000	1.498	92.607	100.000	0.000	9.305	0.743	1.601	3.567
340	26.546	9.006	2.993	2.994	5.987	16.929	44.740	1.833	0.676	1.484	1.924	4.914
341	24.782	9.996	1.496	1.498	2.994	40.916	44.778	0.914	1.146	0.741	1.253	3.232
342	25.901	15.171	2.254	2.254	4.508	37.467	44.764	1.378	1.495	1.117	1.463	3.950
343	26.619	20.283	3.002	3.001	6.004	30.442	44.765	1.837	1.455	1.489	2.013	5.012
344	27.755	8.695	0.749	0.749	1.497	57.486	44.799	0.457	1.119	0.371	1.127	2.684
345	24.988	17.373	1.501	1.500	3.001	53.756	44.826	0.915	1.927	0.743	1.295	3.386
346	25.983	25.988	2.251	2.250	4.501	49.424	44.781	1.375	2.434	1.115	1.539	4.122

347	26.692	34.818	3.004	3.002	6.006	41.758	44.772	1.837	2.385	1.490	2.109	5.280
348	27.674	13.530	0.750	0.747	1.497	67.154	44.913	0.456	1.692	0.372	1.159	2.796
349	25.136	26.923	1.499	1.501	3.001	63.799	44.772	0.916	2.922	0.742	1.324	3.354
350	26.029	40.561	2.248	2.249	4.497	59.099	44.767	1.374	3.595	1.114	1.627	4.235
351	26.847	54.264	2.986	2.995	5.981	51.180	44.674	1.834	3.475	1.481	2.258	5.591
352	27.764	20.311	0.748	0.752	1.500	75.315	44.663	0.459	2.532	0.371	1.163	2.717
353	25.321	40.570	1.499	1.502	3.000	71.862	44.750	0.916	4.235	0.742	1.378	3.478
354	26.284	60.797	2.249	2.250	4.499	63.679	44.733	1.377	4.368	1.114	2.008	4.714
355	26.921	80.853	2.919	2.977	5.896	59.088	44.270	1.822	4.723	1.448	2.475	5.938
356	27.878	30.406	0.751	0.752	1.503	81.872	44.789	0.459	3.753	0.372	1.175	2.742
357	25.551	60.786	1.502	1.498	2.999	81.788	44.851	0.914	7.446	0.744	1.175	3.583
358	26.358	91.055	2.249	2.250	4.499	70.742	44.735	1.377	6.024	1.114	2.182	5.079
359	27.029	121.553	2.417	2.988	5.405	68.811	39.595	1.829	6.679	1.199	2.633	6.253
360	27.912	47.214	0.750	0.751	1.501	87.312	44.751	0.459	5.713	0.372	1.199	2.771
361	25.731	94.454	1.501	1.504	3.005	83.593	44.746	0.918	8.465	0.743	1.607	3.927
362	26.359	142.025	2.242	2.247	4.489	76.813	44.701	1.375	8.237	1.111	2.488	5.755
364	27.940	60.799	0.753	0.751	1.504	89.659	44.838	0.459	7.213	0.373	1.223	2.781
365	25.838	121.418	1.501	1.498	3.000	85.864	44.827	0.915	10.076	0.744	1.736	4.253
366	26.493	182.181	2.237	2.245	4.482	80.878	44.661	1.374	10.501	1.109	2.505	5.780
368	27.983	81.146	0.750	0.749	1.499	91.834	44.834	0.458	9.326	0.372	1.263	2.855
369	25.948	162.380	1.500	1.501	3.002	88.761	44.758	0.917	13.113	0.743	1.785	4.332
370	26.581	242.604	2.042	2.234	4.277	84.154	42.549	1.367	12.639	1.013	2.772	6.212
372	28.061	115.134	0.750	0.751	1.501	93.748	44.764	0.459	12.453	0.372	1.342	3.023
373	25.986	230.278	1.499	1.499	2.998	90.546	44.768	0.916	15.889	0.743	2.089	4.767
376	28.171	182.912	0.750	0.752	1.502	95.540	44.711	0.459	17.800	0.371	1.492	3.333
379	28.236	250.337	0.750	0.751	1.501	96.652	44.766	0.459	23.978	0.372	1.516	3.721
401	28.651	8.008	0.002	3.001	3.003	15.576	0.057	1.839	0.339	0.001	1.459	3.431
402	28.510	70.247	0.005	1.997	2.001	71.625	0.187	1.224	3.095	0.002	1.546	3.299

403	29.694	24.533	0.503	4.504	5.006	36.520	8.291	2.761	1.732	0.250	2.067	4.628
404	31.496	68.633	0.200	1.805	2.005	84.510	8.239	1.107	6.582	0.099	1.531	3.261
405	27.963	23.808	0.300	2.700	3.000	55.502	8.266	1.654	2.249	0.149	1.536	3.471
406	28.026	99.726	0.248	0.748	0.996	94.641	21.200	0.458	10.271	0.123	1.409	2.848
407	27.688	64.026	0.750	2.250	3.000	75.843	21.271	1.379	5.498	0.372	1.688	3.735
408	27.004	71.222	1.249	3.745	4.994	61.843	21.277	2.293	4.721	0.620	2.182	5.076
409	27.546	71.142	0.799	1.200	2.000	88.100	35.081	0.734	8.370	0.397	1.232	3.225
410	26.653	27.515	2.399	3.597	5.996	37.037	35.090	2.201	1.995	1.190	1.993	4.899
411	25.411	36.817	1.599	2.400	3.999	57.646	35.151	1.463	3.071	0.793	1.725	4.002
412	29.542	80.989	0.751	0.752	1.502	91.789	44.693	0.461	9.317	0.372	1.268	2.936
413	27.747	34.834	2.996	2.996	5.992	45.165	44.706	1.837	2.736	1.485	1.846	5.008
414	27.956	79.508	1.199	0.798	1.996	88.740	54.856	0.489	8.537	0.594	1.351	3.156
415	27.538	26.541	3.599	2.400	5.999	40.376	54.802	1.472	2.205	1.784	1.744	4.635
416	27.546	24.822	3.381	1.131	4.512	50.286	70.722	0.694	2.397	1.676	1.500	3.959
417	27.478	77.225	4.467	1.494	5.961	62.105	70.715	0.917	5.132	2.214	2.180	5.369
418	27.549	125.269	2.249	0.255	2.504	89.805	87.641	0.157	11.207	1.115	1.620	3.717
419	27.155	41.794	4.502	0.498	5.001	58.367	87.949	0.306	3.557	2.232	1.700	4.182
420	26.980	36.933	3.001	0.000	3.001	51.153	100.000	0.000	1.558	1.487	1.605	3.429
421	26.910	92.022	5.003	0.000	5.003	51.905	100.000	0.000	2.676	2.480	2.095	4.972